

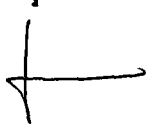
15492

**GEO TECHNICAL EVALUATIONS AND DETERMINISTIC DESIGN
CONSIDERATIONS FOR PITWALL SLOPES AT ESKİHİSAR
(YATAĞAN-MUĞLA) STRIP COAL MINE**

**A DOCTOR OF PHILOSOPHY THESIS
in
Geological Engineering
Middle East Technical University**

**By
ULUSAY, Reşat
September - 1991**

Approval of the Graduate School of Natural and Applied Sciences.


for Prof. Dr. Alpay ANKARA

Director

I certify that this thesis satisfied all the requirements as a thesis for the degree of Doctor of Philosophy in Geological Engineering.



Prof. Dr. Vedat DOYURAN

Chairman of the Department

We certify that we have read this thesis and that in our opinion it is fully adequate, in scope and quality, as a thesis for the degree of Doctor of Philosophy in Geological Engineering.



Prof. Dr. Vedat DOYURAN

Supervisor

Examining Committee in Charge :

Prof. Dr. Vedat DOYURAN

Assoc. Prof. Dr. Erdal ÜNAL

Assoc. Prof. Dr. Nurkan KARAHANOĞLU

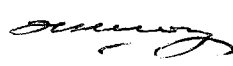
Assist. Prof. Dr. Hüsnü AKSOY

Prof. Dr. K. Erçin KASAPOĞLU











Committee Chairman

ABSTRACT

GEOTECHNICAL EVALUATIONS AND DETERMINISTIC DESIGN CONSIDERATIONS FOR PITWALL SLOPES AT ESKIHİSAR (YATAĞAN-MUĞLA) STRIP COAL MINE

ULUSAY, Reşat

PhD in Geological Engineering Department

Supervisor : Prof. Dr. Vedat DOYURAN

September 1991, 340 pages

In this study it is aimed to reveal the geotechnical characteristics of the lithological units exposed at the Eskihisar strip coal mine, to establish the causes and mechanisms of slope failures, to estimate shear strength parameters mobilized along the sliding surfaces at the time of failure, and to determine optimum slope parameters for safe and economical operation of the mine.

Paleozoic(?) schist and Mesozoic(?) marbles constitute the basement rocks in the mine area. The Neogene deposits comprising Turgut, Sekköy and Yatağan formations overlie the basement rocks unconformably. The coal seam having a maximum thickness of 20 m occurs at the base of the Sekköy formation. All units are crossed by normal faults and numerous joints.

Geotechnical investigations involve core drilling, in-situ and laboratory testing to determine material, discontinuity and mass properties of the lithological units. Groundwater level measurements, slope monitoring and back analyses of various possible modes of failure are also performed.

Slope instabilities are mainly controlled by structural features yielding multiplanar and plane shear failures, and small-scale wedge failures. Mass failures occur in soils and highly jointed rock masses. The parameters derived from laboratory shear tests are compared with those obtained from the back analyses of instabilities encountered in the pit. The results suggested that the residual shear strength of discontinuities and of soils are mobilized along the sliding surfaces at the time of failure.

Stability analyses involved kinematic approaches and limit equilibrium analyses incorporating dry and saturated slopes as well as effects of tension cracks. The results of analyses indicated that the overall stability is most sensitive to toe configuration, weak clay bed appearing at the basin margins, and orientation of major structural elements. Design considerations for multi-bench sidewall slopes, highwalls and individual benches are discussed with the consideration of the initial pit design plan proposed by Turkish Coal Enterprises.

Keywords : Slope stability, Eskihisar strip coal mine, Back analysis, Failure mechanism, Limiting equilibrium, Sensitivity analysis, Design evaluation.

Science Code : 606.04.01

ÖZET

ESKİHİSAR (YATAĞAN-MUĞLA) KÖMÜR AÇIK İŞLETMESİNDE JEOTEKNİK DEĞERLENDİRMELER VE İŞLETME ŞEVLERİNİN DETERMİNİSTİK YÖNTEMLERLE TASARIMI

ULUSAY, Reşat

Doktora Tezi, Jeoloji Mühendisliği Bölümü

Tez Yöneticisi : Prof. Dr. Vedat DOYURAN

Eylül 1991, 340 sayfa

Bu çalışmada, Eskihisar kömür açık işletmesinde yüzeylenen litolojik birimlerin jeoteknik özelliklerinin araştırılması, şev duraysızlıklarının nedenlerinin ve mekanizmalarının belirlenmesi, duraysızlık sırasında kayma yüzeyleri boyunca etkin olan makaslama dayanımı parametrelerinin saptanması ve güvenli ve ekonomik maden işletmeciliği için optimum şev parametrelerinin araştırılması amaçlanmıştır.

Paleozoyik(?) şistler ve Mesozoyik(?) mermerler maden sahasının temel kayaçlarını oluştururlar. Turgut, Sekköy ve Yatağan formasyonlarından oluşan Neojen çökelleri temel kayaçları üzerinde uyumsuz olarak yer almaktadır. Maksimum kalınlığı 20 m olan kömür zonu seviyesi Sekköy formasyonunun tabanında bulunur. Tüm birimler normal faylar ve çok sayıda eklemler tarafından kesilirler.

Jeoteknik etüdüler, karotlu sondajları ve litolojik birimlerin malzeme, süreksizlik ve kütle özelliklerinin tayini amacıyla yerinde ve laboratuvarda yapılan test çalışmalarını içermektedir. Ayrıca yeraltısuyu tablası ölçümleri, şevlerde hareketlerin izlenmesi ve çeşitli duraysızlık modellerinin geriye dönük analizleri de gerçekleştirilmiştir.

Şev duraysızlıkları yapısal özellikler tarafından denetlenen, başlıca çok düzlemlili ve düzlemsel makaslama kaymaları ve küçük ölçekli kama tipi kaymalar şeklindedir. Zeminlerde ve oldukça eklemli kayaçlarda kütleli yenilmeler gelişmektedir. Laboratuvar makaslama testleri ile saptanan parametreler işletmede karşılaşılan duraysızlıkların geriye dönük analizlerinden elde edilen değerlerle karşılaştırılmıştır. Sonuçlar, duraysızlık sırasında süreksizliklerin ve zeminlerin artık makaslama dayanımlarının etkin olduğunu göstermiştir.

Duraylılık analizleri, kinematik yaklaşımları ve kuru ve suya doygun şevlerle birlikte gerilim çatlaklarının etkilerini de içeren limit denge analizlerini kapsamaktadır. Analizlerin sonuçları, nihai şev duraylılığının topoğrafya konumuna, havza kenarlarında görülen zayıf kil tabakasına ve ana yapısal elemanların yönelimine karşı çok duyarlı olduğunu göstermiştir. Çok basamaklı kalıcı kenar şevlerinin, yüksek şevlerin ve münferit basamakların tasarımıyla ilgili hususlar, Türkiye Kömür İşletmeleri tarafından önerilen ilk tasarım planı dikkate alınarak tartışılmıştır.

Anahtar Kelimeler : Şev duraylılığı, Eskişehir kömür açık işletmesi, Geriye dönük analiz, Yenilme mekanizması, Limit denge, Duyarlılık analizi, Tasarım değerlendirilmesi.

Bilim Kodu : 606.04.01

ACKNOWLEDGEMENT

The author would like to express his wholehearted and indebted appreciation to Prof. Dr. Vedat DOYURAN for his very kind and restless supervision of the thesis from the very beginning to the end, and especially for his constant encouragement in all stages of the study.

The author is thankful to Prof. Dr. K. Erçin KASAPOĞLU not only for encouragement and advises he gave during the study, but also his permission to make use of the laboratory and personal computer facilities at Hacettepe University.

The constant encouragement during the thesis and invaluable help of Assist. Prof. Dr. Hüsnü AKSOY on using stereoplot programs and making use of the laboratory facilities are greatly acknowledged.

The author is indebted to Assoc. Prof. Dr. Erdal ÜNAL for his valuable criticisms on rock mass classification. Sincere appreciation is extended to his research assistant İhsan ÖZKAN for performing computer analysis in evaluation of rock mass classification and for carrying out slake durability tests.

Thanks are due to Assoc. Prof. Dr. Nurkan KARAHANOĞLU for his valuable criticisms and suggestions on the statistical part of this investigation. The author is grateful to Assist. Prof. Dr. Can AYDAY for his invaluable help and guidance on statistical analysis of discontinuity parameters by using his computer program.

Special thanks are due to Mr. M. Fatih YOLERİ, from M.T.A., for his kind assistance and enthusiasm in the field work, experimental measurement programme and drawings.

This study is supported by the General Directorate of Mineral Research and Exploration of Turkey (M.T.A.) and the author gratefully acknowledges the support and permission provided by M.T.A..

The author wishes to acknowledge the cooperation of personnel at TKİ Eskişehir Coal Mine. He would also like to thank to colleagues and laboratory technicians employed in Rock and Soil Mechanics Division of M.T.A..

He also cordially thanks research assistants Dinçer ÇAĞLAN and Candan GÖKÇEÖZLU (Hacettepe University) and Mrs. Nuray SAHİLLİ for their very kind assistance in typing and printing the manuscript.

Finally, the author records with pleasure the affection, patience and support of his wife Yıldız ULUSAY and his son KAYA.

CONTENTS

	Page
ABSTRACT	iii
ÖZET	v
ACKNOWLEDGEMENTS	vii
LIST OF TABLES	xv
LIST OF FIGURES	xvii
LIST OF PLATES	xxvi
1. INTRODUCTION	1
1.1. Purpose and Scope	1
1.2. Location and Accessibility	4
1.3. Previous Investigations	6
2. PHYSIOGRAPHY	10
2.1. Topography and Drainage	10
2.2. Climate and Vegetation	12
3. CURRENT MINING PRACTICE	14
4. SITE GEOLOGY	20
4.1. Geological Mapping	21
4.2. Stratigraphy	22
4.2.1. Basement Rocks	22
4.2.1.1. Schists	22
4.2.1.2. Marbles	24
4.2.2. Neogene Deposits	26
4.2.2.1. Turgut Formation	26
4.2.2.2. Sekköy Formation	27

	Page
4.2.2.2.1. Coal Seam	29
4.2.2.2.2. Main Sekköy Formation (Tms)	31
4.2.2.2.3. Detrital Facies of Sekköy Formation (Tms ¹)	33
4.2.2.2.4. Transition Zone Deposits (Tms ²)	35
4.2.2.3. Yatağan Formation	36
4.3. Structural Geology	39
4.3.1. Faults	39
4.3.1.1. Pre-Neogene Faults	39
4.3.1.2. Neogene Faults	40
4.3.2. Joints	45
4.3.3. Bedding	48
4.3.4. Schistosity	50
4.3.5. Unconformities	52
5. SITE INVESTIGATIONS	53
5.1. Discontinuity Surveys	53
5.1.1. Discontinuity Orientation	55
5.1.2. Aperture and Infilling	60
5.1.3. Asperities of Discontinuity Features	62
5.1.4. Water Conditions on Discontinuity Surfaces	62
5.1.5. Spacing of Discontinuities	63
5.1.6. Persistence of Discontinuities	67
5.2. Drilling and Geotechnical Logging	68
5.3. Groundwater Conditions	74
5.3.1. Groundwater Monitoring	76

	Page
5.3.2. Mass Permeability and Determination of Water Losses	81
5.3.3. Assessment of Groundwater Conditions .	83
5.4. Monitoring of Pit Slopes and Observations on Previous Slides	86
5.4.1. Observations on Previous Slides	87
5.4.2. Monitoring of Pit Slopes	89
5.5. Schmidt Hammer Tests	100
5.6. Field Sampling	101
 6. LABORATORY INVESTIGATIONS	 104
6.1. X-ray Diffraction Analyses	105
6.2. Index Properties	106
6.2.1. Unit Weight Determinations	106
6.2.2. Atterberg Limits and Moisture Content Determinations	109
6.2.3. Grain Size Distributions	113
6.2.4. Soil Classification	115
6.2.5. Slake Durability Index	121
6.3. Intact Rock Strength	121
6.3.1. Uniaxial Compressive Strength	122
6.3.2. Classification of Intact Rock	125
6.3.3. Shear Strength of Intact Rock	127
6.4. Shear Strength of Discontinuities	130
6.4.1. Shear Strength Characteristics of Joints	130
6.4.2. Shear Strength Characteristics of Bedding Surfaces	135
6.4.2.1. Shear Strength of Smooth- Planar Bedding Surfaces	135
6.4.2.2. Shear Strength of Undulating Smooth Bedding Surfaces	138

	Page
6.4.3. Shear Strength Characteristics of Fault Gouges	141
6.5. Shear Strength Characteristics of Soil Materials	146
6.5.1. Shear Strength of Claystone in Sekköy Formation	146
6.5.2. Shear Strength of Transition Zone	148
6.5.3. Shear Strength of the Soils of Turgut Formation	149
 7. EVALUATION OF ROCK MASS STRENGTH	 151
7.1. Rock Mass Strength and Classification	151
7.2. Application of Rock Mass Classification System	154
7.3. Estimating Rock Mass Shear Strength From RMR Values and Empirical Failure Criterion	162
 8. BACK ANALYSES AND ASSESSMENT OF MECHANISM OF SLOPE FAILURES	 168
8.1. History of Slope Failures at Eskihsar Open Pit	169
8.2. Back Analysis of Plane Failure in Footwall ...	171
8.3. Back Analysis of Multiplanar Failure	175
8.4. Back Analysis of Wedge Failure and Monitoring Data	182
8.4.1. Back Analysis of Slide 6	182
8.4.2. Evaluation of Monitoring Data From the Highwall of Ninth Slice	187
8.5. Back Analysis of Mass Failure in the Transition Zone Soils	190
8.6. General Evaluation of Other Slides	194

	Page
8.7. Failure Modes of Slides of the Eskihisar Open Pit	197
9. DESIGN SECTORS AND KINEMATIC ANALYSES OF PIT SLOPES	199
9.1. Design Sectors	199
9.2. Kinematic Analysis of Slopes	201
10. DETERMINISTIC ANALYSES AND DESIGN EVALUATIONS ...	214
10.1. Design Methodology	214
10.2. Design Sector I	215
10.3. Southeast Wall (Design Sector II)	226
10.4. Southwest Wall (Design Sector III)	238
10.4.1. Stability of Slopes in Transition Zone Soils	240
10.4.2. Analysis of Mass Failure Possibility in Main Sekköy Formation	242
10.4.3. Overall Stability of Southwest Wall	246
10.5. Stability of West and East Sidewalls (Design Sectors IV and V)	248
10.6. Stability of Highwall Slopes	257
10.6.1. Possibility of Mass Failure in Highwalls	258
10.6.2. Structurally Controlled Failure Analysis for Highwalls (Design Sectors VIII and IX)	263
10.7. Analysis of Possible Wedge Failures	266
10.7.1. Design Sector VI	268
10.7.2. Design Sector VIII	270
10.7.3. Design Sector IX	273

	Page
11. CONCLUSIONS AND RECOMMENDATIONS	275
REFERENCES	283
APPENDIX A. RESULTS OF PETROGRAPHICAL-MINERALOGICAL AND X-RAY DIFFRACTION ANALYSES	297
APPENDIX B. ROCK AND SOIL MECHANICS LABORATORY TEST RESULTS	299
APPENDIX C. ROCK MASS CLASSIFICATION SYSTEMS	311
APPENDIX D. METHODS OF LIMITING EQUILIBRIUM SLOPE STABILITY ANALYSIS	314
APPENDIX E. FLOW CHARTS OF THE COMPUTER PROGRAMS DEVELOPED FOR THE STUDY ..	328
VITA	340
PLATES	

LIST OF TABLES

Table	Page
1. Major discontinuity sets	59
2. Analysis of joint spacing data and cross-correlation test results	66
3. Average percentage of total and intact core recoveries (TCR and ICR) and rock quality designation (RQD) for each unit in terms of boreholes	71
4. Groundwater level observations	79
5. Results of falling head permeability tests	82
6. Statistical results of unit weight determinations	108
7. Results of general statistical evaluation of the Atterberg limits	110
8. Unified Soil Classification	117
9. Uniaxial compressive strength values of various rock types of the study area	123
10. Strength classification for rock units of the study area	126
11. Shear strength parameters of rock substances of the study area	129
12. Results obtained from the analyses of laboratory shear test on discontinuities and soil samples	134
13. Rock mass characteristics of main Sekköy formation	161
14. Design sectors and potential instabilities	208
15. The amounts of shifting (toe) with respect to factors of safety 1.4 and 1.5 for design sector II	239
16. Results of the stability analyses for highwall slopes against mass failure	262

Table	Page
17. Limiting equilibrium analysis of wedge failures- Design Sector VI	269
18. Limiting equilibrium analysis of wedge failures- Design Sector VIII	272
19. Limiting equilibrium analysis of wedge failures- Design Sector IX	274



LIST OF FIGURES

Figure	Page
1. Location map of the study area	5
2. Drainage pattern of the study area and its vicinity	11
3. Average monthly precipitation histogram	13
4. General view of the Eskihişar strip coal mine and striping operation	15
5. Working principles of dragline at Eskihişar open pit : (A) typical range of dragline (B) stripping of dragline on a single coal seam	16
6. Layout plan of the Eskihişar strip coal mine	18
7. Generalized stratigraphic column of the study area	23
8. View of a marble quarry located at the west of existing pit	25
9. A view of the black clay, closely located to basin margins and a plane failure developed along the clay	28
10. The coal seam and its distinct upper boundary	30
11. A view of the medium to thick bedded compact marls in main Sekk�y formation	32
12. Alternation of thinly bedded limestone, claystone and marl in the upper levels of main Sekk�y formation (Tms) and sandy limestone pocket (S1m)	34
13. A view of local folding and raveling developed in the uppermost alternating sequence of main Sekk�y formation	34

Figure	Page
14. A view from the transition zone deposits (Tms ²) and the thin marker coal seam (MC) lying on the main Sekköy formation (Tms)	37
15. A view from a stable bench (18 m high) constructed in massive sandstone of Yatağan formation	37
16. Probable graben boundary identified along the contact between the Neogene deposits and marbles at the south of Aldağ	41
17. Rose diagrams and histogram analysis of fault measurements carried out in the site	43
18. A normal fault affecting overburden and the coal seam at Ertrans section-approximate throw is 2 m	44
19. A view of a well-developed cross joints in the compact marl - length of tape: 1.2 m	46
20. Rose diagrams and histogram analyses of joints measured from Eskihisar strip coal mine	47
21. Rose diagrams and histograms of bedding at different domains of the study area	49
22. Rose diagrams and histogram analysis of schistosity planes	51
23. View showing discontinuity survey conducted on compact marls and joint pattern developed in this rock unit	54
24. Lower hemisphere Schmidt plots illustrating the joint orientations in the main Sekköy formation and the coal seam	56
25. Lower hemisphere Schmidt plots illustrating the orientations of schistosity planes and faults in the study area	57
26. Lower hemisphere Schmidt plots of bedding surfaces in different sections of the study area	58

Figure	Page
27. Separation and local plane failure along the bedding surfaces in the main Sekkøy formation	61
28. A view of a fault plane and the gouge material ..	61
29. Discontinuity spacing histograms for the main Sekkøy formation	65
30. Geotechnical borehole logs	70
31. Views of cores taken from geotechnical boreholes: (a) limestone and alternating upper sequence of main Sekkøy formation (Borehole No. JT1); (b) compact marls (Borehole No. JT3)	72
32. Core orientation technique based on the marker method: (a) reference line and the angles α and β ; (b) simple method of measuring β ; (c) goniometer for measuring α	75
33. Seepage from the coal seam and compact marl/coal seam boundary at the new higwall face - south of ninth slice	77
34. A monitoring target consisting of reflector prism, tripod and labeled steel bar for the monitoring of surface displacements	90
35. (a) General view of slide 6 (b) Tension crack and separation in the rock mass parallel to the steeply dipping joints	92
36. Slope instability map of the slide 6 and monitoring information	93
37. Cumulative vertical displacement versus time plots for stations at +552 bench(A) and +539 bench(B)	95
38. (a) General view of monitored area II and tension cracks (b) slope instability map and monitoring information	96

Figure	Page
39. Plots of movements measured during September 1989 proceeding failure at the end of ninth slice: (A) vertical displacement versus time plot; (B) tension crack separation versus time graph ..	98
40. Slide initiation and separations along faults B and C in the new highwall at the south of ninth slice	99
41. Undisturbed and oriented sampling from a fault gouge using metal specimen cutter	102
42. Unit weight histograms of rock and soil units in the study area	107
43. Distribution of soils of the study area on the "Swelling Potential" chart proposed by Van der Merwe (1964)	112
44. Typical grain size distributions of soil materials of the study area	114
45. Distribution of fine-grained soils of the study area on the plasticity chart	118
46. Graphical presentation of coefficients of permeability values of different types of soils and the methods of determination of permeability	119
47. Uniaxial compressive strength histograms of marl, lignite and conglomerate	124
48. Typical Mohr circles and failure envelope for an intact sandstone sample representing Yatağan formation	128
49. Shear failure envelopes and typical shear stress-shear displacement graphs for smooth-planar joints developed in main Sekköy formation	133
50. Shear failure envelopes and typical shear stress-shear displacement graphs for smooth-planar bedding surfaces developed in main Sekköy formation	137

Figure	Page
51. Shear strength of undulating-planar bedding surfaces developed in the limestone of detritic facies	140
52. Failure envelopes for sample LB47 from limestone	142
53. Direct shear test results on fault gouges	144
54. Direct shear test results on different soil materials encountered in the study area	147
55. Simplified representation of the relationship between size of slope, discontinuity spacing and mechanism of slope failure	153
56. Comparison of the original and modified RMR values determined from geotechnical boreholes and scanline survey data	157
57. Histograms of RMR for all samples from main Sekköy formation: (a) histogram of RMR based on Bieniawski (1989); (b) histogram of modified RMR based on Ünal and Özkan (1990)	158
58. Histograms and normal probability plots of RMR values for weak zone and compact marls with respect to RMR and modified RMR classification system	160
59. Graphical representation of stress conditions for rock failure and empirical failure criterion equations	163
60. Shear strength envelopes and variations of c and ϕ with normal stress for compact marls (A1, B1) and weak zone (A2, B2)	166
61. General view of slide 1 occurred in Ertrans section	170

Figure	Page
62. Plane failure on footwall material-slide 8: (A) instability plan and structural features; (B) sliding surface and linear traces parallel to movement direction; (C) kinematic check of the failure	172
63. Back analysis of slide 8 developed along the black clay	174
64. Kinematic check (a), instability plan (b), and mode of failure (c) for slide 2	176
65. Back analysis of slide 2 developed along multiplanar failure surface	179
66. Kinematic analysis of possible lines of intersection and monitoring station movements for slide 6	183
67. Back analysis of slide 6	185
68. Kinematic analysis of possible lines of intersection and monitoring station movements for the highwall instability at the end of ninth slice	188
69. Back analysis of slide 7 located within the transition zone soils	191
70. View from plane sliding surface developed along a clay bed in footwall at Ertrans section-slide 1b	196
71. General view of slide 5, developed along a circular slip surface within a highly decomposed sandstone (SSt)	196
72. Typical mode failure experienced at the Eskihisar open pit	198
73. Design sectors at Eskihisar open pit	200
74. Steps involved in kinematic analyses of plane, wedge and toppling failure modes	202
75. Configuration of highwall slopes	203

Figure	Page
76. Kinematic analyses used to identify potential slope stability problems for design sectors	205
77. Design sections and comparison of the initial design by TKI and modified design based on a factor of safety of 1.3 for design sector I ...	216
78. Multiplanar failure analyses for design section 3-3' at sector I	219
79. Multiplanar failure analyses for design section 4-4' at sector I	220
80. Multiplanar failure analyses for design section 5-5' at sector I	222
81. Multiplanar failure analyses for design section 6-6' at sector I	223
82. Multiplanar failure analyses for design section 7-7' at sector I	224
83. Design sections and mine layout based on the initial design by TKI at sectors II and III	227
84. Stability analysis of various slope configurations for southeast wall-section 2D1-1', at sector II	229
85. Analysis of planar failure developed after multiplanar failure in hangingwall at southeast wall-section 2D1-1', at sector II	231
86. Stability analysis of various slope configurations for southeast wall-Section 2D2-2', at sector II	232
87. Stability analysis of various slope configurations for southeast wall-Section 2D3-3', at sector II	234
88. Stability analysis of various slope configurations for southeast wall-Section 2D4-4', at sector II	235

Figure	Page
89. Stability analysis of various slope configurations for southeast wall-Section 2D5-5', at sector II	236
90. Slope stability curves for the soils of transition zone in southwest wall (Sector III) ..	241
91. Design sections for design sector III	243
92. Stability analysis of weak portion of main Sekkøy formation based on the mass failure	245
93. Mass failure analyses for slopes involving different rock and soil units at sector III and south of sector IV	247
94. Design sections selected at sectors IV and V ...	249
95. Design section 4D1-1' and computer solutions for the tension crack positions under different groundwater conditions (Sector IV)	252
96. Design section 4D2-2' and computer solutions for the tension crack positions under different groundwater conditions (Sector IV)	253
97. Design section 4D3-3' and computer solutions for the tension crack positions under different groundwater conditions (Sector IV)	254
98. Design section 5D1-1' and computer solutions for the tension crack positions under different groundwater conditions (Sector V)	255
99. Design section 5D2-2' and computer solutions for the tension crack positions under different groundwater conditions (Sector V)	256
100. Stability analysis of highwall slopes constructed in blasted material with dragline load	261
101. Analyses of safe bench width and combined effects of dragline and fault systems on the stability of slopes oriented E-W (Sector VIII and IX)	265

Figure

Page

102. Stereoprojections and sections showing the basic elements of wedge problem	267
103. Plan and section views of wedge problem and most critical wedge occurrences along highwalls at design sector VIII	271



LIST OF PLATES

Plate

- 1 Geological map of Eskihişar coal strip mine
- 2 Geological map of Eskihişar coal strip mine
and its vicinity
- 3 Documentation and groundwater table contour
map
- 4 Geological cross sections

CHAPTER 1

INTRODUCTION

1.1. Purpose and Scope

The cost of oil has increased substantially over the last decade. As a result, electric power generated from oil and gas has placed other alternative means of power. Accordingly, increasing emphasis is now being placed on the use of coal to generate electricity. In many of the countries, like Turkey, major economic pressures are developing subsequently to explore these deposits for the generation of power. These include a number of large lignite deposits which are being developed by strip mining methods.

In order to minimize the cost of power and to maximize the economy of mining it is essential to control the rock mass stability as mining operations progress. In order to maintain the continuity of the production design engineers should evaluate the stability of slopes, and in particular the stability of highwalls in strip mine projects.

Since the commencement of mining in the strip coal mine at Eskihisar (Yatağan-Muğla), where thermal coal is being produced for Turkish Electricity Authority's power generating plant, some stability problems have been faced both in working benches and in permanent slopes. As mining of strips advanced southwards, instability appeared to be more serious due to the movements of the slopes adjacent to the state highway running parallel to the pit boundary. This situation increased the importance of a successful re-design of pit slope based on detailed geotechnical considerations.

The purpose of this investigation is to study the geological and structural features of the pit and its close vicinity; to determine the geomechanical parameters and geotechnical properties associated with both the intact rock material and discontinuities which govern the stability of slopes; to assess the general hydrogeological characteristics of the pit area for stability considerations; to identify the mechanisms and modes of instability by monitoring slope movements and by carrying out back analyses of old and monitored slope failures; to predict rock mass strength of weak and blasted highwall material utilizing empirical criterion for analyzing mass failures; to assess kinematically possible failure modes involving structural discontinuities in different design sections; and finally, to conduct stability analyses based on deterministic approach for the safe slope design with the consideration of operational constraints and of the possible advantages of remedial measures.

The investigations were conducted in four stages. In the first stage extensive literature survey and the desk study which included collection of previous data and reports written for the site vicinity and published literature on strip coal mines and related stability considerations were carried out.

The second stage of investigations included the field work which started in June 1989 and continued until the end of November 1989. However, in 1990, previous field work was also supported by short-term studies conducted in the pit for the purposes of additional data collection and monitoring. During this period, large scale geological and documetation maps were constructed; the scan-line surveys carried out along pitwall faces and discontinuity parameters from 59 scanline stations were entered in data sheets; the long-term monitoring using optical prisms was conducted at two unstable locations in the pit and observations were

performed in previously failed slopes to assess the failure mechanisms. Besides, nine fully cored boreholes were drilled down to the base of the coal seam and then each borehole was geotechnically logged. Groundwater data were obtained from the available boreholes and blastholes, and from the standpipe piezometer installed in a geotechnical borehole. Schmidt hammer tests were also carried out in the field on undulating bedding surfaces to assess their shear strength parameters. Undisturbed block samples and borehole cores were taken from each of the major lithologies and discontinuity surfaces.

The third stage of investigations involved an extensive laboratory testing. Uniaxial and triaxial tests were carried out on samples prepared from existing cores. Index properties of soils and rock units, such as unit weight, water content, Atterberg limits, grain size distribution and slake durability index were also determined. Multiple-reversal shear box tests were performed both on soil materials and discontinuity surfaces to determine their shear strength parameters. Finally, rock mass strength was assessed by employing empirical failure criterion in conjunction with rock mass classification.

The fourth stage of studies involved detailed stability analyses for safe slope design. Several failures, using the information gained from the monitoring and observations, have been back-analysed to assess the failure mechanisms and the results obtained were compared with the laboratory derived shear strength parameters. Pit slopes, grouped into nine design sectors, were analysed to assess kinematically possible failure modes involving structural discontinuities. Finally, design of pit slopes within safety and economical limits stability of highwalls, working benches and permanent slopes were analysed by utilizing two-dimensional limit equilibrium methods based on the deterministic approach.

Different computer programs have been developed by the author for stability calculations of several failure modes and for determination of the rock mass strength using the empirical criterion proposed by Hoek and Brown (1988). IBM 4331 type of main frame computer has been used during analyses.

1.2. Location and Accessibilty

The study area, Eskihisar strip coal mine, is located 8 km west of Yatağan (Figure 1). The area, covered by 1:25000 scale topographic map of Aydın-N20-a4 sheet, is about 36 km to Muğla and 32 km to Milas and surrounded by hills from west, northeast and south. The site is accessible throughout the year through asphalt paved Yatağan - Milas state highway, which follows the southern boundary of the pitwalls.

The closest settlement to the site area is Eskihisar village where ancient ruins called "Straenikea" were located. The village had been evacuated due to mining operations. It is now under the protection of the Ministry of Tourism. Other settlements include Şahinler and the town of Yatağan at the east, Bağcılar village and town of Turgut at the north and Yeni Eskihisar village at the southwest. The roads connecting Yatağan to Şahinler, Turgut and to Yeni Eskihisar are asphalt paved, whereas between Eskihisar and Bağcılar, the road is unpaved.

Boundaries of the study area were determined in accordance with the direction of advance of the pit to the west and to the north, locations of the state highway and spoil pile areas, and the permanent slopes planned in the corridor between Eskihisar and Bağcılar. In this manner, it was aimed to investigate the stability problems of the existing pit and the future excavation areas. For this purpose, the area of detailed study is decided on the

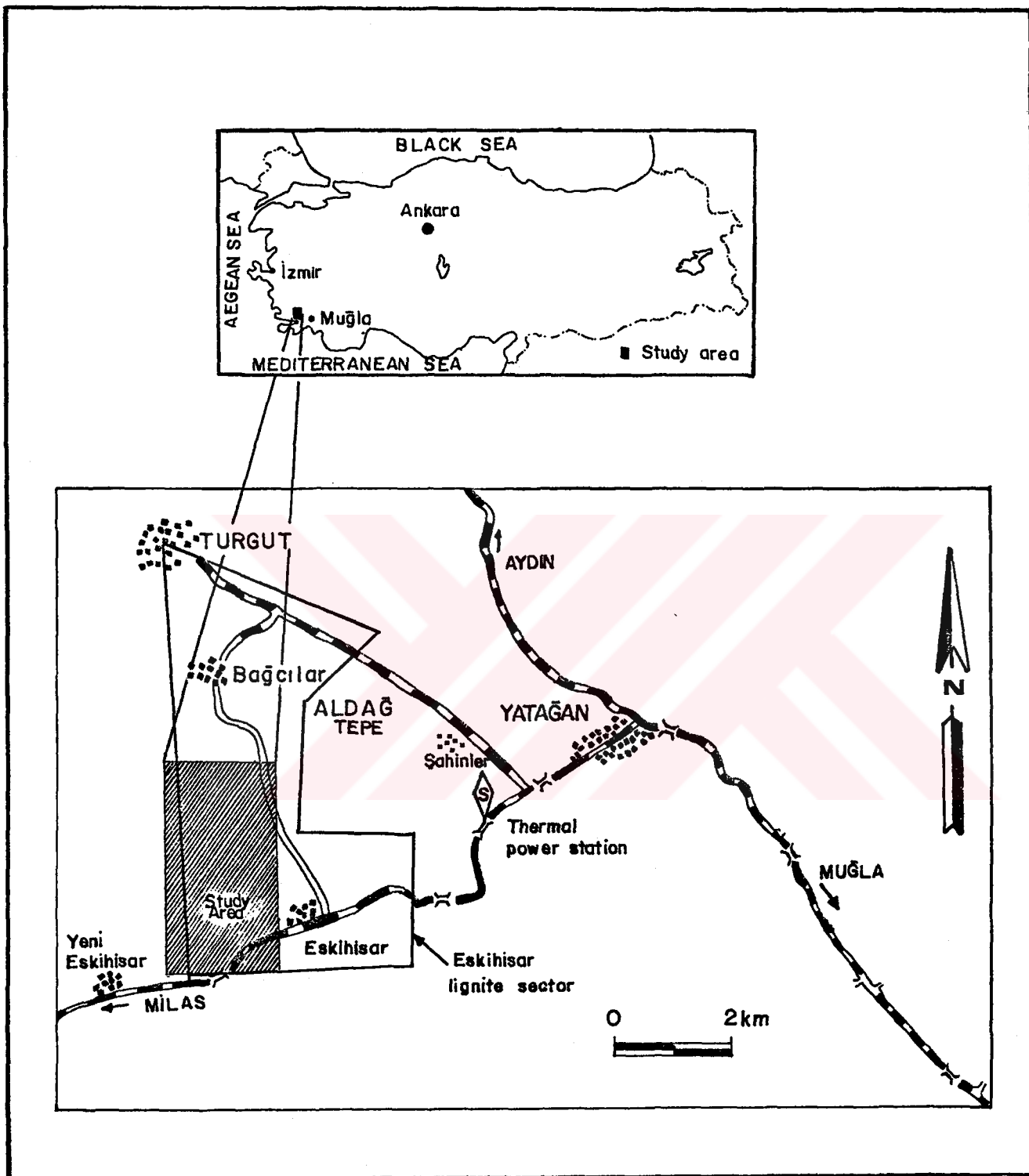


Figure 1: Location map of the study area.

basis of 1:2000 scale production plan covering the existing pit and its vicinity.

1.3. Previous Investigations

Previous investigations at the study area were performed for the purposes of general geological interests and evaluation of lignite potential. The majority of the geological studies were conducted as regional investigations around Muğla including Yatağan and its vicinity.

The earliest geological investigation at the study area was performed by Abdüsselamoğlu in 1965. He prepared a geological map at 1:100.000 scale involving Yatağan and its vicinity. He suggested that the basement rocks, consisting of micaschist, calcschist and marble at Eskihisar area, probably belong to Paleozoic(?) and Mesozoic(?), respectively. Neogene deposits of continental facies were differentiated as conglomerate, sandstone, clay and lacustrine limestone.

Platen and Bering (1966) constructed a geological map at the scale of 1:33000 between Eskihisar and Turgut. In this study two types of deposits, as river and lake deposits, were distinguished. They were the first to differentiate the detritic facies of lake deposits which crop out along the basin margins. This unit was described as conglomeratic travertines.

First detailed investigation involving geology and biostratigraphy of the area was conducted by Becker-Platen (1970) in Muğla and Denizli regions. According to his study, Neogene in Eskihisar area consists of three formations as Yatağan formation (fluviatic), Sekköy formation (fluviatic) and Turgut formation (limnic-fluviatic). He also claimed that the detritic facies of Sekköy formation along the basin margins was represented by conglomeratic travertines,

laterally grading into the main lake sediments. Moreover, he recognized thin and local transition zone deposits between Yatağan and Sekköy formations.

Yücelay (1970) studied the stratigraphy, tectonics and lignite potential of the Neogene deposits within the corridor lying between Eskihisar and Bağcılar. He distinguished the boundary between the basement rocks and Neogene deposits. He proposed the stratigraphical sequence in three major sections as : (1) fluviatic deposits (equivalent of Turgut formation), (2) lake deposits (equivalent of Sekköy formation), and (3) fluviatic deposits (equivalent of Yatağan formation). He also distinguished the crystallized sandy limestones and conglomerates along the basin margins from the lake deposits and claimed that the faults, which were active prior to Neogene, have formed the basin which is then filled with Neogene deposits.

Atalay (1980) studied the Neogene stratigraphy of Muğla, Yatağan and Milas. He argued that two formations named as Eskihisar and Yatağan were recognized in the study area and both were formed from river and lake deposits. In this study the fossils identified suggested that the Sekköy and Turgut members of Eskihisar formation belong to Middle Astracian and Late Astracian, respectively.

Denizli and Muğla Neogene sequences were investigated by Gökçen (1982) in terms of their litho-chrono-stratigraphy and ostracoda biostratigraphy. In conclusion it was understood that although the lower marine parts of Neogene can easily be correlated with the Tethys province by ostracodas, the upper continental facies has some similarities, but a sound correlation among continental fauna seems difficult.

The first coal exploration in Eskihisar coalfield was carried out by Engin (1965) as a general prospecting study.

This study was followed and extended by Benda (1967). Three boreholes were drilled to investigate the position of coal seam. Benda estimated that coal reserves were 20 to 40 million tons in Eskihişar area. He also pointed out that the locations of the state highway and the historical ruins in Eskihişar village would cause some problems and restrictions during future mining operations.

The detailed studies aimed to explore the lignite potential in the corridor between Eskihişar and Bağcılar were conducted by M.T.A. geologists under the management of Gökmen (1975). In this study, a large area between Eskihişar and Turgut was mapped at the scale of 1:10000, totally 170 boreholes were drilled, and Neogene deposits were distinguished according to their lithological differences. Gökmen also indicated that the approximate minable thickness of coal seam ranged between 15 m and 20 m.

Has, et al. (1975) estimated the coal reserves based on the information obtained from detailed studies conducted by Gökmen (1975). According to their reserve estimations based on the methods of polygon and isopach, extractable coal reserves through open pit mining was 106.159.000 tons.

Demirok (1978), based on the available geological information re-evaluated the reserve estimations for prefeasibility studies.

Position and extend of the coal seam at the western and northeastern parts of the current open pit, where excavation has not been started yet, were examined by a M.T.A. team (Kasap and Ünal, 1987 a and b), through a total of 41 boreholes, which were not fully cored. The study pointed out that the coal seam gets thinner and the dips of individual layers increase towards the basin margins.

Two hydrogeological studies were performed in the vicinity of Yatağan and Eskihisar coalfield. Ersoy (1957) investigated the irrigation water potential of the alluviums of the Eskihisar stream.

Canik (1975) tried to determine the hydrogeological parameters of the lithological units, such as hydraulic conductivity, transmissivity and coefficient of storage, through pumping tests around Eskihisar village. He concluded that the coal seam is permeable only in zones where lignite was fractured. The marls overlying coal seam contain some groundwater. He also suggested that sudden inflows were not anticipated from the deposits overlain by the coal seam.

The only investigation involving rock mechanics tests at the Eskihisar coal strip mine was carried out by Paşamehmetoğlu, et al. (1988). This study was performed to investigate the diggability, rippability and blastability characteristics of lignite and compact marl in the overburden. For this purpose, uniaxial and triaxial compressive strengths, elastic constants, unit weight, hardness, tensile strength and slake durability index of the samples were determined. Diggability and rippability classification, equipment selection and cost analysis, based on the experimental results, were introduced.

CHAPTER 2

PHYSIOGRAPHY

2.1. Topography and Drainage

General topographical characteristics of the study area are still distinguishable in spite of the excavations performed and spoil piles created as consequences of continuous mining operations. The study area is located within a depression starting from northwest of Yatağan extending in the southwest direction toward Muğla. The area is connected with the main depression at the east and the northwest through a passageway and a corridor, respectively. Consequently, the study area is developed in the form of an "L" shaped basin.

A large part of the site vicinity is characterized by undulations and flood plains. Average elevation ranges between 400 m and 450 m. Elevations exceeding 800 m along the basin margin are uncommon. The prominent hills of the site vicinity include Aldağ (776 m.), Yeldeğirmen (635 m.), and Hürlek (804 m.) (Figure 2).

In the study area the typical drainage pattern is dentritic. Most streams are intermittent and flow only after heavy rains. The main streams of the basin include Deliömer, Ömeroğlu, Kenker, Sirtlan and Sarıçay (Figure 2). In the scarpland areas, after readjustment to the structure, the streams follows main faults (Plates 1, 2). In this system consequent streams cut at right angles all the cuesta scarps of the resistant basement rocks and form shallow "V" shaped channels.

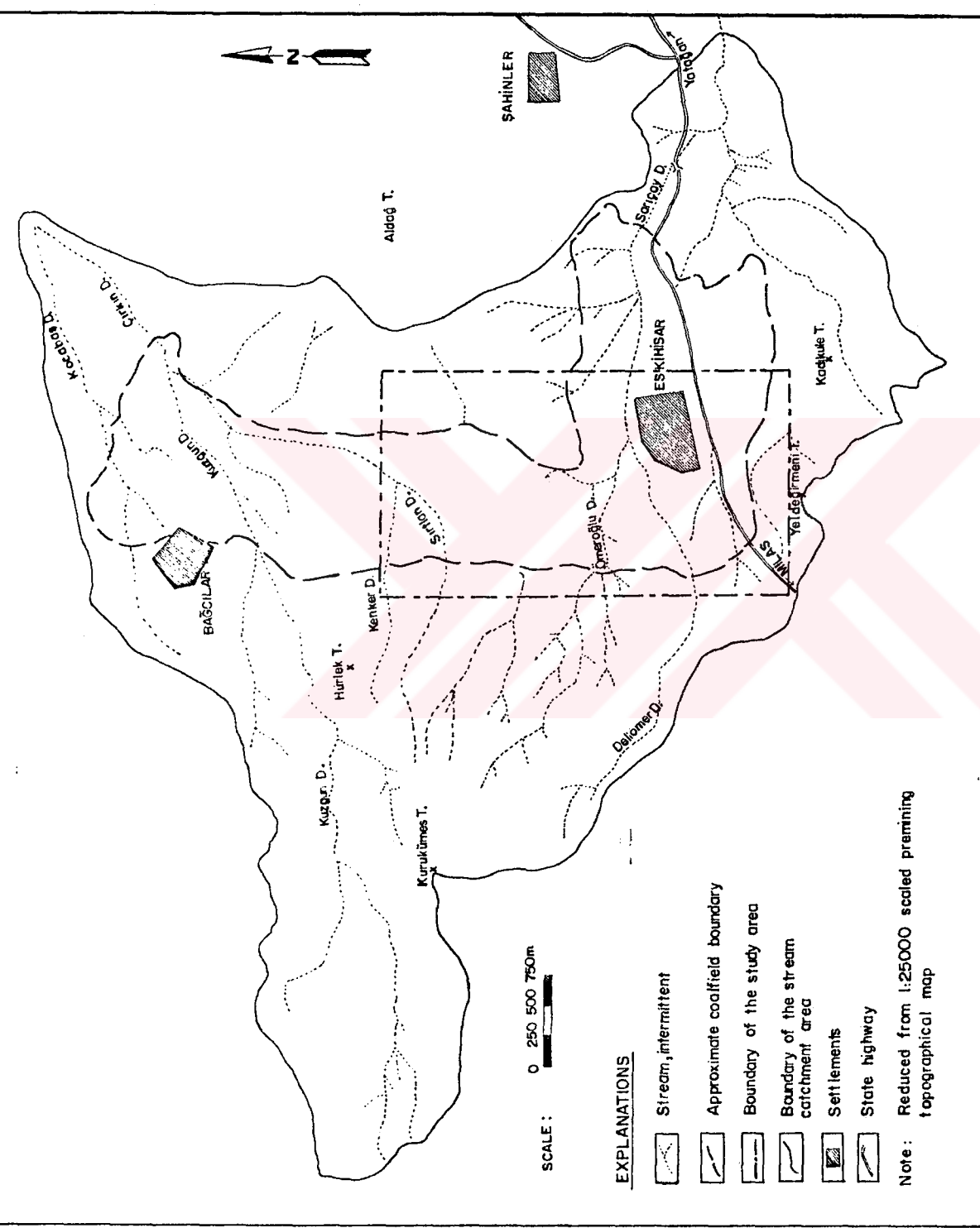


Figure 2: Drainage pattern of the study area and its vicinity.

2.2. Climate and Vegetation

The climatic characteristics of Mediterranean Region, hot and dry summers and warm and rainy winters, prevail throughout the study area. The precipitation is in the form of rain. Meteorological station at Yatağan is the only station closest to the pit. The precipitation records for the period 1971-1981 are evaluated in the form of average monthly precipitation histogram (Figure 3). The highest precipitation occurs during winter and spring and the lowest during July and August.

The study area is poorly vegetated. Only the hills surrounding the depression are covered by lemons and pine forests. The plains, where mining operations have not been extended yet, are used for agricultural purposes.

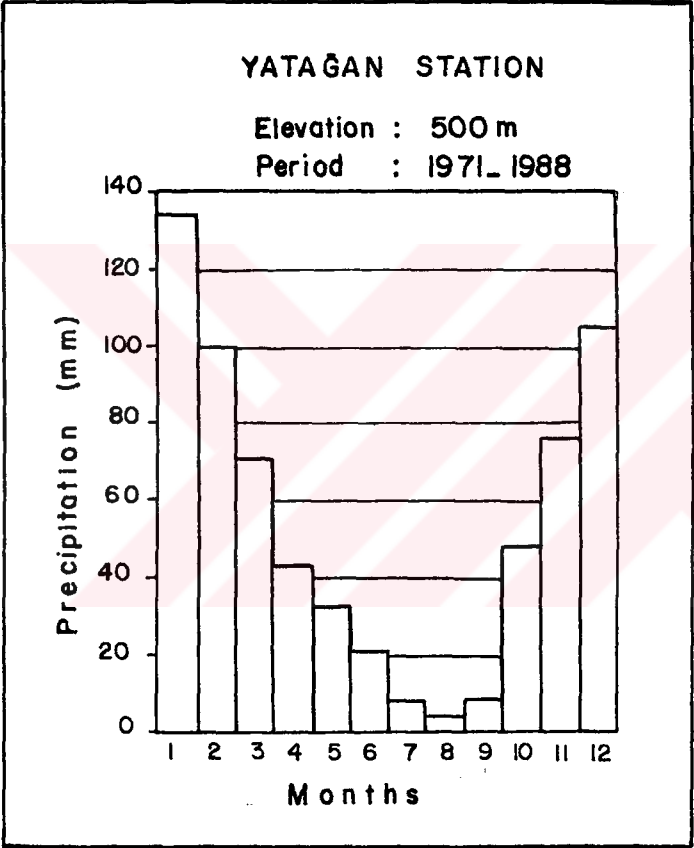


Figure 3: Average monthly precipitation histogram.

CHAPTER 3

CURRENT MINING PRACTICE

The Eskihişar coal mine (Figure 4) operated by Turkish Coal Enterprises (TKİ) produces thermal coal for 3x210 MW Yatağan Power Station of Turkish Electricity Authority (TEK). The mine has been operating since 1984 and produced approximately 3.5 million tons of lower calorific value coal annually. The stripping ratio in the present pit is 4.34:1.

The Eskihişar coalfield contains only one coal seam which is flat, tabular and relatively uniform in thickness. Besides, the overburden thickness is relatively small and thus the coal was planned to be exploited by strip mining technique. Standart dragline stripping methods are employed to uncover the coal in Eskihişar open pit. A single dragline, Marion M8050-36 with a 99 m boom and 50 m³ bucket, is scheduled to remove about 20-25 m overburden above the coal seam. Dragline operates from the top of highwall and works the overburden on its own level. The overburden material excavated is dumped into the void created by the previous strip. The stripping sequence consists of "key cut" removal and then final cut is stripped. Typical range of dragline with plan view and section of a single coal seam stripping operated in Eskihişar open pit are illustrated in Figure 5. A bulldozer assists in preparation of the dragline's tub seat, levelling the roll, pulling electrical cables and other miscellaneous operations as required.

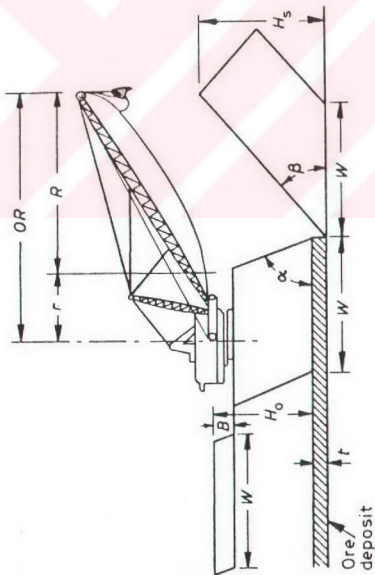
To minimize handling costs highwalls are made as steep as practicable, with angles of slopes ranging between 55° to 70°. The inner spoil piles, in which local failures occurred during the period of site investigation, are constructed of their angle of repose, viz. 30°-35°. The height of the spoil piles ranges between 20 to 30 m.



BM: Basin margin **DA:** Dam **DR:** Dragline **HW:** Highway **OD:** Outside dump **SP:** Spoil pile
YE: Yeni Eskihisar Village

Figure 4: General view of the Eskihisar strip coal mine and stripping operation (View to S; Plate 3-Photo. No.1).

(A)



OR, operational radius; R, reach factor; r, position factor; W, pit width; B, advanced bench height; H_o , overburden depth; H_d , maximum dump height; H_s , spoil height; α , highwall angle; β , spoil angle; and t , ore bed thickness

(B)

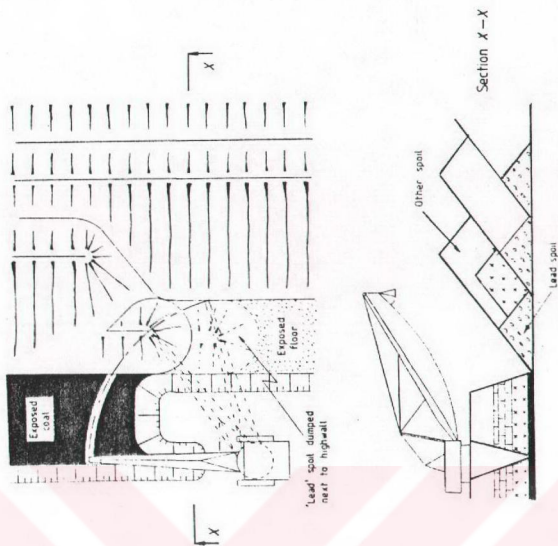


Figure 5: Working principles of dragline at Eskihsar open pit : (A) typical range of dragline (after Chugh, 1980); (B) stripping of dragline on a single coal seam (after Walton and Atkinson, 1978).

Highwalls and advance (working) benches are oriented roughly north-south, in widths of 80 m and a length of about 1200 m and advancing to the west (Figure 6). But, this direction is thought to be reoriented east-west at the northern part of the actual pit, Börükçüdüzü location, where the depth of overburden decreases and the basin becomes narrower.

Permanent slopes involving several benches are planned to be constructed parallel to basin margins in the west and east and adjacent to the highway. Instabilities, noted in Figure 6 and Plate 1 indicate that certain areas of the pit, especially slopes adjacent to the highway, are susceptible to failures.

Geometry of advance benches are variable with angles ranging between 60° to 70° and heights from 10 to 12 m. Material rehandled from advance-bench stripping, which is carried out by 15 yd³ PH2100 excavators, is transported by CAT 777 trucks with a 85 short tons capacity, to the outside dump areas adjacent to Milas-Yatağan highway (Figure 6).

Coal is mined by two electrically operated PH 1900 excavators with a bucket capacity of 10 yd³ and then transported from the pit to screening plant of the power station by Terex 34-11 C trucks having 150 short tons capacity.

Three Reedrill machines with a maximum drilling capacity of 30 m are used for blasthole drills. Vertical holes, 9 inch in diameter and approximately on 10 m x 10 m grid, are drilled and the overburden is loosened by means of technical ammonium nitrate. The shock caused by blasting is not violent.

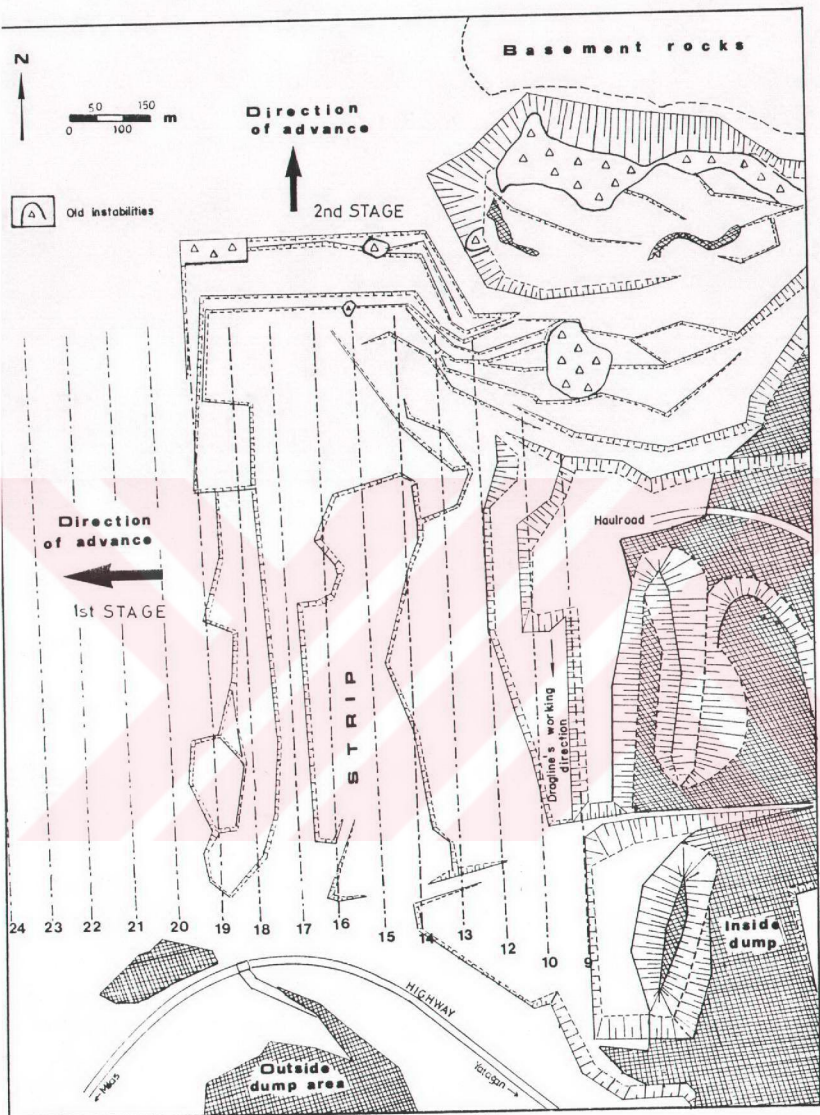


Figure 6: Layout plan of the Eskihisar strip coal mine.

The position of the haulroad was planned so as to cut over the coal reserves at the narrowest extent of the pit, but was governed by the location of the screening plant of the power station.

CHAPTER 4

SITE GEOLOGY

The geological investigations are carried out within the area shown in Plates 1 and 2. Detailed geological investigations of the region for solving basic geological problems have not been aimed in this study. Special emphasis was placed on the actual pit and its close vicinity where mining will advance in the near future. However, information gained from the early regional geological studies were also utilized for the evaluation of local geology and for the interpretation of major structures.

At this stage of the investigation, geological mapping was carried out to confirm lithological boundaries and principal discontinuity systems. 65 lump samples collected from different locations, where visual lithological description is difficult and/or suspicious, have been petrographically analysed in M.T.A. Laboratories. The locations of these samples are shown in Plate 3 and the results of petrographical and mineralogical analyses are summarized in Table A.1 of Appendix A.

The overall rock and soil colour is difficult to quantify and unaided assessments can be very misleading. Therefore, Munsell Colour Charts of Geological Society of America (1963) were used throughout the study to avoid subjective colour descriptions

4.1. Geological Mapping

The geological maps of the site vicinity prepared by previous investigators (Abdüsselamoğlu, 1965; Platen and

Bering, 1966; Becker-Platen, 1970; Yücelay, 1970; Gökmen, 1975) are small scaled and do not include details required for geotechnical investigation. Additionally the formations and/or lithologies have also been identified and described in a rather broad manner. Thus a new geological map of the site area given in Plates 1 and 2 has been prepared by the author to suit the requirements of the study.

Geological mapping of the site vicinity was conducted in two stages. In the initial stage, the geological map of the existing pit at the scale of 1:2000 was prepared (Plate 1). For this purpose the open pit production plan prepared by TKİ in August, 1989 was utilized. The second stage required a more general geological field mapping at the scale of 1:5000 (Plate 2) of an area covering the pit and its vicinity.

Premining aerial photographs were also utilized to obtain an overall impression of the geological condition and to clarify some uncertainties encountered at the basin margins which are covered by dense vegetation. Lateral continuity of the major structural features such as faults recognized in the pit, were also determined through the use of previously prepared borehole logs (Gökmen, 1975; Kasap and Ünal, 1987 a, b).

On 1:2000 scale geological map, directional data of bedding and joints are noted in closely spaced form to reflect the variations in their orientation in different localities. Besides, considering the important role played by the faults on the stability of slopes, all primary and subordinate faults are also indicated on the same map.

4.2. Stratigraphy

The Paleozoic(?) schists and Mesozoic(?) marbles constitute the basement rocks of the area. These are unconformably overlain by Neogene deposits, comprising Turgut, Sekköy and Yatağan formations (Figure 7). Descriptions of these units are given in the following sections.

4.2.1. Basement Rocks

The basement rocks surrounding the study area are represented by schists and marbles. Description of these units are summarized in the following sections.

4.2.1.1. Schists

The oldest rocks of the study area include schists of Paleozoic(?) age (Yücelay, 1970; Gökmen, 1975; Atalay, 1980). They crop out only in the valleys and along the ridges at the south of the state highway (Plate 1) and form the southern extension of the Menderes Massif (Yücelay, 1970). Generally similar colour tones, such as 'dark gray-N4', 'greenish black-5GY 2/1' and 'grayish olive green-5GY 3/2' are differentiated by use of Munsell Rock Color Chart.

Based on the petrographic identification of the samples collected from outcrops and boreholes, the rock is named as micaschist, which is rich in biotite and occasionally possesses characteristics of a calcschist. The thickness of the rock is unknown. Schistosity is well developed in NE-SW direction. Marble bands are uncommon. Schist and marble transition is also recognized in borehole JT9. Due to this and the presence of dense vegetation the boundary between the two is not quite clear (Plates 1 and 2).

4.2.1.2. Marbles

The dominant basement rock surrounding the basin is marble. The best outcrops of this rock are observed along the hills in the northeast of Aldağ, in the west of Kurukümes and Hürlek, and along the ridge in the southwest of the highway. In spite of some uncertainties, an age of Mesozoic(?) has been assigned to this rock unit (Abdüsselamoğlu, 1965; Becker-Platen, 1970; Yücelay, 1970; Atalay, 1980). The thickness of marbles is not known.

White (N9) and occasionally light gray (N7) marbles are coarse crystallized, strong and massive. However, at the rock exposures close to the surface, the rock is occasionally easily crumbled in the form of sugar crystals due to weathering. The other distinguishable property of the rock is that it produces bad smell when struck by hammer. Thus, the rock is named as "dolomitic marble" by Ersoy (1957). Based on petrographic identifications the rock has been named as "marble", "quartz-serisite marble" and "micromerocrystalline limestone".

Joint systems in the rock mass are distinct and can be observed clearly in the quarry situated at the west-central hills of the basin (Figure 8). No karstic features have been detected on exposures. However, in some of the boreholes, JT1 and JT5, small and partially calcite filled solution cavities have been observed.

It is rather difficult to distinguish the boundary between the marbles and the limestones of Sekköy formation due to their similar surface expressions and dense vegetation cover. However, the marbles show distinct crystalline texture and produce smell when broken. The darker tones produce by marble outcrops on the aerial



Figure 8: View of a marble quarry located at the west of existing pit (Photo. No.2).

photographs were also helpful in distinguishing the boundary between the two units. In this manner, boundary of the two rock units is drawn more accurately than those of the earlier prepared maps.

4.2.2. Neogene Deposits

The Neogene deposits are confined to a depression extending approximately in the NW-SE direction from Çine to Muğla. Some of the previous investigators (Becker-Platen, 1970; Atalay, 1980; Gökçen, 1982; Göktaş, 1989) included the Neogene deposits within the Muğla group and distinguished various formations. At the site vicinity three formations were distinguished. From oldest to youngest, these are Turgut (Tmt:Limnic-fluviatile deposits), Sekköy (Tms: Limnic deposits containing coal), and Yatağan (Tmy:Alluvial fan deposits) formations.

4.2.2.1. Turgut Formation

The formation is named after Turgut town where best exposures are observed. It transgressively overlies the basement rocks. At the site area only the upper levels of the formation are exposed.

The formation is very dark gray (5Y 3/1), dark gray (2.5Y 4/1), black (5Y 2.5 5/1) and olive gray (5Y 4/2). It consists of thin bedded plastic clay, moderately dense clayey silts containing thin coal seams at its uppermost levels. Locally medium dense sand lenses and fine gravel alternations may also be observed.

Black, highly plastic clay of 5 to 10 cm thick is first noted by the author at some unstable benches in Ertrans section (Figure 9) and within several boreholes drilled in the southern part of the pit. The clay is mostly situated very close to the basement rocks and due to transgressive overlapping along basin margins its thickness ranges between 5 cm to 20 cm.

At the lower levels, the sequence grades through fine grains into quartz, gravels and coarse clastic elements (Becker-Platen, 1970; Gökmen, 1975). At locations where the thickness of the sequence decreases, fragments of the basement rocks are also noted. The light coloured mica flakes (muscovite) observed in dispersed form are the most distinguishing feature of the sequence.

Based on the borehole data, thickness of the formation ranges between 0.2 m and 5 m in locations very close to the basin margins. Gökmen (1975) reported that the thickness is more than 180 m at the northeast of Bağcılar. Based on the fossil determinations an age of Middle Miocene was assigned to this formation (Atalay, 1980).

4.2.2.2. Sekköy Formation

The formation starts with a coal seam and continues with the main Sekköy formation (Tms), the detrital facies at the basin margins (Tms¹) and the transition zone deposits (Tms²). This subdivision is based on the observations of the author as well as the findings of previous investigators including Platen and Bering (1966), Becker-Platen (1970), Yücelay (1970), Gökmen (1975) and Göktaş (1989). The age of the formation is Middle Miocene (Becker-Platen, 1970; Atalay, 1980).



Figure 9: A view of the black clay, closely located to basin margins and a plane failure developed along the clay (NE of Ertrans section; Plate 3-Photo. No.3).

4.2.2.2.1. Coal Seam

The coal seam corresponds to the base of Sekköy formation and conformably overlies the Turgut formation. It can only be observed in slices (strips) when the overburden is removed.

The type of the coal is lignite with a low calorific value. It is very dark brown (10YR 2/2) and strong in its original state and starts to crumble and turns to black when it loses its moisture. The coal seam is overlain by compact marls of the main Sekköy formation. The boundary between the two is distinct (Figure 10). At its lower boundary, alternations of thinly bedded clays and clayey silts with coal traces are common. There is only one coal seam. However, it is rarely possible to encounter thin coal seams up to 1 m thick below the main coal seam as identified in the boreholes JT2 and JT3.

The coal mined is classified as "ksiolite lignite" and "board lignite (woody lignite)" according to the coal classification systems of Duparque and Francis, respectively (Gökmen, 1975).

The coal shows distinct bedding and joint sets. The thickness of the coal ranges between 15 m and 20 m in the central part of the Neogene basin, but its thickness decreases towards the basin margins. The position and the extend of the coal seam in different directions are shown in cross sections given in Plate 4.

Based on the Mollusca fossils an age of Middle Miocene was assigned to the coal seam (Atalay, 1980).



Figure 10: The coal seam and its distinct upper boundary (South of Üzdemirler section; Plate 3-Photo. No. 4).

4.2.2.2.2. Main Sekkōy Formation (Tms)

This sequence forms the largest part of the Sekkōy formation and extends from south to north within the Eskihisar-Bağcılar corridor (Plates 1 and 2). It is well observed in the pit and occasionally crops out in the stream beds.

The sequence conformably overlies the coal seam. At the bottom, it is composed of grayish olive (10Y 4/2) and light olive (10Y 5/4), medium to thick bedded compact marls (Figure 11). The marls occasionally contain very small lignite fragments close to the coal boundary. Locally claystone and silstone layers ranging between 1 to 10 cm were recognized in some boreholes and on the pitwalls. Towards middle, compact marls grade into thinly laminated marls of the same colour. Towards top, the sequence grades into an alternation of moderately hard clayey limestone, poorly consolidated claystone and marl beds of thickness ranging between a few centimeters to 20 cm (Figure 12). This working benches at higher elevations in the west and in unexcavated area (Plate 1). Pale greenish yellow (10Y 8/2) and pale olive (10Y 6/2) clayey limestones contain Gastropoda fossils. Based on the thin section studies, the rock is classified as a "micritic clayey limestone" containing cryptocrystalline calcite minerals ranging between 70 to 90%. The marls are mostly thinly laminated. Due to variations of the clay and carbonate contents transition between marls and limestones is very common. Light olive gray (5Y 6/2) and olive brown (2.5Y 4/4) claystones are evaluated as clays in engineering sense. They soften and possess highly plastic characteristics particularly when they come into contact with water.

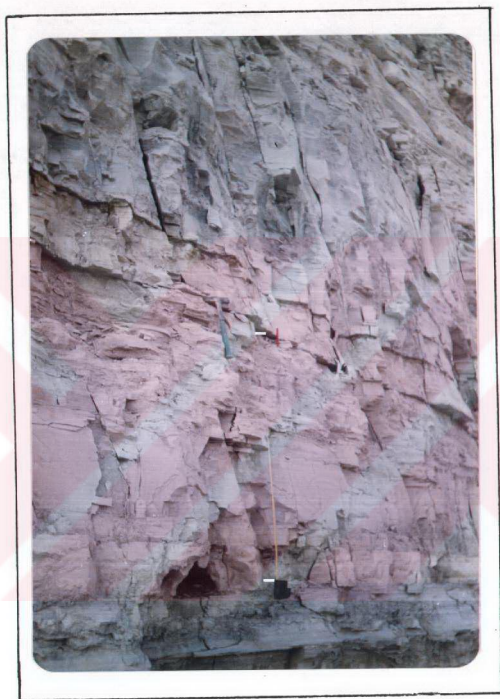


Figure 11: A view of the medium to thick bedded compact marls in main Sekkőy formation (Length of tape: 1.25 m; Plate 3-Photo. No. 5).

In the uppermost levels of this alternation, in Özdemirler section and in the working benches farther west, locally deposited micritic limestone nodules and moderate yellowish brown (10YR 5/4) sandy limestones (Figure 12) are recognized. The sandy limestones are deposited in the form of lenses, pockets and locally extended beds of varying thicknesses. They are generally very hard and locally very weak and can be crumbled by hand. Petrographical analyses indicate that fragments of micritic limestone and other rocks are embedded within a matrix of small calcite crystals.

Small scaled local foldings due to the plastic behaviour of the lithologies and raveling are common (Figure 13). The thickness of the whole sequence ranges between 5 to 90 m. (Gökmen, 1975).

4.2.2.2.3. Detrital Facies of Sekköy Formation (Tms¹)

Sekköy formation is represented by a detrital facies along the slopes formed by basement rocks (Plate 2). This facies was described in a different manner by previous investigators as travertine and slope debris (Platen and Bering, 1966), conglomeratic travertines being transited with Sekköy beds (Becker-Platen, 1970), conglomerates and sandy limestones of pre-Neogene overlapping the marbles (Yücelay, 1970), and conglomerates and sandy limestones of Yatağan formation (Gökmen, 1975). Based on the stratigraphical relations with other formations and correlations between the previously drilled boreholes at the basin margins this facies is included within the Sekköy formation as its detrital facies. Besides, this argument is also confirmed by the studies of Göktaş (1989) who is presently studying the stratigraphy and sedimentology of the Neogene basins in Muğla and Denizli region.

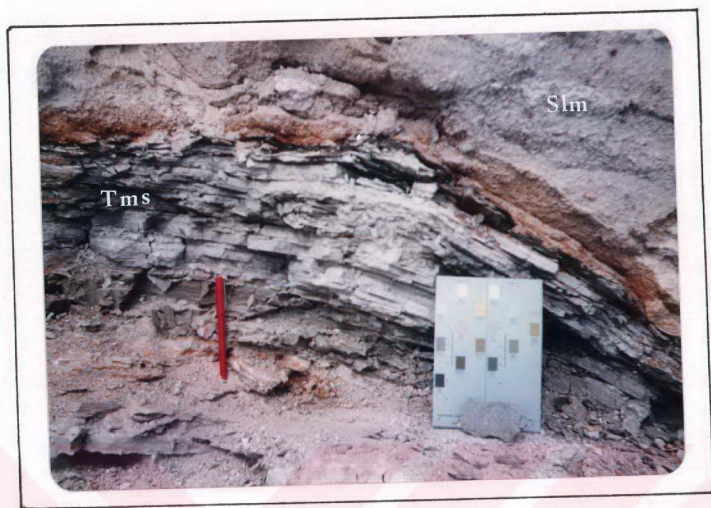


Figure 12: Alternation of thinly bedded limestone, claystone and marl in the upper levels of main Sekköy formation (Tms) and sandy limestone pocket (Slm) (Scale: Rock colour chart and pen; Özdemirler section; Plate 3-Photo. No.6).

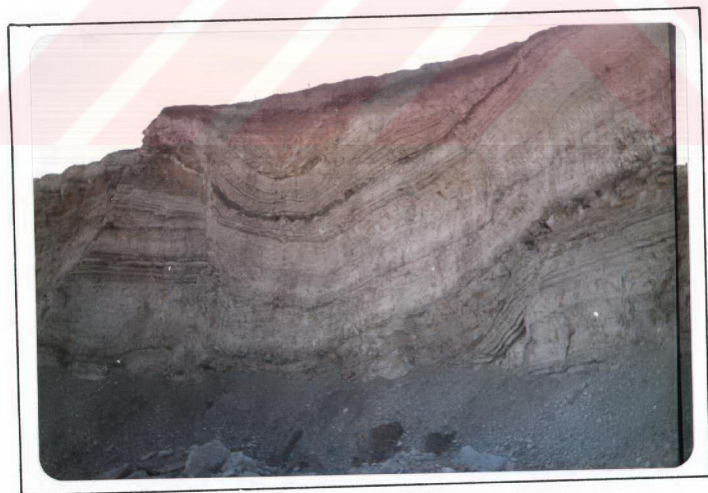


Figure 13: A view of local folding and raveling developed in the uppermost alternating sequence of main Sekköy formation (Plate 3-Photo. No.7).

This facies transgressively overlapping the basement rocks, and laterally transitional to the main Sekköy formation (Plate 4 - Sections I, IV, V, VI). This stratigraphical relation is well observed along the Deliömer stream. The best outcrops are observed in the northern part of energy supply building and along the highway cuts.

At the lower levels, the sequence is composed of very light gray (N8), yellowish gray (5Y 7/2) and pale yellowish orange (10YR 8/6), well cemented, generally hard conglomerates. The rock contains angular and subrounded fragments of micritic limestone, marble and fewer schists in a calcareous matrix. As observed in the cores of borehole JTS, very small solution cavities can be recognized. The cementing material is weaker in the northeast Ertrans section. The upper levels are composed of micritic limestones containing microfossils. Bedding in limestones is more distinct than in conglomerates.

Göktaş (1989) argued that this facies is the detrital product of the tectonic activities associated with the margins of Eskihisar-Bağcılar depression resulting from graben tectonism initiated in early Miocene. The maximum thickness of the sequence is determined as 60 m (Yücelay, 1970).

4.2.2.2.4. Transition Zone Deposits (Tms²)

The presence of a transition zone was first reported by Becker-Platen (1970). He pointed out that a thin transition due to mixed deposition, in some locations between Yatağan and main Sekköy formations, can be observed. Based on the similarities of clays and colour tones identified in both the main Sekköy formation and in this zone, stratigraphic

relations and differences in colour from the typical tile colour of Yatağan formation reflecting the effects of paleooxidation (Göktaş, 1989), the zone is first included in the Sekköy formation and named by the author.

The transition zone is mainly composed of olive gray (5Y 5/2), poorly consolidated claystone and clayey and sandy siltstone alternations and occasional medium dense sand lenses and/or pockets. The sequence contains light coloured mica flakes. The dominant type of deposit in the sequence is claystone.

A very thin and poor quality coal seam of thickness ranging between 0.5 m to 1 m comfortably lies at the bottom of the zone. This bed can be used as a marker to distinguish the boundary between the transition zone and the main Sekköy formation (Figure 14).

Based on the measurements carried out in borehole JT9, in previous boreholes and the faces of pitwalls, the thickness of the zone ranges between 20 m to 25 m.

4.2.2.3. Yatağan Formation

The best outcrops of this formation are observed around Yeni Eskihisar village. The formation extends in the NE-SW direction at the southern boundary of the actual pit (Plates 1 and 2). Becker-Platen (1970), Yücelay (1970) and Atalay (1980) described the formation and reported that the deposits of the sequence represent a fluvial environment. However, Göktaş (1989) argues that they are originally alluvial fan deposits. Yatağan formation (Figure 15) comfortably overlies the transition zone and detrital facies at the basin margins.

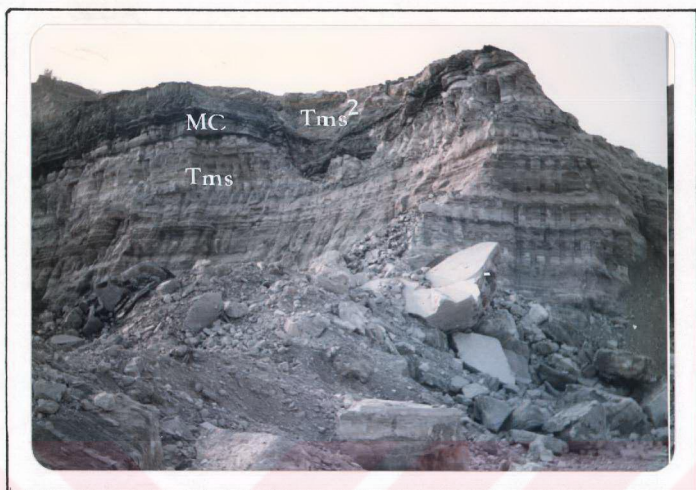


Figure 14: A view from the transition zone deposits (Tms²) and the thin marker coal seam (MC) lying on the main Sekköy formation (Tms) (South of 17th slice; Plate 3-Photo. No.8).



Figure 15: A view from a stable bench (18 m high) constructed in massive sandstone of Yatağan formation (Plate 3-Photo. No.9).

The most distinguishable feature of the formation is its moderate yellowish brown (10YR 5/4), light brown (5YR 5/6) and dark yellowish orange (10YR 6/6) colour tones. The formation is mainly represented by sandstones (Figure 15). Based on the thin section studies calcite, plagioclase, biotite and volcanic rock fragments are embedded within a calcareous matrix. The rock is classified as "calcareenite". It is generally massive and moderately strong. At shallow depths, however, it is weaker due to weathering. Bedding is rather difficult to recognize and jointing is indistinct.

Orange, moderately cemented and poorly graded conglomerates containing limestone, marble and fewer schist fragments and blocks of different dimensions may be observed at the upper levels. They occur in the forms of lenses, banks and channel fillings. The gravels are angular close to the basin margins (north slope of Deliömer Stream) and rounded elsewhere. The maximum thickness of conglomerates is 2 m.

Sandstones occasionally include tuffite intercalations. This material is the deposition product of ashes transported by wind from Bodrum Peninsula where a volcanic activity had been initiated during late Middle Miocene (Ercan, et al, 1984; Göktaş, 1989). Tuffites are composed of fragments of volcanic rocks, idiomorphic micas cemented with volcanic glass and partly transformed into carbonates and clay minerals.

The deposits representing the Yatağan formation in the study area is equivalent of the Bayır member of Atalay (1980) and Göktaş (1989). Based on the information gained from the previous borehole logs, the maximum thickness of the formation is approximately 50 m. Based on the paleontological determinations an age of Late Miocene was assigned to this formation (Atalay, 1980).

4.3 Structural Geology

Considering the important role of discontinuities on the stability of slopes, the structural features of the study area were investigated through systematic surveys. The scanline method, discussed in detail in Chapter 5, was employed for measuring the orientations of discontinuities on pitwalls, outcrops and in stream beds. The data were then evaluated in terms of rose diagrams employing a computer program named EAPR developed by the Geological Engineering Department of Hacettepe University. The structural geology of the site are discussed under five headings as faults, joints, bedding, schistosity and unconformities. Physical and mechanical properties of the discontinuities are discussed in detail in Chapter 5.

4.3.1. Faults

The region including site vicinity gained its structural skeleton through Neogene (Gökmen, 1975). Thus based on the previous studies (Becker-Platen, 1970; Yücelay, 1970; Gökmen 1975) and observations performed by the author the faults were categorized into two groups as pre-Neogene faults and Neogene faults.

4.3.1.1. Pre-Neogene Faults

Yücelay (1970), Gökmen (1975) and recently Göktaş (1989) argued that the tectonic activities at the site were controlled by the graben tectonism. They also pointed out that the lateral boundary between the basement rocks and the Neogene deposits corresponds to the boundary of a graben as well. Steep slopes identified on the wall-like contact at

the northeast of the pit may be evaluated as an indicator of this boundary (Figure 16).

Previous investigators (Yücelay, 1970; Gökmen, 1975) described two concealed major faults striking N-S and dipping east and west along the basin margins. Gökmen (1975) also reported that these faults, formed in pre-Neogene, also continued their activity during Neogene and caused the formation of a depression filled by Neogene deposits. His approach was based on only a limited number of boreholes drilled in locations adjacent to the basin margins. Both site investigations as well as aerial photo interpretations conducted by the author yielded no sound evidences for the existence of these faults. Gradual increase of the dips of Neogene deposits towards the basement margins may be attributed to a fault controlled basin. Considering the present position and extent of the coal seam, which normally thins out towards the basin margins, there is no justification for the existence of alleged faults indicated on the previous maps (Platen and Bering, 1966; Gökmen, 1975). However, near Beybağ, NE and outside of the study area, a distinct, steep and continuous break within the conglomerates was recognized. This surface may be considered as the probable extension of the fault. Thus, the probable faults pointed out by previous investigators are shown on the geological map (Plate 2) as concealed faults. Additional investigations, especially boreholes, are required to verify these faults.

4.3.1.2. Neogene Faults

Faults affecting the Neogene deposits and the coal seam are well observed in the open pit. However, it is rather difficult to identify the faults in unexcavated areas around the pit without the review of previous borehole logs. The

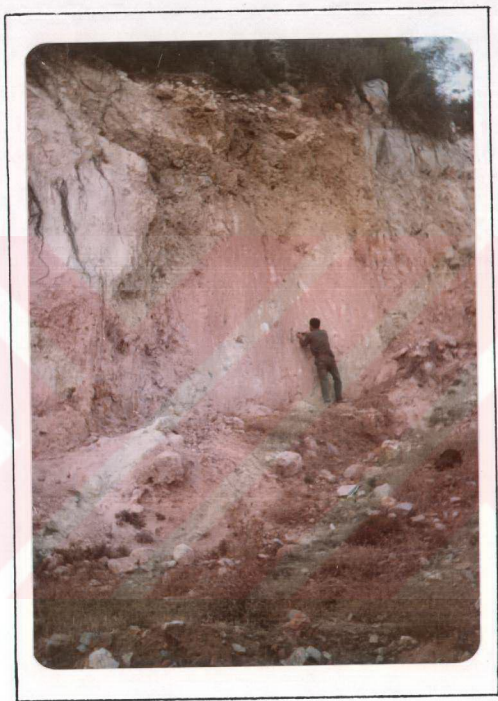


Figure 16: Probable graben boundary identified along the contact between the Neogene deposits and marbles at the south of Aldağ (Plate 3-Photo. No.10).

Neogene faults identified by surface investigations performed on the pitwalls, in stream beds and confirmed by core drilling are classified as: those having throws ranging between 0.4 m to 3 m and those having throws of 5 m or more. The latter are labeled from A through J (Plates 1 and 2) and are important from the mining operations point of view. On the other hand, faults, having throws ranging between 0.10 to 0.20 m are referred to as subordinate faults.

The normal faults identified in the study area dip 60° to 80° SE, NW or SW and strike NEE-SWW, NE-SW and NW-SE (Figure 17). Some fault sets show distinct parallelism and they are closely spaced. Some faults clearly affect the coal seam (Figure 18). Faults having throws ranging between 0.4 m and 3 m are dominant, although they may not be very significant from mining operations point of view. However, slope instabilities associated with such faults may clearly be observed.

The greatest fault is the one labeled as A. It strikes NE-SW and dips about 60° - 70° SE. It has a throw of approximately 60 m. The overburden bounded by this fault on the north is planned to be excavated without use of dragline. Other major faults located in the southern part of the pit adjacent to the highway have throws ranging between 5 to 10 m. Based on the correlations between boreholes and observed strikes of faults on pitwalls, it is believed that they converge in front of the highway bridge (Plate 1). This argument was also confirmed by TKİ's geophysical investigations on the faulted block (Koçak, et al., 1991). The faults (F to J) located at the western and northern parts of the pit may be recognized from their offsets on the pitwalls and from correlations between boreholes. The fault-J may be interpreted as an oblique fault due to its offset characteristics observed between the main Sekköy formation and its detrital facies in the NE.

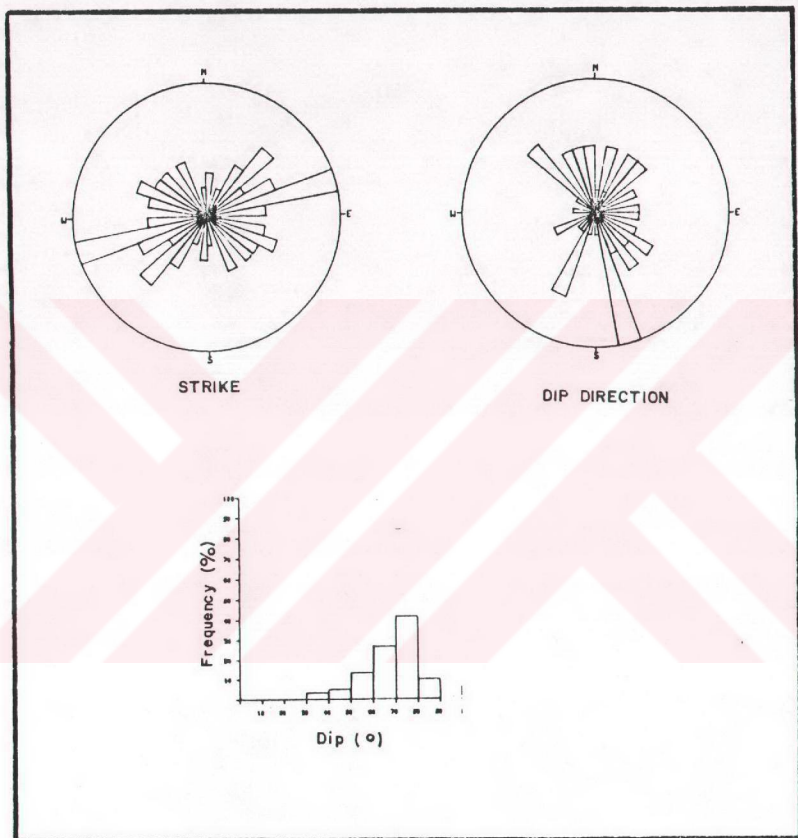


Figure 17: Rose diagrams and histogram analysis of fault measurements carried out in the site.



Figure 18: A normal fault affecting overburden and the coal seam at Ertrans section-approximate throw is 2 m (Plate 3-Photo. No.11).

The subordinate faults are almost all normal faults. Some normal faults having throws of a few centimeters are also observed in the upper sequence of the main Sekköy formation and in the Yatağan formation around Yeni Eskihişar village. They are mostly synsedimentary faults. Observations performed on the pitwalls and its close vicinity suggest that additional faults may be expected in the unexcavated parts of the pit as well.

4.3.2. Joints

In the study area the cross joints are well observed within the laminated and compact marls and clayey limestone of the main Sekköy formation, as well as in the coal seam. The joints are more continuous in marls and coal seam (Figure 19). In sandstones of Yatağan formation the joints are poorly developed.

Joints of moderate persistence developed parallel and/or subparallel to the faults observed in the Sekköy formation generally strike NE-SW and NW-SE. Excepting local deviations, there are three dominant joint sets dipping 80° - 90° NE and SW (Figure 20a). Their persistence is greater in compact marls and reach up to 8 m.

Reasonably well developed cross joints which strike essentially parallel to the joints developed in the Sekköy formation are also identified in the coal seam (Figure 20b). Although only a few measurements were taken, it may be stated that the joints developed in sandstone are discontinuous and show similar orientation to those developed in marls.

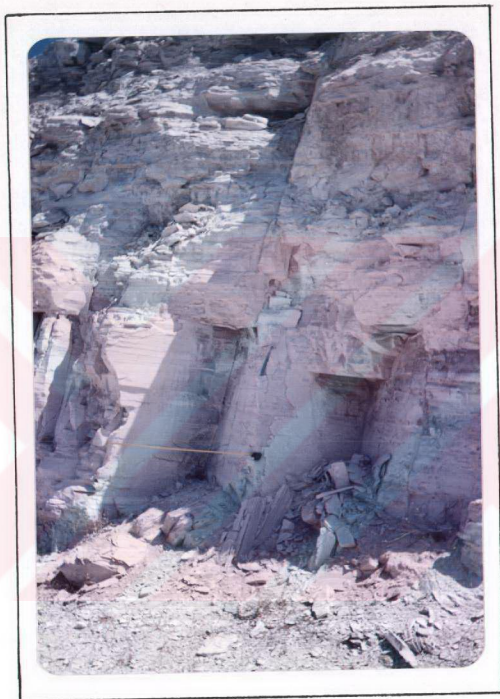
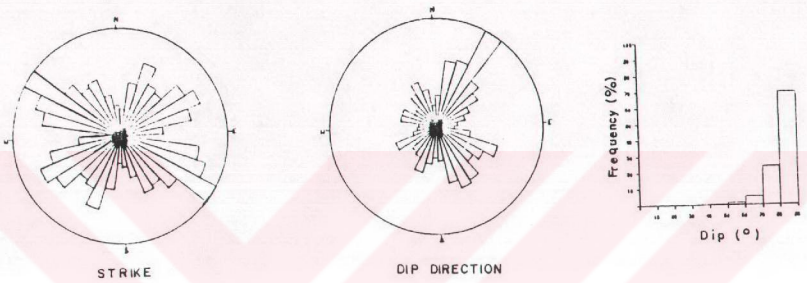


Figure 19: A view of a well - developed cross joints in the compact marl - length of tape: 1.2 m (Plate 3-Photo. No.12).

a) Joints measured in the Main Sekkoy Formation



b) Joints measured in the coal seam

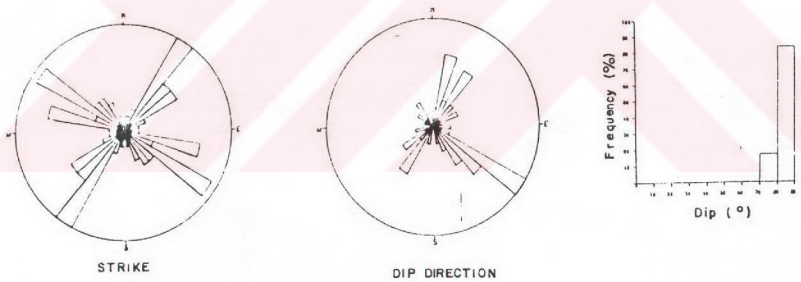


Figure 20: Rose diagrams and histogram analyses of joints measured from Eskihisar strip coal mine.

Sufficient orientation data could not be obtained from the limestone and conglomerate of the detrital facies along the basin margins due to their limited and small outcrops. No well-defined trends, however, were noted in the orientation of the joints.

4.3.3. Bedding

The orientation of bedding in Neogene deposits is closely related with the paleogeography of the depositional environment. At locations close to the basin margins orientation of bedding is controlled by the inclination of the surface of basement rocks. Thus, bedding orientations are evaluated by dividing the study area into the domains where orientations show similarities.

Beds in the southern part of the pit adjacent to basement rocks strike NW-SE and NE-SW and dip 10° to 30° towards excavation (Figure 21a). If the local deviations are ignored, bedding planes along the basin margins in both west and east strike approximately NS and dip between 15° to 25° to the east and west, respectively (Figure 21 b and c). However, dips occasionally increase upto 30° to 40° at basin margins where permanent slopes will be constructed.

Towards the center of the pit flat-lying or gently dipping strata are encountered. This area is evaluated in two domains as north and south, which is separated by an imaginary line passing through the boreholes I-97 and I-93. In the northern domain, beds generally strike NW-SE and NE-SW and dip about 3° - 10° into the pit excavation. Whereas in the south, beds strike NE-SW and dip 5° to 10° NW (Figure 21d). Bedding orientations identified in both north and south suggest the existence of a broad syncline whose axis is approximately parallel to the boundary line of these two

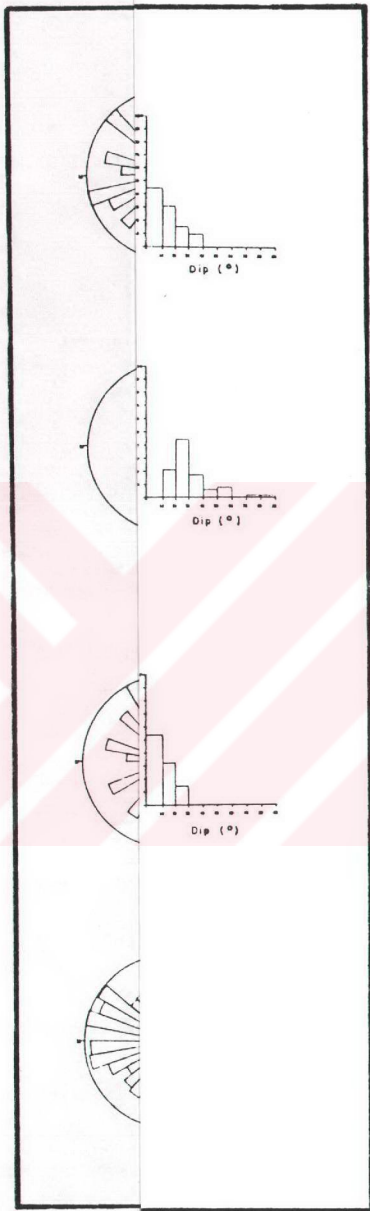


Figure 21

domains. On the basis of bedding orientation a similar local fold may also be recognized at the southern part of fault A (Figure 21e).

As material fails by sliding into the pit along bedding surfaces, like black clay in Figure 9, Ertrans section in NE is distinguished as another domain. Here the beds strike E-W and dip 30° or more towards south area (Figure 21f).

Based on the limited data obtained from the sandstones of the Yatağan formation, it is noted that the beds strike approximately E-W and gently dip towards south (Figure 21g).

The coal seam maintains the same bedding orientation with that of the overburden. Local undulations identified in the upper levels of the Sekköy formation do not occur in the coal seam. Measurements taken from the bedding surfaces of the borehole cores indicated that orientations determined in laminated and compact marls persist throughout the coal as well. The coal seam in Börükçüdüzü location occurs at shallow depths and the beds are generally flat-lying (Plates 1 and 4-Section II).

4.3.4. Schistosity

Measurements taken from the planes of schistosity around the outer spoil pile in the south indicated that the strike and dip of schistosity is generally NE-SW and 65° - 80° NW (Figure 22). Considerable variation in strike are not noted.

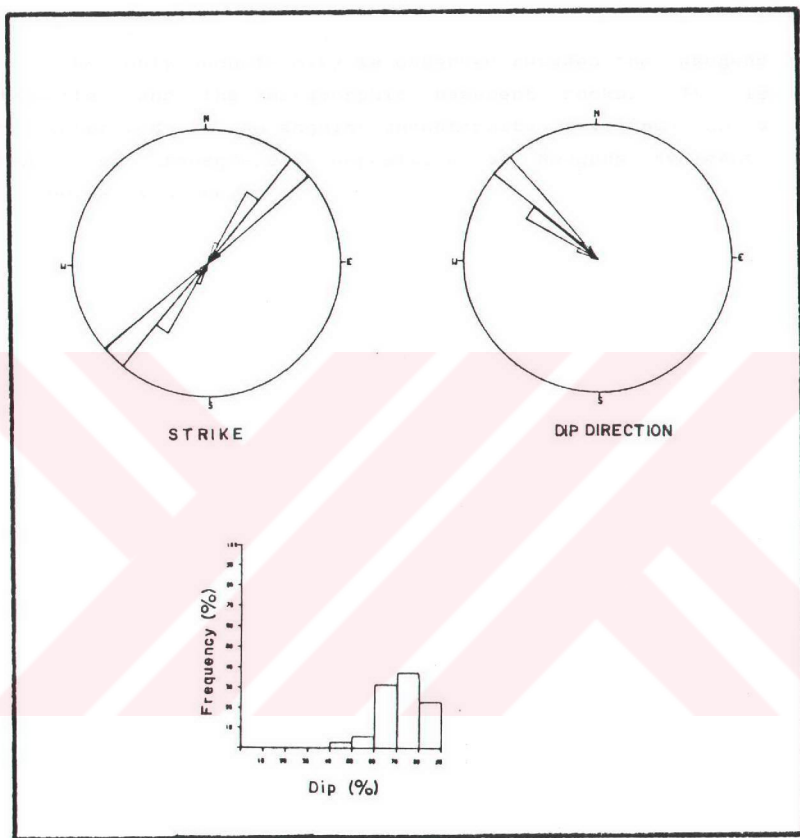


Figure 22: Rose diagrams and histogram analysis of schistosity planes.



Figure 23: View showing discontinuity survey conducted on compact marls and joint pattern developed in this rock unit (Plate 3-Photo No. 13).

Yatağan formation. In these units only limited number of discontinuities (mostly bedding planes) were measured.

Scanline surveys were performed at 59 stations by setting two nearly perpendicular lines in the N-S and E-W directions to avoid sampling bias. The length of each line is not maintained constant. Measurements of discontinuity parameters, such as orientation, aperture, infilling, surface roughness, and water conditions were carried out quantitatively or qualitatively in accordance with the procedures recommended by ISRM (1981). Besides, spacing and persistence of joints were also measured at 20 additional scanline stations where the length of line is fixed as 20 m.

5.1.1. Discontinuity Orientation

A total of 907 joint, 1307 bedding, 61 fault, and 35 schistosity orientation measurements were statistically analysed. Directional data were plotted using computer packages developed by Darton Software (1987) and Jeran and Mashey (1970) which produce output in the form of pole and contoured pole nets.

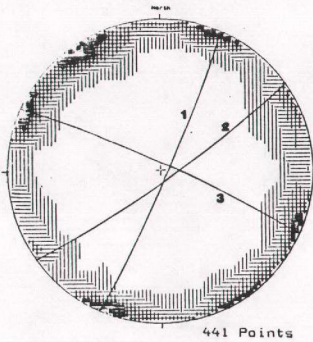
Directional data of bedding was evaluated for eleven domains. These domains were based on the observations of distinct bedding orientations in different areas and the directional relationships noted between the strikes of bedding and slopes.

A summary of the structural data is presented in Figures 24 through 26. Each figure shows the contoured pole plot and major sets identified for a specific type of discontinuity. Major sets of each discontinuity type, based on the peak concentrations are summarized in Table 1.

For the evaluation of joints the field measurements

(a) Joints measured in E-W direction

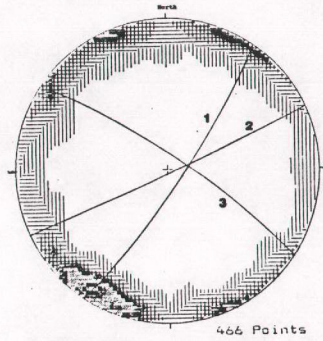
(b) Joints measured in N-S direction



LEGEND (for First 9 Intervals)

□ 1-1	□ 8-9	Contour Method: Schmidt (1928)
□ 2-2	□ 9-0	Counting Area: 0.010
□ 3-3	□ 0-0	Contour Interval: 10 Points per 1% Area
□ 4-4	□ 0-0	Maximum Contour: 10
□ 5-5	□ 0-0	

NOTE: Contour Patterns Repeat Every 9 Intervals.



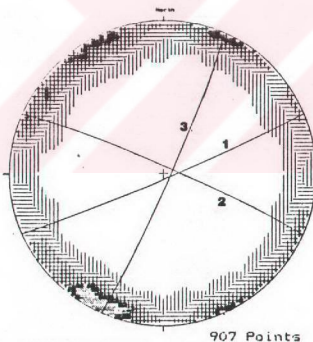
LEGEND (for First 9 Intervals)

□ 1-1	□ 6-7	Contour Method: Schmidt (1928)
□ 2-2	□ 7-8	Counting Area: 0.010
□ 3-3	□ 8-9	Contour Interval: 10 Points per 1% Area
□ 4-4	□ 9-0	Maximum Contour: 10
□ 5-5	□ 0-0	

NOTE: Contour Patterns Repeat Every 9 Intervals.

(c) All joints

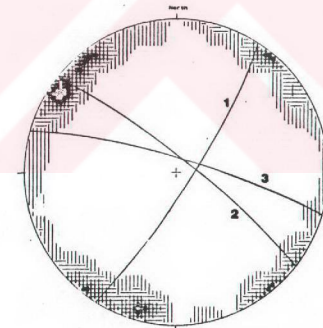
(d) Joints measured in the coal seam



LEGEND (for First 9 Intervals)

□ 1-1	□ 7-7	Contour Method: Schmidt (1928)
□ 2-2	□ 8-8	Counting Area: 0.010
□ 3-3	□ 9-9	Contour Interval: 10 Points per 1% Area
□ 4-4	□ 0-0	Maximum Contour: 7
□ 5-5	□ 0-0	

NOTE: Contour Patterns Repeat Every 9 Intervals.



LEGEND (for First 9 Intervals)

□ 1-1	□ 11-10	Contour Method: Schmidt (1928)
□ 2-2	□ 12-11	Counting Area: 0.010
□ 3-3	□ 13-12	Contour Interval: 20 Points per 1% Area
□ 4-4	□ 14-13	Maximum Contour: 10
□ 5-5	□ 15-14	

NOTE: Contour Patterns Repeat Every 9 Intervals.

Figure 24: Lower hemisphere Schmidt plots illustrating the joint orientations in the main Sekkōy formation and the coal seam.

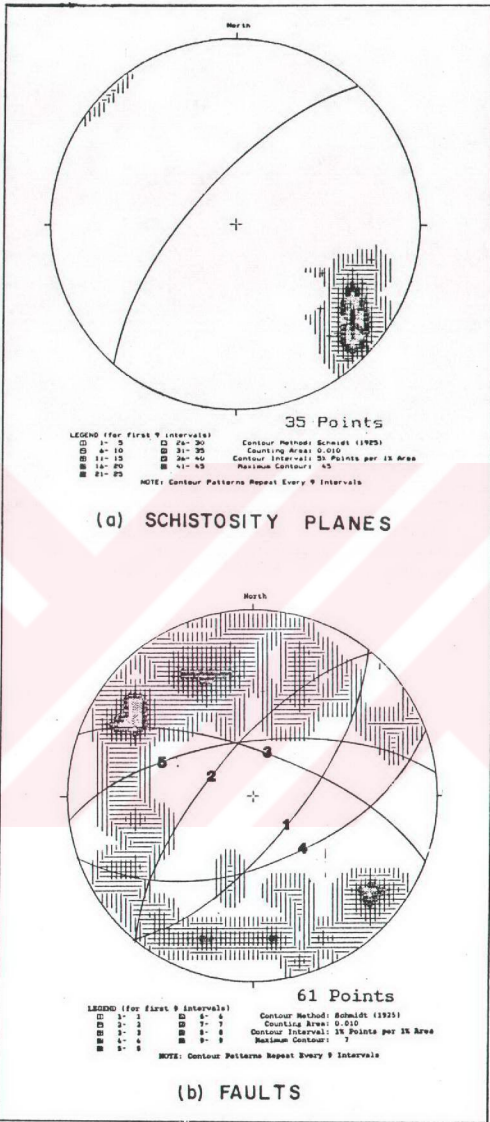


Figure 25: Lower hemisphere Schmidt plots illustrating the orientations of schistosity planes and faults in the study area.

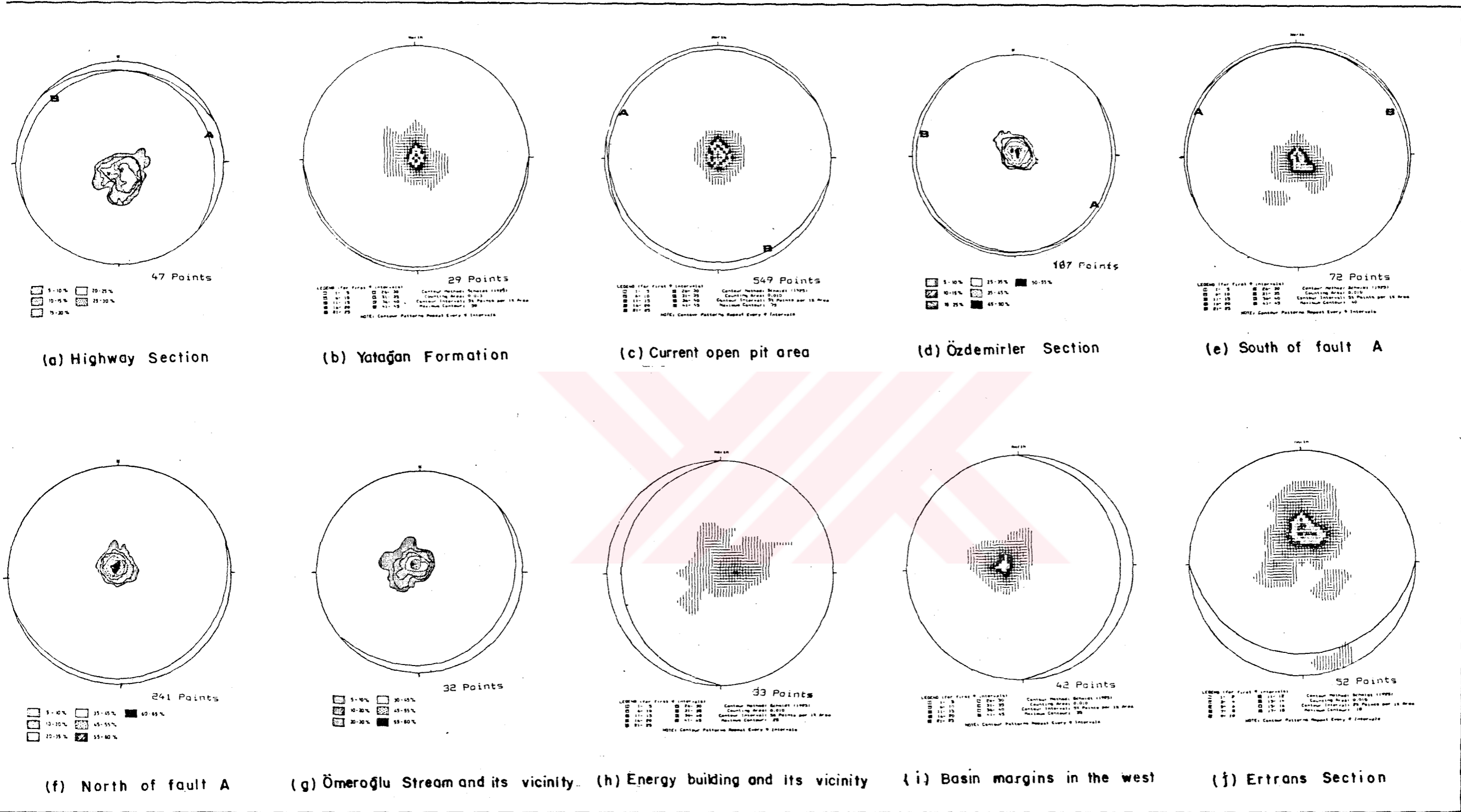


Figure 26: Lower hemisphere Schmidt plots of bedding surfaces in different sections of the study area.

Table 1 : Major discontinuity sets

Type of discontinuity	Figure No.	Data analysed	Major sets	
			Dip/Dip direction (deg)	Strike/Dip
Joints in Serikçi fa.	24a	E-W measurements	86/114 (1)	N24E/86SE
			94/146 (2)	N56E/84SE
			86/024 (3)	N66E/86NE
	24b	N-S measurements	82/125 (1)	N35E/82SE
			88/126 (2)	N66E/88SE
			82/034 (3)	N56W/82NE
24c	All	87/157 (1)	N67E/87SE	
Joints in the coal seam	24d	Pit only	86/024 (2)	N66W/86NE
			86/114 (3)	N24E/86SE
			82/123 (1)	N33E/82SW
			82/038 (2)	N52W/82NE
			82/015 (3)	N74W/82NE
Schistosity	25a	South of highway	71/312	N42E/71NW
Faults	25b	All	70/130 (1)	N40E/70SE
			70/310 (2)	N40E/70NW
			70/020 (3)	N70W/70NE
			55/160 (4)	N70W/55SE
			66/353 (5)	N83E/66NW
Bedding	26a	East of highway	12/040 (A)	N50W/12NE
	26b	West of highway Yatağan fa. (SW of the pit) Open pit:	12/340 (B) 03/130	N70E/12NW EW/3S
Bedding	26c	Southern section	05/332 (A)	N62E/5NW
	26c	Central section	03/190 (B)	N60W/9SW
	26d	Özdesirler section	05/144 (A) 04/234 (B)	N54E/5SE N54W/4SW
	26e	South of fault A	04/332 (A) 04/034 (B)	N62E/4NW N56W/4NE
	26f	North of fault A	06/162	N72E/6SE
	26g	Överoğlu stream and its vicinity	10/140	N50E/10SE
	26h	Energy supply building and its vicinity (lsth.,cong)	14/270	NS/14W
	26i	Basin margins (W) (lsth.,cong.)	12/094	N4E/12SE
	26j	Extrans section	21/181	N89W/21SW

lsth. : Limestone
congl : Conglomerate

Note : Numbers and letters in parantheses refer to great circles shown in Figures 24 through 26.

were divided into two groups, as measurements taken along N-S and E-W directions. Peak concentrations yielded very similar joint systems in both directions (see Figure 24a and b). As a next step all joint orientation data were plotted together (Figure 24 c). Statistical analyses indicated that major joint sets developed in the main Sekköy formation and in the coal seam show similarities in their orientation.

5.1.2. Aperture and Infilling

The thickness of infilling material and its composition are important factors in modifying the shear strength of the discontinuities. For example, if the thickness of the infilling material is greater than the amplitude of surface asperities, the shear strength of the discontinuity is controlled by the shear strength parameters of the infilling material. However, in the Eskihisar open pit the discontinuities generally lack infilling material with the exception of faults.

The bedding planes in the sequence of main Sekköy formation are generally closed features with apertures ranging between 0 to 0.5 mm. Besides, these surfaces are easily separated especially when they are exposed to air (Figure 27). It is possible that the stress relaxation caused by excavation may be responsible for the separation. Very thin coating composed of finest material is recognized along bedding surfaces.

The width of the fault zone ranges between 5 to 40 cm. Along the fault zone intense shearing is observed. The fault gouge (Figure 28) contains rock clasts in a matrix of greenish gray to olive clay of high plasticity. The rock clasts show a floating texture in which they are usually not in contact with each other.

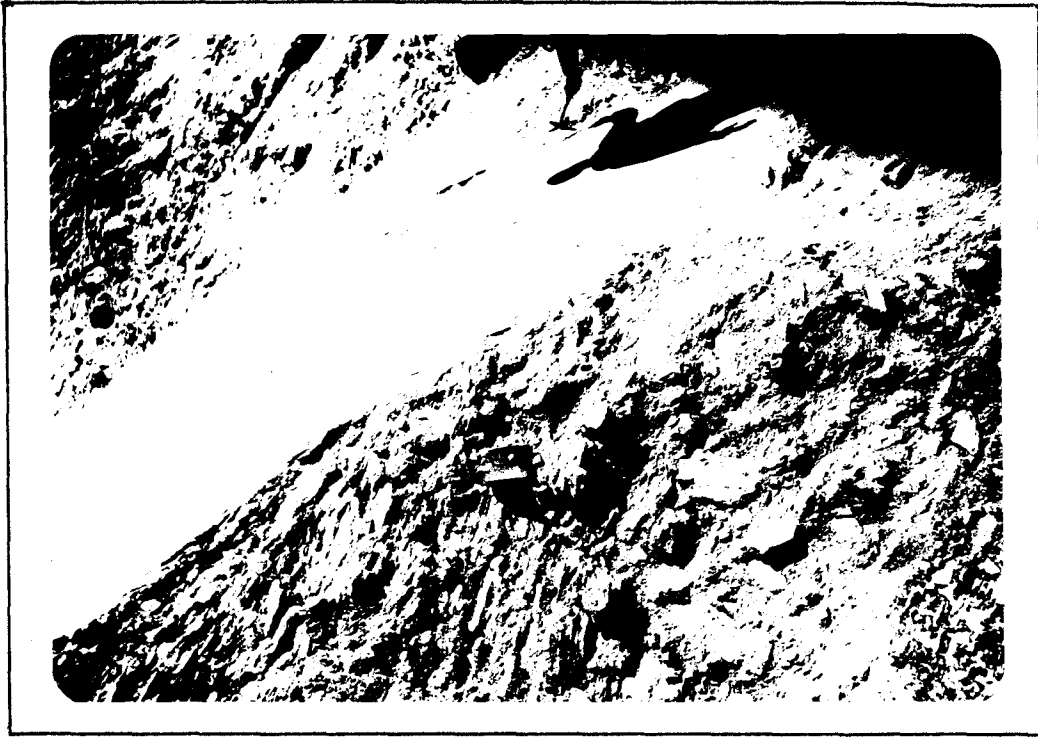


Figure 28: A view of a fault plane and the gouge material (Plate 3-Photo. No. 15).



Figure 27: Separation and local plane failure along the bedding surfaces in the main Sekkøy formation (Plate 3-Photo. No. 14).

The aperture of joints are similar to those of bedding. It ranges between 0.1 to 1 mm and rarely reaches up to 2 mm and contains clay and silt sized material. Limestones and conglomerates along the basin margins show relatively tight apertures along close bedding surfaces. In some places apertures less than 2 mm are filled with clay stained by limonite. Apertures of sandstone beds are generally very tight.

5.1.3. Asperities of Discontinuity Features

The surface asperities of unfilled discontinuities constitute an important component of the shear strength. Generally two different scales of discontinuity asperities are considered. These include roughness and waviness. In this study, these two parameters are quantitatively described. The descriptions are based on the surface roughness profiles provided by Barton and Choubey (1977).

Excepting the bedding surfaces of the detrital facies, all discontinuity surfaces are generally planar-smooth with joint roughness coefficient (JRC) of 2. Fault planes are planar and slickensided (see Figure 28). Bedding planes in limestone and conglomerate show smooth-undulating surfaces with average JRC value of 6.

5.1.4. Water Conditions on Discontinuity Surfaces

Discontinuity surfaces at the upper benches of the pit are normally dry. However, moisture appears when the surfaces are scraped by the geological hammer. Fault gouges are generally softened due to moisture. During field

investigation no seepage along the upper working benches were noted.

5.1.5. Spacing of Discontinuities

Spacing of bedding planes are determined from the borehole data since it is practically impossible to examine the entire pitwall faces. Therefore only the spacing of joints developed in the main Sekköy formation, which are easily sampled on the pitwalls, were systematically measured. Joint spacing in the coal seam is determined through limited data due to the difficulties caused by raveling on the coal faces. Considering the dimensions of the pit, additional scanline surveys at the 20 predetermined stations were conducted for spacing studies.

Şen and Kazı (1984) suggested that the amount of bias decreases as the length of the scanline increases. In the study area the optimum length is determined as 20 m. Thus, a steel tape with a minimum length of 20 m is stretched along the bench face and the joints that cross the tape are sampled. A total of 774 measurements were taken from 20 scanlines in the N-S and E-W directions (Plate 3).

Priest and Hudson (1976) noted that discontinuity intersection points may be evenly spaced, clustered, random or combination of these. Therefore, standard statistical theory was applied to determine the spacing distributions. In order to check different distribution patterns and get some statistical parameters, a computer program STATDIS, which includes most popular distribution patterns utilized in geology such as normal, gamma, log-normal and negative exponential, developed by Ayday (1989) was used. In the analyses closely spaced stations are grouped and evaluated separately.

For most of the scanline data comparison of the theoretical and real frequencies of exponential distribution show distributions resembling negatively exponential distribution with a 90% confidence level. There is also a close agreement between mean spacing and standard deviation which is one of the most important indication of negative exponential distribution. Discontinuity spacing histograms of groups C and E for the joints developed in the main Sekkőy formation are given in Figure 29. Statistical parameters obtained from the analyses are summarized in Table 2.

Analyses based on 21 joint data collected from the coal seam indicated no similarity between the observed and standard distribution for all types of patterns. It is thus concluded that additional data are needed for reliable results.

Generally in statistical spectrum there is a common problem in determining the variation of the observed distribution from the theoretical one Chi-square test can give an answer to this question. In addition, cross-correlation developed for comparison of two time series in statistics provides valuable geologic information (Davis, 1973). Sliding of these two series, in the studied series corresponds to real and theoretical frequencies of the given data, with respect to one another and correlation gives cross-correlation coefficients for different lags. At the end, similarity or nonsimilarity of observed data and negative exponential, log-normal and gamma distribution are decided. In addition to Chi-square tests, cross-correlation tests were also performed.

Above conclusions reached from the distribution models have also been supported by cross correlation tests between the real and the theoretical frequency distributions of discontinuity spacing values (Table 2).

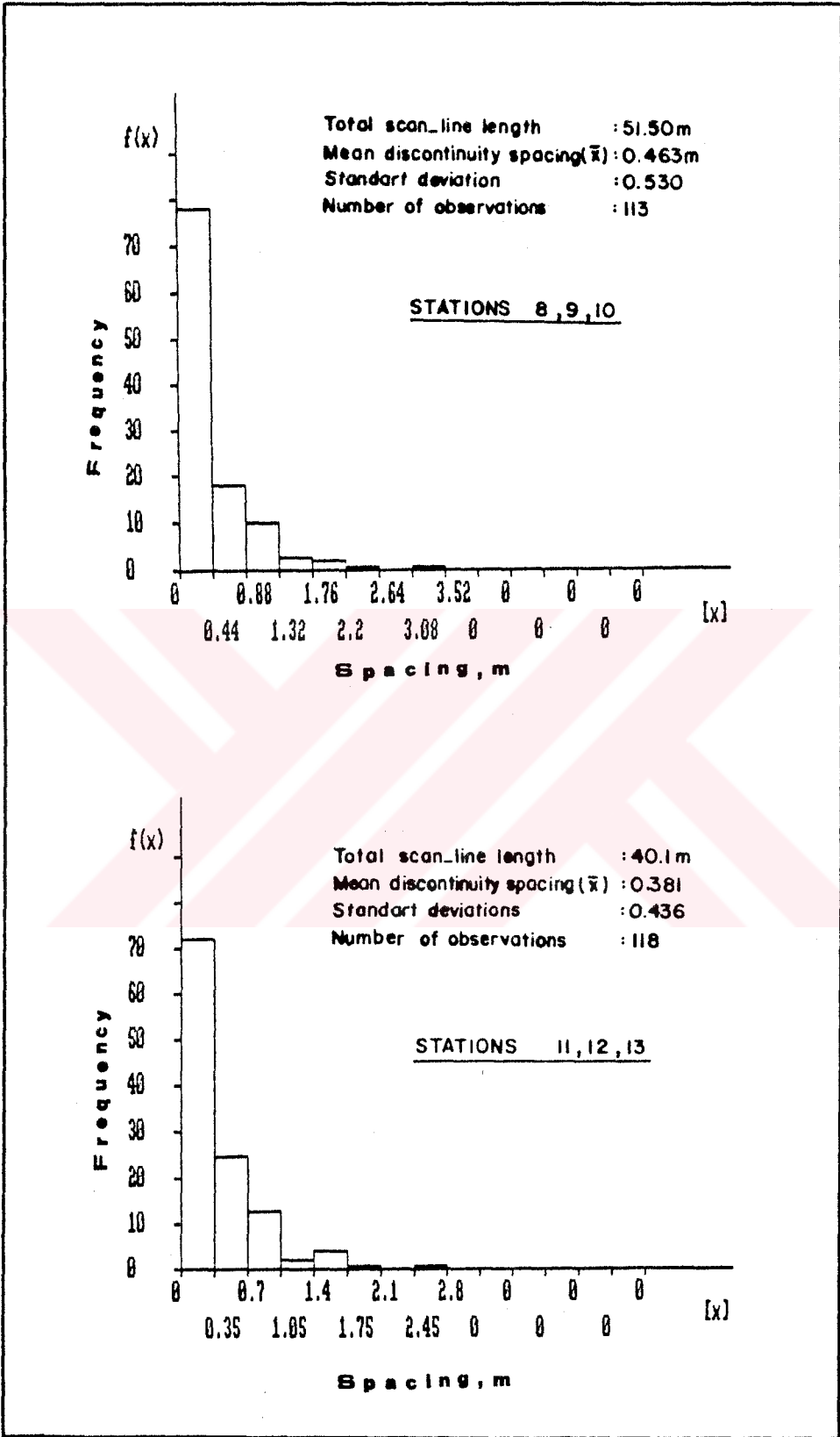


Figure 29: Discontinuity spacing histograms for the main Sekköy formation.

Table 2 : Analysis of joint spacing data and cross-correlation test results

No. of scanlines combined	Group symbol	Number of data	Mean Spacing \bar{X} (m)	SD	Number of joint (n-1)	Chi-square test*		Cross-correlation coefficient		
						Tabulated	Calculated	N.Exponential	Log-normal Gamma	
(a) 1,2,3	A	108	0.461	0.497	2.17	10.61	15.97	0.96	0.29	0.91
(a) 4,5,6,7	B	118	0.618	0.743	1.62	10.61	8.45	0.99	0.92	0.89
(a) 8,9,10	C	113	0.463	0.530	2.16	10.61	12.64	0.99	0.94	0.98
(a) 20	D	43	0.171	0.167	5.85	9.20	9.45	0.96	0.76	0.95
(b) 11,12,13	E	118	0.361	0.436	2.62	10.61	7.87	0.99	0.90	0.99
(b) 14,15,16	F	139	0.262	0.268	3.82	11.98	12.98	0.96	-0.12	0.99
(b) 17,18,19	G	114	0.351	0.290	2.85	10.61	8.16	0.96	0.09	0.97
(a) 20**	H	21	0.300	0.212	3.33	7.74	12.03	0.42	0.76	0.53

* Chi-square values are given only for negative exponential distribution.

** Scanline in the coal seam.

(a) Scanline setup in N-S direction.

(b) Scanline setup in E-W direction.

Cross-correlation coefficients of all scanlines, with the exception of the one performed in the coal seam, generally indicate similarity to negative exponential distribution. The same result is also obtained from the Chi-square tests as well.

Joint spacing distribution patterns determined in the study area confirm the results of Attewell and Farmer (1982). They have shown that weak rocks are more structurally prone to contain more random field of terminated discontinuities and if a rock is materially weak it should satisfy a negative exponential distribution with respect to its discontinuities. Priest and Hudson (1976) also suggests this distribution for homogeneous rock masses.

Mean joint spacing (x) and the average number of joints per meter (λ) of the main Sekköy formation are calculated as 0.386 m and 2.59 m^{-1} , respectively. The joints are classified as "moderately spaced joints" according to the classification proposed by ISRM (1981).

Spacing between bedding planes were assessed from borehole information. In the upper levels of the main Sekköy formation, bedding spacing ranges between a few millimeters to 20 cm. Whereas in compact marls overlying the coal, excepting occasionally laminated levels, spacing ranges between 0.3 to 1 m. Based on the observations in the borehole JT9, spacing of bedding in the sandstone is about 2 to 3 m or more.

5.1.6. Persistence of Discontinuities

In this study, statistical evaluation of joint persistence is performed in a similar way as with spacing. The results of statistical analysis suggest that persistence

data does not belong to a single distribution. Thus it is concluded that persistence of joints does not fit to any distribution. The persistence of the joints, both in the main Sekkøy formation and in the coal seam, ranges between 1 m to 5 m. However, in the central part of the pit the persistence value occasionally exceeds 5 meters (Figure 23).

In a sample of 774 joint measurements taken from the Eskihisar open pit, 149 (19%) with an average length of 1.43 m had both ends exposed, 522 (67.5%) with an average length of 2.3 m had one end exposed, and 103 (13.5 %) with an average length of 7.8 m had no ends exposed. This situation indicates that the majority of the joints do not run throughout the entire benches. On the other hand, distribution of termination types of joints determined in this study shows close similarity to those of Piteau (1973) who has demonstrated that discontinuities where both terminations can be seen are generally smaller than discontinuities where one or no terminations can be seen. Bedding planes and faults are characterized as very highly persistent structural features.

5.2. Drilling and Geotechnical Logging

Nine fully cored geotechnical boreholes designated by the author were drilled vertically during the 1989 field programme. The locations of boreholes (Plate 1) were marginally amended according to the developments at the site and particularly with due regards to the position and importance of the slopes adjacent to the highway. At closer locations to the basement rocks, boreholes were drilled to penetrate the basement rocks to determine their position.

Double tube NQ, 3.05 m long wireline core barrels with diamond surface set bits were used to obtain 47.6 mm diameter cores. Mud was used as flush in drilling.

The borehole cores were geotechnically logged following the stipulated and demonstrated procedures described by the Geological Society of London (1970, 1977), Franklin et al. (1971) and ISRM (1981). Greater emphasis was given to the discontinuity logging.

A summary of the borehole logs in the form of histograms showing intact core recoveries, rock quality designation (RQD) and the frequency of discontinuities is given in Figure 30. Average values of the three mechanical parameters (total and intact core recoveries and RQD) for each geologic unit are given in Table 3.

Low core recoveries and RQD values recorded in the alternating sequence located at the upper levels of main Sekköy formation may be seen in Figure 31a. Presence of weak and soft materials in the sequence and the low spacing between bedding planes have an important role on their core quality. Whereas, at lower levels, particularly in compact marls, mechanical parameters show significant improvement (Figure 31b). According to the rock type, location and depth, rock quality trends are clearly identifiable from the borehole logs. A perceptible improvement in the core quality towards the central part, however, is noted particularly in the upper zone of the rocks of hangingwall. In boreholes JT1, JT4, JT6 through JT8, drilled at locations close to the basin margins, approximately 84 % of all RQD values recorded in the main Sekköy formation are below 50%. On the contrary, 50% of all RQD values are above 50% in boreholes JT2 and JT3 which are located at the central part.

In boreholes JT1 and JT5, low mechanical parameters were noted in the cores of limestone located in the upper

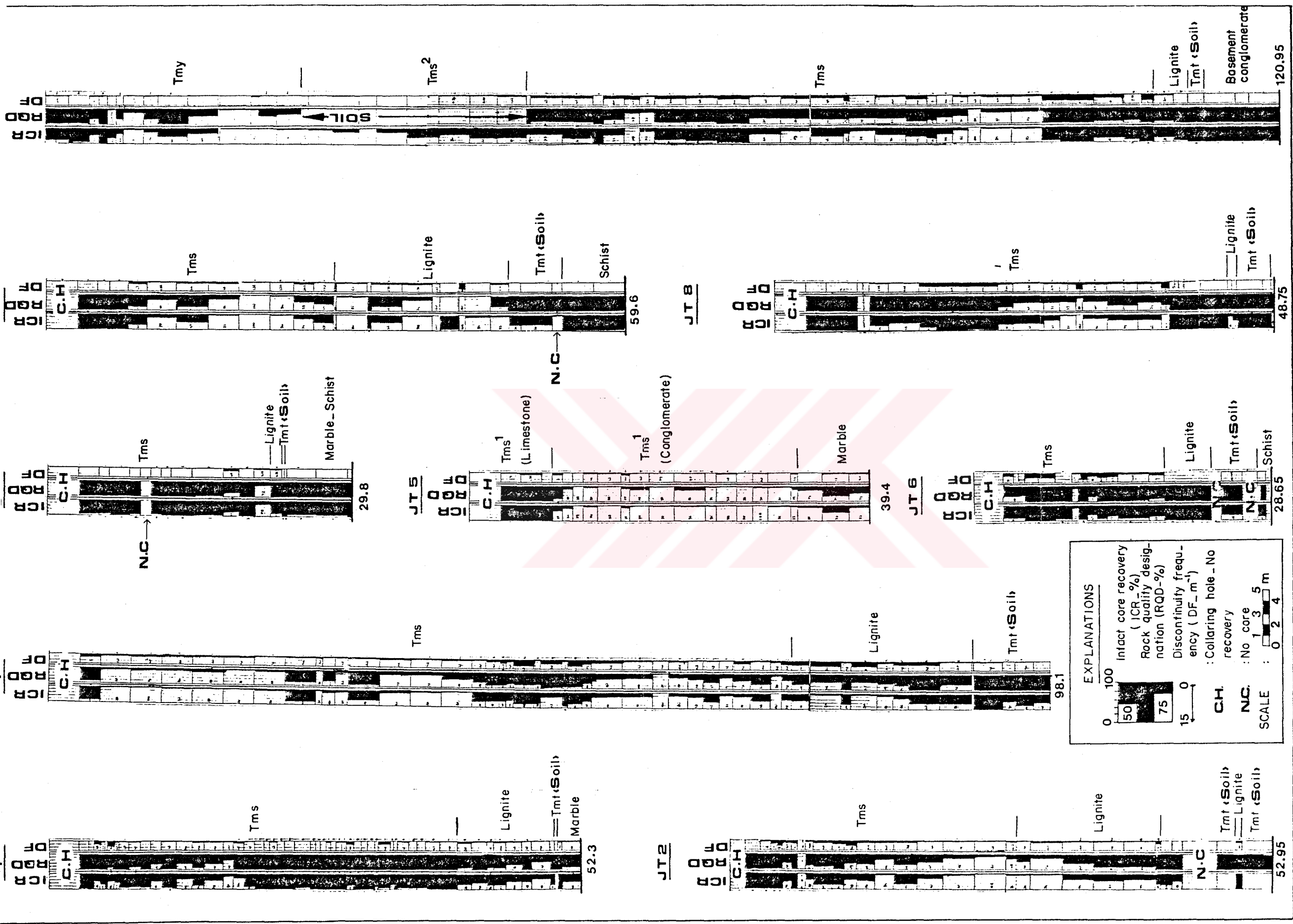


Figure 30: Geotechnical borehole logs.

Table 3 : Average percentage of total and intact core recoveries (TCR and ICR) and rock quality designation (RQD) for each unit in terms of boreholes.

Borehole No	T _{ny}	T _{zs} ²	T _{ms} ¹		T _{zs}	Lignite	T _{at}	Marble	Schist
			Last.	Congl.					
JT1 (TCR)	-	-	77	-	45	93	100	46	-
(ICR)	-	-	35	-	9	45	100	17	-
(RQD)	-	-	17	-	0	19	NA	7	-
JT2 (TCR)	-	-	-	-	69	88	38	-	-
(ICR)	-	-	-	-	53	71	19	-	-
(RQD)	-	-	-	-	37	38	NA	-	-
JT3 (TCR)	-	-	-	-	84	75	29	-	-
(ICR)	-	-	-	-	69	62	23	-	-
(RQD)	-	-	-	-	49	29	NA	-	-
JT4 (TCR)	-	-	-	-	27	30	100	100	27
(ICR)	-	-	-	-	7	21	0	0	10
(RQD)	-	-	-	-	1	0	NA	0	0
JT5 (TCR)	-	-	21	56	-	-	-	79	-
(ICR)	-	-	6	88	-	-	-	77	-
(RQD)	-	-	0	86	-	-	-	55	-
JT6 (TCR)	-	-	-	-	39	25	36	-	-
(ICR)	-	-	-	-	17	2	36	-	-
(RQD)	-	-	-	-	7	0	NA	-	-
JT7 (TCR)	-	-	-	-	69	93	44	-	11
(ICR)	-	-	-	-	59	83	40	-	2
(RQD)	-	-	-	-	50	65	NA	-	0
JT8 (TCR)	-	-	-	-	48	75	2	100	-
(ICR)	-	-	-	-	34	69	1	100	-
(RQD)	-	-	-	-	18	0	NA	0	-
JT9 (TCR)	78	82	-	-	61	68	4	19	-
(ICR)	64	59	-	-	47	19	0	0	-
(RQD)	43	NA	-	-	27	11	NA	0	-

TCR : Total core recovery (%)
 ICR : Intact core recovery (%)
 RQD : Rock quality designation (%)
 T_{ny} : Yatağan formation
 T_{zs}² : Transition zone deposits
 T_{ms}¹ : Detrital facies of Sekköy formation
 T_{zs} : Main Sekköy formation
 T_{at} : Deposits of Turnut formation
 NA : Not applicable (soil)

SYMBOLS

Lmst : Limestone of detrital facies (Tms¹)

U.Tms: Alternating upper sequence of Sekkøy formation

J : Joint

B : Bedding

Note : Length of tape is 1 m



(a)



(b)

Figure 31: Views of cores taken from geotechnical boreholes: (a) limestone and alternating upper sequence of main Sekkøy formation (Borehole No. JT1); (b) compact marls (Borehole No. JT3)

levels of detrital facies. This may be the results of weathering and the fractured nature of the rock at upper levels (Figure 31a). However, based on the observations made on outcrops, this situation is not quite representative for the rock exposed throughout the site. Conglomerates in the lower levels of the same facies have marginally higher quality.

The quality of the coal seam increases away from the basin margins. This property was also confirmed by the observations performed on operating highwalls. Sandstones are generally massive. However, lower parameters were noted at shallow depths in borehole JT9 due to the effect of weathering and crumbling of moderately cemented conglomerate banks at upper levels probably due to the effects of circulation fluid.

In the boreholes penetrating the transition zone and the Turgut formation considerably low core recoveries were obtained. Presence of dense and medium dense silty sand lenses played a major role in the low core recovery. The major soil type of these deposits include clays and clayey silts.

Alteration adversely affected the core quality in the upper zone of the basement rocks, particularly in the schists (see Table 3). The core quality of marble tends to increase with depth, as noted in boreholes JT5.

To check the directional features of discontinuities geological marker method suggested by Rosengren (1970; in Goodman, 1976) was employed. For this purpose, bedding plane orientation in the vicinity of borehole is used as a marker. The procedure was rewarding in the sections of boreholes where the core recoveries were high or excellent. The entire length of the core is divided into a series of continuous sub-lengths; a continuous reference line with respect to the

dip direction of the marker identified on the cores was painted down for each such sub-length. Dips and dip directions were determined with the use of contact goniometer and circumference scale, respectively (Figure 32). In sections where the core pieces could not be fitted to each others due to core losses, only the dips of discontinuities were recorded. The processing of data obtained from cores pointed out that excepting small local deviations, orientation of discontinuities generally maintain their original position through the boreholes. Besides, sharp increments recorded in dips through certain depths were attributed to the existence of faults which are barely detected at the surface. Joints also maintain their general features all around the pit. Both joints and bedding surfaces recognized in boreholes are smooth-planar and occasionally slickensided. They are generally narrow and/or thinly coated with silt or clayey material.

5.3. Groundwater Conditions

Groundwater is one of the most important factors which contributes to instability of slopes. This influence occurs for a number of reasons, either singly or in combination:

- a. Reduction in the shear strength by reducing the normal load on the potential failure surface due to bouyancy.
- b. Existence of seepage forces created by head loss of water flowing through the slope towards the mining face.
- c. Tension cracks or existing joints formed as a result of stress relief which allow water to build hydrostatic pressure at the back of potential

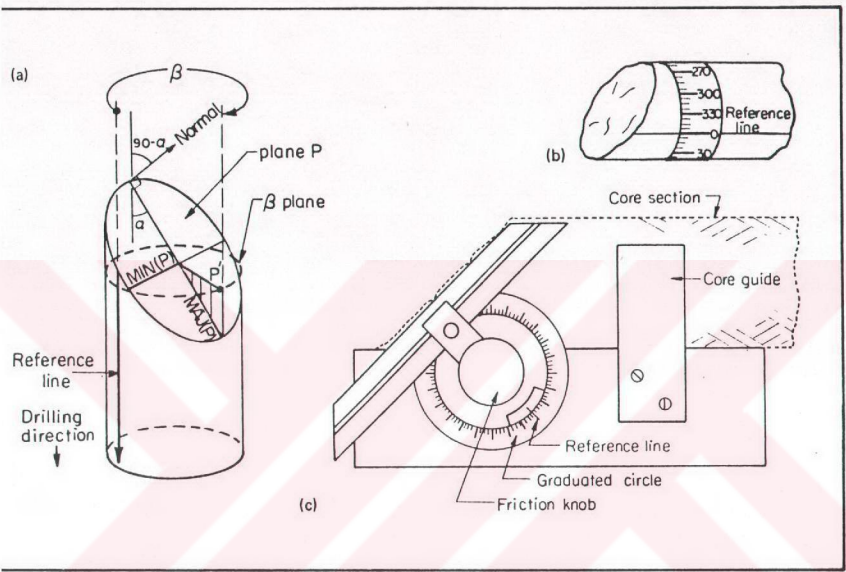


Figure 32: Core orientation technique based on the marker method: (a) reference line and the angles α and β ; (b) simple method of measuring β ; (c) goniometer for measuring α (After Goodman, 1976).

hydrostatic pressure at the back of potential failure blocks.

- d. Increase in shear stress due to hydrodynamic shocks caused by seismic acceleration force due to blasting
- e. Reduction in the discontinuity shear strength properties after periods of heavy rain.

As part of this geotechnical investigation general hydrogeological conditions of the site are also studied for the slope stability and practical design considerations. The studies conducted for this purpose included the followings:

1. Water level measurements in boreholes, blast-holes, water wells, and piezometer installations to establish the seepage points for groundwater monitoring.
2. Bulk permeability determinations for each lithologic unit through predetermined borehole sections.
3. Preparation of groundwater contour map and the general assessment of the groundwater conditions.

5.3.1. Groundwater Monitoring

In the first stage of groundwater monitoring studies, individual seepage points and seepage lines were identified all around the pitwalls (Plate 3). Zones of seepage are noted along the boundary between the compact marls and the coal seam, particularly within the coal seam. Slow rate of flow observed on the coal face along the ninth slice was evident (Figure 33). However, flow rate measurements could not be performed on the wall faces due to uncontrolled flow.



Figure 33: Seepage from the coal seam and compact marl/coal seam boundary at the new higwall face - south of ninth slice (Lg: Lignite; Ma: Marl; Plate 3-Photo. No.16).

A marked drop in the seepage rate was noted during the site investigation stage. A few seepage points were also observed on the sloping ground above some of the faults located NW of the pit. This is attributed to the perched water above the less pervious fault gouge.

In the second stage, to estimate the general configuration of the groundwater table in the open pit and its close vicinity, standing water levels were measured periodically in the vertical boreholes, which remained uncollapsed and penetrated the coal seam. In addition, shallow boreholes GWH1 through GWH12 were drilled using TKI's Reedrill blasthole drilling machine and two water wells previously constructed in the western part of the pit were used. Some of the boreholes GWH6 and GWH9 through GWH12 were drilled down to the coal seam, whereas others (GWH1, GWH3 and GWH4) penetrated both marls and the coal seam.

Boreholes were flushed with a solution of sodacaustic to remove the mud cake on the borehole walls. However, the reliability of measurements taken from previously drilled boreholes were in suspect, since the holes were drilled using bentonitic mud and it was not known whether or not the mud was flushed from the holes upon completion of drilling. Thus, some of the boreholes with anomalous water level measurements and those that are collapsed are eliminated. The groundwater levels were then monitored in 24 boreholes and 9 blastholes. No data concerning groundwater levels along the basin margins were available. This is because previously drilled boreholes were already abandoned. The groundwater level measurements are given in Table 4 and the monitoring wells are shown on Plate 3.

The measurements indicated that the groundwater level fluctuations generally range between 3 to 50 cm. The highest levels were recorded during December and February. This corresponds to the highest precipitation period in the site

Table 4 : Groundwater level observations

Borehole No	Ground elevation (m)	Water elevation (m)	Coal seam elevation (m)	Remarks (Coded)
I-129	554.88	545.88	538.12	A
I-130	553.34	543.94	544.04	B
I-131	551.03	533.03	531.73	B
I-135	552.52	529.72	532.52	C
I-138	585.16	547.16	530.00	A
I-139	581.80	545.05	528.50	A
I-143	541.55	513.35	478.55	A
I-144	525.37	494.17	480.97	A
I-146	530.74	500.54	479.24	A
I-147	517.81	498.61	472.41	A
I-149	503.46	467.16	469.66	B
I-150	505.54	492.39	479.44	A
I-151	537.64	499.84	447.04	A
I-162	537.60	527.06	529.30	B
I-166	559.60	509.70	498.40	A
I-170	573.89	525.39	482.89	A
I-171	590.20	548.85	526.70	A
I-172	579.88	551.31	529.18	A
JT3	564.66	524.76	491.56	A
JT4	522.72	504.12	500.82	A (Water loss)
JT5	536.76	507.26	No coal	D (Water loss)
JT6	508.74	503.34	490.00	A (Water gain)
JT7	508.77	493.27	480.11	Confined water
JT8	530.25	507.25	485.90	A (Water loss)
GWH1	504.25	497.5	483.50	A
GWH2	512.44	497.44	470.00	B
GWH3	486.10	485.60	485.60	A
GWH4	531.84	517.44	505.00	A
GWH6	540.19	515.56	460.00	A
GWH9	504.15	483.00	468.00	A
GWH10	504.96	483.46	473.00	A
GWH11	527.50	503.30	480.00	A
GWH12	507.50	495.30	480.00	A
W1	608.00	592.7	519.83	A
W2	601.00	590.00	488.00	A

- 'I' series boreholes were drilled by TKI
- 'JT' series boreholes were conducted for geotechnical purposes.
- 'GWH' series holes are drilled by blasthole machine for monitoring purposes
- 'W' series are water wells
- Water loss between 4 to 10 m section of boreholes JT1 in limestones (Tms¹)
- WL : Water level
- CM : Compact marl
- A : Water level above the coal seam
- B : Water level at compact marl/coal seam boundary
- C : Water level in the coal seam
- D : Water level in conglomerate

as shown in Figure 3. The water levels are generally above the coal seam. Towards the highwalls the water level tends to decline, particularly close to the compact marl/coal seam boundary (see Figure 33).

High water table was noted in 22 m deep borehole JT6 which is located on a faulted block. No quantitative conclusion can be drawn from this observation, however, it probably indicates a local confinement due to faulting which may create a barrier against groundwater flow. Thus, in order to obtain more information on the groundwater pressure prevailing within the rock mass in the vicinity of faulted blocks, piezometers were installed in boreholes JT6 and JT7 (Plate 3). Taking into account the depth to water table one piezometer in each borehole was installed into the coal seam.

The installations were conducted in accordance with the procedure recommended by Sharp et al. (1977). The standpipe in borehole JT7 was installed at a depth of 33.3 m. Unfortunately, piezometer in borehole JT6 slid down and became blocked at the end of installation without any reading and installation was not operative.

Groundwater monitoring data for a seven months period suggested that water table at this location lies above the coal seam. This situation indicated that the groundwater is confined due to the faults and the impervious character of intact marls overlying the coal seam. However, in view of observations on seepage along the highwall of ninth slice (see Figure 33), which is 150 m far from the borehole JT7, it is concluded that the groundwater in this area cannot maintain its confined state for a long time. Because, the highwall face produces a free discharge and the pressure dissipates with time.

5.3.2. Mass Permeability and Determination of Water Losses

The hydraulic properties of rock masses are required for classifying rock types into similar hydrogeologic units. The hydraulic property most frequently required for groundwater studies is the mass or bulk permeability of the rock. For the assessment of permeability conditions of the site, downhole permeability tests, which are conditionally suitable and cost effective method for this case, were carried out in geotechnical boreholes using the falling head method. Standard test procedure recommended by Sharp et al, (1977), was adopted.

Tests were conducted within the Neogene units excluding the basement rocks. Core evaluation during geotechnical drilling was used to select test section 3 m in length. Totally ten permeability determinations were made (Table 5).

Data given in Table 5 indicate that Neogene units have generally moderate bulk permeability. Lower intact permeabilities are anticipated from the clay-bearing units of main Sekköy formation. However, moderately spaced and continuous joints in this formation served as the possible avenues of recharge. Movement of water becomes easier due to direct entry to the formation through joints. As a result of the presence of relatively free draining joints, considerable higher bulk permeabilities were obtained. In other words, in spite of the lower primary permeability of the rock units, the continuous joints which are generally perpendicular to bedding, have played a major role in increasing the secondary permeability. This situation also indicates that mass permeability is greatest along joints rather than across the bedding planes .

Table 5 : Results of falling head permeability tests

Borehole No	Rock/Soil Type	Test Section (m)	Permeability Coefficient k (cm/sec)	*Degree of Permeability
JT2	Laminated MARL	9.40-12.40	1.95×10^{-4}	Moderate
JT2	Laminated MARL	15.30-18.30	7.4×10^{-6}	Low
JT3	Laminated MARL	18.30-21.30	10^{-5}	Moderate-Low
JT7	Laminated-Compact MARL	21.35-24.50	4.2×10^{-4}	Moderate
JT9	SANDSTONE	12.20-15.20	1.33×10^{-3}	Moderate
JT9	SANDSTONE	17.30-20.30	8.48×10^{-4}	Moderate
JT5	CONGLOMERATE (with small-size solution features)	15.15-17.80	6.4×10^{-4}	Moderate
JT6	LIGNITE	19.20-22.05	3.3×10^{-3}	Moderate
JT7	LIGNITE	30.50-34.75	4.1×10^{-5}	Moderate
JT8	SILT (clayey, sandy with fossil shells-Turgut formation)	46.00-48.75	1.48×10^{-3}	Moderate

*Degree of permeability : High : 10^{-2} to 1 cm/sec.
 (after Sharp et al., 1977) Moderate : 10^{-2} to 10^{-5} cm/sec.
 Low : 10^{-5} to 10^{-7} cm/sec.
 Effectively impermeable : (10^{-7} cm/sec.)

Bulk permeability of the coal seam increases particularly in places where the coal is highly fractured. Considerably higher permeability value obtained for Turgut formation underlying the coal seam does not reflect the actual situation, because the upper levels of this sequence are composed of clays and silts having lower permeabilities. On the other hand, these deposits occasionally show lateral transitions into sand lenses and/or sand-silt mixtures. As a result of such local heterogeneities, a permeability value higher than the anticipated limits could be obtained.

Sandstones also have moderate bulk permeability. Calculated permeabilities are confirmed by those of similar sandstones given in the literature (Hoek and Bray, 1977; Sharp et al., 1977). Excepting near surface layers, secondary permeability of sandstone may be lower than those of marls of the Sekköy formation due to its well-cemented nature and scarcity of joints.

Along some geotechnical boreholes water losses were noted during drilling (Table 4). Considerable water losses were noted in limestones and in the upper levels of conglomerates penetrated by boreholes JT1 and JT5. It was concluded that the losses were caused by small solution openings and fractures within the rock masses. As a result, conglomerates revealed moderate bulk permeability. No signs of moisture was observed on bench faces at Extrans section where limestones are cut by slopes.

5.3.3. Assessment of Groundwater Conditions

Holes used for groundwater level monitoring are categorized as follows:

- 1) Twentyfour unequipped boreholes that tap different

lithological units.

- 2) Holes that penetrate marl and coal seam (GWH1,3,4)
- 3) Holes drilled down to the bottom of marl (GWH 2, 6, 9, 10, 11,12).

Data obtained from the first group represent an overall water table. Whereas data from other groups represent marls only. Thus, the assessment of general groundwater table and flow directions were based on the information obtained from the first group boreholes and two water wells (Plate 3). The differences in groundwater levels in various faulted blocks are not accurately known. However, this is not a major consideration in the general assessment of groundwater conditions.

Groundwater level contours representing marls in a local area are shown by dashed lines (Plate 3). These contours do not show considerable deviations from the general trends. However, it may be possible that perched water table may also exist in some levels of the hangingwall because of the alternations involving clay beds.

It is obvious that the groundwater flows will occur towards excavation. According to the position of groundwater table all around the pit, direction of flow is from west to east and from north to south along the N-S and E-W oriented pitwall, respectively.

Current information on groundwater conditions in the pit and its close vicinity is assessed as follows:

- a) The coal seam acts as the principal aquifer particularly in zones where the coal is fractured.

- b) Groundwater level generally lies above the coal seam in compact marls. While close to the highwalls, where the coal seam exposes, groundwater table tends to decline and approaches the compact marl/coal seam boundary. This situation indicates that a steady seepage condition is present.
- c) Vertical percolation seems to be highly effective. Moderately spaced joints within the Sekköy formation serve as avenues for recharge. Joints are more conducive to seepage flow than bedding.
- d) Direct recharge through joints varies seasonably depending on the amount of rainfall which can easily be drained.
- e) Bulk permeabilities are classified as moderate based on the results of in-situ tests. However, the permeability of the deposits underlying the coal seam is very low. The upper levels of these deposits are exposed after the removal of coal and then covered by the spoil material. Therefore, no significant hydrogeological problem is anticipated from these deposits.
- f) Groundwater condition of the sandstone is available only from the boreholes I-166 and I-170. In these boreholes water levels are below the top of sandstone sequence and no significant seepage was observed on benches constructed in this rock unit. Thus, for stability analyses the sandstones may be considered as forming the dry zones.
- g) The lignite bearing basin is enclosed by limestones and conglomerates. The topography rises to an elevation of about 650 m both in the west and in the northwest of Eskihisar basin. Flow of

groundwater would be expected to occur from higher elevations to the lower parts. The magnitude of the flow would depend on the permeability of these rock units. The hydrogeological data for these rocks, however, is quite limited. However, their bulk permeabilities could be moderate particularly in their near-surface layers. It should also be noted that no sign of seepage was observed on benches constructed in limestone at Ertrans Section during the studies. Thus, it may be concluded that water percolating through these units will probably reach to the lower marl level when permanent slopes are to be constructed.

h) Local groundwater reserves may be expected in the vicinity of faults and in local folds situated within the hangingwall material.

i) Confined groundwater conditions are not considered to be significant in the study area. This is due mainly to the fractured and free draining nature of the overburden material and the coal seam.

5.4. Monitoring of Pit Slopes and Observations on Previous Slides

A knowledge of the slip surface, mechanism of instabilities and the shear strength mobilized along the sliding surface at the time of failure are essential for stability analysis and for designing appropriate remedial measures. The available methods for providing information about instabilities are divided into two groups; those applicable only to moving slopes and those applicable to stationary ones. The first group requires application of a monitoring program. The second group includes in-situ

observations from access holes, observations on recovered samples and surface.

Taking into consideration the above mentioned matter, observations on previous slides in different parts of the pit and surface displacement measurements using conventional surveying equipment in two unstable areas were conducted for the following purposes:

- a) To provide geotechnical information for analysing the slope failure mechanism, for the assessment of the weighed mean value of the shear strength parameters along the failure surface and for conducting future re-design considerations of the slopes, and
- b) To maintain safe operational procedure for the protection of personnel and equipment.

5.4.1. Observations on Previous Slides

Seven slides developed within the benches in the northern part of the actual pit were identified during the site investigations and labeled from 1 through 7. Their boundaries were established by topographical surveys and are shown with their most probable movement directions in Plates 1 and 3. In addition to these, another instability, which developed progressively in June 1990 during the last visit of the author to the site and is labeled as 8 was also investigated in detail.

As pointed out by Sancio (1981), Hutchinson (1983), and Carter and Bentley (1985), it is required that the pre-failure geometry of the slope or bench should be known for a

valuable back analysis. Slope geometries or profiles of the slides 2,6,7 and 8 before failure are known. Whereas those of others are not available because of the insufficient records kept by the contractor who was responsible from the mining operations at the northern part of the pit, before 1988. In addition to this, severe disturbance in slide areas makes it rather difficult to perform a detailed observation. Therefore, for these instabilities (1,3,4,5) only the present state of the failed benches and largest blocks with the orientation of structural features were studied.

Detailed slope instability maps at the scale of 1:200 and cross sections of slides 2,6,7 and 8 were prepared by means of surveying technique. These drawings include the position of benches, present state of the failed mass and the extent of tension cracks. Directional data from the structural features in the close vicinity of the instabilities and of the failure surface were collected in a closely spaced pattern. In addition, trends of the fresh traces parallel to the direction of movement on soft sliding surfaces and wet locations were also noted.

Based on the observations conducted on the slides it can be concluded that the geologic structure has had a significant influence on the mechanism of failures both in hangwall and in the footwall. Except the slides 5 and 7, all the instabilities are structurally controlled failures resulted in movements along the individual discontinuities subject to plane failure or combinations of discontinuities. Slide 8, which developed along the black clay surface (see Figure 9) is a best example of the plane failure mode evidently observed in the open pit. The slides 5 and 7 developed in soil and soil like material are mass failures rather than structurally controlled mode of failure.

No sign of instability was noticed in the south slopes of the pit and the highway during the studies.

5.4.2. Monitoring of Pit Slopes

As a part of this research, slope monitoring studies were conducted in two localities of the pit where evidences of instability were detected. Many techniques are available (Franklin, 1977; Wyllie and Munn, 1979; Call, 1982; Hanna, 1985) for the monitoring of the slope behaviour. One of such method is the surface displacement measurement using conventional surveying equipment. This method was preferred in this study because of its availability and cost-effectiveness for the case.

A survey network consisted of targets installed at various strategic locations throughout the slide and the station on a stable ground some distance from the pit were established for each monitored location. Targets themselves consists of reflector prisms mounted on a sturdy tripod by means of a conic catcher specially made for this study. Prisms were installed on steel bars which were labeled and fixed permanently to the unstable ground (Figure 34).

Stable bases of station for each monitoring location were established with concrete monuments. Monitoring was conducted by means of electronic distance measuring (EDM) equipment consisting of 1200 informatic theodolite and D14 distomat connected with a Wild Heerbrug Gre3 data terminal. The coordinates and the elevation of each target, from which vectors of movement between successive readings can be calculated, were recorded in certain time periods depending on the rate of movement and the availability of TKI's surveying team. Monitoring studies, performed at two unstable locations, are briefly discussed below.

Unstable area I (Slide 6) : Slide 6 had occurred at the south boundary of the Özdemirler section in May 1989, before this study had commenced. The bench constructed in the coal



Figure 34: A monitoring target consisting of reflector prism, tripod and labeled steel bar for the monitoring of surface displacements (TC: Tension crack; Plate 3-Photo. No.17).

seam was shifted back to the next mining bench resulting in a considerably high and steep individual bench including marl and coal and then instability has started to develop (Figure 35a). Direction of the movement, which was estimated from the considerations on the positions of the failed blocks and the fault surface limited the failure in the west, is approximately SE. On the other hand, tension cracks with a large extend behind the crest and the toe of the upper bench caused a suspicion that a subsidiary bench movement into the void created by previous failure may be expected. Thus, a monitoring system consisting of 17 monitoring targets, which were installed in a vertical pattern to the main cracks, were set up on the +539 and +552 benches (Figure 36). Monitoring was started in July 28, 1989 and continued until September 14, 1989. After this date the equipment was not available due to the intensive surveying program of TKI.

Resultant displacement vector of each target station were calculated at the end of monitoring. These are shown in slope instability map with the orientation of tension cracks and the structural features (Figure 36). The plunges of the displacement vectors at +552 bench are very similar and range between 33.5° and 40° , except one, while those of others at +539 bench are more uniform around 26° . Their trends are mostly parallel in the SW direction towards the void created by the previous slide 6.

A point on the surface of a sliding soil or rock mass will move in a direction parallel to the slope of the slip surface beneath provided that the mass moves as a rigid body. Carter and Bentley (1985) suggest a method to predict position of the slip surface when the surface movement directions and the positions of the toe and the backscar of the sliding are known. But this method gives accurate result for translational or planar and circular failure surfaces. In spite of the lack of information from the bench faces,



(a)



(b)

Figure 35: (a) General view of slide 6 (F: fault);
(b) Tension crack and separation in the
rock mass parallel to the steeply dipping
joints (J) (Plate 3-Photo. No.18 and 19).

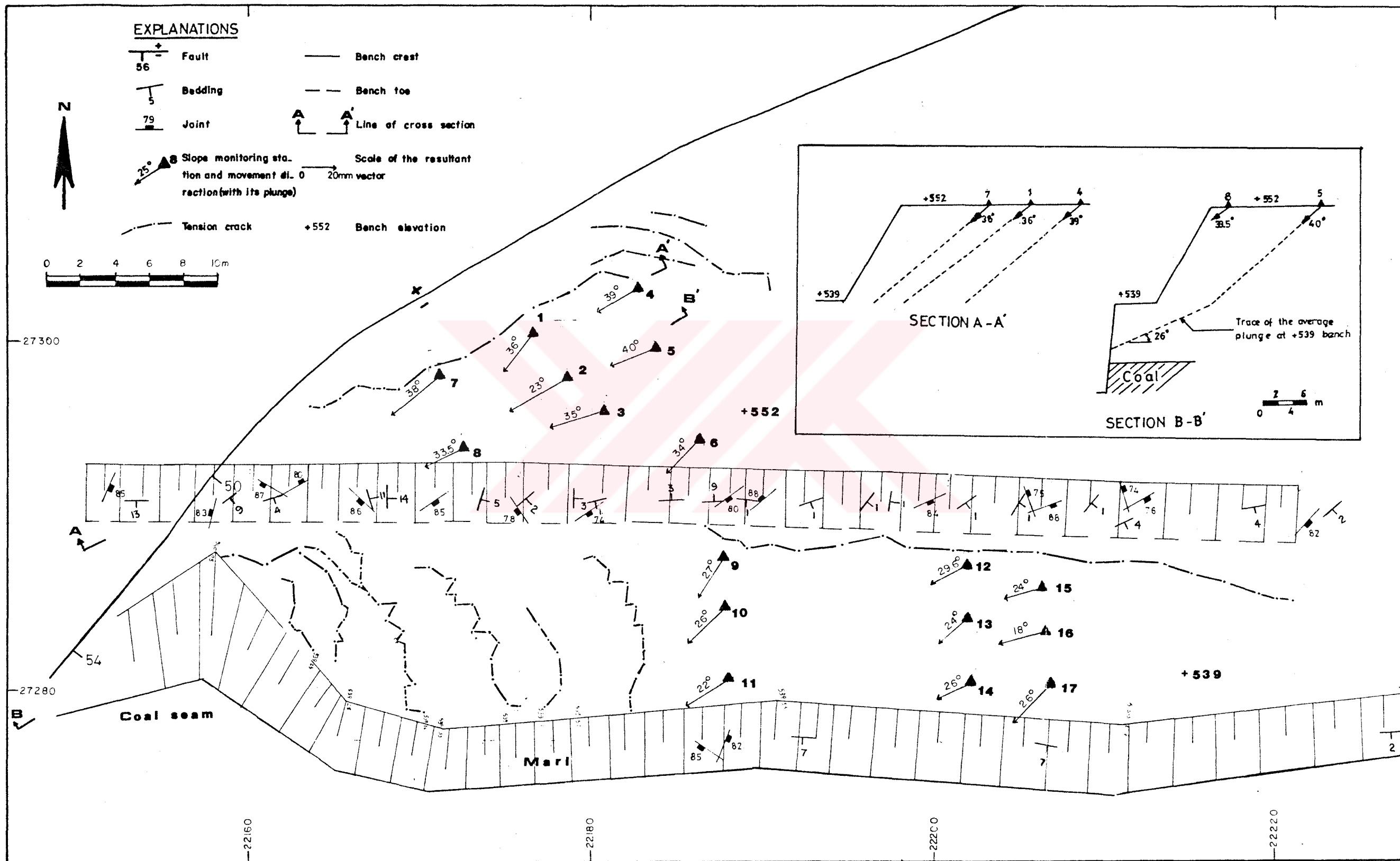


Figure 36: Slope instability map of the slide 6 and monitoring information.

the monitoring sections based on the above mentioned method brings to mind a translational type of slip surface along discontinuities rather than a circular shape. In the unstable area, bedding planes dipping to the opposite way of the vector and steeply dipping joints are considered kinematically not to cause a planar sliding. But orientations of the fault and tension cracks developed parallel to the joints (Figure 35b) and the displacement vectors indicate that a wedge type of failure is more likely. This information was also employed for back analyses to assess the mechanism in detail using the kinematical and limit equilibrium techniques.

Monitoring data were also graphically displayed in the form of vertical cumulative displacement versus time plots (Figure 37). Greater increases in the rate of movement was recorded in August 1989 while the rates decreased in September. During the monitoring stage no rainfall was observed whereas occasional blasting for loosening purposes was carried out near this location along some working benches at the mid of current pit. It can be possibly concluded that seismic waves generated by blasting might be the cause of an increase in the rate of movement or of the acceleration.

The monitoring study pointed out that the movement still continues with small rates into the void created by the previous movement. Therefore the exploitation of the coal from this part has been terminated until the end of winter season of 1990 when the unstable portion of +539 bench reached to an equilibrium after complete failure through rainy months.

Unstable area II : Development of tension cracks parallel to fault-B and sub-parallel cracks were observed on the new highwall at the south part of the ninth slice in August 28, 1989 (Figure 38a). This situation was taken as a sign of instability. The following day preparation of an

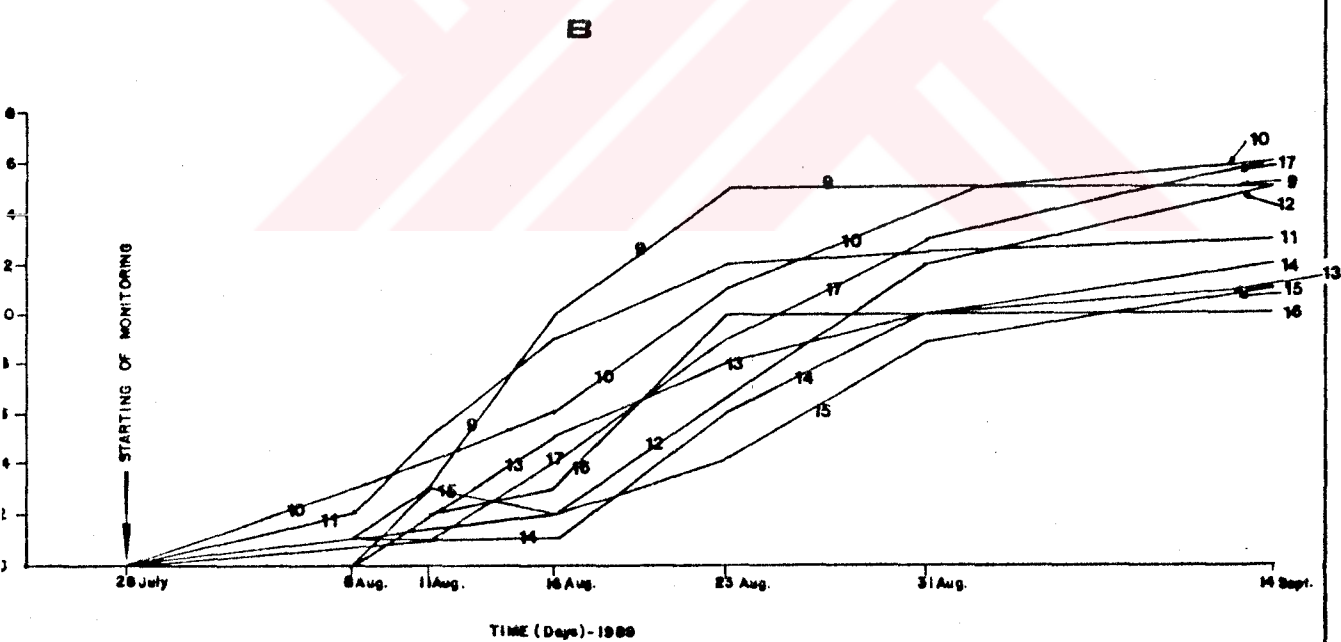
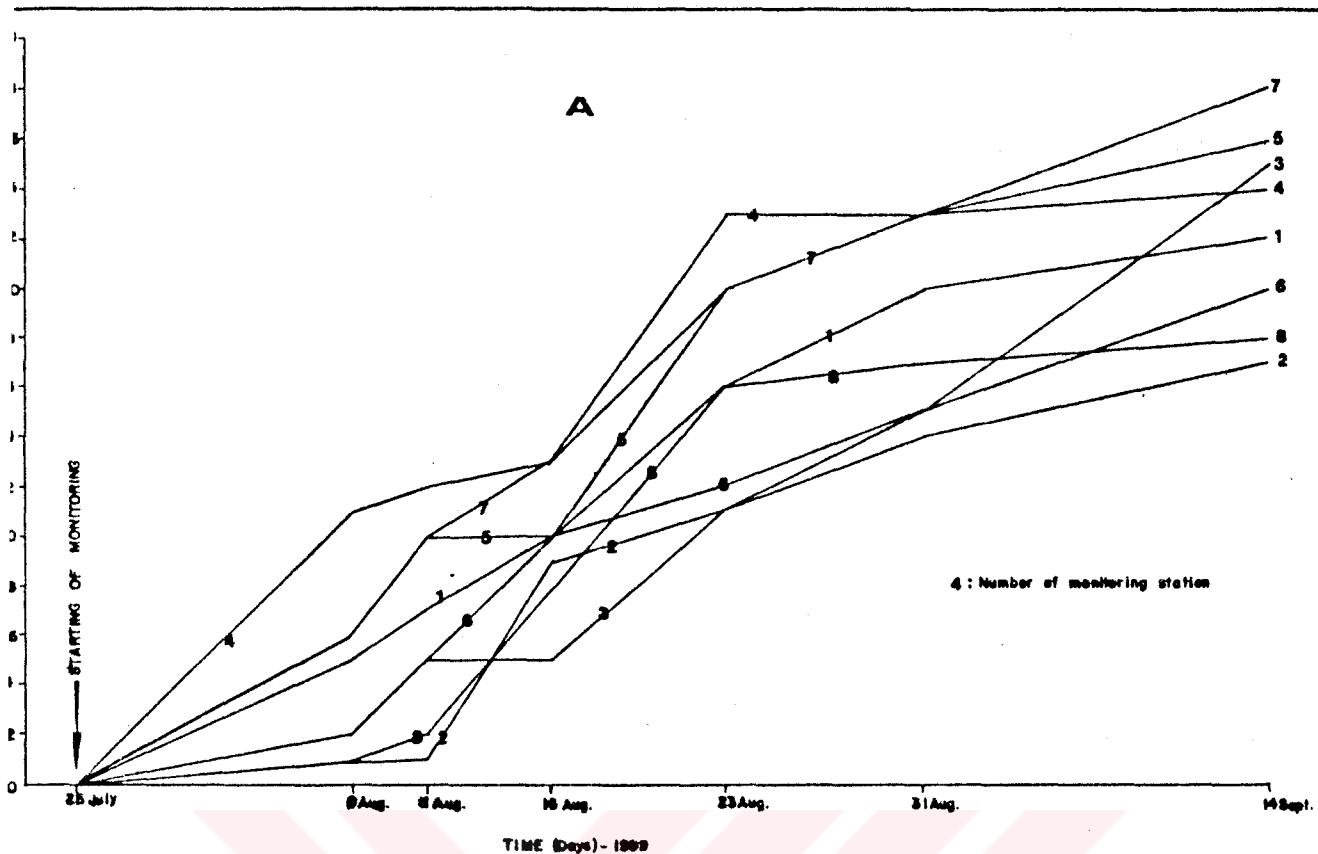


Figure 37: Cumulative vertical displacement versus time plots for stations at +552 bench(A) and +539 bench(B).

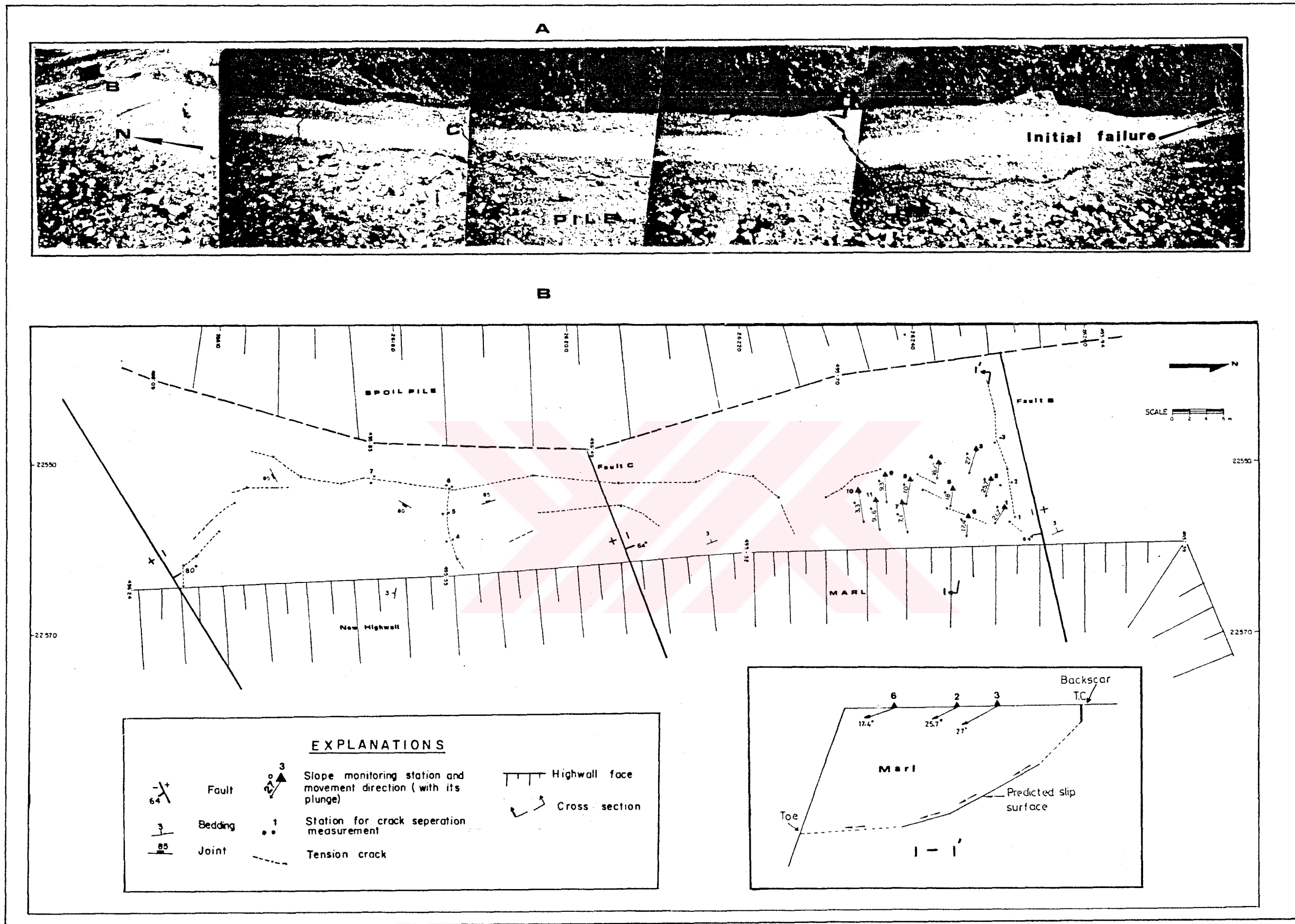


Figure 38: (a) General view of monitored area II and tension cracks (Plate 3-Photo. No.20);
 (b) slope instability map and monitoring information.

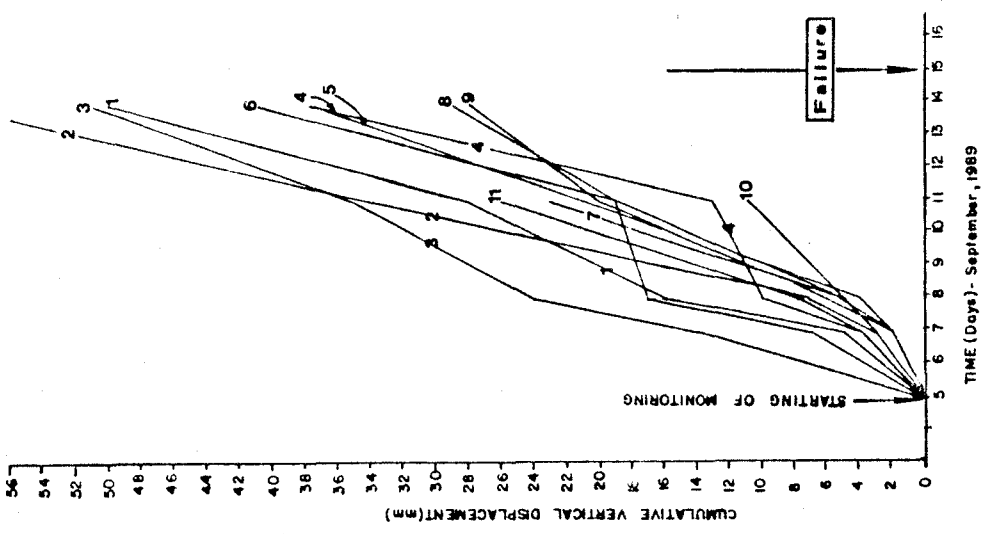
instability map was started (Figure 38b). A monitoring network consisting of 11 target stations was set up behind the crest of the highwall near fault-B in September 5, 1989. In addition, 7 pairs of steel bars were fixed one on either side of the main cracks and opening of tension cracks were measured with a steel tape.

The rate of movement and separation of the rock mass through the tension cracks was considerably fast. As a result of this, tension crack development extended to south in a pattern parallel to other faults and joints. The movement was limited in the west by a continuous crack probably 2 m deep which developed parallel to the toe of temporary spoil pile. Thus, this part of the slice, where the coal was eventually mined, was omitted.

A projection of vertical displacement data of each station, plotted in Figure 39a, was made. By 11 September when the rate of movement drastically increased it was evident that highwall failure was inevitable. The first slide, which is bounded by the fault, occurred in the south (Figure 40). It was a spoon shaped, shallow seated slide within the marls. In this area this slide was followed by similar instabilities. The equilibrium was reached in September 15.

Plunges of the resultant displacement vectors of the stations near the crest are shallower than those of others (Figure 37b). This probably indicates that failure is more likely to occur along a shallow seated slip surface in the form of a curve. This approach was also visually confirmed by the shape of first failure shown in Figure 39. On the other hand, in this section sliding on an individual discontinuity seems to be kinematically impossible due to their orientations. Besides, it should be noted that planar failures may occur with much less warning (Wyllie and Munn, 1979). However, trends of tension cracks generally

A



B

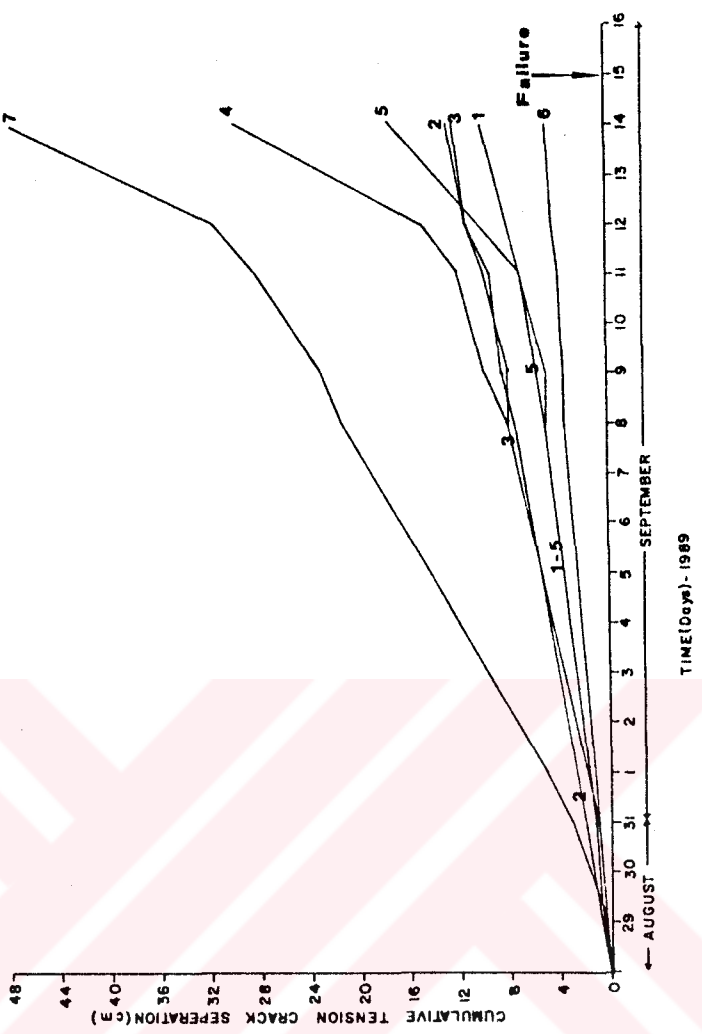


Figure 39: Plots of movements measured during September 1969 proceeding failure at the end of ninth slice: (A) vertical displacement versus time plot; (B) tension crack separation versus time graph.



Figure 40: Slide initiation and separations along faults B and C in the new highwall at the south of ninth slice (SP: spoil pile; Plate 3-Photo. No.21).

correspond to the strikes of discontinuities in the unstable area. Thus, it can be stated that discontinuities more likely act as release surface or surfaces of separation. Detailed discussion of the failure mode in this area, which is based on kinematic assessments, are introduced in Chapter 8.

5.5. Schmidt Hammer Tests

Non-planar bedding surfaces included in the limestone rock mass of detrital facies along the basin margins have not been sampled for laboratory shear strength determinations. Thus, the shear strength of these surfaces were amended to be determined by empirical equation proposed by Barton (1976), and Barton and Choubey (1977). One of the parameters employed in the empirical equation is joint wall compressive strength (JCS). The Schmidt hammer, which is a simple field test recommended by Deere and Miller (1966), provides the ideal solution to determine this parameter.

Schmidt rebound number can be obtained as a result of this test. Deere and Miller (1966) have shown that the uniaxial compressive strength of rocks can be graphically determined by using Schmidt rebound number and the unit weight. Due to sampling difficulties of the limestone, additional data for the uniaxial strength were also aimed to be obtained by means of this test.

L type Schmidt hammer, which is applied vertically downward, was used in this research. The application surface was smoothed by emery-stone before testing. Unit weights were determined experimentally in the laboratory. Tests were performed in 13 locations where suitable limestone outcrops including representative bedding surfaces exist. The test locations, situated in the boundaries of 1:2000 scale

documentation map, are shown in Plate 3 and the test results are given in Table B.1 of Appendix B. The values of JRC and unit weight range between 32 to 47.6 kPa and 22.7 to 26.5 kN/m³, respectively. Statistical analyses yield that average JRC is equal to 41.7 kPa with a standard deviation of 5.1. However, considering weathering effects and small size solution features in the rock mass, the lower bound of JCS which is 36.6 kPa may be used in calculations. Based on the average values of JRC (36.6 kPa) and unit weight (24.9 kN/m³), average uniaxial compressive strength of the rock is estimated as 30 MPa from the "Schmidt hardness-uniaxial compressive strength" chart given in Hoek and Bray (1977).

5.6. Field Sampling

Samples required for geomechanical laboratory tests were collected through a field sampling program. In this program block, disturbed and core samples were taken in accordance with the sampling standards (BSI, 1981). Totally 58 block samples from each of the principal lithological units and from discontinuity surfaces, with the exception of basement rocks, were taken from locations shown in Plate 3.

It was rather impossible to obtain test samples for shear strength from the lignite blocks because of the difficulty of sampling from a heavily cleated block sample. Then only two suitable lignite block samples were available. On the other hand, blocks from conglomerates could not be sampled due to unsuitable outcrops.

Samples from the fault gouges were recovered with an orientation parallel to the displacement. In some locations where digging of sampling face was difficult, 100 mm square by 20 mm thick specimen cutters were utilized for undisturbed sampling (Figure 41). Some of the blocks were



Figure 41: Undisturbed and oriented sampling from a fault gouge using metal specimen cutter (Plate 3-Photo. No.22).

also sampled from the surface of failures and by excavating borrow pits. Disturbed samples, which are labeled with the letter Z (Plate 3), were taken from the soil materials for soil classification tests.

In addition, borehole cores of different lithologies and the coal were sampled. Taking into consideration the possibility of sample losses during specimen preparation in the laboratory, sufficient amount of core samples were taken. After labelling, all the samples were coated with a succession of layers of microcrystalline wax using layers of muslin and then were transported to the Rock and Soil Mechanics Laboratories of M.T.A..

CHAPTER 6

LABORATORY INVESTIGATIONS

Material strength together with geological structure, groundwater and mining strategy are critical factors in determining slope stability. Failure occurs when the shear strength of a material is exceeded. A wide variety of instability mechanisms are operative in Eskihisar open pit which involve failures along discontinuities and within weak zones. Therefore, strength is an unceasing input parameter of the stability analyses.

On the other hand, some simplified tests, called as index tests, provide indirect information about the engineering properties of soils and rocks. These tests are also indicative of other physical properties and help in defining the limits of engineering classifications. It is presumed that materials in a limited area with similar index properties will have similar engineering properties.

In this study, an extensive laboratory testing program, using the samples collected from the site, was applied in order to determine engineering properties of the materials and discontinuities encountered in the pit. The tests were performed in M.T.A. Rock and Soil Mechanics Laboratories in Ankara. Laboratory testing program consisted of two stages. In the first stage, disturbed and undisturbed soil samples and rock cores were used for index tests. The second stage tests were carried out for the determination of strength parameters. Strength tests were tried to be performed under specific conditions as close as possible to in-situ conditions, such as normal loads and moisture conditions.

The methods in accordance with the procedures recommended by the most popular international test standards were employed. The test data were evaluated using some

computer packages, which are general statistical computing systems. Testing program involved the followings:

- a) X-ray diffraction analyses
- b) Unit weight determinations
- c) Atterberg limits tests
- d) Grain size distribution analyses
- e) Slake durability tests
- f) Intact rock strength tests (uniaxial and triaxial compression tests)
- g) Rock shear tests on discontinuity surfaces
- h) Soil shear tests

6.1. X-ray Diffraction Analyses

Sixteen X-ray diffraction analyses were carried out on soil materials from the pit. They were representative samples of scrapings from fault gouges, the deposits of transition zone and Turgut formation. Atterberg limits of most of these samples were also determined. The tests were performed to investigate the type and relative quantity of the minerals present in each of these soil materials.

The XRD diffractograms were obtained in M.T.A. X-ray micro analysis laboratory with the use of JOEL JBX-8P diffractometer. Diffractograms from normal, ovened and treated with ethylene glycol preparates in the order of abundance of each mineral (Appendix A, Table A.2).

X-ray analyses revealed that fault gouges and transition zone deposits mainly consisted of Ca-Na montmorillonite and illite with smaller quantities of kaolinite. They also contain non-clay minerals such as calcite, quartz, dolomite, aragonite and traces of feldspar. On the contrary, deposits of Turgut formation were found to

contain significant quantities of kaolinite and illite, while montmorillonite was the secondary. These deposits also contain muscovite, chlorite, small quantities of quartz, calcite, dolomite and very few feldspars. Derivation of this deposit from the local mica schists basement rock is shown by the presence of mica minerals within it.

6.2. Index Properties

6.2.1. Unit Weight Determinations

Unit weight is used as an index property in determining the overburden loads acting upon the sliding surfaces for stability analyses. In this study unit weight determinations were conducted on 365 test specimens composed of the lithologic units in Neogene and the fault gouges. Machined rock core specimens of cylindrical shape and soil specimens prepared using 60 mm square 20 mm thick specimen cutter of soil shear box were used for determinations. Test procedure suggested by ISRM (1981) was employed. On the other hand, unit weight of a few lump samples were determined according to the bouyancy technique (ISRM, 1981).

A computer package, named GEO-EAS (Englund and Sparks, 1988) was used in statistical analyses. The results of the unit weight determinations are illustrated as histograms in Figure 42. The mean value of each histogram was calculated as the representative of the unit weight of each unit (Table 6). The results show that the unit weights are distributed in an approximately normal form.

Considerably similar unit weights were obtained for main Sekköy formation, transition zone material, deposits of Turgut formation and the fault gouges which are rich in clay size material.

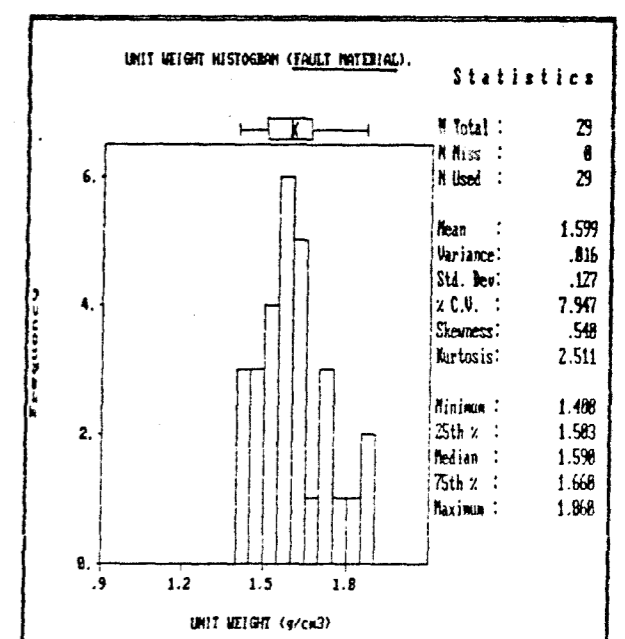
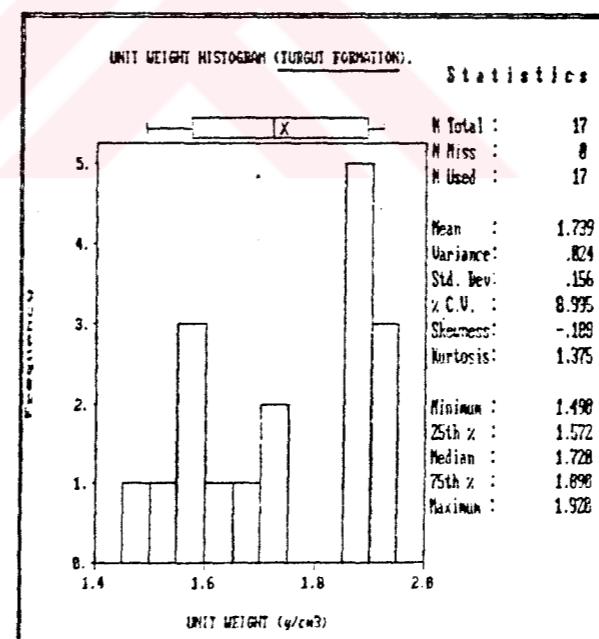
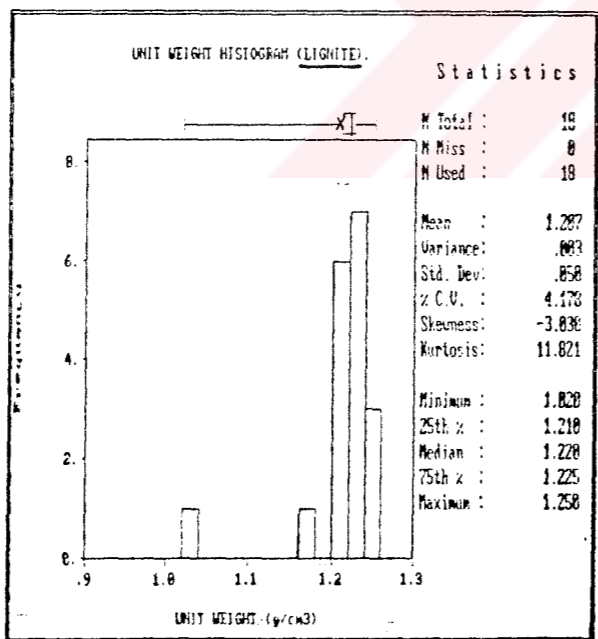
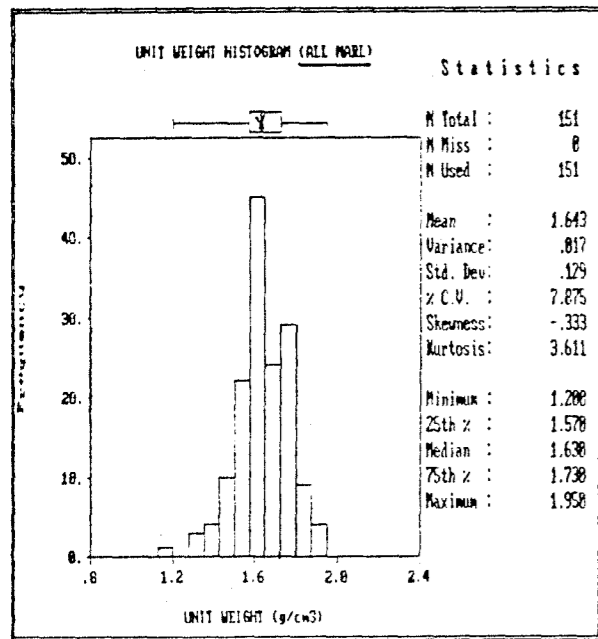
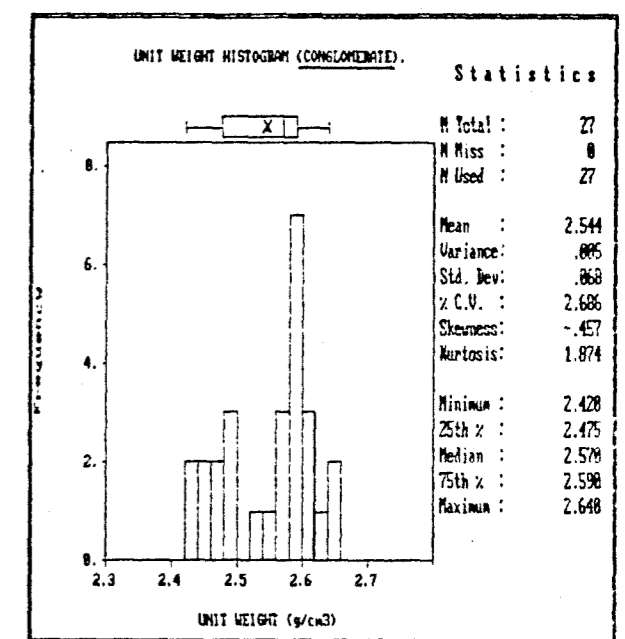
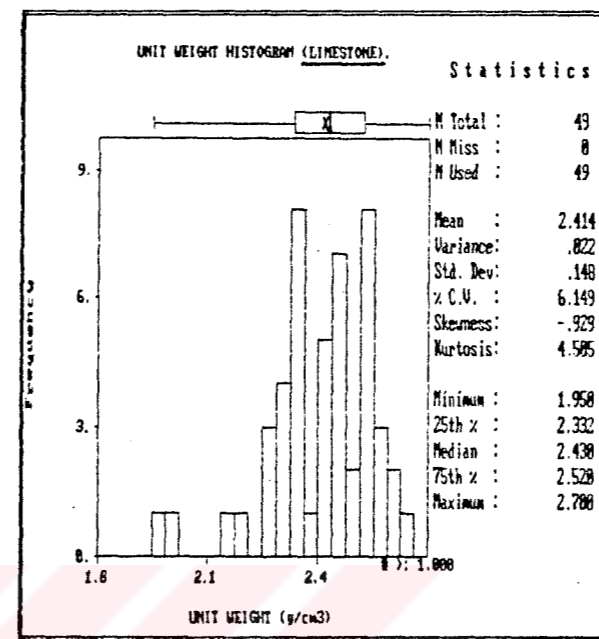
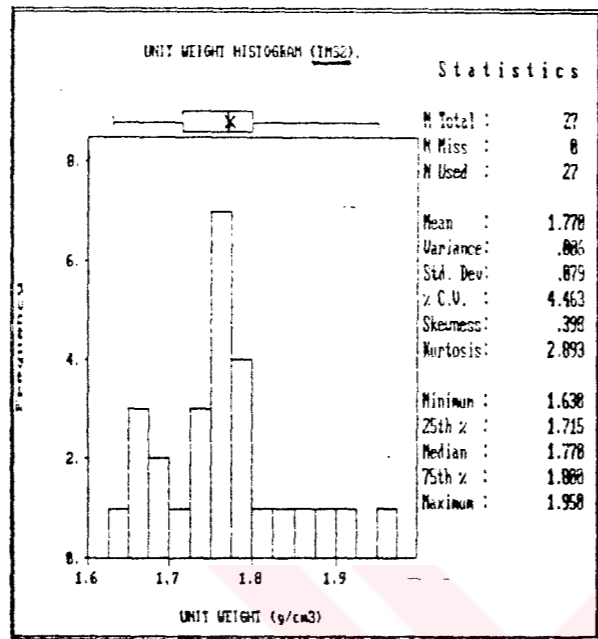
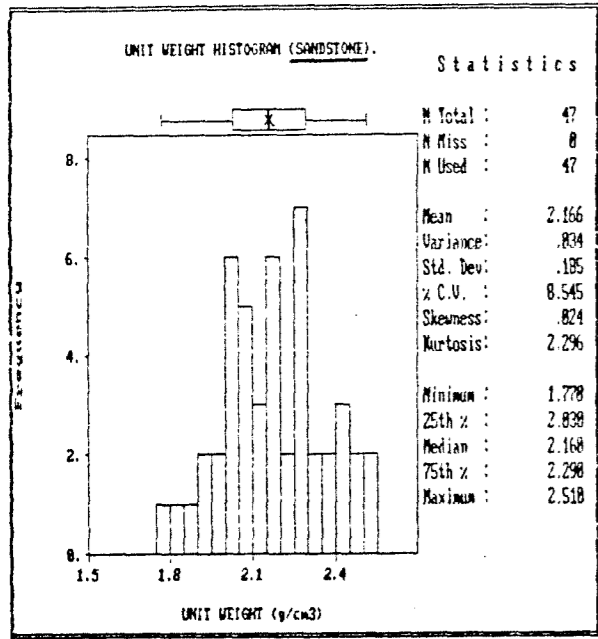


Figure 42: Unit weight histograms of rock and soil units in the study area.

Table 6 : Statistical results of unit weight determinations

LITHOLOGICAL UNIT OR FORMATION NAME	UNIT WEIGHT						Number of values
	Range		Mean	Standard Deviation		SD	
	Min. (g/cm ³)	Max. (g/cm ³)	X (g/cm ³)	(KN/m ³)*			
Sandstone (Tey)	1.770	2.510	2.166	21.24	0.185	47	
Transition zone deposits (Tas ²)	1.630	1.950	1.770	17.36	0.079	27	
Limestones (Tas ¹)	1.950	2.700	2.414	23.67	0.148	49	
Conglomerate (Tas ¹)	2.420	2.640	2.544	24.95	0.068	27	
Main Sekkôy forz./Marl (Tas)	1.200	1.950	1.643	16.11	0.129	151	
Lignite	1.020	1.250	1.207	11.84	0.050	18	
Deposits of Turgut formation (Tet)	1.490	1.920	1.739	17.05	0.156	17	
Fault gouges	1.400	1.860	1.599	15.68	0.127	29	

* : 1 g/cm³ = 9.807 KN/m³

6.2.2. Atterberg Limits and Moisture Content Determinations

Atterberg limits of soil materials (liquid limit, LL; plastic limit, PL; plasticity index, PI), which are most useful for engineering purposes and necessary for soil classification, were determined in this study. Totally 25 samples from fault gouges, claystone of Sekköy formation, transition zone and Turgut formation were selected for the tests. The material passing the 425 μm (No. 40) sieve of each sample was used. Tests were carried out following the method proposed by ASTM (1985; D4318-84). In addition, the moisture content of some test samples, which preserved their natural moisture were also determined according to ASTM D2216-80(1985).

The test results are summarized in Table B.2.1. of Appendix B. The ranges of Atterberg limits determined for each soil type and their mean values are given Table 7. The majority of the tests indicate that the liquid limits are greater than 50%. Means and Parcher (1963) suggest that soils with liquid limits of 50 per cent or above probably indicate the presence of montmorillonite. This was confirmed by X-ray diffraction analyses.

Fine-grained materials sampled in the study area, with the exception of two samples, have plasticity indices greater than 20%. Based on the plasticity classification system (Leonards, 1962), these soils may be classified as plastic and highly plastic soils. The variation in the plastic limits probably resulted from the presence of nonclay minerals as pointed out by Grim (1962). However, it increases for materials rich in montmorillonite.

Table 7 : Results of general statistical evaluation of the Atterberg limits

LITHOLOGY OR FORMATION	Number of test	LL (%)				PL (%)				PI (%)			
		Min.	Max.	Mean	SD	Min.	Max.	Mean	SD	Min.	Max.	Mean	SD
Fault gouge	10	34	106	71.2	20.6	19	51	35.2	10.5	15	59	36	14.5
Transition zone	7	41	77	57.6	10.2	26	37	32	3.9	15	43	25.6	8.2
Claystone *	3	42	60	53.3	8	21	34	29	5.7	21	26	24.3	2.4
Turgut formation	5	36	87	68.8	18.2	22	46	34.8	9.6	14	52	34	12.6

* Claystone in the upper levels of main Sekköy formation.

Natural moisture contents of the fault gouges range between the liquid limit and the plastic limit. This indicates that fault gouges are in plastic state. Heave potential may be estimated from index test data. Soils were grouped by Van Der Merwe (1964) into four classes from very high to low potential expansivity. Clay fraction versus plasticity index data of the soils of which Atterberg limits and grain size distributions were determined, were plotted on a graph (Figure 43). Distribution of the plotted data indicates that transition zone deposits and fault materials belong to the categories of low and medium potential expansiveness, respectively. Whereas, fine-grained deposits from Turgut formation have expansivenesses ranging between low and very high.

Skempton (1953) gave quantitative expression to the influence of the clay grade upon plasticity of soils by defining a parameter termed the activity. This is the ratio of the plasticity index to the clay fraction of the soil expressed as the percent dry weight of less than 2 μ fraction. According to the activity classification suggested by Skempton (1953), soils from transition zone and fault gouges are active and normal active soils. Whereas, fine-grained soils of Turgut formation show lower activities. On the other hand, according to Mitchell (1975), the approximate activity values for smectite group, including montmorillonite, range from 1 to 7; for illite 0.5 to 1 and for kaolinite 0.5. The result of the analyses (Figure 43) showed that soil samples rich in kaolinite and illite (Table A.2) had activity values smaller than one or approximately one, whereas increase in montmorillonite resulted in higher activity values ranging between 1.5 and 4.3.

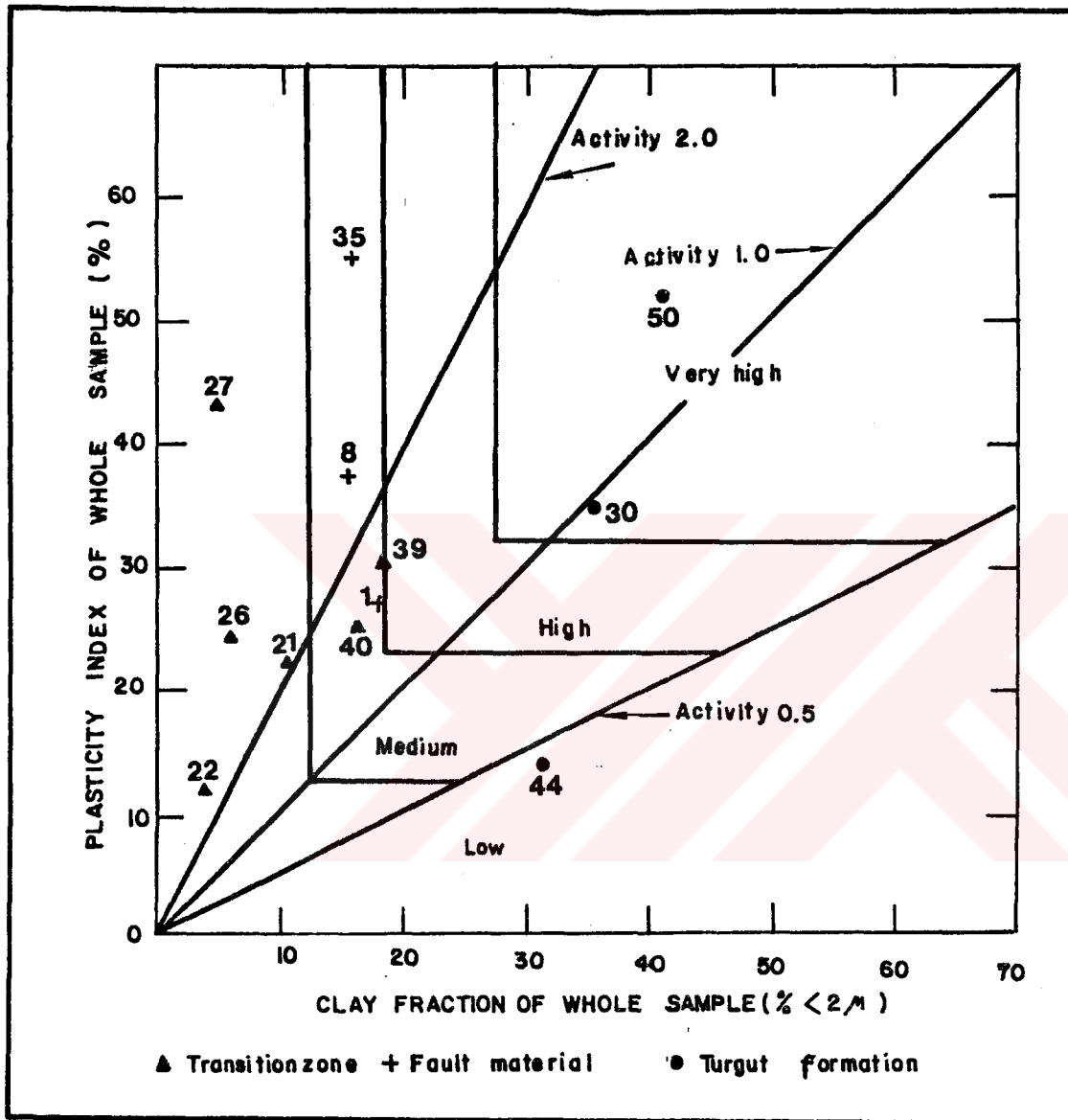


Figure 43: Distribution of soils of the study area on the "Swelling Potential" chart proposed by Van der Merwe (1964).

6.2.3. Grain Size Distributions

In order to investigate the characteristics of the soil materials and to classify them for engineering purposes and shear testing, particle size analyses were carried out. Tests could not be performed on claystones of Sekköy formation because of the very limited quantity of core samples. Based on the basic field identification procedures performed on fine-grained soils with very high plasticity, some of the Atterberg limit samples were not needed for testing. Thus a total 20 samples were selected from different soils for the purpose.

Tests were conducted in two stages consisting of sieve and hydrometer analyses because of the presence of various size grains in the soils. Method of wet mechanical analysis were employed to prevent probable underestimations due to clay and silt proportions. Analyses were carried out using the method suggested by BSI (1975; BS 1377).

The laboratory results are summarized in Table B.2.1. of Appendix B. In addition, some of them are presented in the form of cumulative grain size curves (Figure 44). In order to determine whether the coarse-grained material is well or poorly graded, coefficients of uniformity (C_u) and curvature, (C_c) were also determined for each sand samples (Table B.2.2.).

In general, majority of fault gouges consists of clay and silt fraction. However, a few samples contain large proportion of poorly graded sand size material. These coarse-grained materials belong to rock clasts resulted from faulting.

(B) Sample No.: LB35 (Fault gouge - Clayey SILT; MH-OH)

(C) Sample No.: LB22 (Transition zone - Low plasticity clayey SILT; ML-OL)

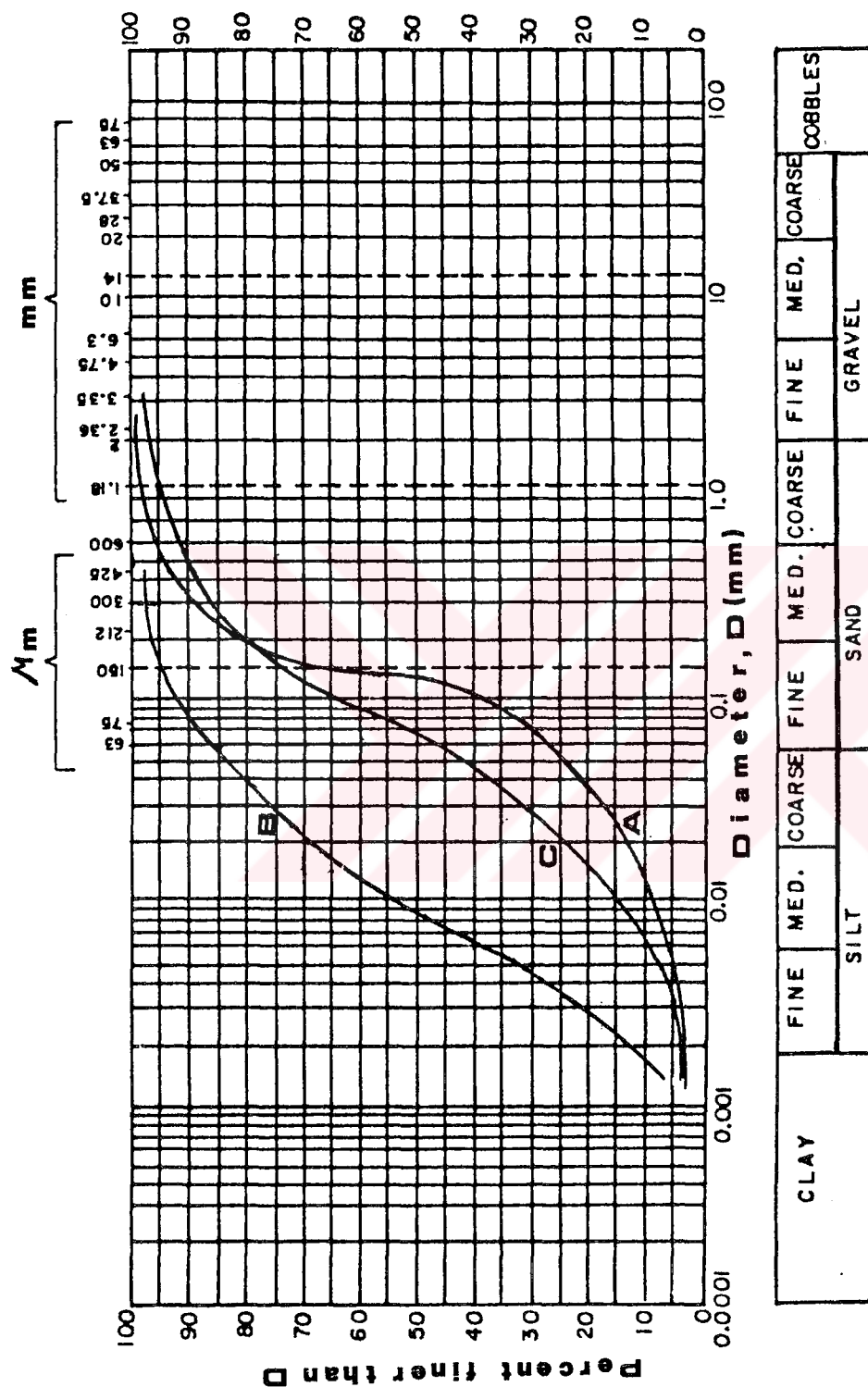


Figure 44: Typical grain size distributions of soil materials of the study area.

Soil samples from transition zone may be considered in two groups. The first group has a significantly higher clay and silt fraction which are the dominant soil type in the zone according to the observations at the site. In the second group soils, which were sampled from thin layers and lenses, sand size grains are dominant with the mixture of silt and clay fraction.

The high percentage of fines were found in the samples taken from the upper zones of Turgut formation which lie just below the coal seam. On the other hand, in the lower levels the materials appear to correspond to reasonably well-graded sands with a relatively small proportion of silt and clay size particles.

A clean sand having both C_u greater than 6 and C_c between 1 and 3 is well graded, otherwise it is a poorly graded sand. According to the values of C_u and C_c given in Table B.2.2. sandy soils are mostly well graded. However, they contain appreciable amount of fines. Therefore, they cannot be accepted as clean sand and their gradation vary between poor and well categories.

6.2.4. Soil Classification

Sorting soils into groups exhibiting similar behaviour is very helpful. Such sorting helps to obtain systematical source of information on probable soil behaviour and guidance for strength test program. Many systems of soil classification for engineering use have been proposed. It appears, however, that the Unified Soil Classification System (UCS) adopted in 1952 by the U.S. Bureau of Reclamation (1974) is the most widely used system. The system is based on the Casagrande's (1948) soil classification for airfield projects.

For the classification purposes, the samples given in Table B.2.1. were divided into two groups with respect to their grain sizes using the 50 percent criterion. With this system the coarse grained soils were classified on the basis of criteria given in Table 8. The fine-grained soils were classified on the basis of plasticity chart using their values of liquid limit and plasticity index (Figure 45).

The soil group symbol of each sample, determined from Table 8 and the plasticity chart, are given in Table B.2.2. Atterberg limits of the majority of 24 samples from the fine-grained soils show a systematic distribution of data points, concentrated around the A line on plasticity chart. About 80% of data points lie within the MH-OH and CH categories. The results indicate that majority of the fine-grained soils in the study area have similar PI/LI ratio and high plasticity. They mainly consist of organic and inorganic clays of medium to high plasticity and micaceous fine clayey silts or elastic silts. About 20% of the samples fall into CL category of inorganic clay of low to medium plasticity. A very small proportion plotting below the A line is in the silt range (ML-OL).

The coarse-grained soils possess the characteristics of the SM category. They mainly consist of poorly-graded sands, silty sands and sand-silt mixtures with a small proportion of clay fraction.

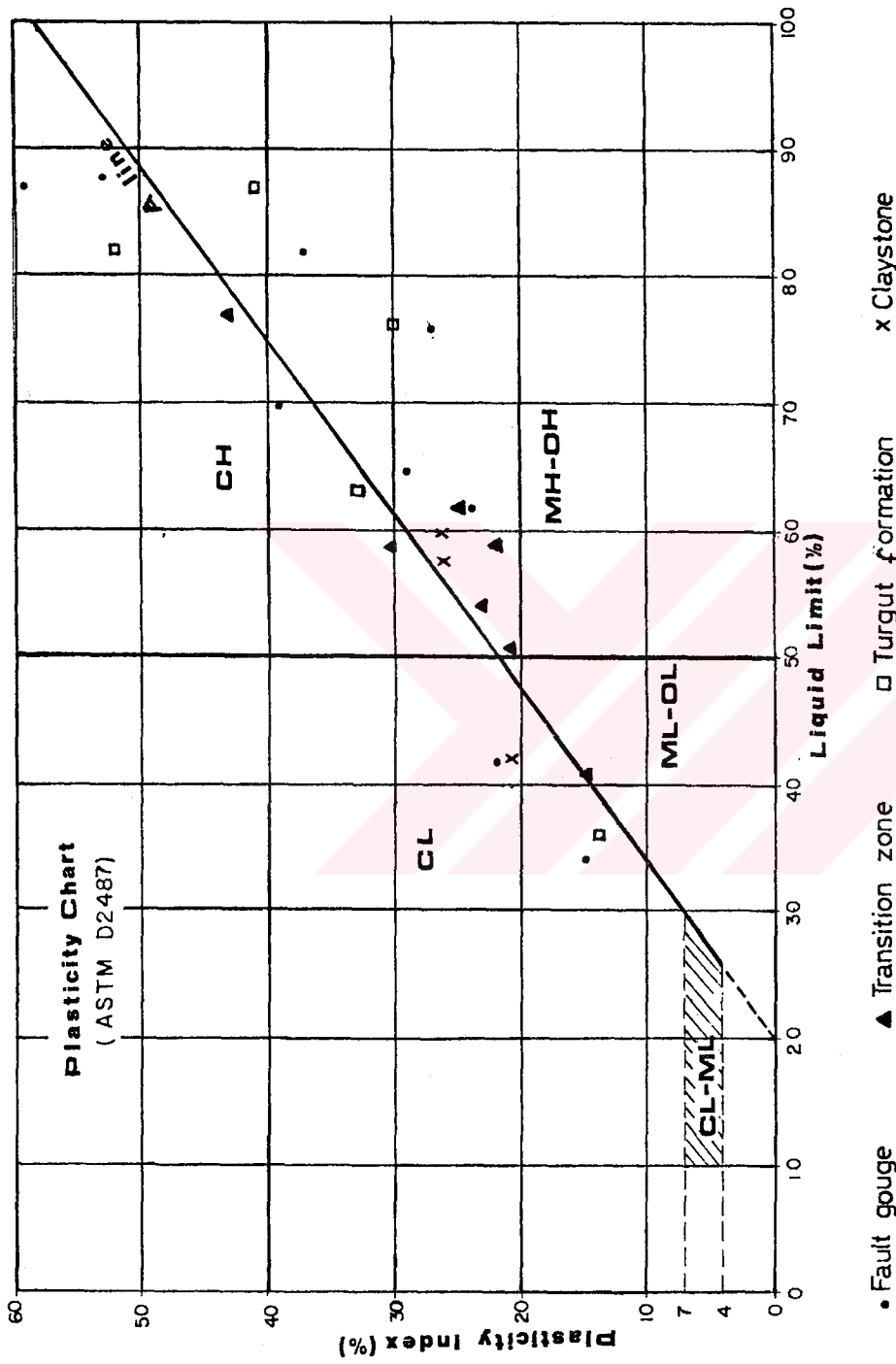
Based on the determined soil groups and engineering use chart (U.S. Bureau of Reclamation, 1974), for the majority of the fine-grained soils of the study area fair to poor shear strengths may be anticipated where they are saturated. Whereas, sands and sand-silt mixtures may probably possess higher strength. On the other hand, the permeability chart involving different soil groups indicates very low permeabilities for the most soils of the site (Figure 46).

Table 8: Unified Soil Classification

Field Identification Procedures (Including particles larger than 3 in. and having fractions on estimated weight)		Group Symbols ^a	Typical Names	Information Required for Describing Soils	Laboratory Classification Criteria
Coarse-grained soils More than half of coarse fraction is larger than No. 4 sieve size More than half of coarse fraction is larger than No. 4 sieve size More than half of coarse fraction is larger than No. 4 sieve size	Gravels More than half of coarse fraction is larger than No. 4 sieve size (For visual classification, the 2 in. size may be used as representative)	GW GP GM GC SW SP SM SC	Well graded gravels, gravel-sand mixtures, little or no fines	Give typical name; indicate approximate percentages of sand and gravel; maximum size; angularity, surface condition, and hardness of the coarse grains; local or regional name; soil use; and symbols in parentheses. For undisturbed soils add information on stratification, degree of compaction, cementation, and drainage characteristics. Example: Silty sand, gravelly; about 20% sand, angular gravel particles 1/4 in. maximum size; rounded coarse sand; about 15% silty plastic fines with low dry strength; well compacted and moist in place; alluvial sand; (SM)	$C_u = \frac{D_{10}}{D_{60}}$ Greater than 4 $C_c = \frac{(D_{30})^3}{D_{10} \times D_{60}}$ Between 1 and 3 Not meeting all gradation requirements for GW Atterberg limits below "A" line, or <i>Pf</i> less than 4 Atterberg limits above "A" line, with <i>Pf</i> greater than 7 $C_u = \frac{D_{10}}{D_{60}}$ Greater than 6 $C_c = \frac{(D_{30})^3}{D_{10} \times D_{60}}$ Between 1 and 3 Not meeting all gradation requirements for SW Atterberg limits below "A" line, or <i>Pf</i> less than 5 Atterberg limits below "A" line, with <i>Pf</i> greater than 7
	Sands More than half of coarse fraction is smaller than No. 4 sieve size (For visual classification, the 2 in. size may be used as representative)		Poorly graded gravels, gravel-sand mixtures, little or no fines Silty gravels, poorly graded gravel-sand-silt mixtures Clayey gravels, poorly graded gravel-sand-clay mixtures Well graded sands, gravelly sands, little or no fines Poorly graded sands, gravelly sands, little or no fines Silty sands, poorly graded sand-silt mixtures Clayey sands, poorly graded sand-clay mixtures		
Fine-grained soils More than half of material is smaller than No. 200 sieve size (The No. 200 sieve size is about the smallest particle visible to naked eye)	Identification Procedures on Fraction Smaller than No. 40 Sieve Size Dry Strength (Crushing consistency near plastic limit) Dilatancy (reaction to shaking) Toughness (consistency near plastic limit)	ML CL OL MH CH OH PI	Inorganic silts and very fine sands, rock flour, silty or clayey fine sands with slight plasticity Inorganic clays of low to medium plasticity, gravelly clays, sandy clays, silty clays, lean clays Organic silts and organic clays of low plasticity Inorganic silts, amaceous or silty, silty, sandy or silty clays, silty clays Inorganic clays of high plasticity Organic clays of medium to high plasticity Peat and other highly organic soils	Give typical name; indicate degree of plasticity of soil; amount and maximum size of coarse grains; colour in wet condition, odour if any, local or geologic name, and other pertinent descriptive information, and symbol in parentheses. For undisturbed soils add information on structure, stratification, consistency in undisturbed and remoulded states, moisture and drainage conditions. Example: Clayey silt, brown; slightly plastic; small percentage of fine sand; numerous vertical root holes; firm and dry in place; (ML)	Use grain size curve in identifying the fractions as given under field identification Determine percentages of gravel and sand from grain size Depending on percentage of fines (fraction smaller than No. 200 sieve size) coarse grained soils are classified as follows: Less than 5% More than 5% to 12% More than 12% to 50% 50% to 75% 75% to 100% Borehole cases requiring use of dual symbols Comparing soils at equal liquid limit Highest and dry strength increase with increasing plasticity index Liquid limit Plasticity chart for laboratory classification of fine grained soils

^a Boundary classifications. Soils possessing characteristics of two groups are designated by combinations of group symbols. For example GW-GC, well graded gravel-sand mixture with clay binder.
^b All sieve sizes on this chart are U.S. standard.

* After Wagner (1957; in Lambe and Whitman, 1969)



Number of tests: 25 (LL > 100 for LB 35-not plotted on the chart)

Figure 45: Distribution of fine-grained soils of the study area on the plasticity chart.

k (cm/s)	10 ²	10	1.0	10 ⁻¹	10 ⁻²	10 ⁻³	10 ⁻⁴	10 ⁻⁵	10 ⁻⁶	10 ⁻⁷	10 ⁻⁸	10 ⁻⁹
DEGREE OF PERMEABILITY	PERVIOUS		GOOD DRAINAGE				POOR DRAINAGE		PRACTICALLY IMPERVIOUS			
TYPE OF SOIL	CLEAN GRAVEL		CLEAN SANDS, CLEAN SAND-GRAVEL MIXTURES				Fine sands, organic and inorganic silts, silt clay mixtures bedded clay			HOMOGENEOUS CLAY		
U.S.C GROUP SYMBOL	GP	GW	SP	SW		GM	SM	SC		CL	CH	OH
DIRECT DETERMINATION OF PERMEABILITY COEFFICIENT	In-situ pumping test											
	Constant head test											
	Falling head test											

Figure 46: Graphical presentation of coefficients of permeability values of different types of soils and the methods of determination of permeability (Rearranged from Jumikis, 1967 and Kezdi, 1974).

Materials or formations possessing soil characteristics were engineering geologically described in accordance with the information yielded from index tests and soil classification:

- a) Fault gouges : These materials contain small proportion of rock clasts in a matrix of olive and light gray, highly plastic clay, rich in montmorillonite, and inorganic elastic silt that locally can be tan-brown due to limonites. The rock clasts, which are in sand or fine gravel, have a floating texture where they are not in contact with each other.

- b) Transition zone soils : This zone is mainly composed of olive and greenish gray micaceous clays and inorganic clayey silts of high plasticity. However, well-to-poorly graded, moderately packaged olive and gray silty sands are also included in the form of pockets, lenses and unpersistent levels.

- c) Deposits of Turgut formation : On the basis of information available from the shallower levels of this formation micaceous, highly plastic, gray and black clays and elastic silts are present just below the coal seam. Below these fine-grained levels, medium to dense, dark gray silty sands and silt-sand mixtures take place in the alternating form with clays and silts.

- d) Claystone : This lithology, in the upper levels of main Sekköy formation behaves as a soil material. It is composed of grayish olive, highly plastic, homogeneous, thinly-bedded clay. It becomes softer when it comes into contact with water.

6.2.5. Slake Durability Index

Many rock materials, notably those with a high content of clay minerals, are prone to slaking. This is the property of an unconfined, undisturbed sample of rock or soil to swell, weaken and disintegrate when subjected to drying and rewetting. It is important from the material behaviour point of view in a slope.

Slake durability index determinations were carried out on marl samples collected from geotechnical boreholes, according to the method suggested by ISRM (1981). The test results (Table B.3), indicate that values of slake durability index (I_{d2}) are very similar. The mean durability index is calculated to be 93.6% with a standard deviation of 2.2. The rock unit has a high slake durability according to Franklin and Chandra's (1972) durability classification.

6.3. Intact Rock Strength

If the discontinuities are not critically oriented but the rock substance is weak, instability may occur through shearing of the intact material. The strength of jointed rock masses in nature lie between the strength parameters of the intact rock substances and the strength of discontinuities. On the other hand, intact rock strength is a most useful index parameter directly and indirectly used in many classification systems of rock substance (Coates, 1964; Deere and Miller, 1968; Stapledon, 1968; Geological Society of London, 1970; Broch and Franklin, 1972; Jennings et al., 1973) and rock mass (Bieniawski, 1973; Barton et al., 1974). Thus, to achieve these objectives, extensive laboratory work including uniaxial and triaxial tests were carried out on intact rock specimens to determine their mechanical behaviour.

6.3.1. Uniaxial Compressive Strength

This method of test is intended to measure the uniaxial compressive strength of a rock sample in the form of specimens of regular geometry. The test is mainly intended for strength classification and characterization of intact rock (ISRM, 1981).

In accordance with the suggested procedures of ISRM (1981), specimens of intact core samples from different rock units were prepared and then tested using the motorized compression machine with 150 ton loading capacity. Loading was controlled by means of load pacing unit. Load on the specimen was applied continuously at a constant stress rate such that failure would occur within 5-10 minutes of loading.

At least five specimens were tried to be tested from each rock unit depending upon the availability of cores of convenient size for the test. But, only three tests could be performed on the limestone. Because only a few cores of limestone were collected from two boreholes. Besides, fractures and small cavities were resulted in sample losses during sample preparation. Problem was also faced on lignite cores, due to their rapid drying and ravelling.

Totally 72 core samples with a diameter of 47.6 mm were tested. The measured uniaxial compressive strengths of the tested samples are tabulated in Table 9 and graphically presented as the frequency versus strength histograms with statistical parameters for three rock units (Figure 47).

It is seen that, conglomerate and limestone of the detrital facies have the highest and weak sandstone at very shallow depths has the lowest compressive strength

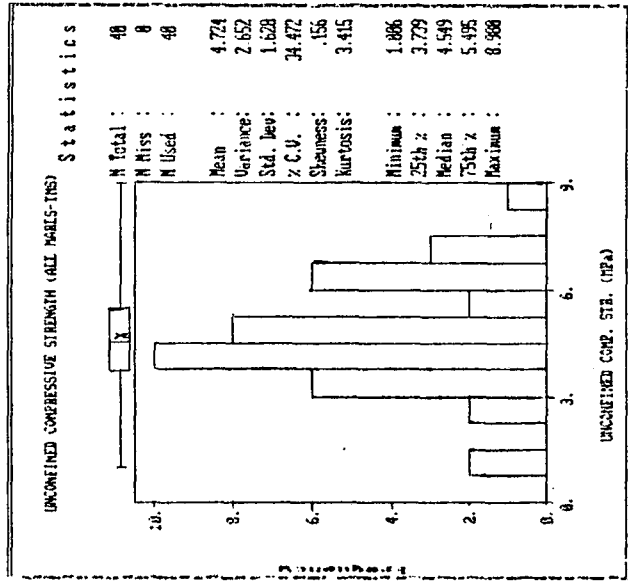
Table 9 : Uniaxial compressive strength values of various rock types of the study area

Rock Type	Range (MPa)		MPa*	Mean (X) kgf/cm ²	Standard Deviation (MPa)	Number of test
	Min.	Max.				
Weak Sandstone (Tmy)	1.15	2.64	1.70	17.36	0.66	5
Hard sandstone (Tmy)	6.21	10.72	9.04	92.21	1.68	6
Limestone (Tms ¹)	20.00	29.80	25.03	255.23	4.91	3
Conglomerate (Tms ¹)	14.30	52.60	30.83	314.32	13.94	8
Laminated marl (Tms)	1.14	6.41	4.15	42.27	1.62	10
Compact marl (Tms)	1.01	8.98	4.92	50.13	1.61	30
All marls (Tms)*	1.01	8.98	4.72	48.17	1.63	40
Lignite	7.00	11.90	9.06	92.34	1.37	10

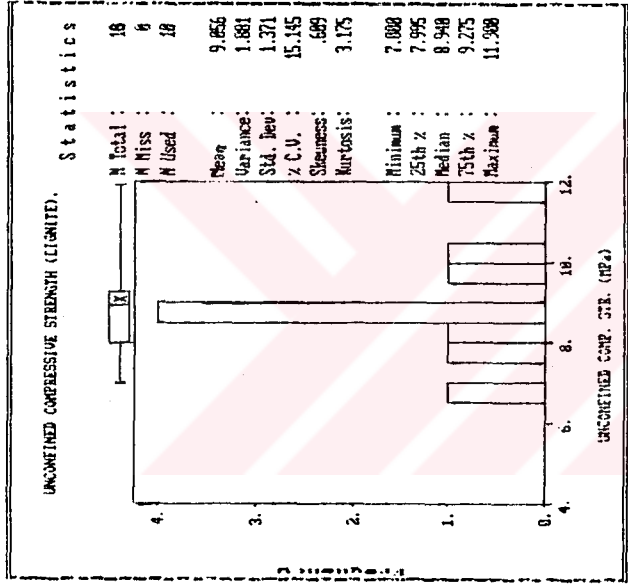
* 1MPa = 10.197 kgf/cm²

• Includes laminated and compact marls

a



b



c

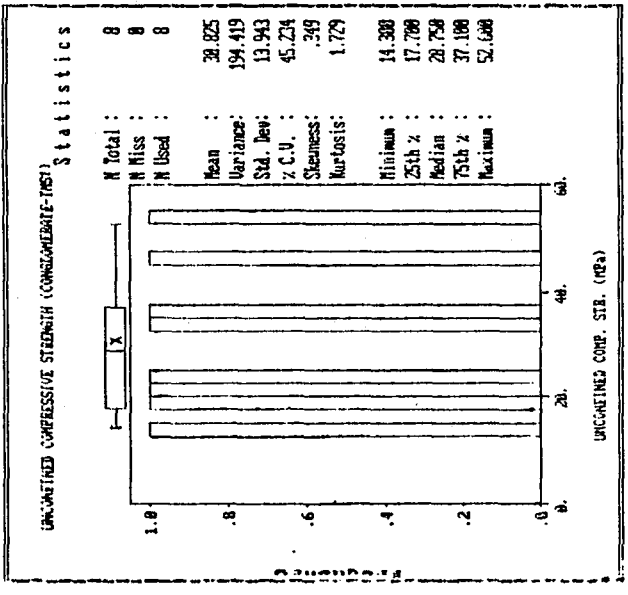


Figure 47: Uniaxial compressive strength histograms of marl(a), lignite(b) and conglomerate(c).

(Table 9). Strength of the sandstone increases with depth where the effects of weathering is negligible. No significant differences between the strengths of laminated and compact marls were noted. Therefore, their strengths were assessed in the same group (Figure 47A). On the other hand, conglomerates indicate high standard deviation value than the other types of rock. This probably resulted from different ranges of weakening due to small cavities and the limited data for statistics. These results show that the uniaxial compressive strength of each rock unit with the exception of conglomerate and limestone are distributed in an approximately normal forms (Figure 47).

6.3.2. Classification of Intact Rock

Classification of intact rock deals with the material removed from its environment and devoid of discontinuities. Rock units of the study area were classified according to the strength classification system for rock substance proposed by Deere and Miller (1966). This covers almost the complete range of the rocks met in mining and civil engineering and is based on both the strength and deformation characteristics of the rock. In this study, the classification based upon uniaxial compressive strength was used (Table 10 a).

The classification (Table 10 b) indicates that the majority of the rock units, also including lignite, lie within the E category rocks with very low strength. However, limestone and conglomerate are classified as low strength rocks.

Table 10 : Strength classification for rock units of the study area

a) Strength classification for rock substance (after Deere and Miller, 1966)

Class	Description	Uniaxial Compressive Strength (MPa)
A	Very high strength	>200
B	High strength	100-200
C	Medium strength	50-100
D	Low strength	25-50
E	Very low strength	<25

b) Strength classes for the rock units

Rock unit	Class
Weak sandstone (Tmy)	E
Hard Sandstone (Tmy)	E
Limestone (Tms ¹)	D
Conglomerate (Tms ¹)	D
Marl (Tms)	E
Lignite	E

6.3.3. Shear Strength of Intact Rock

The cohesion and internal friction angle for coal measures rock types of the study area were evaluated on 27 test sets by triaxial tests. The machined intact core specimens of 47.6 mm (NQ) diameter were tested by a technique described by ISRM (1981).

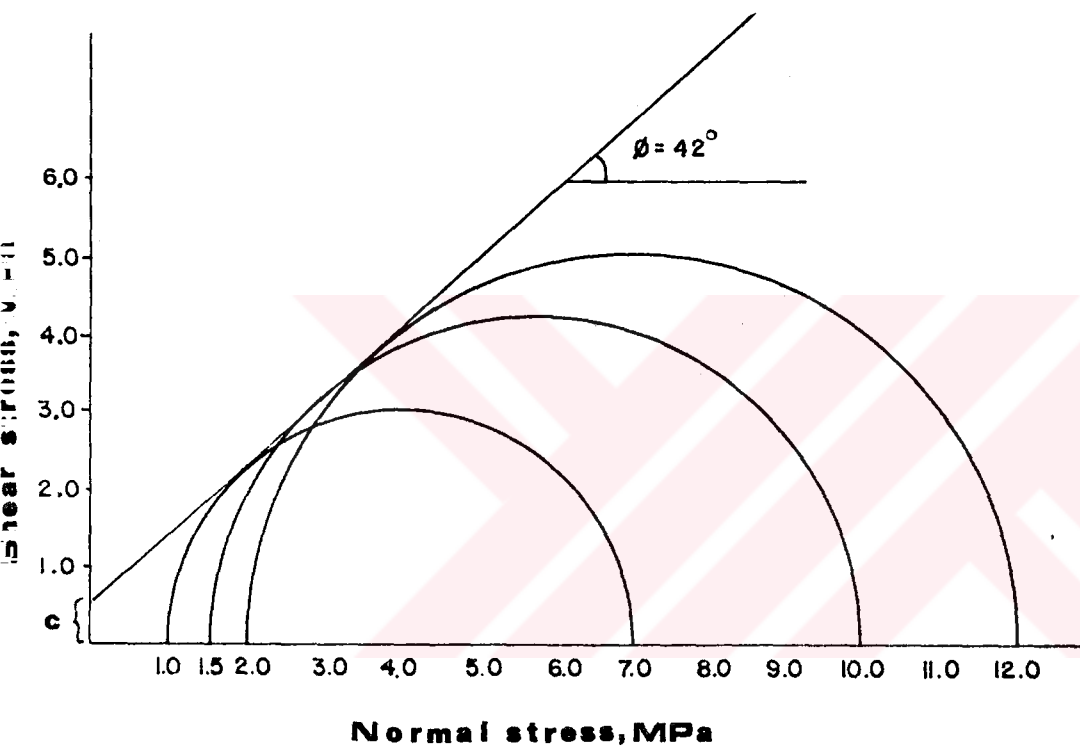
In spite of the specimen losses of the limestone and lignite cores at least two test sets consisted of three specimens for each rock unit were prepared. The tests were carried out at different confining pressures. The minimum confining pressure applied is 1 MPa. The confining pressures ranging between 1 to 3 MPa were selected. Loading was performed in a Hoek triaxial cell. Specimens from the sandstone were tested in three groups on the basis of their degree of weathering.

The shear strength of each sample was determined from the graphical Mohr circle method as the intercept of each failure envelope with the shear stress axis. Figure 48 shows a family of Mohr's circles for failure stress of a sandstone sample. The confining pressure (σ_3) and the corresponding axial stress value (σ_1) for each specimen with the derived strength data and statistical evaluations are given in Table B.4 of Appendix B and Table 11, respectively.

Test results indicated that sandstone in each category has more uniform strength parameters than those of others, probably due to their homogeneous nature. Majority of marls also show similar strength parameters amongst themselves. Variations in strength parameters of limestone and conglomerate may be explained by factors such as the presence of small cavities, weathering effects and the presence of different blocks of which strength properties are not uniform.

Sample No. : JT9 / 11, 12_1, 12_2

Rock type : Moderately weathered SANDSTONE



c (Cohesion) = 0.6 MPa

ϕ (Internal friction angle) = 42°

Figure 48: Typical Mohr circles and failure envelope for an intact sandstone sample representing Yatağan formation.

Table 11 : Shear strength parameters of rock substances of the study area

Rock Type	Cohesion, c (MPa)			Internal friction angle, ϕ (degrees)			Number of test sets
	Min.	Max.	Mean SD	Min.	Max.	Mean SD	
SANDSTONE-moderately weathered, weak	0.6	1.0	0.83 0.17	42	42.5	42.2 0.23	3
SANDSTONE-slightly weathered, medium hard	0.3	1.75	0.73 0.6	49	55	52.3 2.38	4
SANDSTONE-unweathered, well cemented	2.5	4.5	3.71 0.75	35	64	47.8 10.50	4
CONGLOMERATE-including very small solution cavities and occasionally lichenitised	3	9	5.23 2.21	48	61	55.2 5.56	5
LIMESTONE-including very small solution cavities fractured and moderately weathered	2	7.3	4.65 2.65	54	55	54.5 0.50	2
MARL	1.3	2.6	1.97 0.54	19	37	27.1 6.25	7
LIGNITE	3.75	3.8	3.78 0.02	16	18	17 1	1

SD : Standard deviation.

6.4. Shear Strength of Discontinuities

6.4.1. Shear Strength Characteristics of Joints

Systematic and easily sampled joints were developed in the main Sekkőy formation. From the stability point of view, it is obvious that this formation, forming the largest part of the excavation, will maintain its importance during the life of the pit. Thus, shear strength determinations of joint surfaces were performed on the jointed samples taken from this formation.

Taking into consideration the highly steep dips of the joints the anticipated full range of in-situ normal stresses acting on these discontinuities in a highwall or bench will vary between a few tens and/or hundreds kPa, respectively. It is also noted (Barton, 1973) that low normal loads encompass almost all slope and dam problems when compared to the underground structures. Thus, it was considered to be essential that this condition should be duplicated in the laboratory.

On the basis of author's experience, the loads applied by the portable shear box apparatus, which is most commonly used in practice, produce normal loads higher than those produced in-situ. The smallest division of the loading gauges mounted on the box is equal to 1MPa. Therefore, it would unquestionably have resulted in more severe damage to the weakness surfaces, particularly for discontinuity surfaces, in marls, as being in this case.

In this study, the general requirements for direct shear test apparatus and testing method clearly set out in the relevant ISRM (1981) procedure was followed. The author believes that these requirements may be achieved with

soil shear machine because of its adequate loading capacity and strain control facilities without any significant difficulty or loss of accuracy. It also provides to determine the residual shear strength parameters which are more important for stability assessments.

Motorised direct/residual soil shear test device with shear box assembly was used for testing. Specimens from block samples were cut to size to fit the shear box of 6x6x2 cm dimensions and then set into two halves of shear box. Difficulties were faced in preparing intact joint samples because the specimens tended to break along the bedding or lamination planes and totally six representative specimens could be prepared for the tests.

Testing can be carried out by either single or multistage procedures (Udd and Pakalnis, 1979; Hencher and Richards, 1989). In this study, single stage procedure in which each sample is sheared at a constant normal load was preferred. Barton (1973) pointed out that the presence of water was found to reduce the shear strength of rough infilled joints, but hardly to affect the strength of planar surfaces. Some of the instabilities in this pit were known to have occurred after periods of precipitation. Thus, tests on wet surfaces were required and water was introduced from the shear box using a squeeze bottle. Tests were carried out with multiple reversals and strain controlled to achieve residual values.

Rates of shearing below a few millimeters per minute do not affect test results as a rule (Hencher and Richards, 1989). Some investigators (Schneider, 1978; Hencher, 1981; Gillette, et.al, 1983) showed that very high rates of shearing may give different strengths. Therefore the rate of shear displacement of 1 mm per minute was applied and the displacement was continued to a travel about 15% of the specimen length (ISRM, 1981).

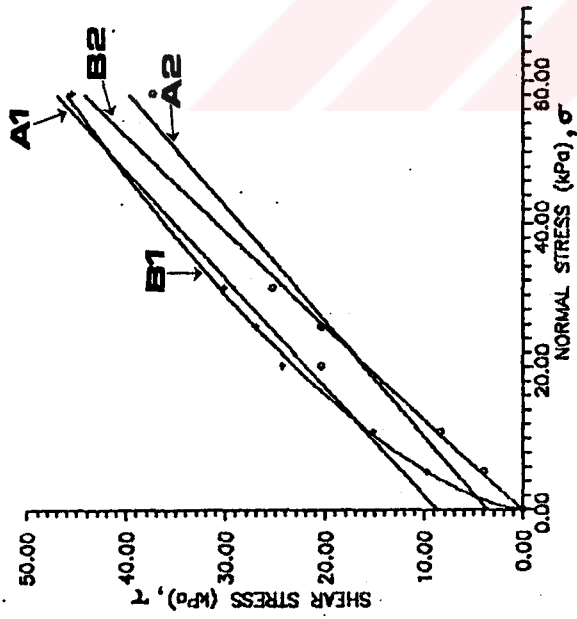
Reading from the displacement and shear force gauges were evaluated to calculate the strengths using the computer programs named SHEAR and REVERSE developed by the author (Appendix E.1). The values of peak and residual shearing stresses which were obtained for all of the tests are plotted in Figure 49a and given in Table B.5 of Appendix B. The results display little scattering.

In the statistical analysis of the data, both linear and power curve (geometric regression) relationships, which fitted to the experimental results best, were derived. Statistical analyses and plotting of the failure envelopes were performed using a conventional statistical computer packaged named GRAPHER (Golden Software Inc., 1986). In both cases very high coefficients of correlation were obtained (Table 12).

During the tests no dilation was noted. Residual shearing was achieved to the last stage of the forward positions for each specimen. This situation is illustrated for some specimens in the form of graphs showing shear stress versus shear displacement in Figure 49b. These plots indicate the behaviour of clean and/or thinly coated joints. For this type of joints shear strength rises to a clear peak followed by a steady decline to an almost constant (residual) value with shear displacement (Papaliangas, et. al., 1990). Thus, the displacement plots also confirm the surface features of the joints.

Many investigators (Udd and Pakalnis, 1979; Hassani and Scobie, 1982; Udd and Betournay, 1983; Hencher and Richards, 1989; Singh and Gahrooe, 1989) indicate that a persistent, clean, smooth and planar discontinuity (not dilating) will show a purely fractional resistance proportional to normal stress. However, Hencher and Richard (1989) also pointed out that cohesion may result due to secondary mineral coatings forming chemical bonds across the surface. This conclusion

a) Failure envelopes



Peak Residual

Linear relationship: (A1) $\tau = 8.71 + 0.6587\sigma$ (A2) $\tau = 3.65 + 0.619\sigma$

Power curve: (B1) $\tau = 3.298\sigma^{0.648}$ (B2) $\tau = 0.865\sigma^{0.968}$

b) Shear stress - displacement curves

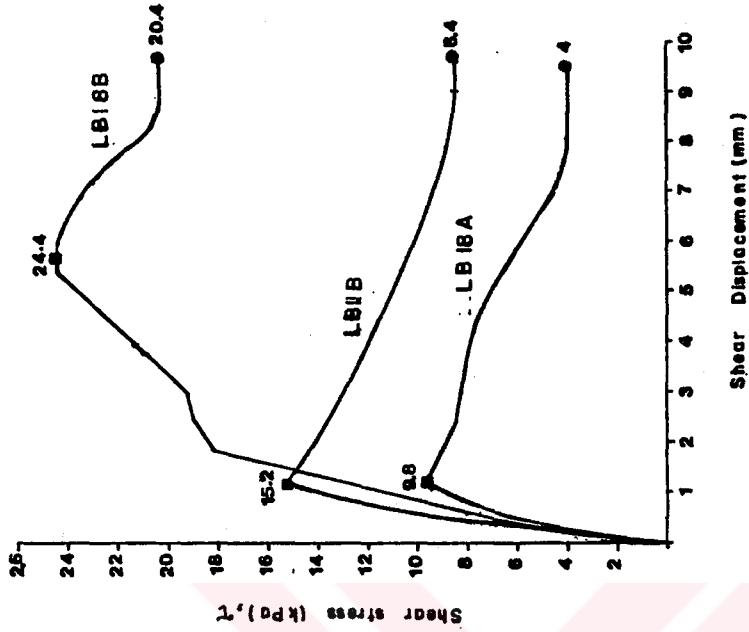


Figure 49: Shear failure envelopes and typical shear stress-shear displacement graphs for smooth-planar joints developed in main Sekkōy formation.

Table 12 : Results obtained from the analyses of laboratory shear tests on discontinuities and soil samples.

DISCONTINUITY/SOIL TYPE		LINEAR REGRESSION ($\tau=c+\tan\theta\sigma$)				GEOMETRIC REGRESSION ($\tau=A\sigma^B$)		
		θ (degree)	c (kPa)	(*) r	Shear Strength	Shear Strength	$\tan\theta$	(*) r
FAULT GOUGE	(Peak)	25.97	18.11	0.902	$\tau=18.11+0.4872\sigma$	$\tau=1.957\sigma^{0.767}$	$1.5\sigma^{-0.233}$	0.902
	(Residual)	17.56	9.73	0.896	$\tau=9.73+0.3164\sigma$	$\tau=0.901\sigma^{0.829}$	$0.746\sigma^{-0.171}$	0.927
BEDDING SURFACES (Smooth-planar)	(Peak)	36.19	22.96	0.963	$\tau=22.29+0.7316\sigma$	$\tau=2.232\sigma^{0.819}$	$1.828\sigma^{-0.181}$	0.97
	(Residual)	26.48	12.51	0.926	$\tau=12.51+0.4982\sigma$	$\tau=0.711\sigma^{0.959}$	$0.682\sigma^{-0.041}$	0.96
JOINT SURFACES (smooth-planar)	(Peak)	33.4	8.71	0.977	$\tau=8.71+0.6587\sigma$	$\tau=3.298\sigma^{0.648}$	$2.137\sigma^{-0.352}$	0.981
	(Residual)	31.8	3.65	0.969	$\tau=3.65+0.619\sigma$	$\tau=0.865\sigma^{0.968}$	$0.837\sigma^{-0.032}$	0.984
BEDDING SURFACES (LB47) (Transition between undulating and smooth)	(Peak)	43.97	5.98	0.978	$\tau=5.98+0.9646\sigma$	$\tau=2.24\sigma^{0.823}$	$1.843\sigma^{-0.177}$	0.976
	(Residual)	30.02	3.05	0.988	$\tau=3.05+0.5778\sigma$	-	-	-
BEDDING SURFACES (Undulating-planar)	(Peak)	-	-	-	-	$\tau=1.757\sigma^{0.908}$	$1.595\sigma^{-0.092}$	1
	(Res.)	33.56	0	0.989	$\tau=0.6635\sigma$	-	-	-
TRANSITION ZONE (Tms ² -fine material)**	(Peak)	26.96	50.07	0.956	$\tau=50.07+0.5085\sigma$	$\tau=13.76\sigma^{0.447}$	$6.15\sigma^{-0.553}$	0.953
	(Residual)	22.52	4.93	0.972	$\tau=4.93+0.4146\sigma$	$\tau=1.076\sigma^{0.818}$	$0.88\sigma^{-0.182}$	0.951
TURBUT FORMATION (Black clay-LB48)	(Peak)	24.71	7.59	0.979	$\tau=7.59+0.4601\sigma$	$\tau=2.15\sigma^{0.683}$	$1.468\sigma^{-0.317}$	0.973
	(Residual)	17.21	0	0.998	$\tau=0.3097\sigma$	$\tau=0.302\sigma$	0.302	0.998
TURBUT FORMATION (Fine material)**	(Peak)	28.90	34.30	0.981	$\tau=34.30+0.5521\sigma$	$\tau=5.755\sigma^{0.606}$	$3.487\sigma^{-0.394}$	0.947
	(Residual)	20.98	0	0.920	$\tau=0.383\sigma$	$\tau=0.374\sigma$	0.374	0.963
CLAY (Main Sekkøy form.)	(Peak)	22.76	15.86	0.992	$\tau=22.76+0.4197\sigma$	$\tau=1.811\sigma^{0.756}$	$1.369\sigma^{-0.244}$	0.97
	(Residual)	14.39	7.96	0.95	$\tau=7.96+0.2566\sigma$	$\tau=1.748\sigma^{0.654}$	$1.143\sigma^{-0.346}$	0.94

r(*) Coefficient of correlation.

** Clay and silt size material.

c Cohesion.

θ Internal friction angle.

A,B Constants expressing the shape of the curve.

is also valid for the joint surfaces investigated in this case, due to the existence of very thin coating.

On the other hand, the envelopes (see Figure 49a) become closer at normal stresses of about greater than 20 kPa which corresponds to a bench height of 7 to 8 m. This suggests that there will be no important difference in using shear strength parameters derived from linear relationship.

6.4.2. Shear Strength Characteristics of Bedding Surfaces

Shear strength determinations of bedding surfaces were conducted on two groups on the basis of surface asperities. Planar and smooth surfaces from the main Sekköy formation were included in the first group. In the second group, undulating planar surfaces from limestone were tested using the combination of experimental and empirical methods. Unfortunately, suitable specimens of coal from the limited block samples could not be prepared due to the crumbly nature of the coal.

6.4.2.1. Shear Strength of Smooth-Planar Bedding Surfaces

Totally 39 specimens were prepared from 8 different block samples of laminated and compact marls. Bedding surfaces tested were partly very thinly coated with fine material and partly fresh with no evidence of gouge infill. The tests were carried out on 8 test sets consisting of minimum of 4 specimens of each to achieve representative failure envelopes for each set. The same methodology and testing equipment previously mentioned for the joints were also used for the bedding surfaces.

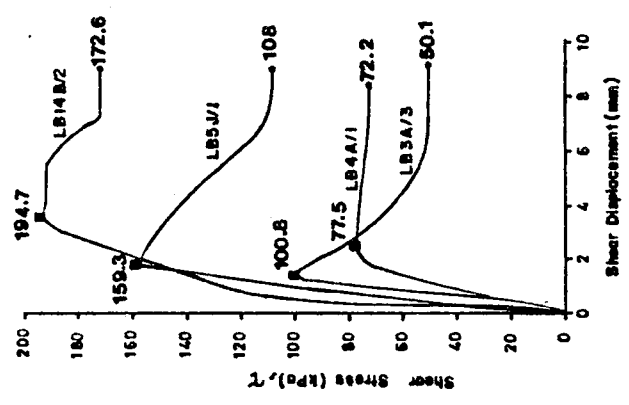
Test results were obtained on samples that were sheared after their surfaces were made wet. In addition, sample LB4 was tested under dry condition to compare the effects of wet and moist conditions on the shear strength. The special tests on sample LB4 yielded that peak cohesion values were 71 kPa and 23.3 kPa for dry and moist surfaces, respectively. These results from adjacent specimens, both at dry and moist conditions, indicated that moisture causes a sharp reduction in the cohesive forces in marl. Cavounidis and Sotiropoulos (1979) and Fazio and Tommasi (1990), who performed shear tests on marls and interbedded marly layers and obtained similar results, argued that saturation or moist results in a large reduction in peak shear strength because of marl's strain softening property. Taking into consideration this effect and site conditions, it was concluded that the shear strength parameters determined under moist conditions would be more realistic for this case.

The test results and the shear strength parameters from the failure envelopes based on the linear regression analysis are summarized in Table B.6 of Appendix B. Statistical analysis of the shear strength parameters are as follows :

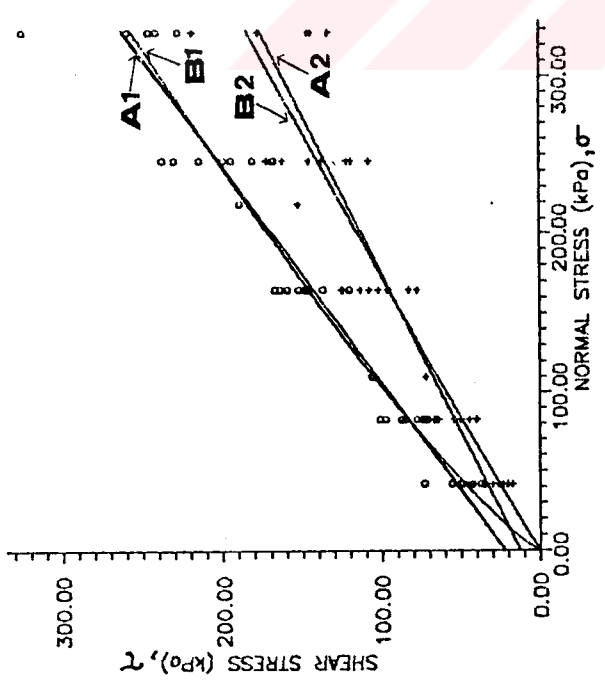
Peak Shear Strength				Residual Shear strength			
Cohesion, c_p (kPa)		Internal friction angle, ϕ_p (degree)		Cohesion, c_r (kPa)		Internal friction angle, ϕ_r (degree)	
Mean	SD	Mean	SD	Mean	SD	Mean	SD
21.68	8.23	36.23	4.07	11.42	9.04	26.32	4.40

Referring to the results, it can be stated that there is a close agreement between the shear strength properties of the samples. Thus, to obtain general failure envelopes of peak and residual strength representing bedding surfaces, all data were plotted on a single σ - τ graph (Figure 50a). Both linear and power curve relationships were fitted to the

b) Shear stress - displacement curves



a) Failure envelopes



Linear relationship : (A1) $\tau = 22.29 + 0.7316 \sigma$ (A2) $\tau = 2.51 + 0.4982 \sigma$
 Power curve : (B1) $\tau = 2.232 \sigma^{0.819}$ (B2) $\tau = 0.711 \sigma^{0.959}$

Figure 50: Shear failure envelopes and typical shear stress-shear displacement graphs for smooth-planar bedding surfaces developed in main Sekkōy formation.

experimental data with very high coefficients of correlation. Although the fitting of power curves yielded coefficients of correlation 1-3% higher than those of linear fit, these two types of curve fit into one another at normal stress level of 100 kPa. This lower stress level corresponds to in-situ conditions, such as a cut of 6 to 7 m high which is the lower bound engineering range encompassing for the slopes under investigation. Thus, it is concluded that the linear failure envelope may confidently be used in slope stability assessments.

Majority of the test specimens reached the residual values at the end of first forward motion of the shear box. However, fewer specimens required greater displacements through multiple reversals to reach residuals. As reported by Fazio and Tommasi (1990), this was probably caused by the progressive reorientation of the scales along the shear plane. Shear stress-shear displacement graphs of some specimens illustrated in Figure 50b, reflect the behaviour of smooth-planar surfaces (Papaliangas, et al., 1990). Referring again to Figure 50b, residual strength of these bedding planes will be mobilized after a short period of time with considerable small displacement. This result is also supported by the studies of Barton (1973) on weakest rock discontinuity surfaces.

6.4.2.2. Shear Strength of Undulating-Smooth Bedding Surfaces

Both undulations and smaller-scale roughnesses contribute to frictional resistance to sliding. Because of this, the value for the angle of friction is comprised of two components. The components (ϕ_b) and (i) are usually termed the base friction angle and the effective roughness for undulating surfaces. Because of the difficulties that

were encountered in obtaining suitable samples from limestone, it was decided that shear strength would be determined by using the empirical shear strength criterion for rock discontinuities proposed by Barton (Barton, 1973; Barton and Choubey, 1977). This criterion is given by the following equation;

$$\tau = \sigma_c \tan [JRC \log_{10}(JCS/\sigma_n) + \phi_b]$$

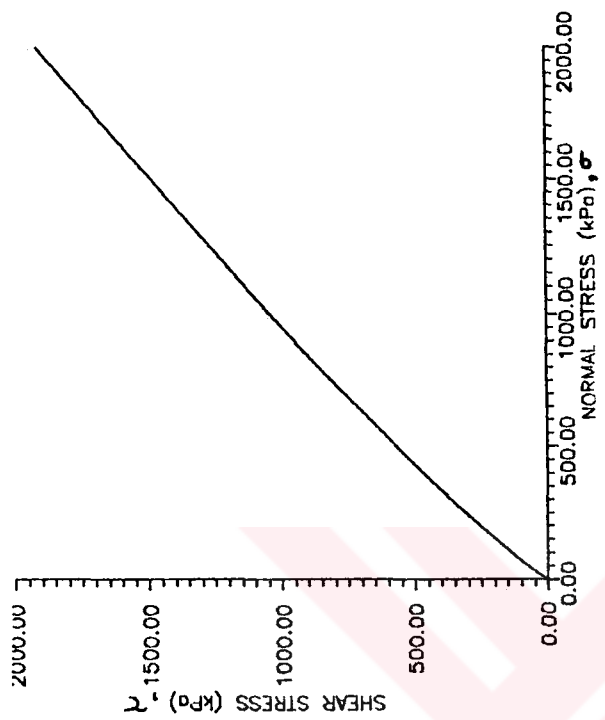
where

- τ : peak shear strength
- σ_n : normal stress
- JRC : joint roughness coefficient
- JCS : joint wall compressive strength
- ϕ_b : base friction angle

Determination of the parameter ϕ_b was carried out on smooth and planar surfaces (Barton and Choubey, 1977; Hoek and Bray, 1977). For the purpose, six artificially produced smooth and planar surfaces from the limestone blocks (LB54) were prepared by means of a smooth diamond saw cut. Following the standard procedures the shearing strengths for a range of applied loads were determined. The results are shown in Table B.7 and Figure 51a. The failure envelope was found to be linear indicating that the basic friction angle was 33.5°. This quantity falls into the range of ϕ_b values for most smooth unweathered rock surfaces which lie between 25° and 35° (Barton and Choubey, 1977).

The mean values of the parameters appearing in the above equation,

$$JRC = 36.6 \text{ MPa}; JCS = 6; \phi_b = 33.5^\circ$$



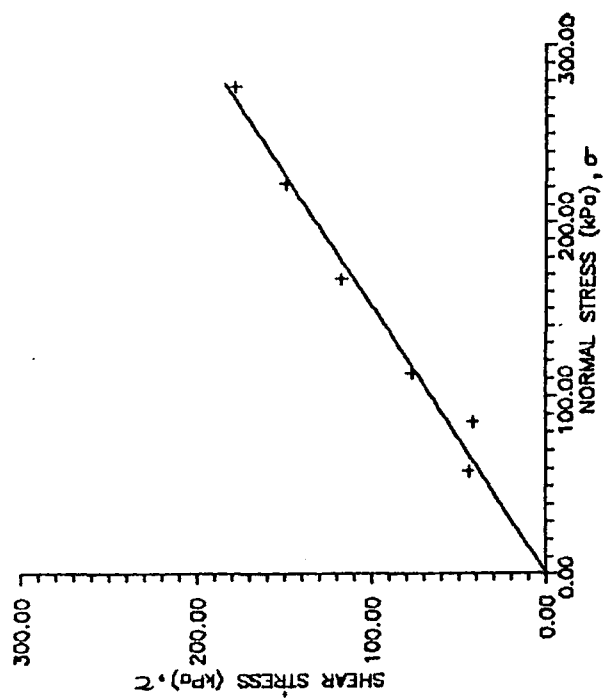
$$\tau = \sigma \tan \left[JRC \log_{10} \left(\frac{JCS}{\sigma} \right) + \phi_b \right]$$

JRC = 6, JCS = 36.6, $\phi_b = 33.5^\circ$

$$\tau = 1.757 \sigma^{0.908}$$

$\tan \phi = 1.595 \sigma^{-0.092}$, $r = 1.0$

(r : coefficient of correlation)



$$\tau = 0.6635 \sigma \quad r = 0.99$$

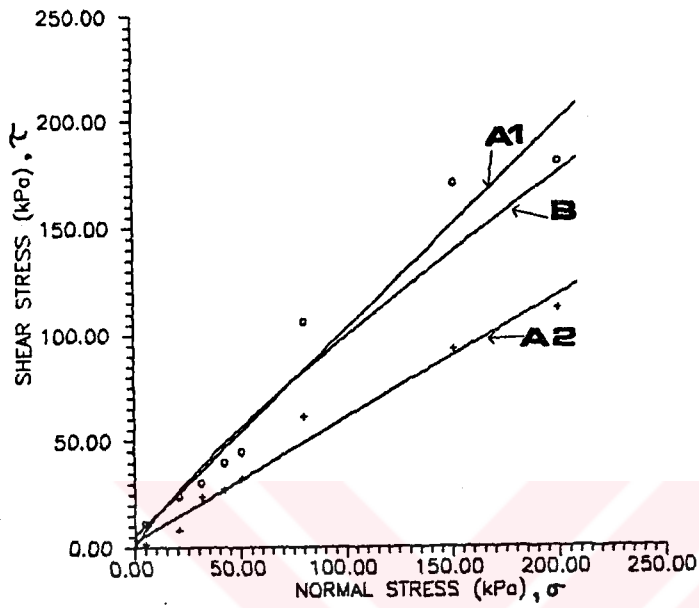
Figure 51: Shear strength of undulating-planar bedding surfaces developed in the limestone of detritic facies.

were employed with selected normal stress values as input parameters to derive the strength envelope shown in Figure 51b. As pointed out by Barton (1973), a non-linear shear strength envelope indicating a stress dependent friction angle was obtained. However, nonlinearity of the envelope is not distinct. Therefore, referring to the envelope and equations in Figure 51b, reduction in internal friction angle from lowest stress levels to the highest, which corresponds to 6 m and 50 m cut heights, is not sharp and ranges between 46° and 41° .

On the other hand, some bedding surfaces showing transition between smooth-planar and undulating-planar features were observed in Ertrans Section and in the vicinity of highway bridge in limestone rock mass. Totally 8 natural surfaces, with very small asperities, prepared from the sample LB47 representing this bedding surface, were also tested in accordance with the test procedure applied for joints and smooth beddings. The test results (Table B.8) are plotted in Figure 52. It is evident from the failure envelopes that at shallow stress levels the angle of internal friction of this type of surface is 6° to 7° smaller than those of more undulated dominant surfaces. Residual strength envelope best fits to linear relationship due to the shearing of small asperities during multiple reversals.

6.4.3. Shear Strength Characteristics of Fault Gouges

Fault gouges in the study area contain very small rock clasts floating in a matrix of highly plastic clays or clayey elastic silts. Barton (in Miller, 1982) pointed out that undulations of the rock surface on either side of the zone would not add to the zone's overall strength. The walls of the faults in the pit are planar with a few



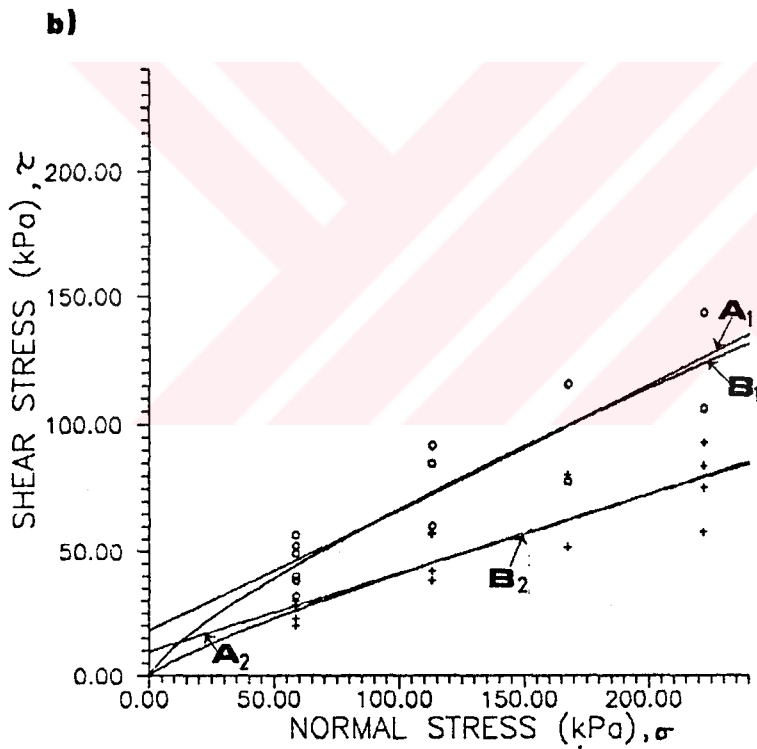
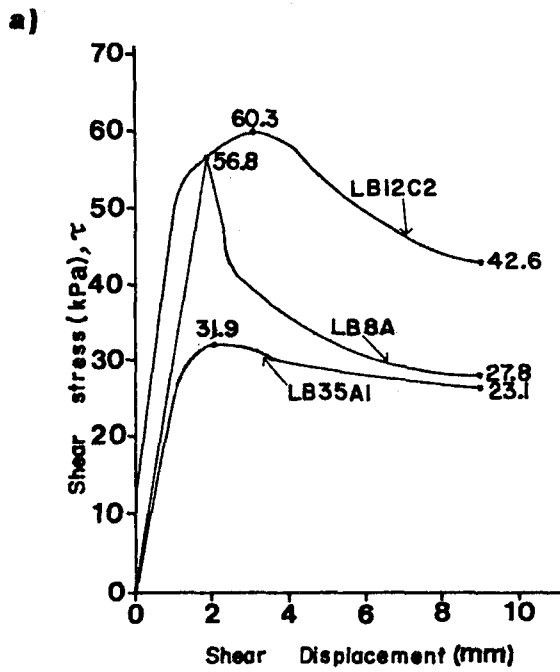
	<u>Peak</u>	<u>Residual</u>
Linear :	$\tau = 5.98 + 0.9646 \sigma$ (A1)	$\tau = 3.05 + 0.5778 \sigma$ (A2)
Power :	$\tau = 2.24 \sigma^{0.823}$ (B)	—

Figure 52: Failure envelopes for sample LB47 from limestone.

exceptions. Even if an undulation is strong enough to support riding up, the gouge is not, therefore over a period of time it will flow around such an undulation. This flowing would require energy from the sliding block and might tend to dampen the slide, but it would not add to the strength of fault zone. This results in the behaviour of fault gouge as a clay. Thus, shear strength determinations along the faults were carried out on the orientated gouge samples.

For a cutting in a clay, the long-term stability is considered critical. Because pore pressures are initially low or negative and gradually increase towards steady seepage pore pressures. The increase in pore pressures causes a decrease in effective stresses (Deen, et al., 1977). Therefore, drained conditions are more important for the end of construction case. Thus, consolidated-drained test method (ASTM, 1985; ASTM D3080-72) was employed. Totally 22 test specimens from 7 different gouge blocks were prepared. The tests were carried out in the multiple reversal shear box, care being taken to arrange the specimens so that the shearing follows the natural direction of movement. Each specimen was consolidated under the appropriate normal load and then sheared until the residual condition was reached. So that a peak and residual shear strength of each specimen was determined for a particular load (Table B.9). All the tests were run at a strain of 0.042 mm/min to allow the contained water to drain and to avoid an undrained loading effect (Lambe and Whitman, 1969).

Generally peak shear strengths were reached after only a few millimeters of displacement, but the residual strengths were reached about 12-13% displacement (Figure 53a). The reversal of shear box means a slightly oblique clay mineral alignment near the shear surface will suffer some particle readjustment with each change in direction (Hawkins and Privett, 1985). For this reason, residuals for some specimens were reached at the end of the reversals.



<u>Peak</u>		<u>Residual</u>	
Linear: $A_1, \tau = 18.11 + 0.4872 \sigma$	$A_2, \tau = 9.73 + 0.3164 \sigma$		
Power: $B_1, \tau = 1.957 \sigma^{0.767}$	$B_2, \tau = 0.901 \sigma^{0.829}$		

Figure 53: Direct shear test results on fault gouges.

Based on linear fit each set (Table B.9) indicated that the samples rich in clay and silt size material (LB8, 12, 23, 35, 36) show similar shear strength parameters. Whereas, other two samples, which were clayey and silty sand, had greater internal friction angles and lower cohesion values. Considering that the majority of the fault gouges in the pit are represented by plastic fine material, the data from the first five samples were plotted to obtain a general failure envelope for the fault gouges. The failure envelopes were fitted by both linear and power curve relationships (Figure 53b). The same coefficients of correlation were obtained from both relationships for peak values (Table 12). Jaeger (1971) noted that the power law tends to better fit the data that turns down at the lower normal stresses. Besides, Skempton (1985) and some other investigators (Bishop, Kenny, Hutchinson, Garga, Chandler, Privett, Hawkins and Privett; all in Hawkins and Privett, 1985) state that for most clays, relation between residual strength and effective normal stress is non-linear. On the contrary, Townsend and Gilbert (1973), Bromhead and Curtis (in Hawkins and Privett, 1985) had straight failure envelopes for clays they tested. Lupini et al. (1981) have also chosen to express residual strength parameters as linear to a good approximation. As it can be seen in Figure 53b for the residual strength the power law represents the test data slightly better than a linear equation. But, for the normal stress level above approximately 70 kPa there is no significant difference between the envelopes and equations. Since the normal stresses on the faults are expected to be above 70 kPa, the simpler Coulomb equation (linear fit) may confidently be used in the stability analyses.

6.5. Shear Strength Characteristics of Soil Materials

Shear strength parameters of soil samples collected from the open pit are determined and discussed in the following sections.

6.5.1. Shear Strength of Claystone in Sekkōy Formation

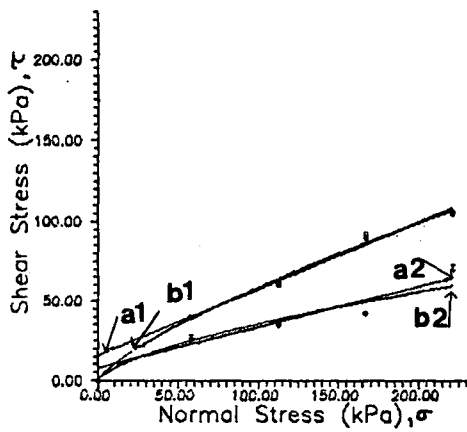
The claystone in the upper zone of main Sekkōy formation, which exhibits clay behaviour, could not be undisturbedly sampled in block shape from the pitwalls. For this reason its shear strength parameters were determined on moderately disturbed specimens prepared from NQ size core samples.

The tests were carried out on 8 specimens under drained conditions, according to the method suggested by ASTM (1985; ASTM B3080-72) as mentioned in the previous section.

The linear and power laws were fitted to the test results (Table B.10a) and the failure envelopes were constructed (Figure 54a). The statistical analyses indicate that linear failure envelopes for both peak and residual strengths are fitted to data better than the power curve.

Disturbance of the specimens tested is inevitable during the drilling and the preparation of 6x6x2 cm specimens from NQ size cores. Therefore, it is concluded that the shear strength parameters obtained from laboratory tests (see Table 12) are probably lower than would be expected for this material. A very close agreement between the peak strength of the clay and residual strength of the undisturbed bedding planes in the same formation was obtained. If this agreement and the effects of soil disturbance are taken into consideration, for stability assessments it would be assumed that the shear strength of this soil and the bedding surfaces might be very similar.

a) Claystone in Sekkoy Formation



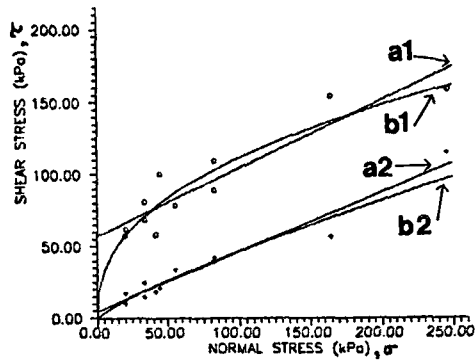
Peak

Residual

Lin. : $\tau = 22.76 + 0.42\sigma$ $\tau = 7.96 + 0.2566\sigma$
 (a1) (a2)

Power : $\tau = 1.81\sigma^{0.756}$ $\tau = 1.748\sigma^{0.654}$
 (b1) (b2)

b) Transition zone soils



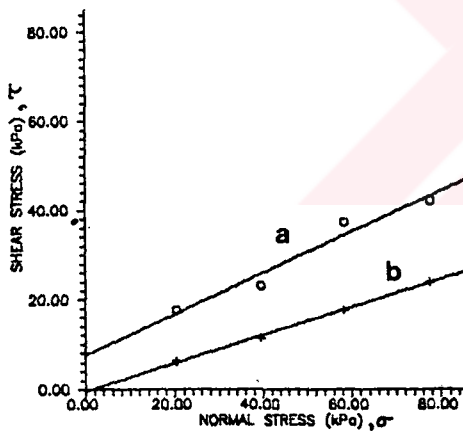
Peak

Residual

Lin. : $\tau = 50.07 + 0.5085\sigma$ $\tau = 4.93 + 0.4146\sigma$
 (a1) (a2)

Power : $\tau = 13.76\sigma^{0.447}$ $\tau = 1.076\sigma^{0.818}$
 (b1) (b2)

c) Black clay



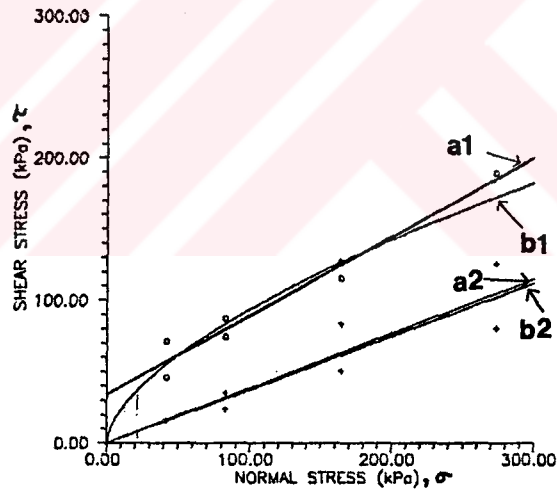
Peak

Residual

Lin. : $\tau = 7.59 + 0.4601\sigma$ $\tau = 0.3097\sigma$
 (a) (b)

Power : $\tau = 2.15\sigma^{0.683}$ $\tau = 0.302\sigma$

d) Finest material in Turgut Formation



Peak

Residual

Lin. : $\tau = 34.30 + 0.5521\sigma$ $\tau = 0.383\sigma$
 (a1) (a2)

Power : $\tau = 5.755\sigma^{0.606}$ $\tau = 0.374\sigma$
 (b1) (b2)

Figure 54: Direct shear test results on different soil materials encountered in the study area.

6.5.2. Shear Strength of Transition Zone

The transition zone, exhibiting purely soil characteristics, is consisted mainly of finest material. The sandy portion included in this zone has a very small extend in the form of small lenses or pockets. According to the site observations on an instability the behaviour of this zone is mainly governed by the finest portion. Thus, shear strength determinations were carried out on clay and clayey silt samples.

On the basis of soil classification test results three undisturbed blocks of finest material were chosen and then totally 11 test specimens were prepared. Taking into consideration the long-term stability condition, consolidated-drained shear tests (ASTM, 1985; ASTM D3080-72) were conducted.

The test results were first fitted to linear relationship (Table B.10.b). A close agreement between the strength parameters of each test set was found. Thus, the linear and power laws were fitted to all data to obtain general strength envelopes characterizing this zone (Figure 54b). In both cases, very high coefficients of correlation were obtained (Table 12). However, coefficients obtained from the linear fit are higher than those of power law. Thus the assumption that the shear strength parameters of this zone are constant and not sensitive to applied normal load may be used confidently for the assessment of stability. On the other hand, in the majority of the samples residual values were achieved at the end of the first run of the shear box. Besides, the difference between the calculated peak and residual cohesive intercepts is high. This probably indicates that the residual cohesive strength of the soil is mobilized after small displacements.

6.5.3. Shear Strength of the Soils of Turgut Formation

After the removal of the coal seam only the upper levels of Turgut formation expose. These levels are consisted of dark coloured, highly plastic clays and clayey silt alternations. Therefore, it was concluded that behaviour of these finest materials plays an important role on the stability rather than the coarse grained portion lying deeper. Failures experienced in Ertrans section (Plate 1) also confirm this conclusion. Thus, shear strength determinations were conducted on clay and clayey silt samples.

The test samples were categorized in two groups. The first group involves clay and clayey silt samples representing the alternations in the upper zone where the coal seam is thicker. While the second group involves highly plastic, homogeneous black clay appearing along basin margins, where the coal seam becomes thinner and/or does not appear. The test procedure applied on other soils were also adopted for these materials.

The tests on the black clay from a sliding surface (see Figure 9) was carried out with care being taken to locate the slip surface as exactly as possible in the plane of the box and to arrange the sample so that shearing follows the natural direction of movement.

In the statistical analysis both linear and power curve relationships were fitted to the experimental data (Table B.10/c.1 and c.2). The linear relationship is better fitted to the data for the first group (Figure 54.d and Table 12). When the shear strength parameters are compared it can be seen that there is a close agreement between the first group in Turgut formation and soils in transition zone. However, soils from Turgut formation behave as a cohesionless soil in residual condition.

The black clay has a very low shear strength (Figure 54 c). Residual strength of this clay was reached after small displacements and the material behaves cohesionless. The coefficients of correlation for both models are equal. This indicates that no considerable difference exists between the strength parameters obtained from these relationships. Thus, it is concluded that the shear strength parameters derived from the linear fit may be used confidently in further analyses for the sake of simplicity.



CHAPTER 7

EVALUATION OF ROCK MASS STRENGTH

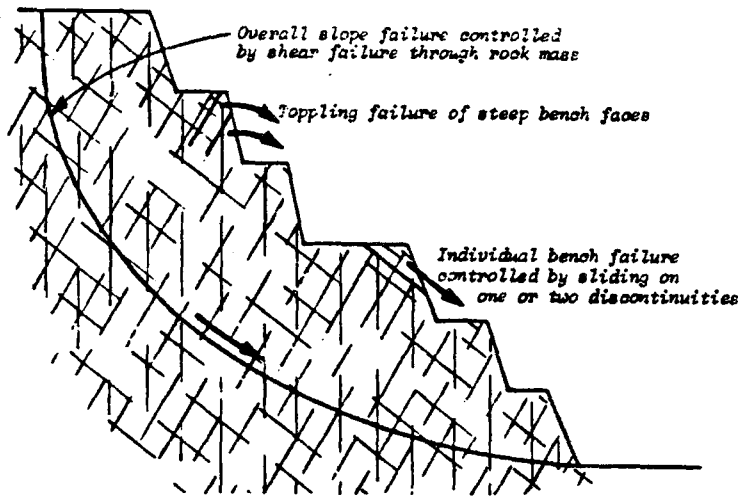
7.1. Rock Mass Strength and Classification

Large walking dragline, employed for the removal of overburden at Eskihisar open pit, necessitated the investigation of the stability of different highwall slopes associated with dragline operation. With the exception of locations close to the basin margins, the dragline operates on very gently dipping strata. Therefore, structurally controlled failures are not generally expected along the highwalls constructed in N-S direction. However, in order to ease the diggability the overburden is blasted. On the basis of observations made on the walls this operation produces artificial haircracks in the rock mass giving rise to an overall strength reduction.

On the other hand, in the southwest, through the planned permanent slopes, bedding planes are nearly horizontal and no fault or shear zones were recognized. This means that the probability of structurally controlled failures is rather low. On the basis of this favorable condition, working with steep final slopes may create additional stresses in the rock mass in conjunction with the heightening of the slope. According to the observations conducted on borehole cores and pitwalls in the south, thinly bedded, fractured marl, limestone and claystone alternations, which also exhibit ravelling behaviour, become the dominant type of rock mass, while the stronger compact marls become thinner or absent. This situation may be evaluated as a transition from intact rock to heavily jointed rock mass. Depending on the number, orientation and the nature of discontinuities the intact rock pieces will translate, rotate or crush in response to stresses imposed on the rock mass (Hoek, 1983). Hoek (1971) also suggests that even for cases of horizontally bedded intact rock, failure may occur along a circular surface.

Because of the reasons mentioned above, the possibility of the mass failure which will tend to occur partly along the discontinuities and partly through intact rock materials following a curved failure surface (Figure 55) was decided to be investigated. The strength of a jointed rock mass in nature lies between the strength parameter of the intact rock and the strength of discontinuities. The former value is too conservative for use in designing rock structures and the latter one is far too optimistic to be of practical application. The mechanical behaviour of such a rock mass is poorly understood. This being in part, due to the difficulties in applying conventional testing program to rock mass. That is why only a few attempts have been made to determine the strength of rock mass experimentally. Triaxial tests in very large cells carried out by Jaeger (1970) is an example to these attempts. An alternative to the difficult and expensive laboratory or in-situ testing of the rock mass to determine its shear strength is to consider the empirical relationships. The author believes that the Hoek and Brown (1980a,b) non-linear failure criterion, which gains an increasing popularity in stability of slopes (Hoek, 1982 and 1983; Priest and Brown, 1983; Rosenbaum and Jarvis, 1985; Singh and Gahrooe, 1989; Abdallah and Helal, 1990), in conjunction with the rock mass classification systems, provides a meaningful estimate of rock mass behaviour. In-situ shear box test data from the blasted marl in Seyitömer coal mine indicated that Hoek-Brown criterion slightly underestimated the shear strength of the same material, exhibiting a better fit to test data obtained from the second sliding of the surface than other criteria (Özgenoğlu, 1990). Thus, this failure criterion was used in order to forecast the behaviour of the controlled blasted overburden in highwalls and the weaker marginal zones of the main Sekköy formation.

a) Cross-section of slope and failure mode



b) Three dimensional view of slope and failure mode

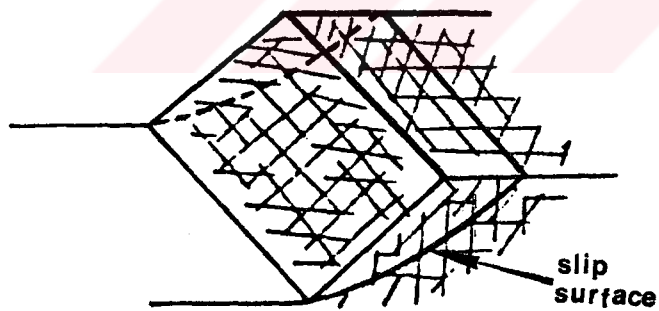


Figure 55: Simplified representation of the relationship between size of slope, discontinuity spacing and mechanism of slope failure (after Hoek, 1982).

7.2. Application of Rock Mass Classification Systems

In order to provide a rational basis for estimating the values of material constants for jointed rock masses, use is made of the rock mass classifications proposed by Bieniawski (1973) and Barton et al. (1974). In this study only the RMR Geomechanics Classification of Bieniawski was used.

The Rock Mass Rating (RMR) system was first proposed by Bieniawski (1973) and has since been modified by the same author (Bieniawski, 1984 and 1989). Table C.1.A in Appendix C shows that the following five parameters are included in the RMR system.

- (1) Uniaxial compressive strength of rock material.
- (2) Rock quality designation.
- (3) Spacing of discontinuities.
- (4) Condition of discontinuities.
- (5) Groundwater conditions.

An additional adjustment for the orientation of the major discontinuity system is made on the basis of the information listed in Table C.1.B. However, greatest difficulty is experienced in determining the rating value for discontinuity orientation in slopes which varies from 0 to -60. Singh and Gahrooe (1989) proposed well described rating adjustment for discontinuity orientation in slopes using the Bieniawski's ratings (Table C.1.E). Their approach was quantified on the basis of rating with regard to the number of possible modes of failure. In this study, only one possible mode of failure, the mass failure, was considered and then (-5) was employed as an adjustment rating.

For better characterization of joint conditions, the guidelines for coal bearing strata proposed by Bieniawski (1984) were preferred (Table C.1.F). On the other hand, in

RMR system groundwater conditions are considered in five categories. The first two categories include completely dry and damp conditions. In the study area, discontinuity surfaces were moist due to the filtering of the surface water through the continuous joints. Thus, water conditions for the discontinuities above the general groundwater level were evaluated using a rating value ranging between those of the first two categories.

Ünal and Özkan (1990) suggest that RMR and Q systems cannot fully describe the specifications of the weak stratified and clay bearing rocks. These kind of rock masses generally include laminated or bedded marl and limestone with continuous beds and bands of consolidated clay as in the upper levels of the Sekköy formation. In order to better characterize this kind of rock mass, interval limits considered in the RMR system were modified (Ünal and Özkan, 1990). In this modification, standard interval limits suggested by ISRM (1981) are used. The effect of water on clay-bearing rock is also expressed by the slake durability index. A summary of this modified RMR system is introduced in Table C.2. of Appendix C.

Considering the applicability of the above mentioned modified RMR system to the clay bearing rocks of the study area and in order to compare the results of the original and modified RMR systems, these two systems were utilized for classification purposes. The modified RMR values were determined by using a computer program called ROCK-MASS developed by Ünal and Özkan (1990), after the arrangements made for one possible mode of failure and for moist discontinuities which were mentioned above.

The data required for rock mass rating determinations were obtained from the geotechnical logs and scanline surveys. Values of RMR for the rock mass in the main Sekköy

formation were determined for 102 individual sections from seven boreholes considering drill-run lengths ranging between 1 to 3 m. In addition, a total of seven scanline sections were also evaluated.

The RMR values obtained from both original and modified systems are given in Figure 56 for comparison. Majority of the ratings of both systems are very close to each other and rock mass descriptions are not affected even after the modification of RMR values. However, below the rating value of 40 modified values show a noticeable variation and a wider band of RMR values as compared with the RMR values obtained from RMR system suggested by Bieniawski (1989), but characterizing the joint conditions given in Bieniawski (1984; see Table C.1.F). It is also noted that in both cases the rock mass under consideration generally falls into the fair rock-mass class.

Histograms of the 109 values of RMR (Figure 57) drawn by using the statistical package of GEO-EAS (Englund and Sparks, 1988) has a bimodal form. It suggests that from a geotechnical point of view the rock should be regarded as comprising two rock mass types. Examination of borehole cores and observations on pitwalls showed that the lower values of RMR tended to occur in the upper and marginal zones of the formation affected by weathering and alternating character of the zone. However, occasionally individual higher RMR values reaching up to 50 were also encountered in this zone. In the lower levels, in compact marls above the coal seam, higher RMR values ranging between 50 and 62 were differentiated. Thus, the rock mass was divided into "more fresh (compact marls)" and "weak zone (alternating zone)" according to depth. It is clear from Figure 56 that in boreholes JT2 and JT3 and along the scanlines the rock mass quality reaches its highest values.

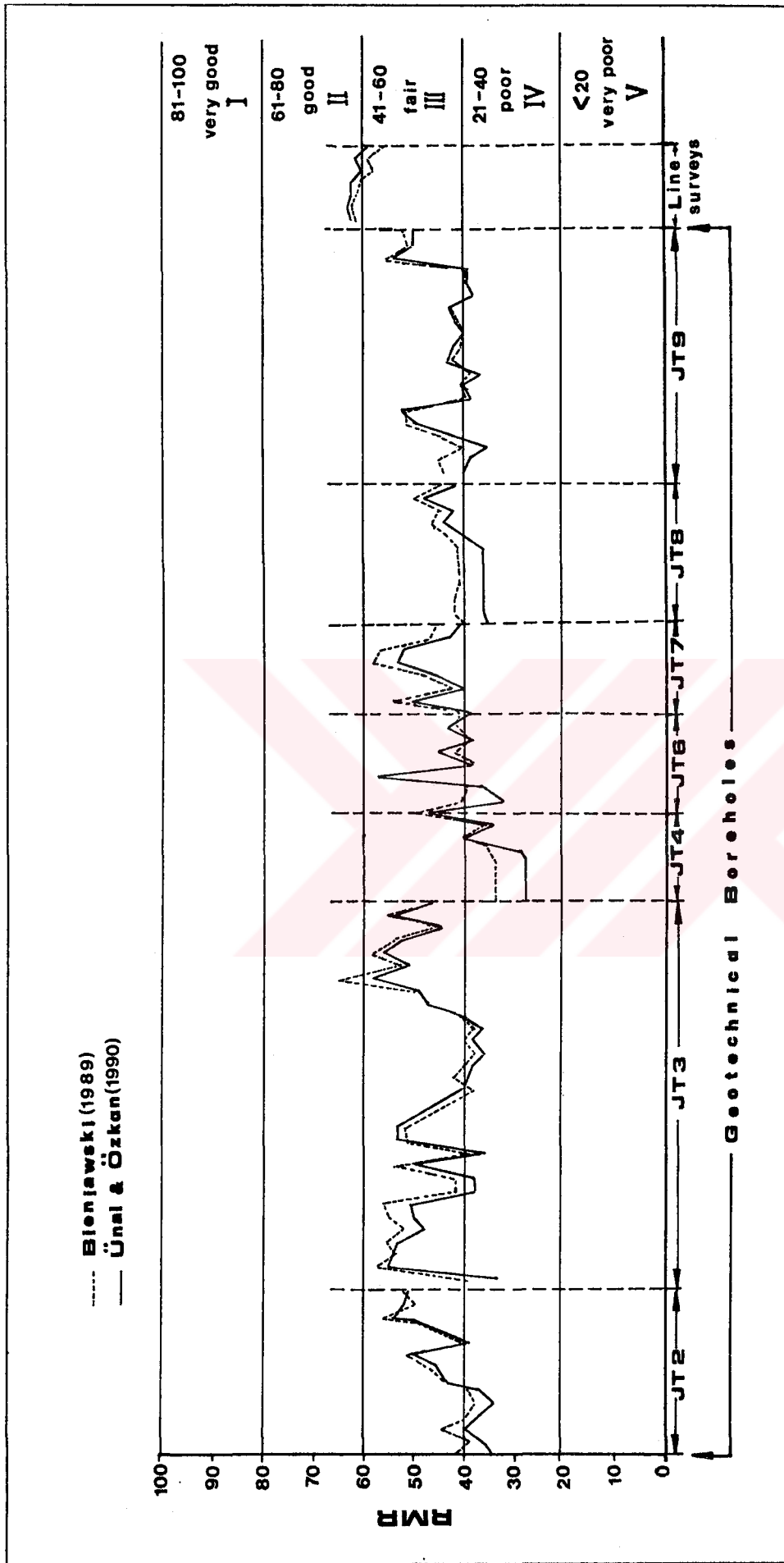
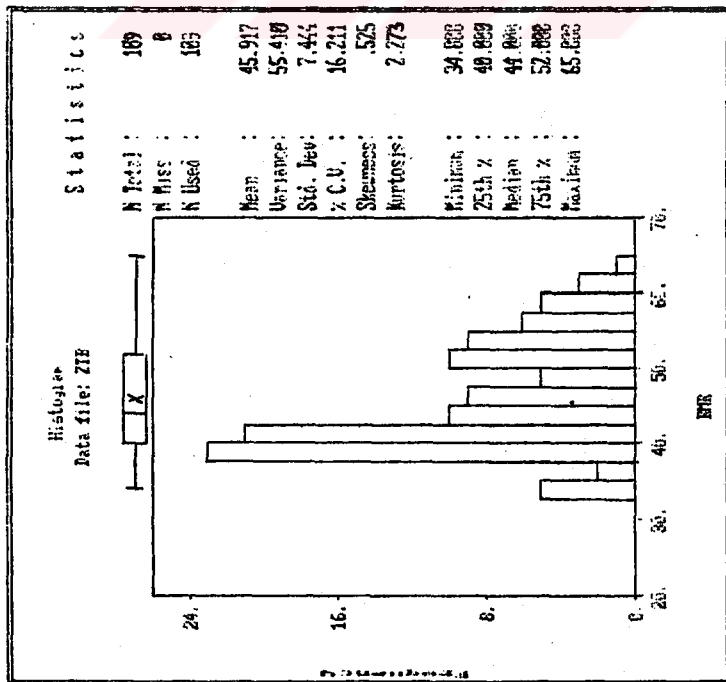
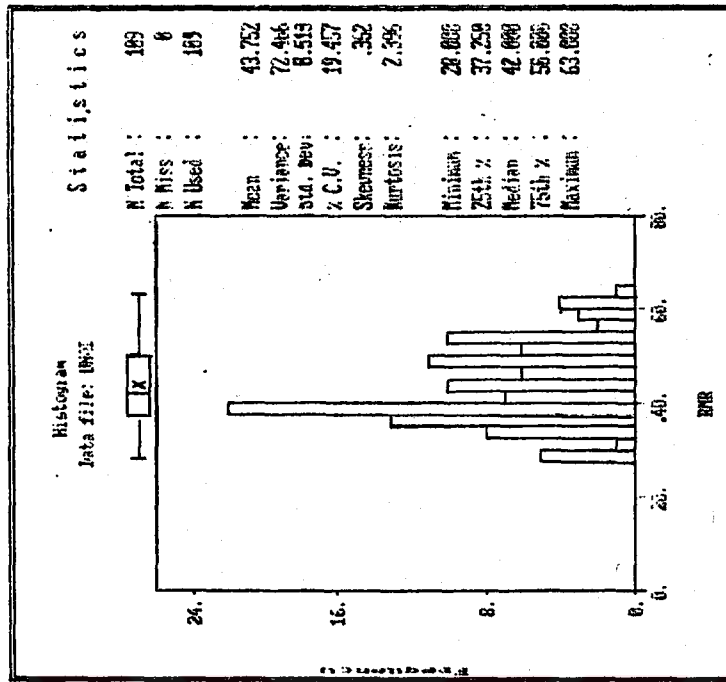


Figure 56: Comparison of the original and modified RMR values determined from geotechnical boreholes and scanline survey data.



a



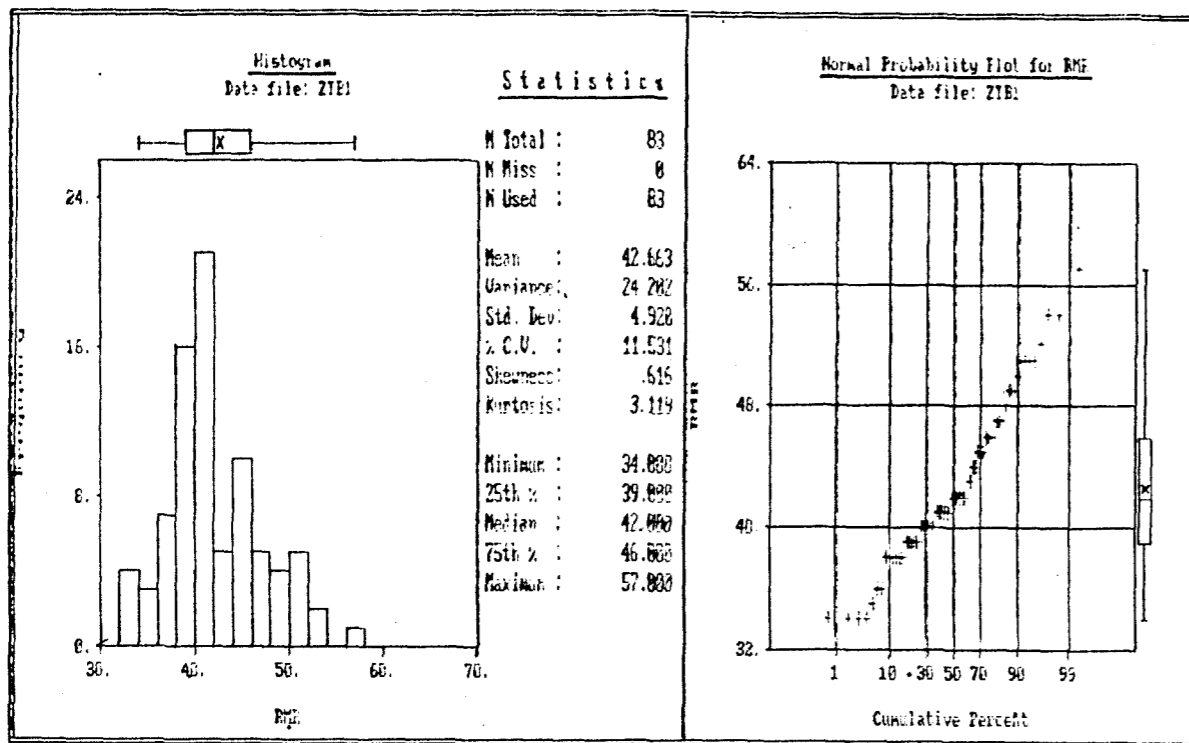
b

Figure 57: Histograms of RMR for all samples from main Sekkőy formation; (a) histogram of RMR based on Bieniawski (1989); (b) histogram of modified RMR based on Ünal and Özkan (1990).

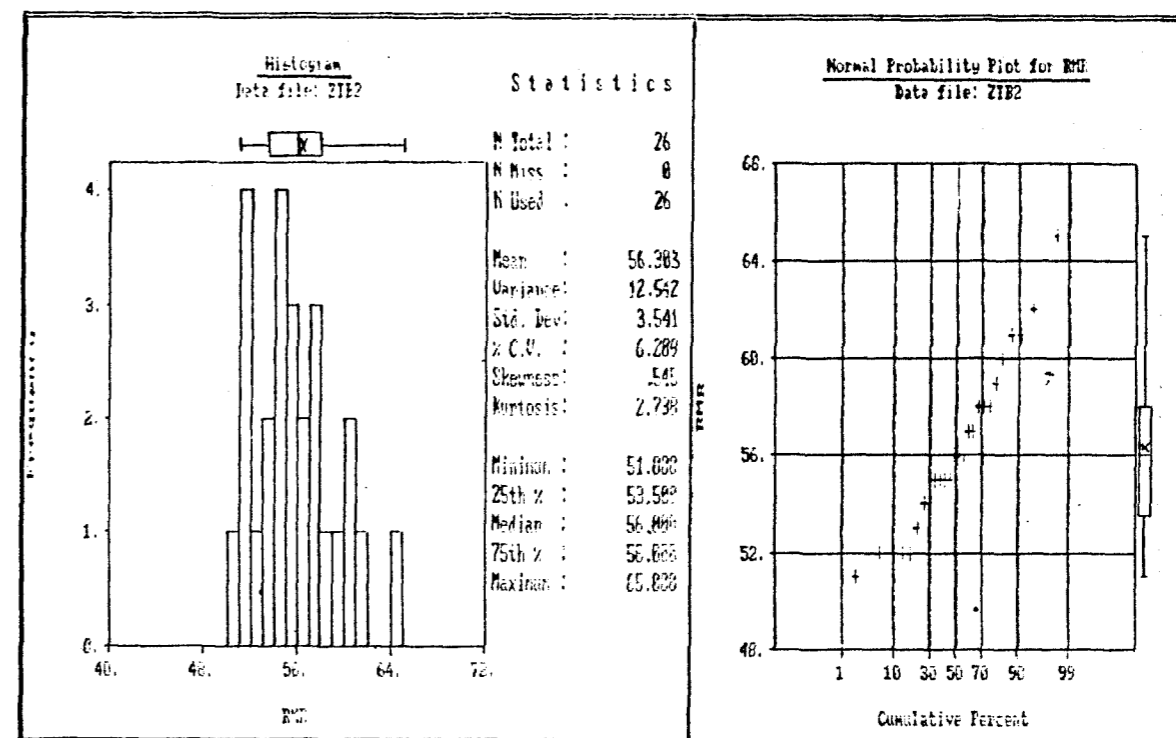
This is because, they were conducted in the central part of the pit where the compact marls exist and become thicker.

To make RMR values independent of the fresh type the highest 26 RMR values encountered just above the coal seam were separated. Histograms for weaker upper zone (Figure 58.a,b) and compact marls (Figure 58.c, d) show that RMR values are distributed in approximately normal forms. The difference between the mean and median values of modified RMR histograms (Figure 58.c, d) are greater than those of the original RMR values. This is due to the scattering of values lying around the boundary between the poor and fair rock masses. According to the RMR values listed in Table 13 weak zone falls into the lower boundary of the fair rock, while compact marls are closer to the upper boundary of the same category.

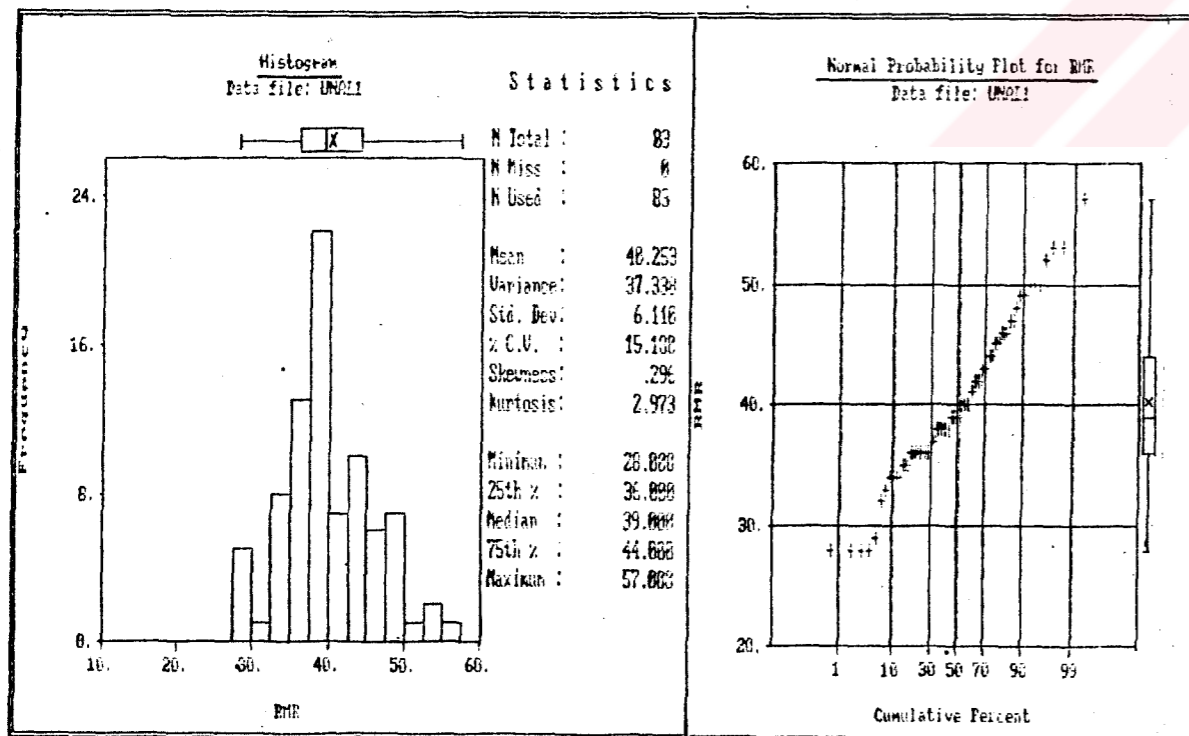
Mining applications include dynamic processes such as blasting and a blasting adjustment for RMR values is recommended (Bieniawski, 1984 and 1989). In Eskihisar open pit blasting is made in compact marls. It is a controlled blasting with a slight damage to loosen the overburden in highwall. For this condition blasting damage adjustment (A_b) ranges between 0.94 to 0.97. Application of the lower adjustment value (0.94) to the RMR values of compact marls yields adjusted RMR values of 53 and 52 for original and modified systems, respectively. The weak zone is generally removed by excavators without blasting. Thus, no adjustment for this rock mass was applied.



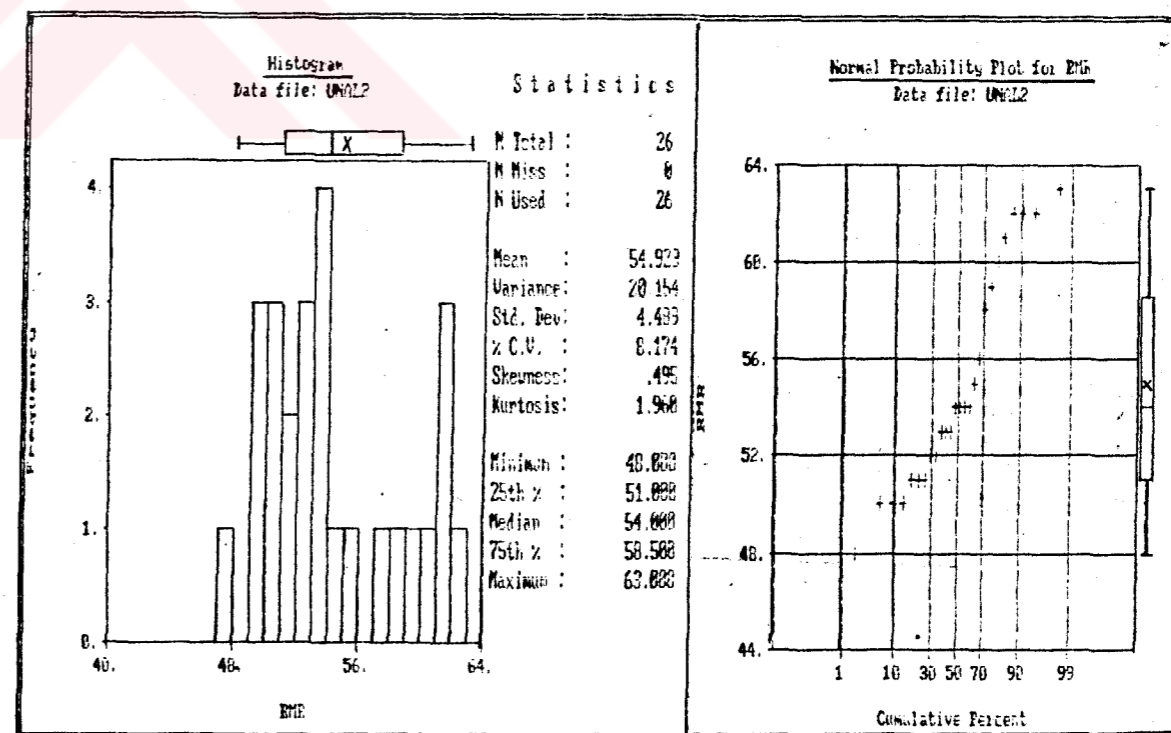
a. Weak zone (RMR System)



c. Compact marls (RMR System)



b. Weak zone (Modified RMR System)



d. Compact marls (Modified RMR System)

Figure 58: Histograms and normal probability plots of RMR values for weak zone and compact marls with respect to RMR and modified RMR classification systems.

Table 13 : Rock mass characteristics of main Sekköy formation

Rock Mass	Mean		Material Constants			
	Rock Mass Rating (RMR)					
	Bieniawski (1989)	Ünal & Özkan (1990)	Bieniawski (1989)	Ünal & Özkan (1990)	Bieniawski (1989)	Ünal & Özkan (1990)
			α	β	α	β
All samples from overburden	46	44	-----			
Compact marls*	53	52	0.344	0.0004	0.32	0.00034
Weak zone	43	40	0.168	0.000075	0.135	0.000045

$\alpha_i = 9.87$ (intact rock)

* Values of RMR adjusted for blasting.

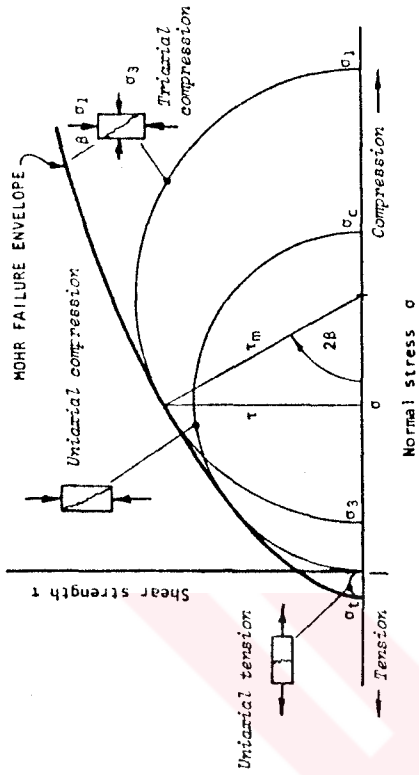
7.3. Estimating Rock Mass Shear Strength From RMR Values and Empirical Failure Criterion

The brittle failure criterion for rock, described by Hoek and Brown (1980 a, b) and Hoek (1983), is widely used for estimating the strength of jointed rock masses. A complete discussion on the derivation of the empirical criterion exceeds the scope of these study. Briefly, the criterion was developed by a trial and error process based upon experience of both theoretical and experimental studies of rock failure. The resulting failure criterion and related equations are expressed in Figure 59.

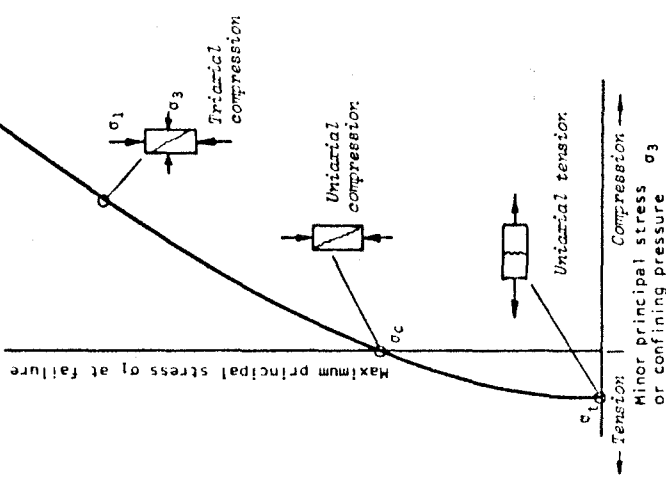
When the material constants (m) and (s) described in Figure 59 cannot be determined experimentally, it is possible to derive the required constants as a function of RMR rating. Hoek and Brown (1988) and Hoek (1990) suggested a set of relations between the RMR from the Bieniawski's (1984) rock mass classification and the constants (m) and (s). Following Priest and Brown (1983), the relations for disturbed rock mass, mainly occurring around the surface mine slopes which have been loosened or damaged by blasting, were presented in the form of following equations:

$$m = m_i \exp \left[\frac{\text{RMR} - 100}{14} \right]$$

$$s = \exp \left[\frac{\text{RMR} - 100}{6} \right]$$



RELATIONSHIP BETWEEN PRINCIPAL STRESSES AT FAILURE



Empirical failure criterion equations:

$$\sigma_1 = \sigma_3 + \sqrt{m\sigma_c\sigma_3 + s\sigma_c^2} \quad (1)$$

$$\tau = A\sigma_c(\sigma_c + \sigma_t/\sigma_c)^B \quad (2)$$

- where:
- σ_1 = major principal stress at failure,
 - σ_3 = minor principal stress at failure,
 - σ_c = uniaxial compressive strength of intact rock pieces,
 - m = material constant which controls the curvature of the σ_1 vs. σ_3 curve,
 - s = material constant which controls the location of this curve in space,
 - τ = shear strength,
 - σ = normal stress at failure,
 - A) = material constants for Mohr envelope,
 - B) = $1/2 \sigma_c (m - \sqrt{m^2 + 4s})$ is the apparent tensile strength of the rock mass.

Figure 59: Graphical representation of stress conditions for rock failure and empirical failure criterion equations (after Hoek, 1982).

where m_i is the value of m for the intact rock, determined from the results of triaxial tests (Hoek, 1983). In addition to compact marls which are blasted, the above equations were also used for the weak rock mass. Because, it will also loosen due to the stress relaxation as a result of slope construction.

The value m_i was calculated by linear regression analysis on the measured triaxial data pairs from intact marl core samples which are tabulated in Table B.4. For the purpose, a computer program called HOBR (Appendix E.2), developed by the author, was used. The shear strength for a specified normal stress is found by solving the following set of equations (Hoek and Brown, 1988):

$$\tau = (\cot \theta - \cos \theta) \frac{m\sigma_c}{8}$$

where

$$\theta = \arctan \frac{1}{\sqrt{4h\cos^2 \theta - 1}}$$

$$\theta = \frac{1}{3} (90 + \arctan \frac{1}{\sqrt{h^3 - 1}})$$

$$h = 1 + \frac{16 (m\sigma + s\sigma_c)}{3m^2 \sigma_c}$$

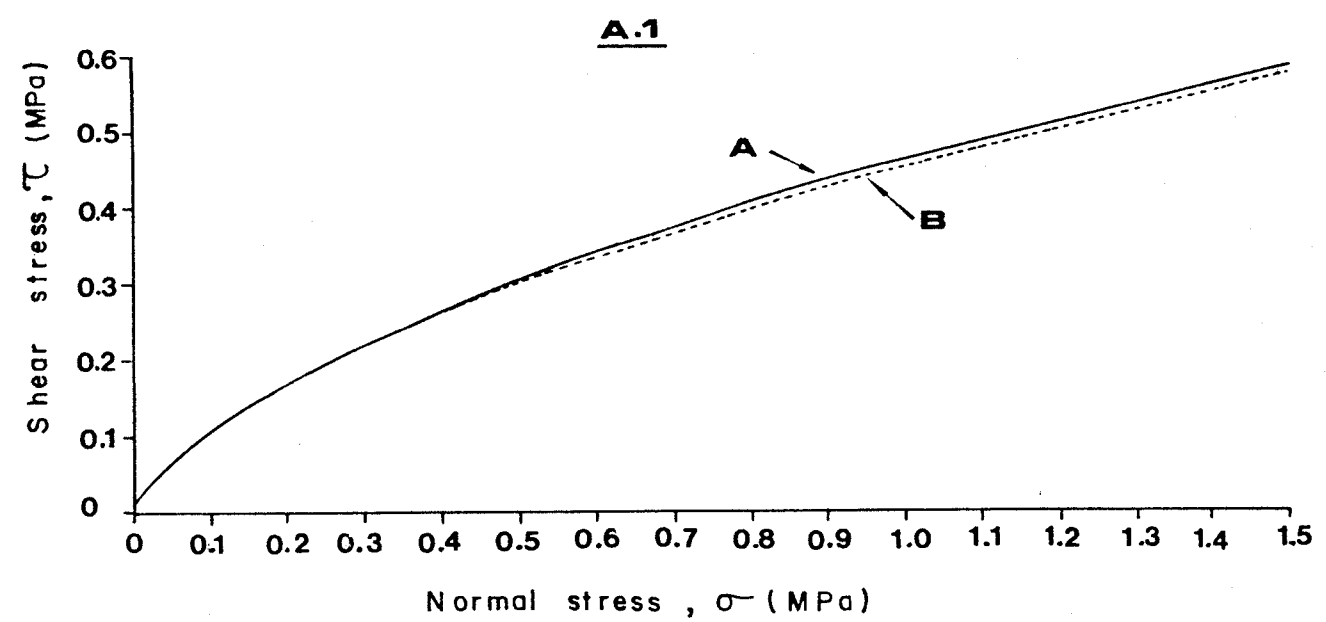
The corresponding instantaneous cohesion is:

$$c = \tau - \sigma \tan \phi$$

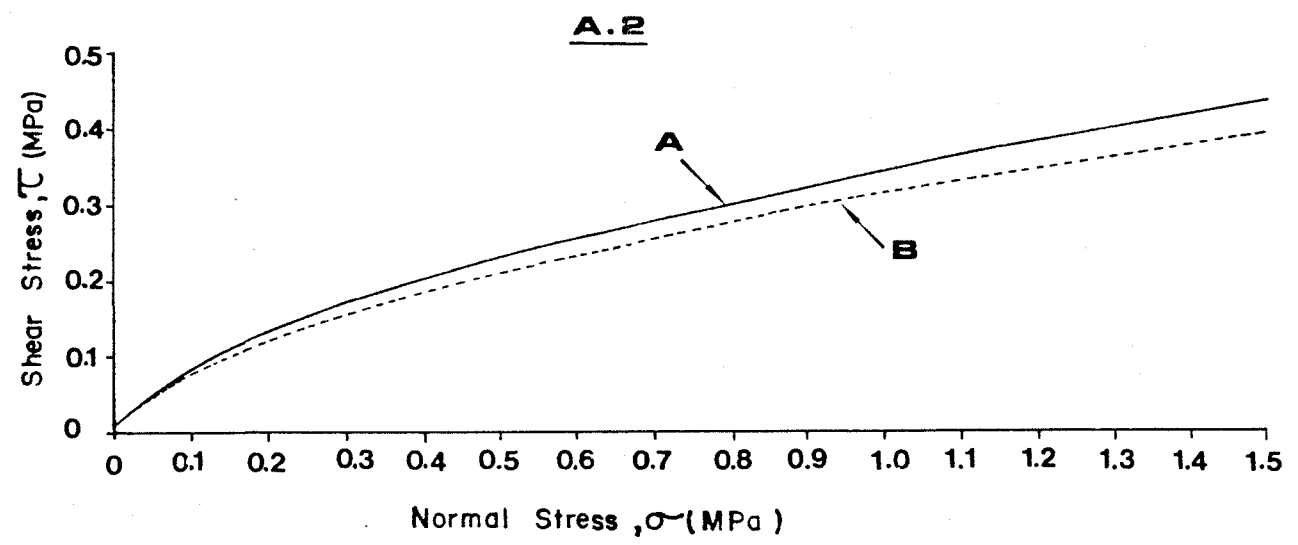
Using the program HOBRE the material constants m and s (Table 13) and shear strengths, cohesion and internal friction angles for normal stress levels ranging between 0 and 1.5 MPa were calculated. The resulting curvilinear shear strength envelopes and the variation in cohesion and internal friction angle with normal stress for both types of rock masses encountered in main Sekkőy formation are illustrated in Figure 60.

One of the main difference between the RMR values obtained from Bieniawski (1984, 1989) and the modified RMR values obtained from Ünal and Özkan (1990) is in the evaluation of joint conditions. In modified RMR system, when intact core recovery (ICR) parameter is equal to zero, whether infilling material exists or not, rating for infill is taken as zero. But infill, which represents a part of joint condition, should not be ignored. It is suggested that to make infill rating independent of ICR values will probably yield more reliable ratings for joint conditions. On the other hand, especially where intact core recovery is less than 25 % joint orientation index suggested by Ünal and Özkan (1990) provides lower values as compared to those suggested by Singh and Gahrooee (1989) for slopes.

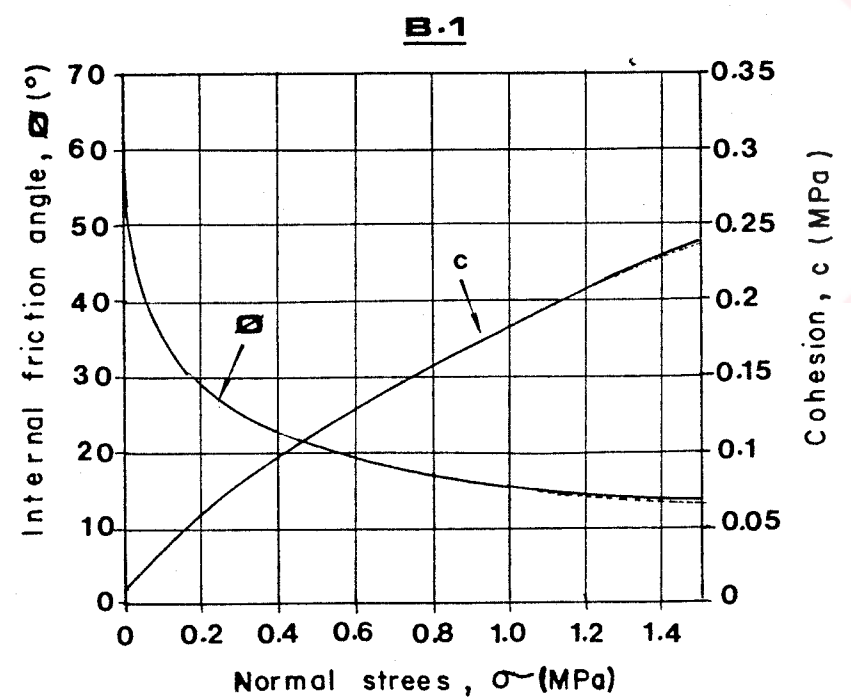
Variation in shear strength parameters c and ϕ for compact marls estimated from both cases (Figure 60 b.1) show a negligible difference. On the other hand, in higher normal stress levels, values of c and ϕ estimated from Bieniawski were slightly higher (max. 1 degree for ϕ and 6-14 kPa for c) than the estimates of Ünal and Özkan (Figure 60 b.2). It is clear that both methods provided similar results due to very similar mean RMR values which did not fall below the



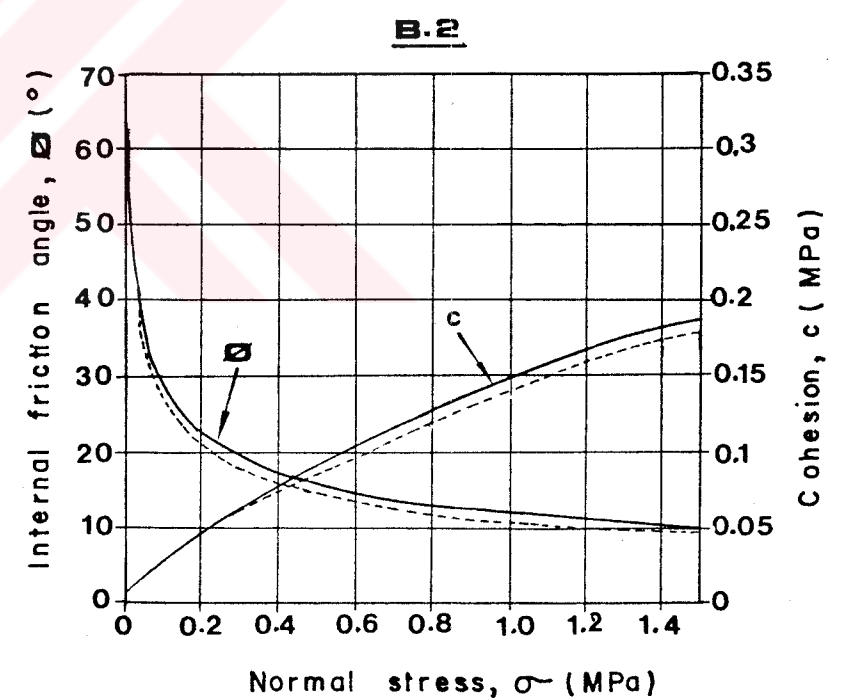
A_ RMR = 53 (Bieniawski; 1989), $m = 0.344$, $s = 0.0004$
 B_ RMR = 52 (Ünal & Özkan, 1990), $m = 0.320$, $s = 0.00034$



A_ RMR = 43 (Bieniawski, 1989), $m = 0.168$, $s = 0.000075$
 B_ RMR = 40 (Ünal & Özkan, 1990), $m = 0.135$, $s = 0.000045$



— $\overline{\text{RMR}} = 53$
 - - - $\overline{\text{RMR}} = 52$



— $\overline{\text{RMR}} = 43$
 - - - $\overline{\text{RMR}} = 40$

Figure 60: Shear strength envelopes and variations of c and ϕ with normal stress for compact marls (A1, B1) and weak zone (A2, B2).

RMR value of 40. Thus, in the light of discussion, it is concluded that the shear strength parameters obtained from Bieniawski may confidently be used without any significant deviation for this case.



CHAPTER 8

BACK ANALYSES AND ASSESSMENT OF MECHANISM OF SLOPE FAILURES

In the case of stability analysis for actually failed slopes, shear strength of material obtained from laboratory tests are not often effective to decide their critical state. The most reliable way to obtain a statistical weighed mean value of shear strength parameters in an extended slope is back calculation. The back analysis of failures using limit equilibrium techniques is fundamental to an improved understanding of both the failure mechanisms and the mobilized shear strength parameters.

Slope failures have occurred both in the hangingwall and footwall materials of Eskihişar open pit. Back analyses of some of these failures are included in this research for the purposes mentioned above. Records have not been kept for all the failures. Consequently back analyses are restricted to five failures for which slope geometries and some important site conditions before and during failure are generally known.

The general approach employed in the analyses was based on the following assumptions:

1. A condition of static equilibrium at the point of failure (limit equilibrium) exists at time of failure. That is, slope failure occurs when the factor of safety is reduced to unity.
2. Since surface roughness and coating of discontinuity surfaces are generally similar throughout the site, there was no need for further simplifications in terms of homogeneity and isotropism (Sancio, 1981).

3. The shear strength obtained from the analyses is the weighed average shear strength of the sliding or slip surface.

8.1. History of Slope Failures at Eskihisar Open Pit

Some multibench and single bench failures have occurred in Eskihisar open pit. With the exception of a large one, they have been limited to small, manageable failures. During the initial operation of the pit, in the north margin of Ertrans section problems were encountered with the stability of permanent slopes (Plate 3 - failure 1a, 1b). The material from multibench failure covered the western part of this section (Figure 61). It was mined by a private sector and thus no valuable information and documentation related to the history of the failure was available.

In 1987 failures occurred progressively with the development of the pit in the Özdemirler section (Plate 3 - slides 2, 3, 4). The slides 3 and 4 could not be adequately observed due to their disturbed nature. But the slide 2, in the hangingwall rock material, apparently involved structurally controlled movement. A shallow seated failure bounded by the fault A (Plate 3 - slide 7) occurred involving a circular movement of a body of essentially clayey material within the transition zone. The second mass failure developed in highly decomposed sandstone. This unit is a very small and relict portion of the Yatağan formation preserved in NE. The failure was shallow seated and covered highly steep slope involving two benches (Plate 3-slide 5).

In 1988, tension cracks were recognized by TKİ staff between the southern edge of the eighth slice and the highway. The displacements were immediately deflected by filling the excavated material into the void to make a toe



Figure 61: General view of slide 1 occurred in Ertrans section (Tms: main Sekkőy formation, Tms1: Detrital facies of Sekkőy formation, M: Marble, 1a, b: Slide 1; Plate 3-Photo. No. 23)

buttressing effect. Unfortunately, no suitable recorded data was available for this movement.

The best observed instabilities occurred during the research period 1989 and 1990. The first one occurred in September 1989 at the southern part of the ninth slice (Figure 39). This instability developed in the hangingwall material.

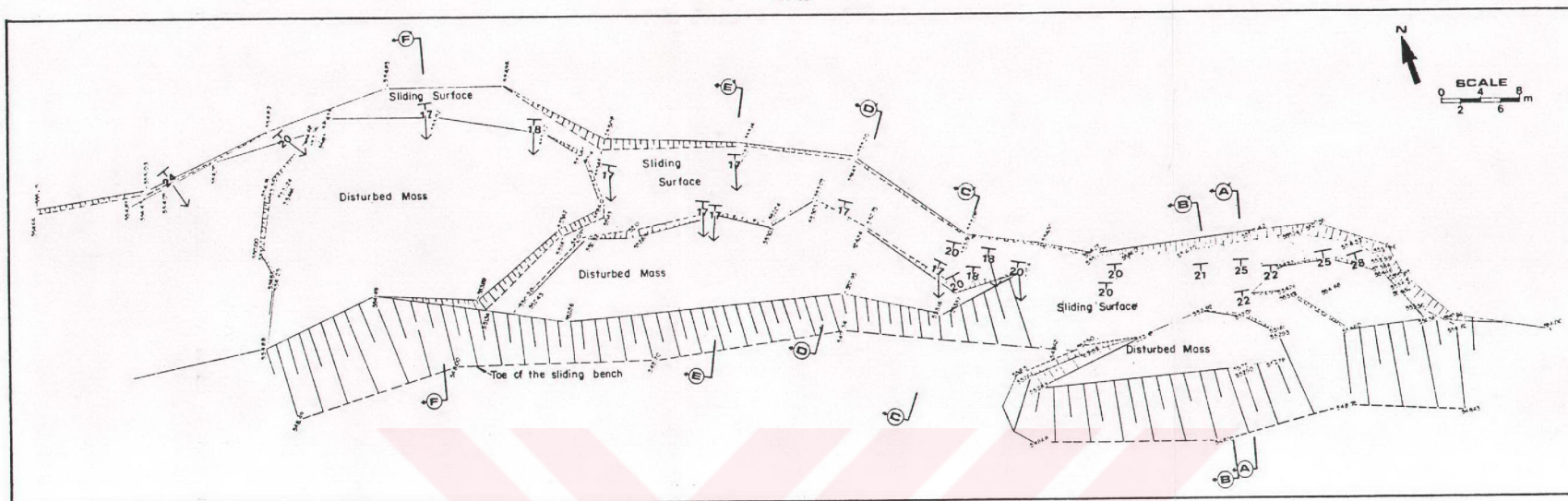
Other failure (Figure 9 ; Plate 3 - slide 8) developed progressively as the bench excavation continued in June 1990. It was apparent that the instability developed in the mode of plane failure along the black clay including a single bench.

B.2. Back Analysis of Plane Failure In Footwall

The slide 8, shown on Plate 3, occurred during removal of overburden in the eastern edge of Ertrans section throughout a single bench of approximately 7 m high. The instability initiated in the east and progressed towards west as the bench construction was continued. The displacement of the sliding mass was considerably fast, occasionally reaching to 1m per day.

The mode of plane failure, which occurred along the black clay representing upper levels of footwall, is apparent for this slide (Figure 9). Bedding strikes measured on different parts of the sliding surface are almost parallel to those of wall face (Figure 62a). On the other hand linear traces produced on the sliding surface by the weight of sliding mass and parallel to the direction of movement were recognized (Figure 62b). The directions of these traces were also in a good agreement with the dip direction of sliding surface (Figure 62a). Besides, sliding

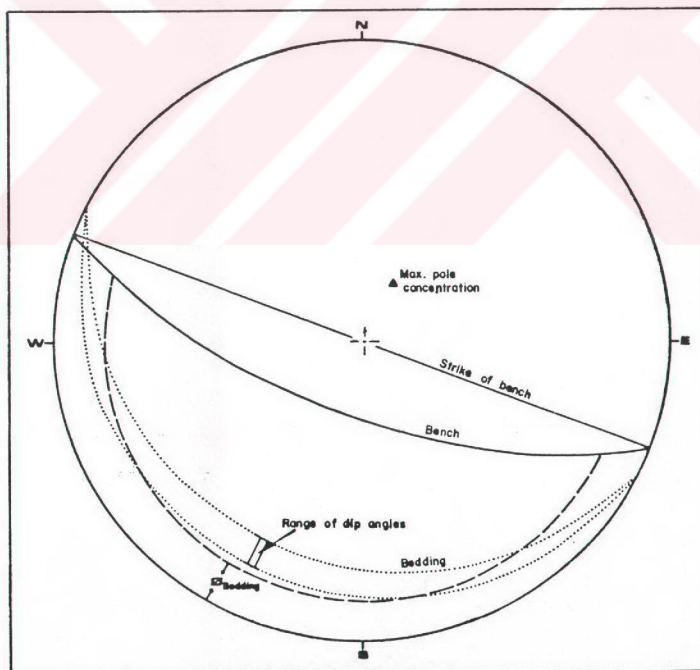
(A)



(B)



(C)



EXPLANATIONS

- $\overline{25}$ Strike and dip of bedding
- \downarrow Section line for back analysis
- $\leftarrow \text{E} \rightarrow$ Direction of linear traces on the sliding surface, parallel to the movement direction
- \downarrow Direction of linear traces on the sliding surface, parallel to the movement direction

Figure 62: Plane failure on footwall material-slide 8: (A) instability plan and structural features; (B) sliding surface and linear traces parallel to movement direction (Plate 3-Photo. No.24); (C) kinematic check of the failure.

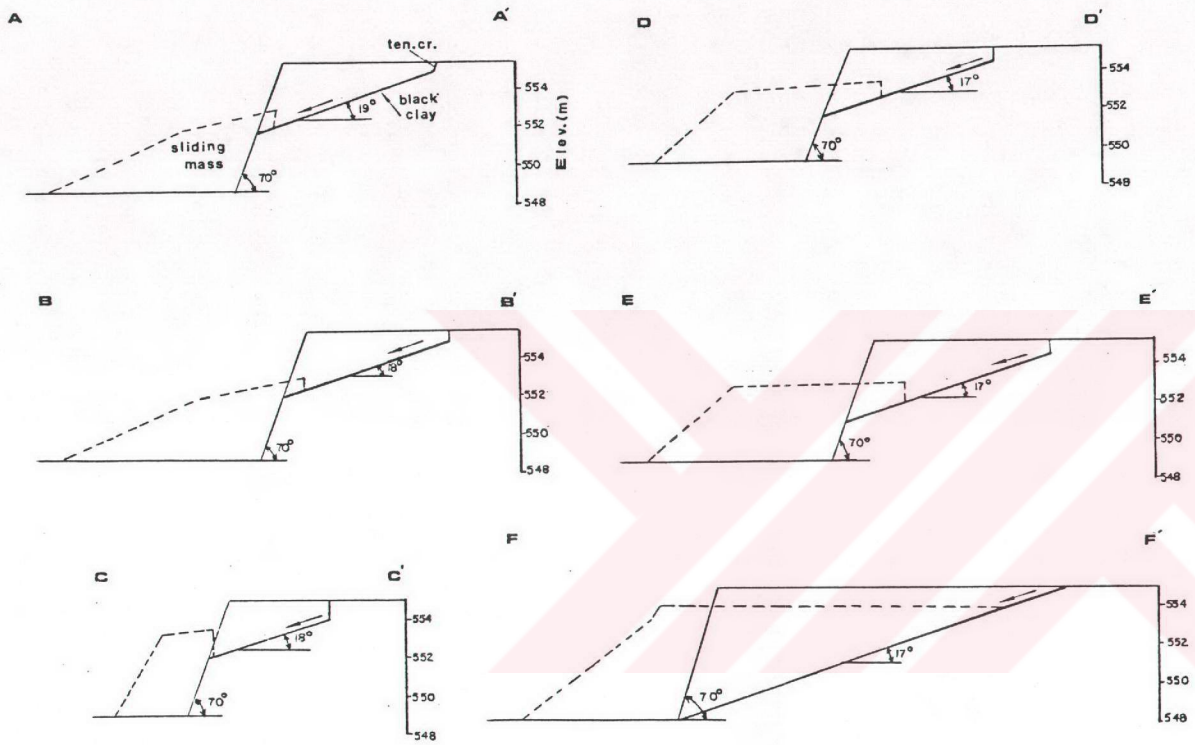
surface daylight on the 70° bench face. It is also noted that the laboratory derived residual internal friction angle of black clay is equal to or from place to place smaller than the inclination of sliding surface. These conditions, illustrated on a stereographic projection in Figure 62c, kinematically satisfy plane failure conditions (Markland, in Bell, 1981 ; Hoek and Bray, 1977; Herget, 1981).

Six bench profiles (Figure 63a) parallel to movement direction were prepared from the instability plan for back calculation of the shear strength parameters of the sliding surface. Observations revealed that in the vicinity of unstable area the slope and very shallow tension crack were dry. However, a few moist zones were recognized on the black clay surface due to the seeping surface water. Thus, no groundwater condition was included in the analyses.

The profiles were back-analysed using two dimensional planar failure analysis method based on Hoek and Bray (1977; Appendix D.1). Calculations were performed with the MBPF (Multi Bench Plane Failure) computer program (Appendix E.3) developed by the author. The method was modified for the computer applications to incorporate slice definition, multi benches, non-linear water table conditions and the effects of static external loads imposed by heavy mining machines such as dragline.

Considering that all parameters to be accurately known, the cohesion was back calculated from the slide only as a function of the predetermined internal friction angle by many iterations of the equation 2 given in Appendix D.1. The diagram given in Figure 63b shows back analysis of plane failure using Mohr-Coulomb linear failure criterion discussed in Chapter 6. Because of the variations in the mechanical properties of the same material in different places, the back calculation of ϕ and c from more than two slopes give as many as $n(n-1)/2$ points of intersections for

a) Back analysis sections



b) Multiple solutions for (ϕ, c) pairs

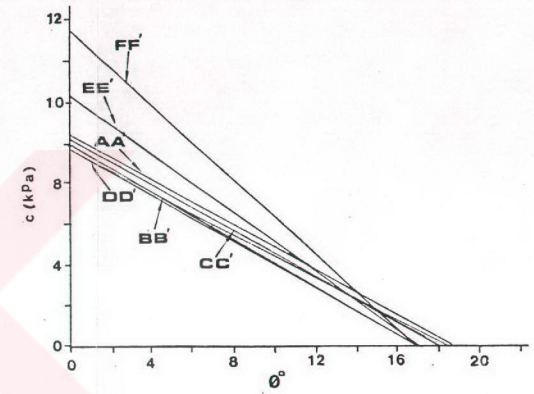


Figure 63: Back analysis of slide 8 developed along the black clay.

curves (ϕ , c) (Sancio, 1981). Accepting this idea of having all the variables affecting the stability, Figure 63b gives bounds for the pair (ϕ , c). In this case, (ϕ , c) varies between (14, 2) and (17, 0). The (ϕ , c) envelopes of profiles DD', EE' and FF' intersect each others at $\phi=17^\circ$ and $c=0$. While, other profiles yielded a factor of safety of about 0.9 for the same strength values. In the former profiles the inclination of sliding surface is 17° which is equal to the laboratory derived residual friction angle of the sliding surface. On the other hand, in other profiles sliding surface inclination ranges between 18° and 19° .

The data derived from the back analyses using planar technique is in very good agreement with laboratory derived residual shear strength data for black clay on the basis of linear relationship (Table 12). The results also indicate that movement on the black clay surface initiates when its inclination reaches to 17° or more with a significant reduction in its shear strength, mobilizing the residual values. Hutchinson et al (1973) and Chandler (in Chandler, 1977) showed that laboratory test methods seem to yield residual strength parameters that are up to 10% or so lower than those derived from back analyses. Thus, it was concluded that residual shear strength parameters of the black clay may confidently be used for stability assessments of permanent slopes which will be constructed along basin margins.

8.3. Back Analysis of Multiplanar Failure

The slide 2 in Özdemirler Section (Plate 3) had occurred in thinly bedded and alternated upper sequence of main Sekköy formation through two benches. The sliding mass is bounded from the west by a normal fault dipping SE with an inclination of 50° to 60° (Figure 64b). With the

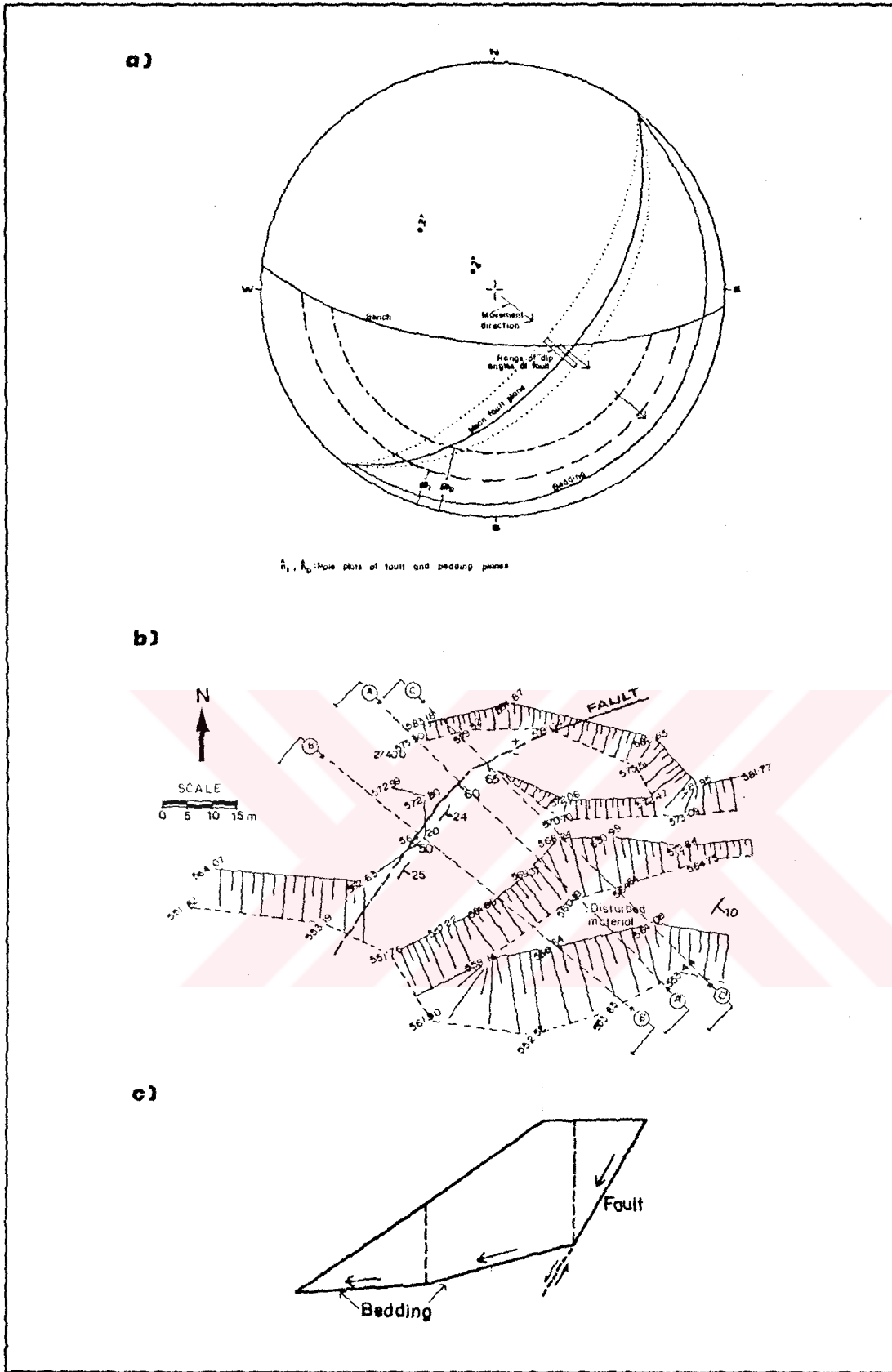


Figure 64: Kinematic check (a), instability plan (b), and mode of failure (c) for slide 2.

exception of strata steepening adjacent to the fault, the inclination of bedding is mostly 10° towards SW. On the other hand, the difference between the strikes of structural features and the slope face is greater than 40° . These directional relationships and the laboratory derived residual friction angles are illustrated on a stereographic projection for kinematical check (Figure 64a). It can be seen that neither fault nor bedding plane alone may kinematically satisfy the plane failure conditions. Besides, the failed zone takes place above the groundwater table (Plate 3) and no identifiable tension crack, which may be filled with water, is observed. These considerations placed focus on the question "how does this slope with such a relatively low bedding inclination fail?"

For this case, it is concluded that the fault may act as a rear release surface and the association of faulting with localized steepening of bedding (25°) may also be a critical factor in the stability (Figure 65c). These kinds of structurally combined failures were reported by Cobb et al. (in Stead, 1990) and Hawley et al. (1986). Similar instabilities with multiplanar failure surfaces have also been experienced in Canadian mines (Munn, 1985; Khan and Nikols, 1989). Stead (1990) suggested an additional possible mechanism in U.K. surface coal mines which may involve the generation of a secondary shear surface between the upper and the lower failure surfaces. This shear surface is determined by a combination of localized strata steepening adjacent to the fault, jointing and intact rock shear through highly disturbed (due to faulting) coal measures rocks of low rock mass quality. The measured inclinations of localized bedding reaching to 25° adjacent to the fault in this vicinity also confirms a high possibility of a multiplanar structurally controlled mode of failure. Thus, back analyzing of the slide was based on this mode.

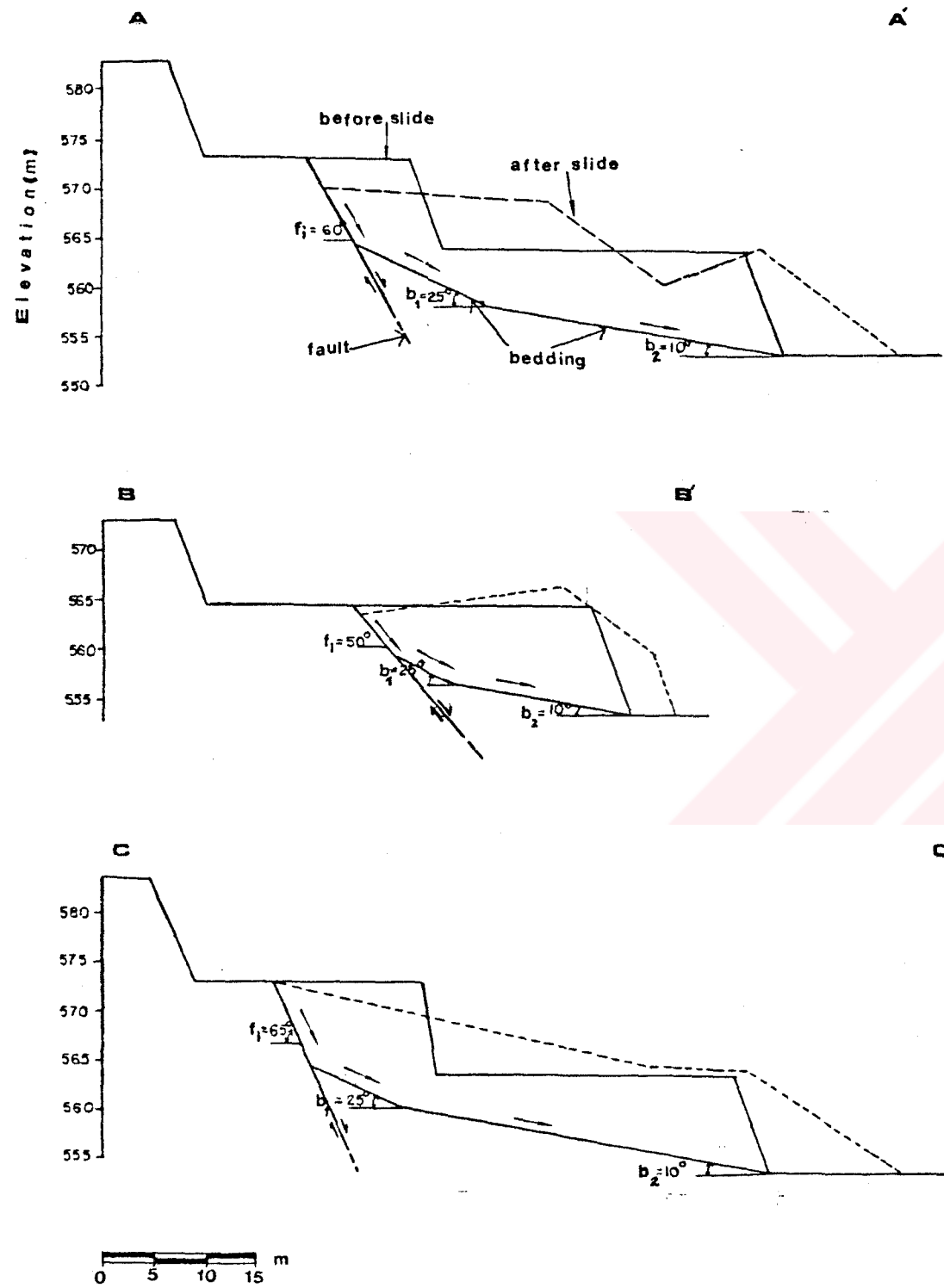
Coulthard (in Stead, 1990), who faced with similar problems in Australian surface coal mines, reported that the Janbu method was not kinematically feasible for the analysis of such failure mode and that an active-passive block method enabled a more realistic modelling of the slope failure mechanism. The approach was also supported by the bi-planar and tri-planar sliding surface methods of analysis (Chowdhury, 1978; Huang, 1983). In these models, as being in this case, the failure surface consists of three discontinuities such as, upper or active wedge, a central or neutral wedge and a lower or passive wedge (Figure 64c).

In this study, the analytical method proposed by Huang (1983) was used (Appendix D.2). The analyses were carried out using the program SWASE developed by the same author. Three typical profiles (Figure 65) involving the pre-failure and post-failure geometries were prepared from the failure plan (Figure 64b) for back analyzing. In the three profiles analyzed the upper failure surface was a fault.

Based on the groundwater conditions, it was concluded that hydrostatic forces did not contribute to the failure and slope was dry. However, the argument that precipitation might have caused reduction in the discontinuity shear strength properties was taken into consideration, as applied in the laboratory tests.

Due to the reasons discussed for bedding surfaces in Chapter 6, linear failure shear strength criterion was used for back analyses. However, power curve criterion was also adopted only for the profile CC' for comparison purposes. It was calculated for both fault gouge and bedding surface. The fault zone was created by shearing which produced flaky clay particles oriented in the direction of shearing. This orientation is believed to produce the major difference between the peak and residual strength of clays (Skempton, 1964).

a) Back analysis sections



b) Comparison of back calculated and laboratory derived shear strength

I : One standart dev.range of peak strength
 II : One standart dev.range of residual strength

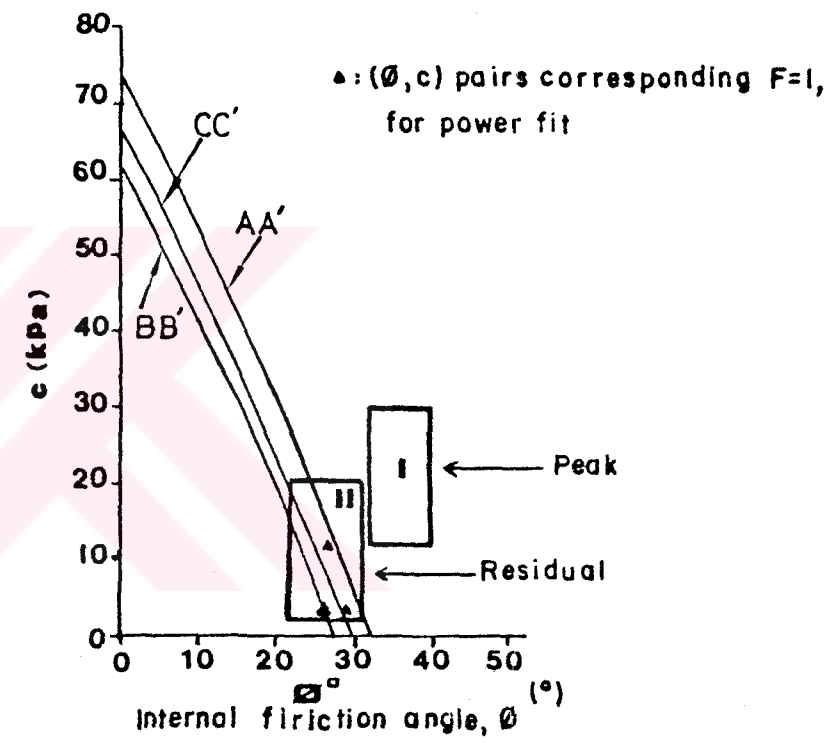


Figure 65: Back analysis of slide 2 developed along multiplanar failure surface.

Skempton (1964) offers another possible explanation by considering that along the oriented domains the shear strength is at its residual value which then transfers additional stress within the material to some other points causing it become oriented. Miller (1982) also showed that laboratory derived residual shear strength was found to be very close to the fault zone strength predicted from a back calculation.

On the other hand, it was shown by Stead (1990) that if negligible effective cohesion and effective friction angle ranging between 15° and 25° were assumed for the fault plane the derived lower wedge failure surface shear strength parameters were in close agreement with residual laboratory shear strength data when slopes without water table and pressurized water were considered. Thus, assuming that the shear strength of the fault gouge was equal to laboratory derived residual values ($c_r=9.7$ kPa ; $\phi_r=17.6^\circ$), the number of unknowns was reduced to two parameters. These pairs of parameters were assumed to be equal for both lower and central bedding surfaces due to their identical surficial properties.

Considering all conditions to be accurately known and that the lower surface runs through toe of the slope, three sections were back-analysed for the combinations of c and ϕ values of bedding. The results are presented in the form of (ϕ, c) functions (Figure 65b). In addition to back-calculated strength, Figure 65b shows the residual and peak shear strength in the range of one standard deviation calculated from the values listed in Table B.6. As can be seen, the back-calculated strength falls within the range of laboratory derived residual shear strength, indicating that the peak strength is not critical. It was noted, however

that the back analysis for profile CC' using power curve criterion produced an equal A and B index values ($\tau=A \sigma^B$) to those obtained from laboratory residual shear tests. This point, represented by a solid circle in Figure 65b, is in a very close agreement with the c- ϕ line of linear relationship.

Based on the back analyses the following conclusions may be derived:

- a) The strength of smooth-planar bedding surfaces in main Sekkøy formation reduces to residual values at the point of failure. As pointed out by Richards et al. (1981), the stress relief due to excavation may result in the separation of bedding planes which dip adversely into the pit and hence would assist in reducing the shear strength.
- b) Water percolating through discontinuities helps to reduce shear strength of the bedding surface.
- c) Based on the very close agreement between the laboratory derived residual shear strength and back analysis results, values of $c_r=12.5$ kPa and $\phi_r=26.5^\circ$ for bedding planes may be used in stability analyses.
- d) The results support the argument that the residual shear strength should be used when large finer material is involved in a fault gauge.

8.4. Back Analysis of Wedge Failure and Monitoring Data

The two monitored wedge failures are back analysed and the results are discussed in the following sections.

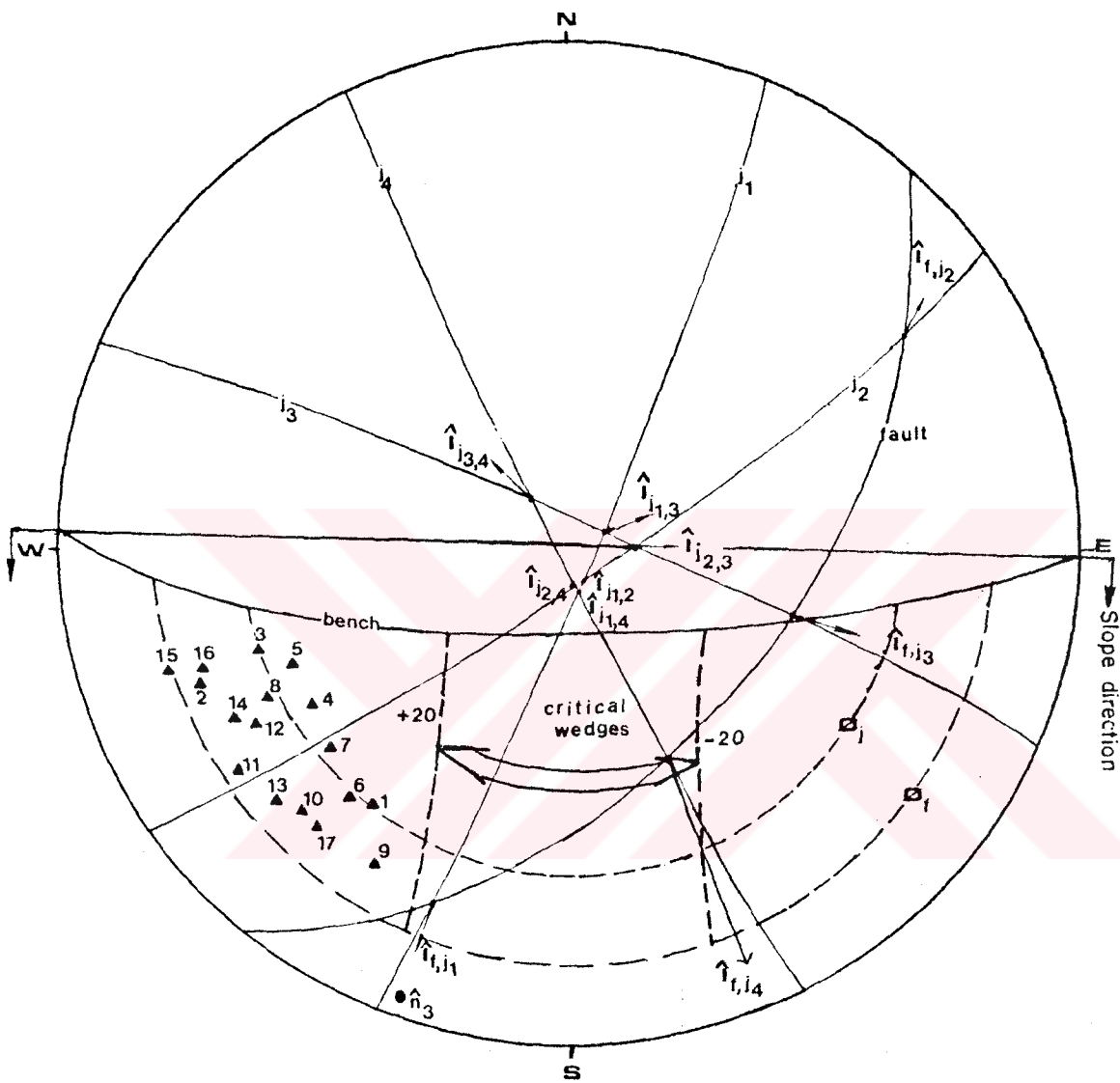
8.4.1. Back Analysis of Slide 6

The slide 6 (see Figures 35,36), as discussed in Chapter 5, seems to have been developed with the combination of discontinuities. The existence of a fault running through the benches and sets of joint oblique to the fault strengthen this approach. In order to investigate the failure mode of this slide kinematic analysis is required.

The orientations of discontinuity sets determined along E-W direction (see Figure 24a) were analyzed to assess kinematically possible failure modes. A lower hemisphere equal area projection of discontinuities with the addition of a local joint set (j4) and the bench face orientation is shown in Figure 66. The residual friction angles from linear fit for the fault and joints were included in the analysis. The bedding planes were not taken into consideration due to their nearly horizontal position.

As it can be seen in Figure 66, neither fault nor each joint set can satisfy the kinematic requirements for plane sliding. Besides, all the lines of intersection of joint sets are steeper than the bench face inclination without any daylighting. Therefore, the only possible mode of failure may be resulted in the combination of the fault and joints. For this purpose, kinematic checks were performed for four intersections, $I_{f,j1}$, $I_{f,j2}$, $I_{f,j3}$ and $I_{f,j4}$ (Figure 66).

The lines of intersections $I_{f,j2}$ and $I_{f,j3}$ are not daylighted by the bench face and they plunge in the opposite direction of the cut face. This situation indicates that



- ▲ : Monitoring station movement direction
- _{i1,3} : Structural intersections
- _{n3} : Pole plot
- J : Joint
- f : Fault
- ◻_{phi1} : Internal friction angle

Figure 66: Kinematic analysis of possible lines of intersection and monitoring station movements for slide 6.

these intersections are not kinematically possible to cause a wedge failure with respect to the face orientation and thus they were eliminated from further considerations. The only two intersection points falling into most critical wedge area (Herget, 1981) were considered (Figure 66). An initial rapid evaluation of likely failure mechanism was made using the stability charts for friction only case presented by Hoek and Bray (1977). The analyses yielded factors of safety smaller than 1 and 2.32 for $I_{f,j4}$ and $I_{f,j1}$, respectively. Hoek and Bray (1977) suggest that a wedge having a factor of safety in excess of 2 is unlikely to fail under the most severe conditions. Besides, the plunge of $I_{f,j1}$ is very flat and ranges between the internal friction circles of two discontinuities. On the other hand, the line of intersection of either plane, fault and joint set 4, lies between the dip direction of the planes (Figure 66). According to Hocking's rule (Hocking, 1976) this geometric relation will satisfy the condition that the wedge will slide down the line of intersection of both planes. Thus, it was concluded that the mode of failure of this instability was wedge type involving the fault and joint set 4.

A more sophisticated analysis was than made of the unstable configuration for back analyzing. The back analysis method for the wedge ($I_{f,j4}$) was based on the analytical solution given by Hoek and Bray (1977 ; Appendix D.3). A computer model named WEDFA (WEDge FAilure), including the conditions of water pressure, tension crack position and external loads were developed by the author (Appendix E.4). A simplified diagram illustrating the forces acting on the wedge is illustrated in Figure 67a.

The sensitivity approach included in the analyses involve:

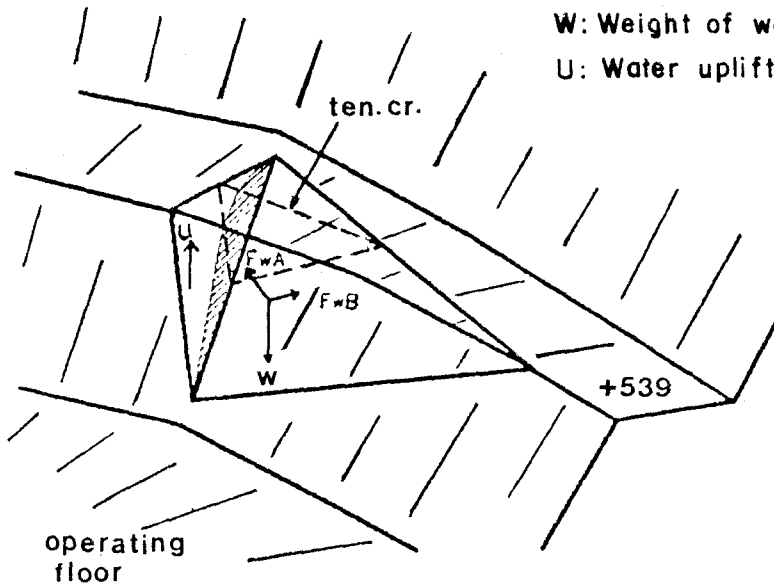
- a) Dry slope with no tension crack
- b) Dry slope with tension crack
- c) Slope with tension crack and water pressure

$F_w A$: Normal force-major plane

$F_w B$: Normal force-minor plane

W : Weight of wedge

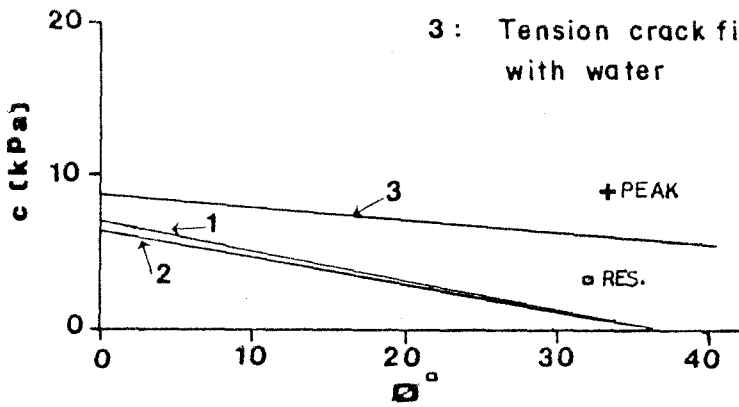
U : Water uplift



a) Sketch showing wedge and forces mobilized

CASES

- 1 : No tension crack
- 2 : Tension crack (dry)
- 3 : Tension crack filled with water



b) Comparison of back calculated and tested shear strength

Figure 67: Back analysis of slide 6.

The tension crack labeled by T was measured approximately 7 m away from the original crest of the bench (Figure 36). This point also coincides with the intersection point of both discontinuities. The residual shear strength parameters of fault gouge were used as input data to estimate the pairs of c and ϕ for the joint surface.

The results of back analyses combined with sensitivity analyses are given in Figure 67b. As can be seen, there is no significant difference between the dry slope with no tension crack and with tension crack cases. The (ϕ, c) function forms of these cases are in a close agreement with the laboratory derived residual shear strength parameters of joint surfaces. While the third case, including also water pressure, requires a shear strength higher than those of laboratory derived to satisfy a factor of safety of 1.0 at the time of failure. On the other hand, no rain was recorded before failure and the failed mass is located above the groundwater table (Plate 3). However, discontinuity surfaces may contain slight moisture due to percolation of surface water through joints during winter, before failure was initiated. This condition was also simulated in the laboratory test environment.

As a conclusion, it is assumed that failure 6 is developed with the combination of fault and joint forming a wedge and that residual shear strength is mobilized along the joint surfaces during failure. However, it is also possible that other joints, which did not directly contribute to the failure, probably helped to develop the failure as release surfaces (Figure 35b).

Monitoring station movements (plunges and trends) are also plotted on the equal area projection (Figure 66) for comparison with the kinematic analyses. These directions, having an average difference of about 30° , generally correspond to the dip direction of the line of intersection

$I_{f,j1}$. Besides, movement vectors are in close agreement with the plunge of $I_{f,j1}$. This situation strengthened the idea that the line of intersection $I_{f,j1}$, which was stable before the slide 6, might be activated towards the void created by the previous failure.

On the other hand, pole of the joint set 3 (n_3), the dominant joint set in the pit (Figure 24a, c), falls very close to monitoring plots (Figure 66). The position of this joint set may kinematically cause initiation of a toppling failure. After the first failure the direction of the bench crest changed to NW-SE. This direction also created a new unsupported face for movement. Thus, it may be concluded that the most probable cause of the movements following slide 6 is attributed to the combined effects of wedge and probably toppling modes of instabilities. Unfortunately, due to the lack of quantitative long term monitoring data after September 1989 and fast operation in the pit restricted the observations on old instabilities. Thus, detailed analytical analysis could not be performed for this secondary instability.

8.4.2. Evaluation of Monitoring Data From the Highwall of Ninth Slice

The movement vector analysis carried out for the failure monitored on highwall of ninth slice has indicated that the failure was more likely to occur along a shallow seated surface rather than fully structurally controlled mode of failure. In order to determine the mechanism of this failure and to compare the monitoring data with those of kinematic analysis, the data obtained from the site was plotted on the equal area projection (Figure 68).

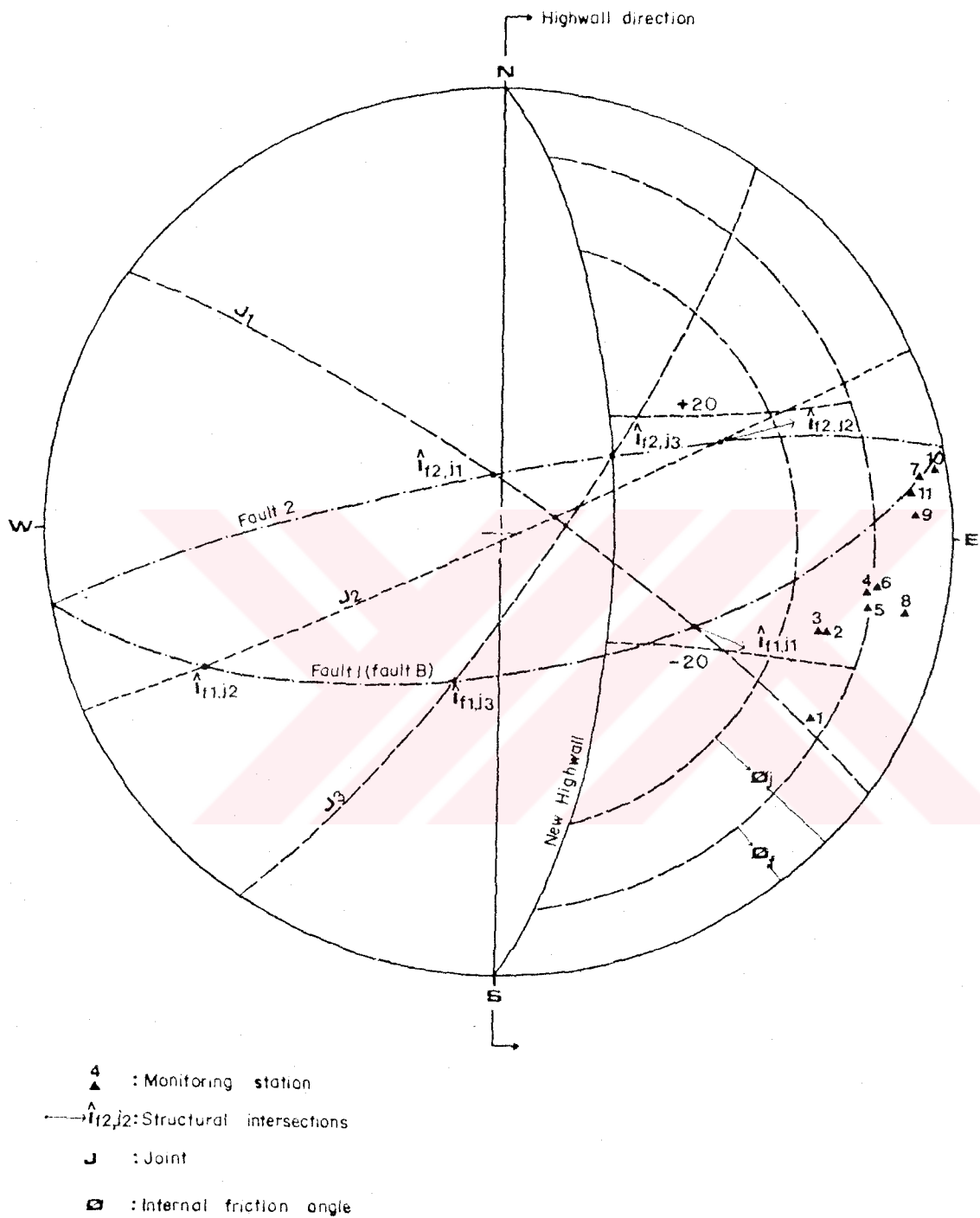


Figure 68: Kinematic analysis of possible lines of intersection and monitoring station movements for the highwall instability at the end of ninth slice.

Examination of Figure 68 indicates that movement directions of the monitoring stations generally corresponding to the dip direction of the lines of intersection of wedges involving faults and steeply dipping joint sets. However, monitoring station movement vectors are generally 25° to 35° shallower than the plunges of lines of intersection. On the other hand, analysis using stability charts (Hoek and Bray, 1977) yielded factors of safety of 0.82 for $I_{f1, j1}$ and 2.85 for $I_{f2, j2}$. The wedge involving fault 2 and joint set 2 has small dihedral angle and may cause forming of a small wedge.

Based on the above discussions it is concluded that the geological structure has had a significant influence on the failure mechanism, although geological structures do not appear to control the entire failure. This introduces a distinct three dimensional nature of the higwall failure and, hence, potential failure surface involves a complex surface formed in part along structural discontinuities and in part through intact rock.

Piteau and Martin (1982) as well as Newcomen and Martin (1988) documented numerous failures which involve more than two planes. The failure by rotational sliding may occur on a plane and separation across the other plane. They suggest that occurrence of a subvertical joint may initiate a tension crack, as being in this case, or backscarping of a wedge. These features would reduce the size of the failure discontinuity planes with different orientation could lead to an ever more complex failure geometry.

The mechanism mentioned above introduced similarities to that of the author's approach. Besides, progressive increase in the amount of movement along tension cracks from right to left, shown in Figure 38, also resembles rotational mechanism for this failure.

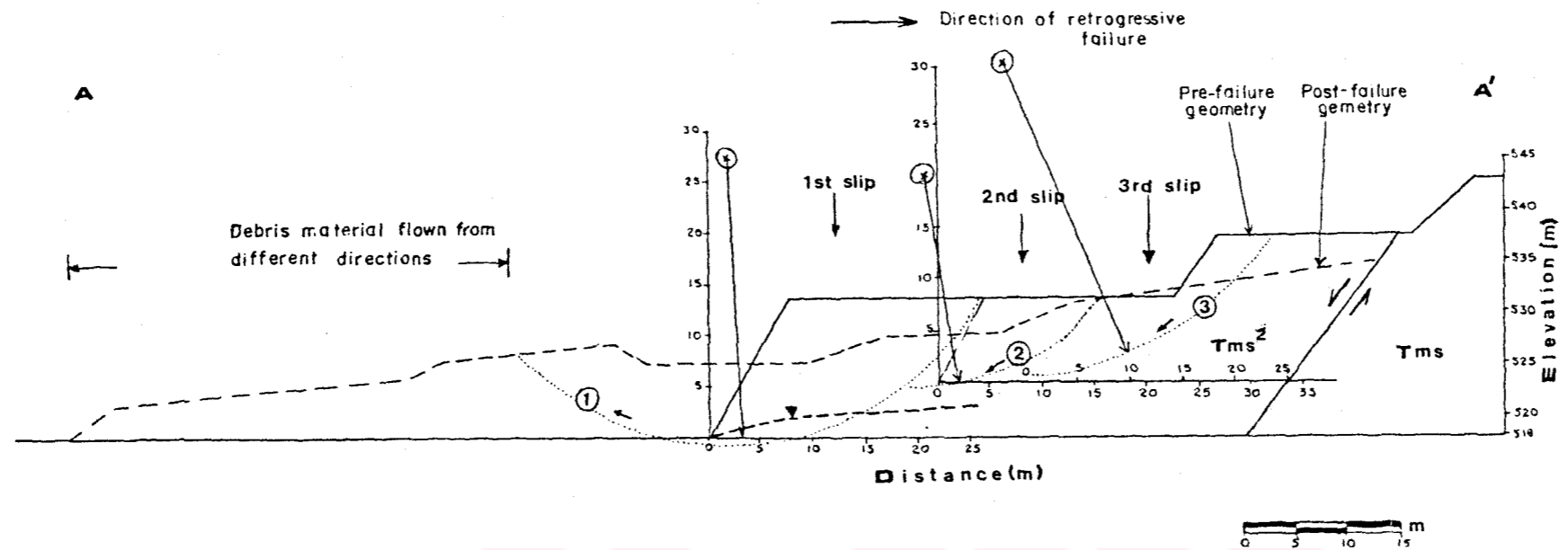
However, the temporary spoil material dumped behind the crest of highwall was not included in the failed mass. It should also be noted that the forces imposed by the spoil pile probably contributed to the forces tending to induce sliding. This surcharge effect makes the mechanism to be more complex. Thus, results of the refined analyses and assessment of monitoring data suggest that failure has developed by a combination of sliding along steeper discontinuities in the marl and failure through the rock mass in the lower portion of the slope.

8.5. Back Analysis of Mass Failure in the Transition Zone Soils

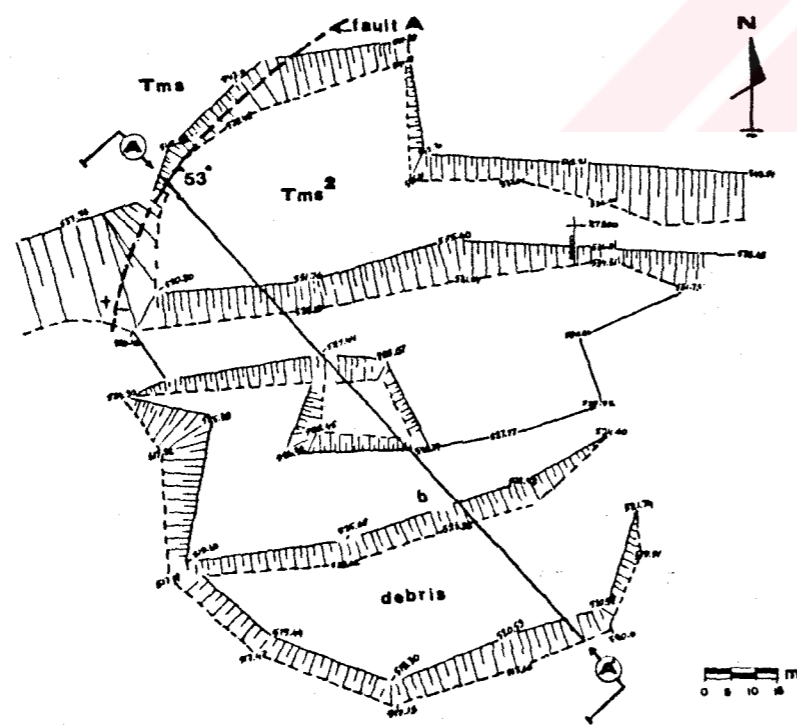
The slide 7, shown in Plate 3, occurred throughout the transition zone soils and was bounded from NW by fault- A. The failed slope involving two benches was not steep. The failed mass was in the form of separated successive blocks (Figure 69a). The mode of failure has been categorized as a rotational slide because of the curved shape of the observed part of the failure surface, tilted position of the failed mass, and the heave at the toe area. In order to understand the failure mechanism and to confirm the mobilized shear strength of the material, systematic back analyses of the slide zone were undertaken along a section (Figure 69b) prepared from the instability plan.

The Bishop simplified method of slope stability analysis (Bishop, 1955) for circular slip surfaces (Appendix D.4) was employed. Calculations were performed with the MTASLP computer program developed at MTA Rock and Soil Mechanics Division. MTASLP is a program that can handle slope stability analysis of slip surfaces for slopes involving many benches, various soil materials and different groundwater conditions. The program has routines that search

a) Failure geometry and successive critical slip surfaces



b) Instability plan



c) Comparison of back calculated and laboratory derived shear strength

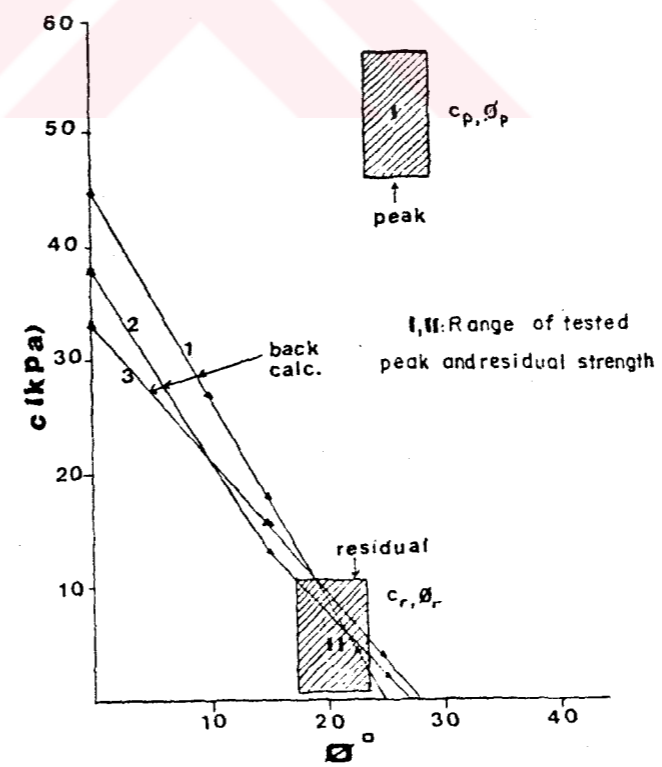


Figure 69: Back analysis of slide 7 located within the transition zone soils.

for more critical failure surfaces in a grid system or automatically. Circular rotation was analyzed using effective stress, since the study is concerned with the long-term stability of slope.

Some factors such as local strength variations, climatic influence, etc., cannot be realistically included in the analysis. However, during site investigations no indication of groundwater was observed and the failed material is consisted of considerably homogeneous finest material involving lenses of coarser material in the upper levels. However, in a silty sand of 1 m thick located at the E of the slide a seepage point was noted.

As a first step, the possibility of a circular slip surface running from the toe to fault A is analyzed. The slope was assumed dry and the mean unit weight (Table 6) was used. Besides, as an initial approximation, the laboratory derived residual shear strength parameters, both for finest material in the failed zone ($c_r=5$ kPa; $\phi_r=22.5^\circ$) and the uppermost portion of the fault ($c_r=9.7$ kPa; $\phi=17.5^\circ$), were employed. The analysis yielded a factor of safety of 2.01. This indicated that the failure could not develop throughout the entire slope involving two benches even if the residual shear strength parameters were mobilized along the slip surface.

Using the same approach the analysis was continued by including a groundwater table of 6 to 7 m high to investigate the saturation effect on the stability of slope. The results yielded a minimum factor of safety of 1.77, suggesting that the slope with a considerable high groundwater table was reasonable stable and failure probably developed by successive slips. Therefore, a different sliding mechanism was adopted. This approach involved a failure in the lower bench along a critical circle that would alter the geometry and consequently the stability of

bench resulting in a succession of rotational slides which tend to retrograde from the toe to the top of slope. The successive position of failed blocks (Figure 69a) and the observed tension cracks represent the boundaries of retrogressive failure slices.

An analytical study of this retrogression was performed on the profile given in Figure 69b. Each time a critical circle with a factor of safety equal to unity was computed for different combinations of (ϕ, c) pairs. The material slumped was assumed not to be removed. The resulting profile with a new steepened face was re-analyzed and each consecutive failure was assumed to occur.

On the basis of the block configuration and observations performed in the slide area, the slip surface indicated as 1 for the initial slide was assumed to be the most predictable slip surface (Figure 69b). Considering the seepage point mentioned above, analyses were carried out to obtain (ϕ, c) function forms for equilibrium conditions ($F=1$). Turning back to Figures 69b and c, analyses showed that there are certain combinations of parameters for which the most critical slip surfaces determined are very close to the predictable surface labeled as number 1.

Additional back analyses were performed for the second and third successive sliding blocks with the assumption that most predictable actual slip surfaces might be the surfaces 2 and 3, as shown in Figure 69b. In the analyses, steepening of the slope due to the void created by the previous failure was taken into consideration. Analyses for (ϕ, c) pairs indicated that there was also a close agreement between the most predictable surfaces and determined slip surfaces at limiting equilibrium condition. Thus, back analyzing of three successive slip surfaces was assumed sufficient for evaluation of shear strength parameters.

Lines showing combined values of c and ϕ producing limiting equilibrium for successive failure conditions are illustrated in Figure 69c. In addition, laboratory derived peak and residual shear strengths of this soil material, in the range of one standard deviation, was also shown as ruled areas in Figure 69c. As can be seen in Figure 69c, the peak laboratory derived strength is considerably higher than the actual state under investigation, while the intersection of two (ϕ, c) function forms plot in ruled area II, which represents residual strength. These intersections may be considered as the right combination of c and ϕ values (Sancio, 1981). On the basis of these back calculated values are concentrated between 5 to 10 kPa and 20° to 22° for c and ϕ , respectively.

It is noted that there is a good agreement between the laboratory derived shear strength parameters and back analysis results. Thus, residual values may be employed in further stability assessments for the slopes in transition zone. The instability has continued in the form of successive slides until a safety factor greater than unity was reached. The stable slope was obtained for the profile given in Figure 69b when the cycles reached to the fault surface behind which a competent marl lies.

The back analyses also indicates that construction of a bench of 10 to 12 m high would not be adequate for transition zone. This situation was taken into account for the stability of slopes as planned in the same material at SW part of the open pit.

8.6. General Evaluation of Other Slides

The probable modes of failure of the slides encountered elsewhere in the pit are evaluated on the basis of

observations and their similarities with those analysed because of the lack of suitable information for back analysing.

- a) Slide 1: Dips of bedding planes encountered along the basin margin in Ertrans section (reaching up to 30° - 35°) are greater than the residual friction angles of planes both in hangingwall and footwall. Besides, there is a close agreement between the strikes of bedding planes and bench faces. In spite of the lack of information for slide 1 (Figure 61) and severe disturbance in the rock mass after failure, it was however, distinguishable that the slope was designed with a highly steep overall slope angle and narrow bench width. These conditions indicated that the plane shear failure would be satisfied. This conclusion is also confirmed by the position of the failed blocks. On the other hand, a portion of sliding surface developed on the footwall clay dipping 33° south, which appeared after removal of sliding material by TKİ in June 1991 in the slide area 1b suggests the mode of plane failure (Figure 70).
- b) Slides 3 and 4: In the slide areas 3 and 4 severe disturbance prevented detailed observation in the failed mass. However, orientations of the faults and bedding planes show similarities with those of slide 2 (see Figure 64) which occurred at the eastern edge of the same bench. Thus, it is concluded that these two failures probably resemble a multiplanar failure involving faults and bedding planes.
- c) Slide 5: It is a local instability developed through highly decomposed sandstone which represents a relict portion of Yatağan Formation in the north. It is obvious from its spoon shaped form (Figure



Figure 70: View from plane sliding surface developed along a clay bed in footwall at Ertrans section-slide 1b (Plate 3-Photo. No.25).



Figure 71: General view of slide 5, developed along a circular slip surface within a highly decomposed sandstone (SSt) (Tms : Sekkøy formation ; Plate 3-Photo. No.26).

71) that the failure developed along a shallow circular slip surface. It may also be concluded that the material showing a soil-like behavior has lost its strength due to steepening of the slope and probable softening after rainfall and then failed through the weaker link in the mass.

8.7. Failure Modes of Slides of the Eskihisar Open Pit

Detailed back analysis of five instabilities and general assessment of other slides located in the pit showed that the most common failure modes are planar and multiplanar slide mechanisms both in the hangingwall and in the upper levels of footwall, subsidiary wedge failure in Sekköy formation and circular failure in transition zone soils. In addition to these, in blasted highwalls with excess external loading, such as those imposed by temporary spoil piles, a complex failure involving discontinuities and the failure through intact rock was also possible.

The main modes of failure experienced at the Eskihisar open pit are illustrated in Figure 72.

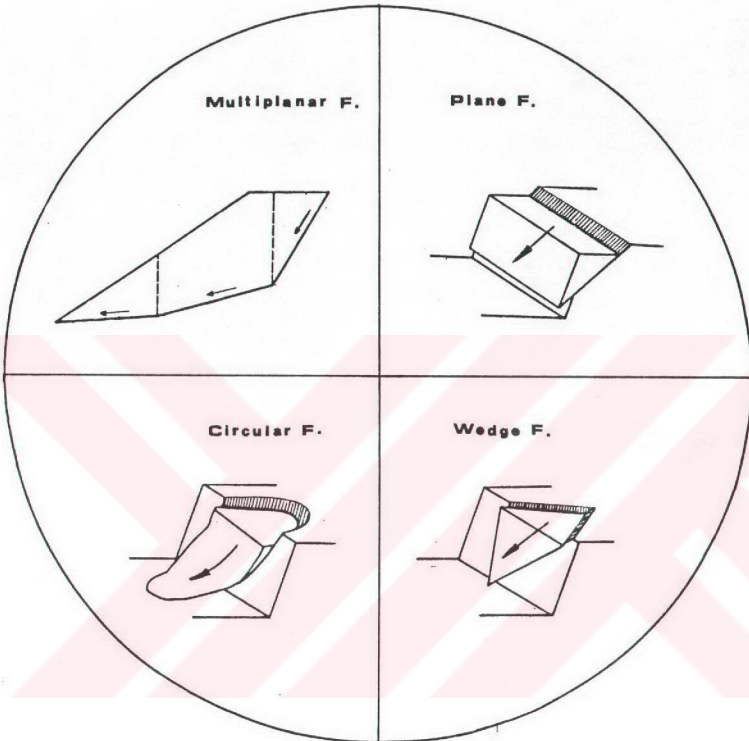


Figure 72: Typical modes of failure experienced at the Eskihisar open pit.

CHAPTER 9

DESIGN SECTORS AND KINEMATIC ANALYSES OF PIT SLOPES

The results of back analyses of slides encountered at Eskihisar open pit showed that the instabilities are mainly structurally controlled failures. As faced in this case, in regularly bedded rocks, cut by faults and joints, there are many possibilities for block movement along weakness planes and a large variety of behavioral modes are exhibited. With an appreciation of the mode of failure, it is possible to evaluate a factor of safety and to investigate remedial measures. Thus, considering that the kinematic model studies help to anticipate the most likely pattern of slope failure in the rock masses, analyses were carried out to assess the kinematically possible failure modes using the results of geological structural analysis. Detailed limit equilibrium (deterministic) stability analyses, were then based on the results of kinematic checks.

9.1. Design Sectors

Structural domains of Eskihisar open pit were divided into nine sectors, where the final slope orientation and operational use are relatively constant, and the types of discontinuities with respect to the pitwalls are similar (Figure 73). In addition to these direction of advance, orientation of highwalls and position of the highway were also considered. The sector boundaries (Figure 73) were kept constant throughout the life of long-term design. Although constant sector boundaries are not required in the analyses, they ease data gathering and interpretation.

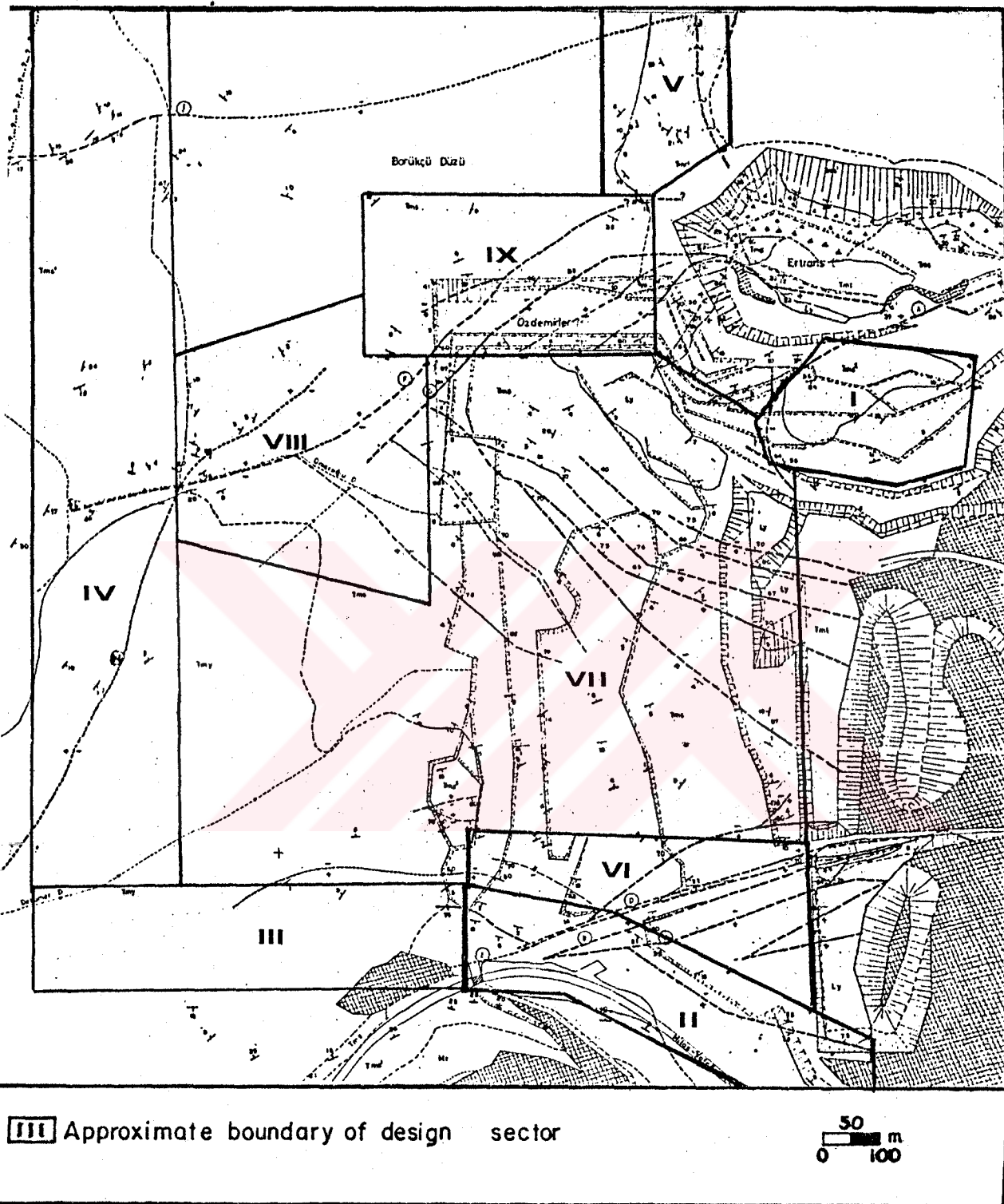


Figure 73: Design sectors at Eskihisar open pit.

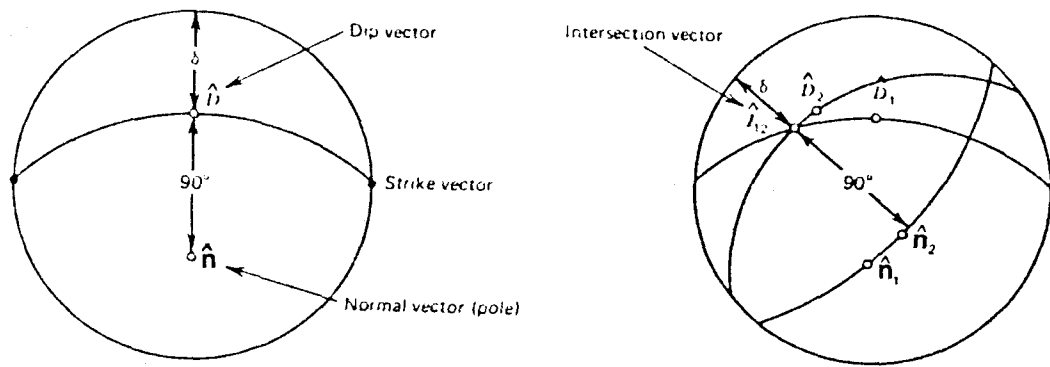
In the southeast of the pit where bedding planes dip into the excavation planned permanent slopes (sidewalls) are adjacent to highway. Besides, this location is also very close to faulted blocks. On the contrary, its SW extension will be constructed through a rock mass involving nearly horizontal structural features and introducing different slope behaviours. Thus, the south face was divided into two sectors (II and III). The basin margins were placed in sectors IV and V. The current pit area was divided into three sectors, because of variable orientations of pitwalls and fault systems with different orientations causing different modes of instability. Within each design sector, the main kinematically possible modes of failure were determined.

9.2. Kinematic Analysis of Slopes

The existing and planned slopes in Eskihisar open pit were kinematically analysed using stereographical projection techniques described in most referenced literatures (Hocking, 1976 ; Hoek and Bray, 1977 ; Goodman, 1980 ; Bell, 1981 ; Herget, 1981). The details of the techniques used herein were not included in this chapter. However, kinematical conditions satisfying the most common types of structurally controlled modes of instabilities are summarized in Figure 74. The symbols for the basic line elements of rock mass used in the analyses are also introduced in Figure 74a.

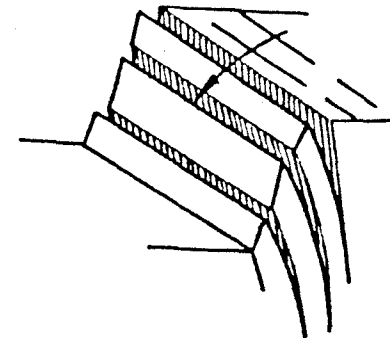
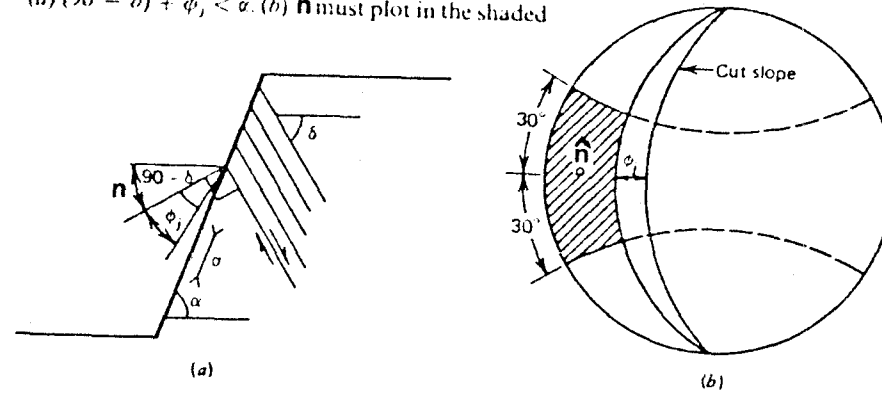
Face angles and strikes of permanent slopes both of working benches and slopes of highwall (Figure 75) are used as input parameters in kinematic check and are based on the values given in TKI project and the current applications in the pit. Friction circle of each discontinuity was drawn on nets using their laboratory derived residual friction angles (Table 12), which were also confirmed by the back analyses.

a) Stereographic projections of line elements



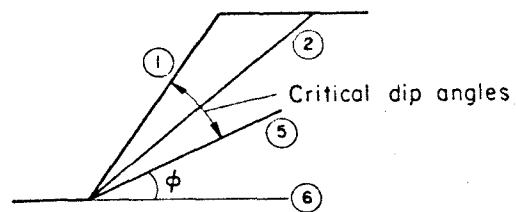
b) Toppling failure

(a) $(90 - \delta) + \phi_j < \alpha$. (b) \hat{n} must plot in the shaded

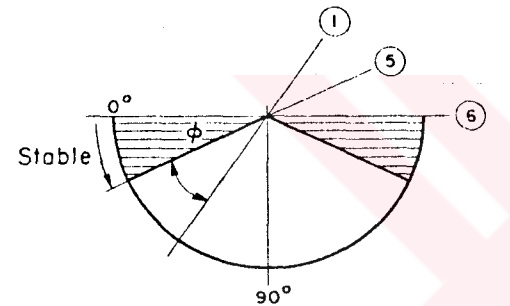


(c) Block diagram

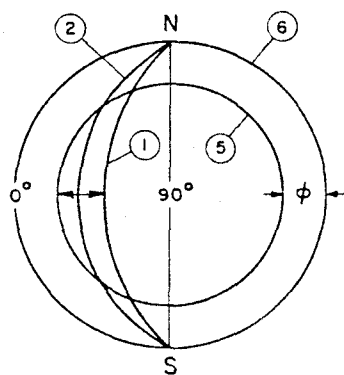
c) Plane failure



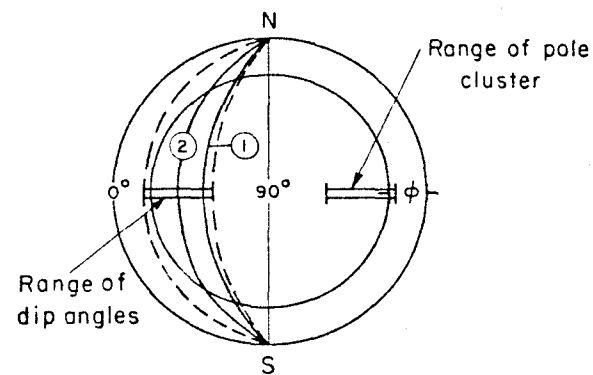
(a) Cross section of simple plane shear



(b) Cross section of lower hemisphere of equal area net with stable dip angles due to friction (ϕ)



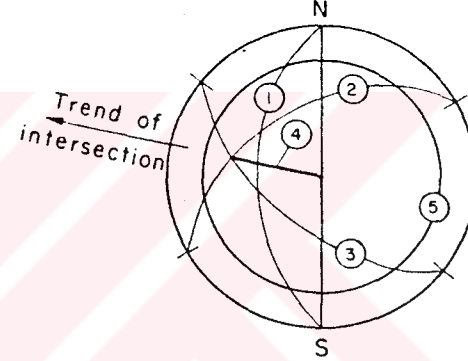
(c) Equal area net presentation of (a) showing range for critical dip angles



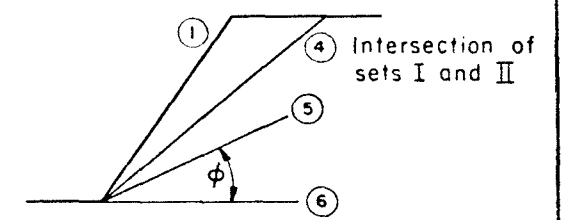
(d) Range of discontinuity dips from pole cluster

All discontinuities with dip angles $< \phi$ are stable
 All discontinuities with dip angles $> \phi$ are unstable

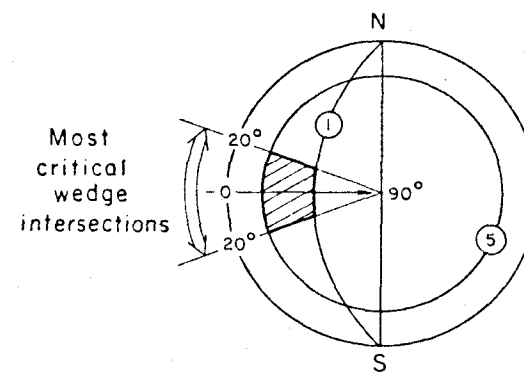
d) Wedge failure



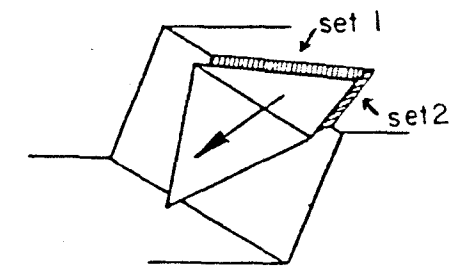
(a) Determination of intersection from mean orientation of sets I and II



(b) Section of wedge instability



(c) Area of critical plunge and trend



(d) Block diagram

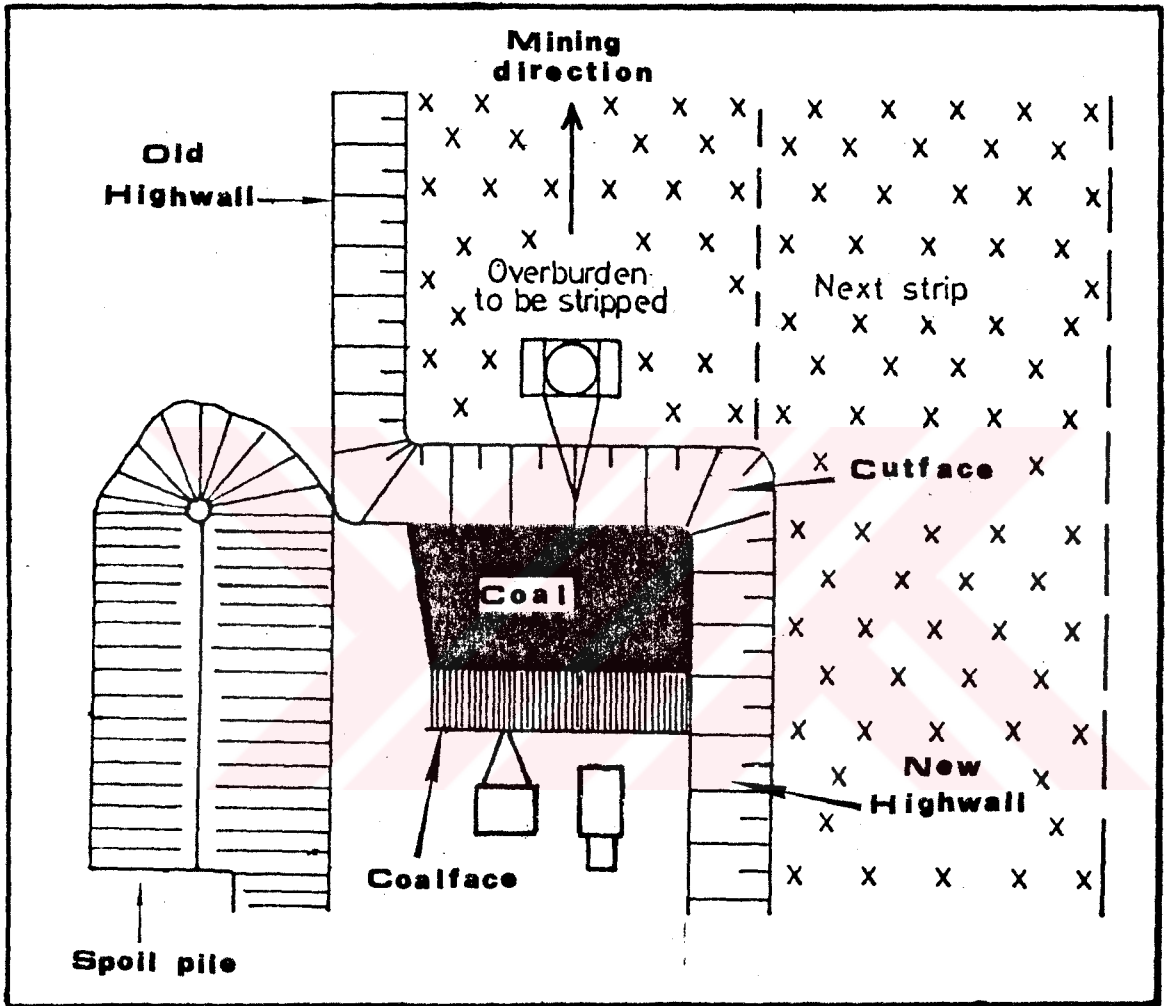


Figure 75: Configuration of highwall slopes.

The stability conditions of each current and/or planned faces were analysed individually using significant discontinuity orientations given in Table 1. However, local steepenings or critical deviations from the highest concentrations recorded in bedding planes were also taken into consideration. With this application, it was aimed to investigate the probable negative effects of deviations in bedding orientations on the kinematical behaviour of slopes. Besides, for slopes where sufficient directional data are not available, the geological cross sections running vertically to the strike of planned slopes were utilized.

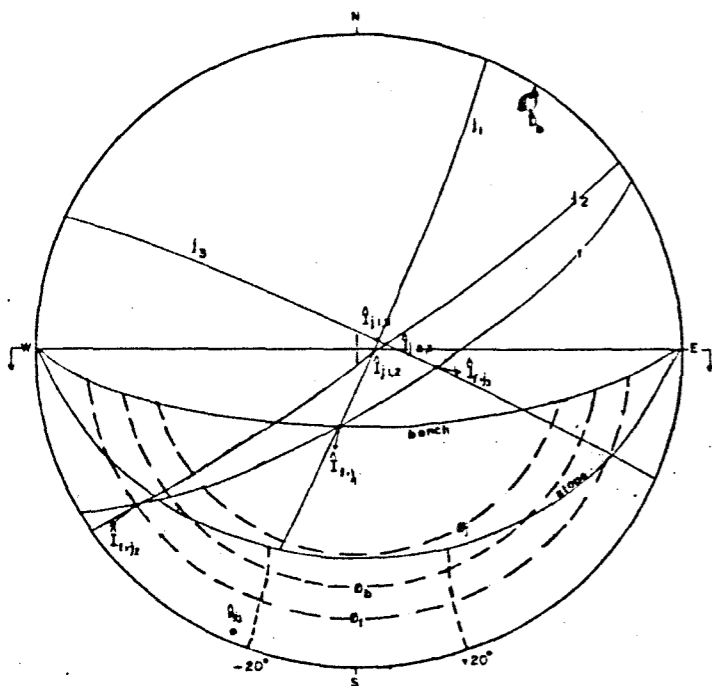
Faults were evaluated by taking their local orientations in each sector into consideration. On the other hand, on the basis of TKI's approach, analyses were carried out alternatively for different highwall orientations and working benches both in the N-S and E-W directions for sectors VIII and IX.

The graphical analyses for each design sector are illustrated in Figure 76a through i. The results of the kinematic analyses are summarized in Table 14. On the basis of information gained from kinematic analyses the following conclusions were drawn for main structurally controlled modes of failure encountered and/or expected in the study area:

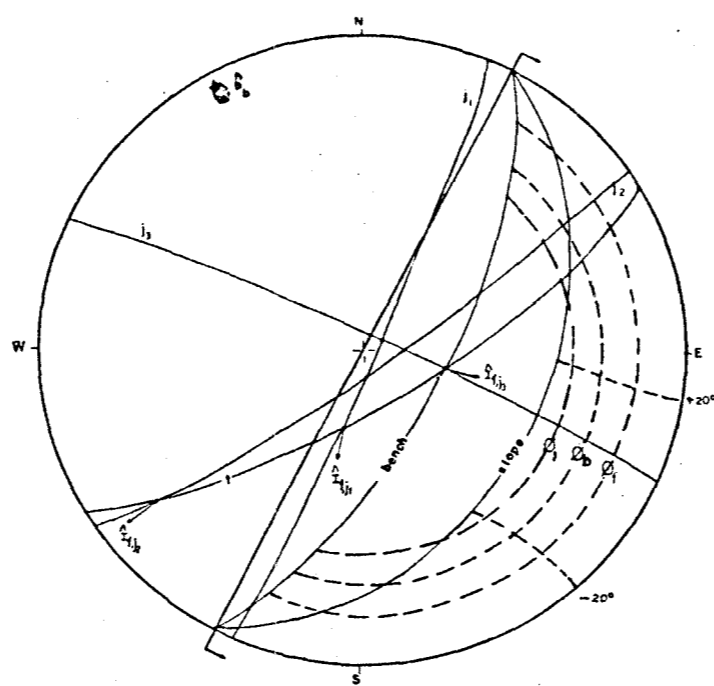
Plane failure: The entire stability of planned permanent slopes in the N-S direction along the E and W basin margins are mainly controlled by plane failures (Figure 76d and e). Bedding planes dipping into the planned excavations make these discontinuities the major structural element contributing to failure. This mode of instability seems to be more critical for footwall involving weak black clay bed, which has a lower shear strength than those of bedding planes in

a. DESIGN SECTOR I

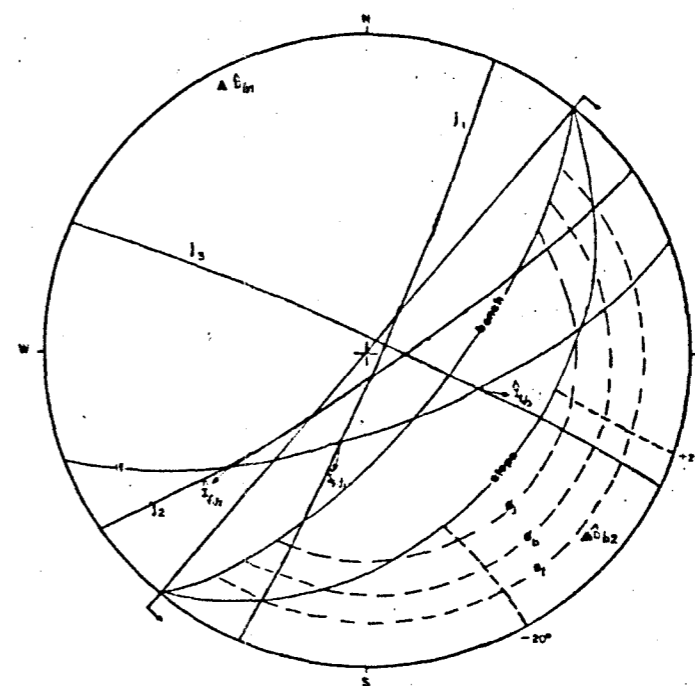
a.1. Section 1-1'



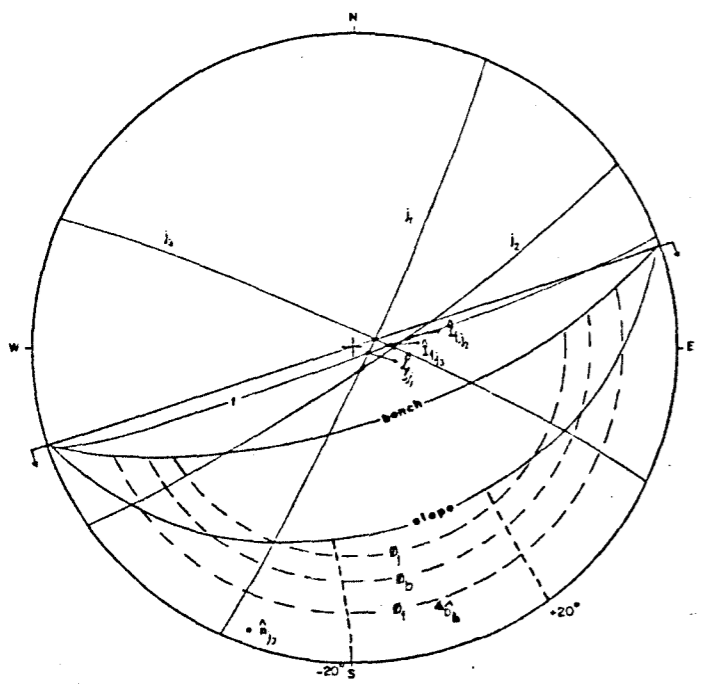
a.2. Section 2-2'



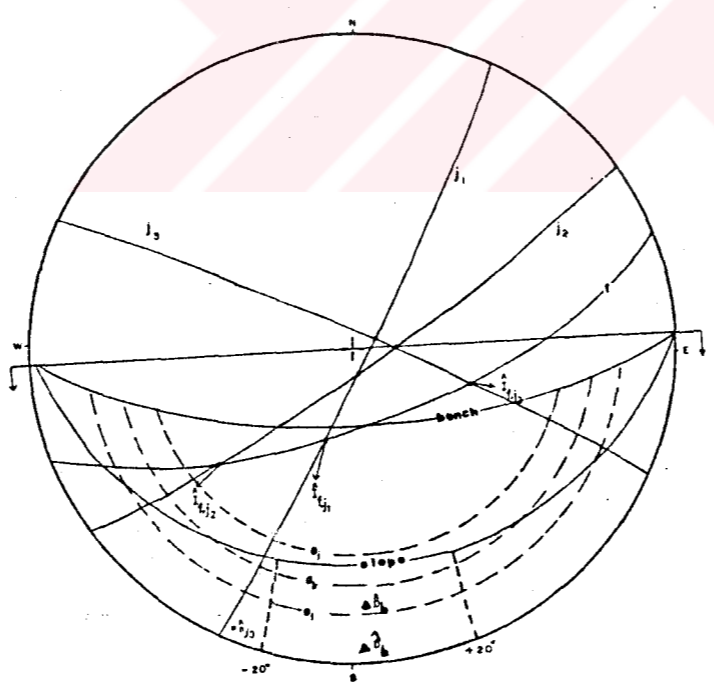
a.3. Section 3-3'



a.4. Section 4-4'



a.5. Section 5-5'



a.6. Section 6-6'

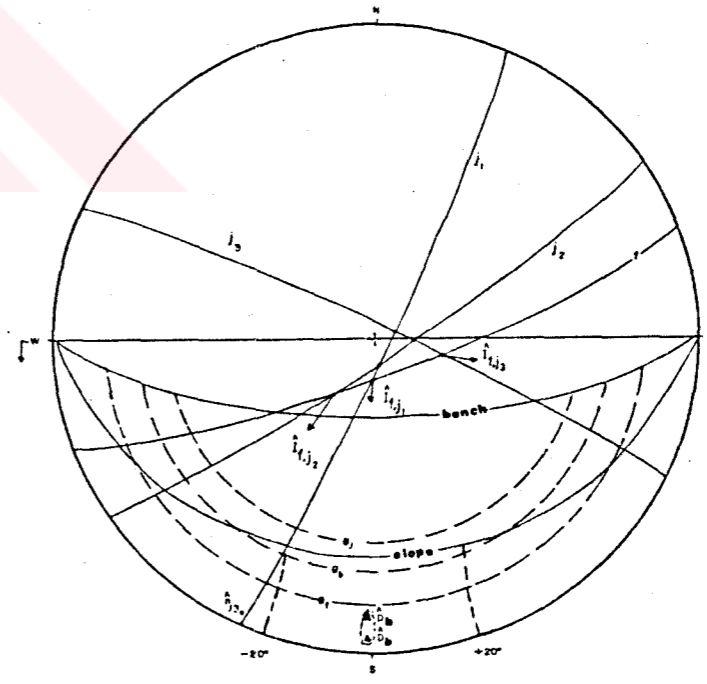


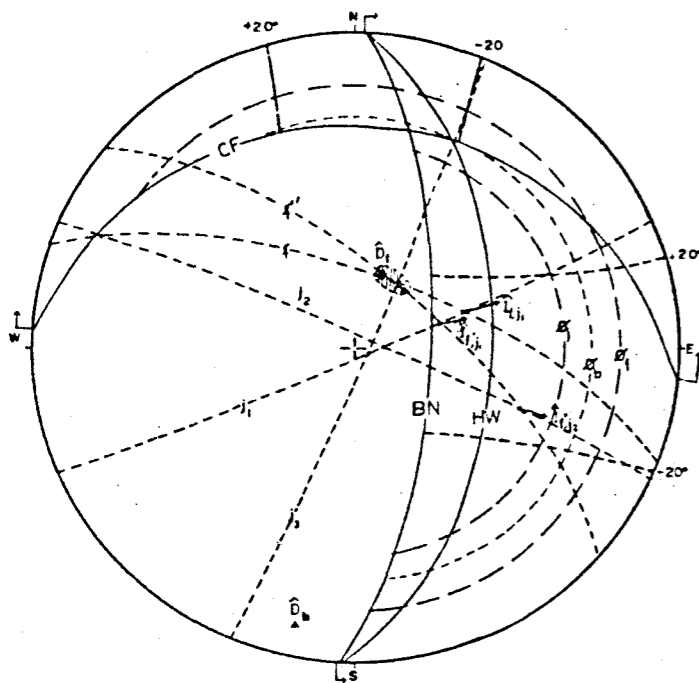
Figure 76: Kinematic analyses used to identify potential slope stability problems for design sectors.

h. DESIGN SECTOR VIII

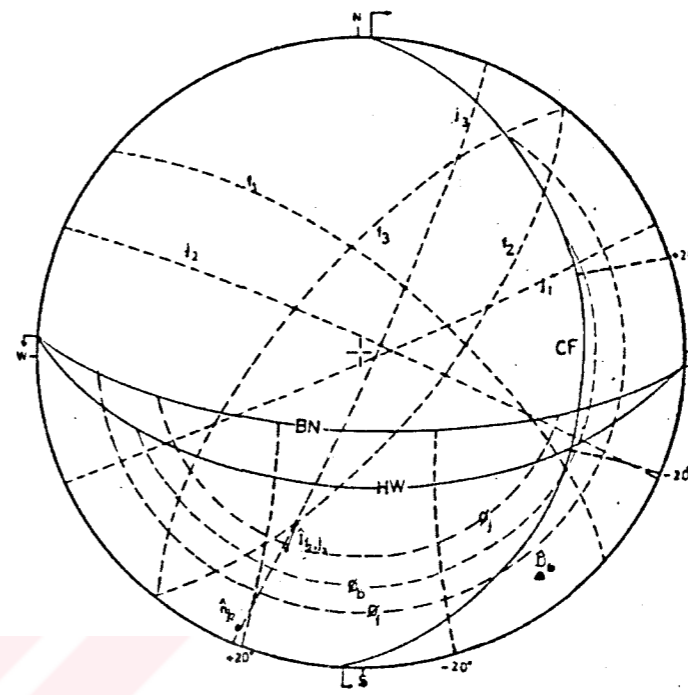
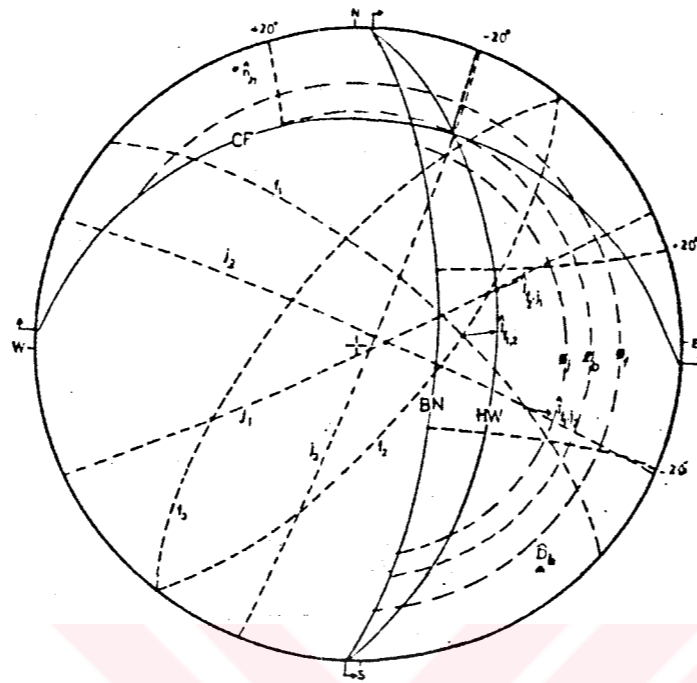
g. DESIGN SECTOR VII

h.1. Slices oriented in NS direction

h.2. Slices oriented in EW direction



f: faults striking NW-SE (east of 15th slice)
f' : " " " (west of 15th slice)



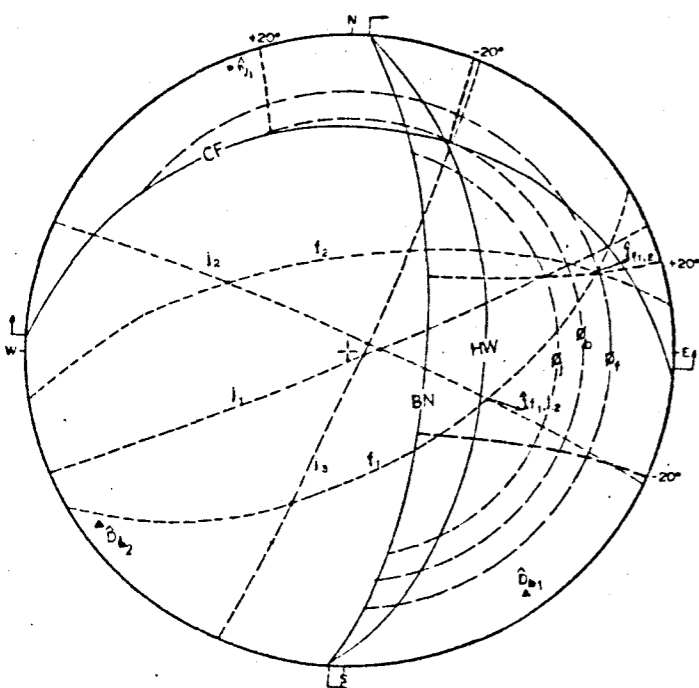
BN: Working bench HW: Highwall CF: Cut face

i. DESIGN SECTOR IX

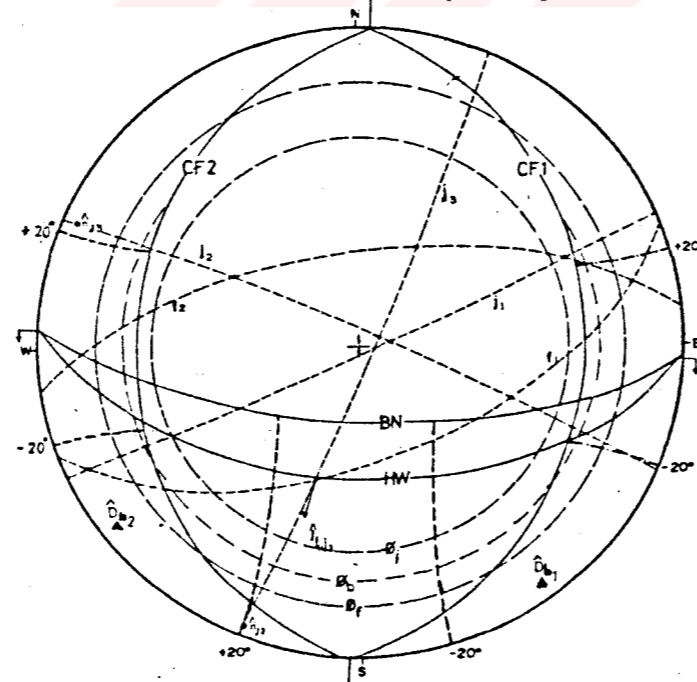
i.1. Slices oriented in NS direction

i.2. Slices oriented in EW direction

j. The relationships between line of intersection and slope face

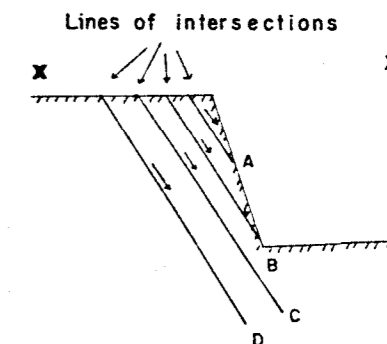
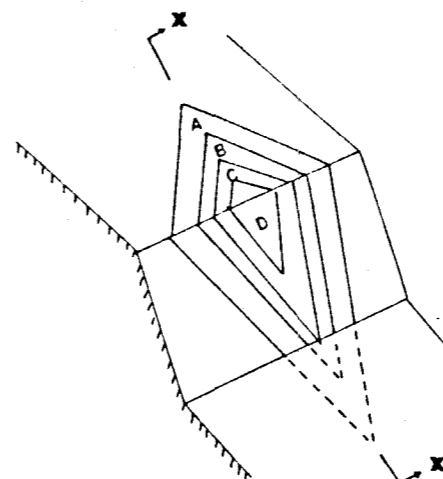


Working from E to W Working from W to E



j.1. Block diagram

j.2. Cross-section



Lines of intersections of wedges
C and D do not daylight and
no wedge failure risk

Figure 76 (Continued)

Table 14 : Design sectors and potential instabilities

Design Sector	Description Domain	*Orientation of slope and bench	Possible mode of instability	Plunge or orientation of critical structure	Instability classification	Considerations
I**	Section I-1'	35/180 (OS) 70/180 (BN)	Toppling involving set 3.	85/024 (J3)	Safe (if joint set 3 is continuous throughout the entire bench face, local separation in the uppermost bench of the slope).	--
	Section 2-2'	42/118 (OS) 70/118 (BN)	Wedge possibility involving fault A and bedding planes.	70° (I _{f,j3})	Safe (plunge of line of intersection is equal to bench inclination, due to this parallelism no daylighting).	--
	Section 3-3'	43/130 (OS) 70/130 (BN)	Multiplanar failure possibility along fault A and bedding planes. Wedge possibility involving fault A and set 3.	70/160 (f) 13/130 (B)	Critical, particularly in slope with groundwater. Detailed analysis is required flattening of slope.	--
	Section 4-4'	41/162 (OS) 70/180 (BN)	Multiplanar failure possibility along fault A and bedding planes	87/150 (f) 15/162 (B)	Critical	As in Section 3-3'
	Section 5-5'	32/177 (OS) 70/177 (BN)		70/160 (f) 5°-19° (B)	Critical	" "
	Section 6-6'	32.5/180 (OS) 70/180 (BN)	Wedge possibilities involving fault A and set1; fault A and set2. Multiplanar failure possibility along fault A and bedding planes.	66° (I _{f,j1}) 44° (I _{f,j2})	Safe (line of intersection is not expected to be daylighted by the slope due to low bench height).	--
	Section 7-7'	30/220 (OS) 70/220 (BN)		80/160 (f) 5°-11° (B)	Critical	As in section 3-3'
				70/160 (f) 0°-17° (B)	Critical	" "
			Wedge possibilities involving fault A and set1; fault A and set2. Toppling involving set3.	66° (I _{f,j1}) 44° (I _{f,j2})	Safe (line of intersection is far from the crest and is not daylighted due to low bench height).	--
				85/024 (j3)	Safe (if the joints are continuous throughout the entire bench, local separations in the uppermost bench of the slope).	--
II	Southeast permanent slopes adjacent to highway	30/022 (OS) 70/022 (BN)	Multiplane failure along faults and bedding planes. Plane failure along bedding planes.	75/021 (f) 56/353 (fault c) 12°-28° (B)	Critical	Detailed analysis is required.
			Wedge possibility involving fault C and set2 between the slices of 13 and 16.	60° (I _{f2,j2})	Safe (line of intersection is not daylighted by the bench face due to low bench height).	--
III	Southeast permanent slopes	45/353 (OS) 70/353 (BN)	Toppling involving set3.	87/157 (j1)	Safe (slope will be cut in the upper zone of Sekkoy formation where joints have lower persistence).	--
IV	Permanent slopes along basin margin in the west	35/090 (OS) 70/090 (BN)	Plane failure along bedding planes in Sekkoy formation and along black clay below the coal seam.	20°-30° (B)	Critical (for both highwall and footwall, particularly in the case of groundwater).	Detailed sensitivity analysis is required. Flattening of slope may be useful.
V†	Permanent slopes, along basin margin in the east.	35/270 (OS) 70/270 (BN)	Same as in Sector IV.	14°-35° (B)	Same as in Sector IV.	Same as in Sector IV.

Table 14 (Continued)

Design Sector	Description of slope and bench	*Orientation of slope and bench	Possible mode of instability	Plunge or orientation of critical structure	Instability classification	Considerations
VI	Highwalls and working benches in the faulted blocks at SE part of the pit.	55/093 (HW)	Wedge failure involving the faults dipping to NW and set 1.	$30^\circ (I_{f1,j1})$	Potential if the highwall crest is excessively loaded by spoil.	Avoiding to be dumped temporary spoil piles sensitivity analysis may be required. Analytical check may be useful.
		70/093 (BN)	Wedge failure involving the faults dipping to SE and set 2.	$48^\circ (I_{f2,j2})$	Safe (plunge of line of intersection is smaller than ϕ_j).	
			As in highwalls.		Safe (if bench height is not exceed 12 m).	--
VII(a)	Current pit-walls between Ozdesirler section and section VI. Slices are in N-S direction.	55/093 (HW)	Wedge failure involving faults and set 2 at the west of 13th slice where strike of faults run towards NW.	$44^\circ (I_{f,j2})$	Not critical if not excessively loaded, only small failures.	--
		70/093 (BN)	Wedge failure involving faults with respect to deviations in their strikes and set 1.	$68^\circ (I_{f,j1})$	Safe (difference between the inclination of bench face and I is very small and then possibility of caving is so low).	--
		30/003 (DF)				--
VIII(a)	West of pit, covering Ozdesirler area and its vicinity-slices are in N-S direction.	55/093 (HW)	Wedge failure involving two faults.	$62^\circ (I_{f1,j2})$	Safe unless dips of faults locally smaller than 50° .	Not steepening highwall more than $55^\circ-60^\circ$.
		70/093 (BN)	Wedge failure involving fault 1 and set 2.	$44^\circ (I_{f1,j2})$	May be critical in the cases including water and heavy external loads as encountered in monitoring area II.	Sensitivity analysis may be required.
			Same as highwall.		Not critical (bench heights in 12 m, if line of intersection cuts the face close to crest small failures may be expected).	Widths of working benches should be kept at 80 m as possible as planned.
		30/003 (DF)	Wedge failure involving faults 1 and 2.	$55^\circ (I_{f2,j1})$	"	"
VIII(b)	Slices are in E-W direction-direction of advance is from E to W	55/183 (HW)	Multiphase failure possibility along fault 2 and bedding	$70/130(F)$ $10/140(B)$	May be critical in the cases involving water and excessive loads.	Detailed analysis may be required.
		70/183 (BN)	Wedge failure involving fault 2 and set 3.	$43^\circ (I_{f2,j3})$	Safe (if line of intersection meets the crest, small separations).	--
		30/092 (DF)	Same as highwall.		Same as highwall.	Same as highwall.
IX(a)	Ozdesirler section and its close vicinity-slices are in N-S direction.	55/093 (HW)	Wedge failure involving fault 1 and set 2.	$52^\circ (I_{f1,j2})$	May be critical if joints are continuous throughout entire wall-shallow seated blocks may be expected.	Detailed analysis may be required.
		70/093 (BN)	Wedge failure involving fault 1 and set 2.	$17^\circ (I_{f1,j2})$	Safe ($I_{f1,j2} < \phi - 17.5^\circ$, even if local deviations in faults orientation exist, the most critical plunge of the intersection will be 17°).	--
		30/003 (DF)	Same as highwall.		In general safe (bench height is smaller with respect to highwall height).	Widths of working bench should be kept as possible as 80 m.

Table 14 (Continued)

Design Sector	Description of slope and bench	*Orientation of slope and bench	Possible mode of instability	Plunge or orientation of critical structure	Instability classification	Considerations
IX (b)	Ozdemirler section and its close vicinity - slices are in E-W direction.	55/183 (HW)	Multiplanar failure along fault 1 and bedding planes.	59/160 (f ₁) 5-10/144 (B ₁)	May be critical under the cases including water and excessive external loads.	Detailed analysis is required.
		70/183 (HW)	Wedge failure involving fault 1 and set 3.	52° (f ₁ , j ₃)	Safe if highwall face angle is not exceeded 55°.	Analytical checks may be useful for steeper face angles.
		30/053 (CF)	Same as highwall.	Same as highwall.	Same as highwall if bench widths are not kept narrow.	

* : Out face angle (CF) : 30° ; Highwall face angle (HW) : 55° ; Working bench face angle (BN) : 70° ; OS: Overall slope (These values are based on the initial design by TKI and current applications in the open pit).

** : Slope orientations used in the analyses was based on 7 slope profiles prepared from an initial design by TKI for Sector I (Figure 77).

+ : Final slope angle of permanent slope along basin margin in east was assumed 35°, as in Sector IV, because of unavailability of initial mine design for Sector V.

f : Fault

B : Bedding

j : Joint

I : Line of intersection

a : Slices and working benches constructed in N-S direction (as in the current pit).

b : Slices and working benches constructed in E-W direction (as in Ozdemirler Section).

hangingwall rocks. Because of the restrictions, the slope configuration on both basin margins is required to maintain their planned position. Thus, as a remedial work, flattening of slopes should be investigated using deterministic (limit equilibrium) models.

Multiplanar shear failure : The most outstanding possible occurrence of multiplanar shear failure instability is expected in design sectors I and II where the slopes are controlled almost exclusively by faults and bedding planes dipping into excavation. The slope faces run almost obliquely or nearly parallel to faults. This mode of failure is also expected to appear in sectors VIII and IX if the wall faces constructed in the E-W direction (Figures 76.h2 and i2). The possibility of occurrence of this mode, which may involve several benches, is evident from the failure in Özdemirler section (Figure 64). This implies that further remedial measures may be required such as maintaining the width of working benches as large as possible as proposed in mine plans. This application will cause an increase in the length of lower gently dipping strata and then increase in resisting forces against failure. Several alternatives will be examined in the next chapter using detailed limit equilibrium method.

3-dimensional wedge failure : In all instances, plunges of lines of intersection of wedges formed from the combinations of steeply dipping joint sets are much greater than the face inclinations and friction angles of joints. This implies that no unstable wedge will be resulted from the combination of joint sets in Sekköy formation. The case that no failures have been observed involving these features in the pit also confirms the results.

The wedges formed by the intersections of faults, which appear locally in sectors VIII and IX, tend to make wedge failures unlikely, unless local steepening in their dips are encountered. On the other hand, their flatter plunges play a positive role on stability (Figure 76 h.2 and i.2).

However, wedges formed from combinations of faults and steeply dipping joints in Sekkøy formation may introduce instabilities involving highwall or benches only. The wedges involving these sets of discontinuity have small dihedral angle and may probably tend to cause small wedge failures. Joint sets 1 and 2 contribute to the wedge forming more than as does set 3.

The kinematic studies are based on the assumption of underground continuity of the surface plane of weaknesses. Even though this may not be the case, the assumption does provide an approach to a first estimate of potential slope stability problems in the preliminary assessments. But, continuity of discontinuities throughout the entire slope is an important factor controlling wedge failures. Faults in the study area are continuous structures, while joint sets mostly terminate in exposures. Therefore, wedge formation throughout the entire bench of 12 m or highwall may not be anticipated for every case. On the other hand, even if plunge of line of intersection is smaller than the face inclination, if line of intersection runs behind the toe of slope daylighting will not occur (Figure 76j). Because of this argument, wedges with a line of intersection plunging slightly shallower than cut face may be categorized as safe or slightly critical. However, considering the wedges with water pressure and external loading, analytical sensitivity analyses were also performed for safer design.

Toppling failure: Toppling is a possibility on a regular, closely spaced and continuous discontinuity set if its normal plots inside the ruled region of Figure 74b. In addition to this, toppling can occur only if the discontinuity strike is nearly parallel to the strike of the slope, say within 30° . As it can be seen from Figure 76, poles of the joints plot very close to the boundaries of the ruled region rather than in the central part. On the other hand, persistence of joints are smaller than the height of walls. This situation also prevents the forming of continuous blocks. No failures have been observed involving columnar structures in the pit. Therefore, it is concluded that possibility of toppling in the study area is not generally expected.

CHAPTER 10

DETERMINISTIC ANALYSES AND DESIGN EVALUATIONS

10.1. Design Methodology

This section considers the geotechnical aspects of mine design. Geotechnical aspects of design of an open pit mine are concerned with deriving the steepest allowable slope angles and bench configurations and formulating any special or remedial measures necessary for stability within given economic and/or environmental constraints. The final design, however will of course devolve from interaction of many contributing factors which are beyond the scope of this study. In this study, slope design parameters are considered as overall slope angle, bench geometry and highwall geometry for given sectors or rock types. Stability of slopes has been defined in terms of "factor of safety" for given conditions.

Stable highwalls and permanent slopes are essential for the success of dragline operation and the continuity of the production. Kinematical assessments are helpful only in determining kinematically possible modes of failure, but do not consider groundwater conditions, seismic acceleration and some important geomechanical parameters, such as cohesion and unit weight. In order to obtain design parameters and to assess possible remedial measures for safer design conditions further detailed analysis of slopes is required.

On the basis of kinematical assessments, stability conditions in each design sector were examined with respect to the anticipated most possible mode(s) of failure and various slope configurations. The analyses were principally based on the methods of two-dimensional limit equilibrium of

forces which are also known as conventional deterministic framework, as described in Appendix D. In addition to various parameters, external loading imposed by dragline was also considered in the analyses where it was necessary.

In the case of an earthquake, a horizontal seismic force is applied at the centroid of the mass under consideration. It is assumed that this force has no effect on the normal force or the resisting moment, so only the driving moment is affected (Huang, 1983). Besides, seismic coefficient depends on the geographic location. An average acceleration of 0.5 g for 225 years of return period has been suggested to the southern part of the Aegean region (Erdik et al., 1985). However, there is no available local information about the acceleration to which the slopes are likely to be subjected throughout the life of the pit. Considering that a degree of risk due to an earthquake acceleration may be assessed in design, it is concluded that the factor of safety will fulfill this requirement. Thus, uncertainties from acceleration, however, was taken into account in the analyses by suggesting higher factors of safety in certain limits obtained from worldwide experiences in open pits (Hoek and Bray, 1977; Huang, 1983).

In the first series of further stability analyses, the applicability of the initial design project by TKİ was investigated. Second series analyses with the combination of sensitivity approach were performed to introduce alternatives to remedial measures when a normally accepted factor of safety could not be achieved for given condition.

10.2. Design Sector I

In the analyses seven design sections (Figure 77) were employed to take local variations such as orientation of

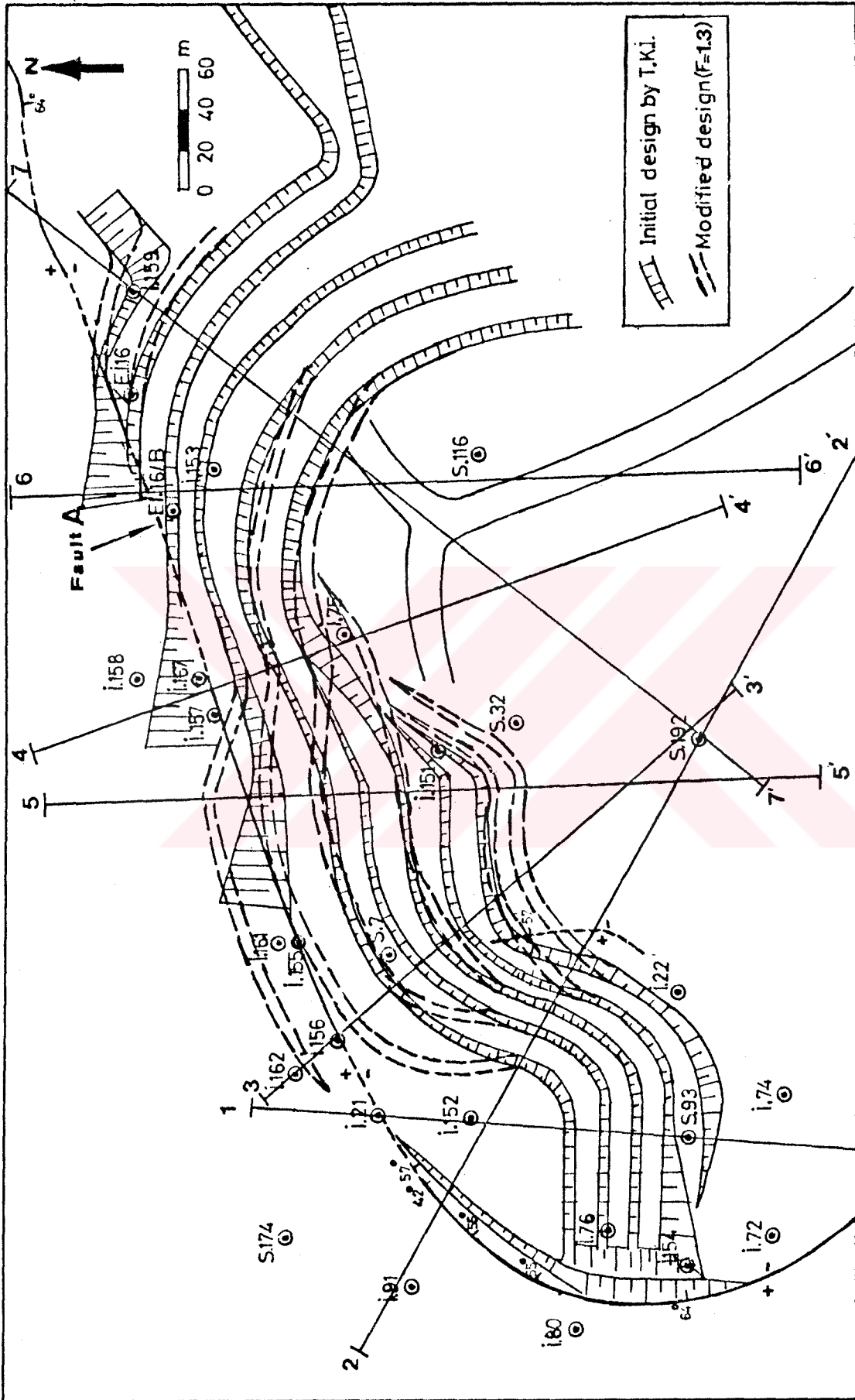


Figure 77: Design sections and comparison of the initial design by TKI and modified design based on a factor of safety of 1.3 for design sector I.

overall slopes and of major structures into consideration. As pointed out in the kinematic analyses (Table 14), the stability in the sector is mainly controlled by multiplanar shear failure. Thus, on the basis of this model, two cases were considered in the analyses:

- 1) Exposed footwall case : Sliding along fault-A and clay bed in footwall where the overall slope reaches to the bottom of coal seam, and where weak clay bed daylights.
- 2) Hangingwall case : Sliding along fault-A and bedding planes during different stages of slope construction in hangingwall material.

The strata overlying the coal seam in the sector consist principally of the main Sekköy formation with a small proportion of transition zone soils. Transition zone, however, was removed in June 1990 and not included in the analyses. On the other hand, shallow excavations behind fault-A indicated that a very thin black clay seam may possibly continue at the upper levels of footwall, this is the Turgut formation. Thus, to be on the safe side it was believed that employing the residual shear strength of finest material of Turgut formation will be more realistic. The residual shear strength parameters (Table 12) for other discontinuities and mean unit weights of each unit (Table 6) were used in all analyses.

As discussed in Chapter 5, the assumption for groundwater was that general groundwater table would tend to follow a drawdown pattern, first towards the compact marl/coal seam boundary and then towards the toe throughout the overall slope. The analyses were conducted using the computer program called SWASE (Huang, 1983).

Section 3-3' : The analysis of the initially designed 42° overall slope profile with respect to exposed footwall case (Figure 78a) yielded a factor of safety of 0.56. This result indicates that a final design angle of 42° for this section will be highly critical. Because of the multiplanar nature of the sliding surface, to improve the overall stability it was concluded that extending the lowest bench or shifting its toe forward towards south in conjunction with several combinations of the upper benches may improve the stability.

On this basis, the examined slope configurations and resulting factors of safety are introduced in Figure 78 b through g. The analyses indicated that a factor of safety of 1.3, which is desirable in a major slope (Hoek and Bray, 1977), could be attained by shifting the initial toe position about 30 m forward (Figure 78 h) while applying the same procedure for upper benches as shown in Figure 78 e through g.

The analyses also indicated that no instability was anticipated in different stages of slope construction in the hangingwall material (Figure 78 i).

Section 4-4' : The first step analysis for initial profile (Figure 79 a) indicated that design of a 41° overall slope yielding a factor of safety 0.93, would be critical. The next step was to analyse the effects of extending the lowest bench and flattening of the slope (Figure 79a and b). The results of exposed footwall case (Figure 79 c and d) imply that flattening of the slope to 30° or shifting the initial position of toe 15 m forward by maintaining the upper benches in their initial position might be considered as a remedial measure satisfying a factor of safety of 1.3. Additional analyses also indicated that slope construction in hangingwall would not cause any stability problem in each stage (Figure 79e).

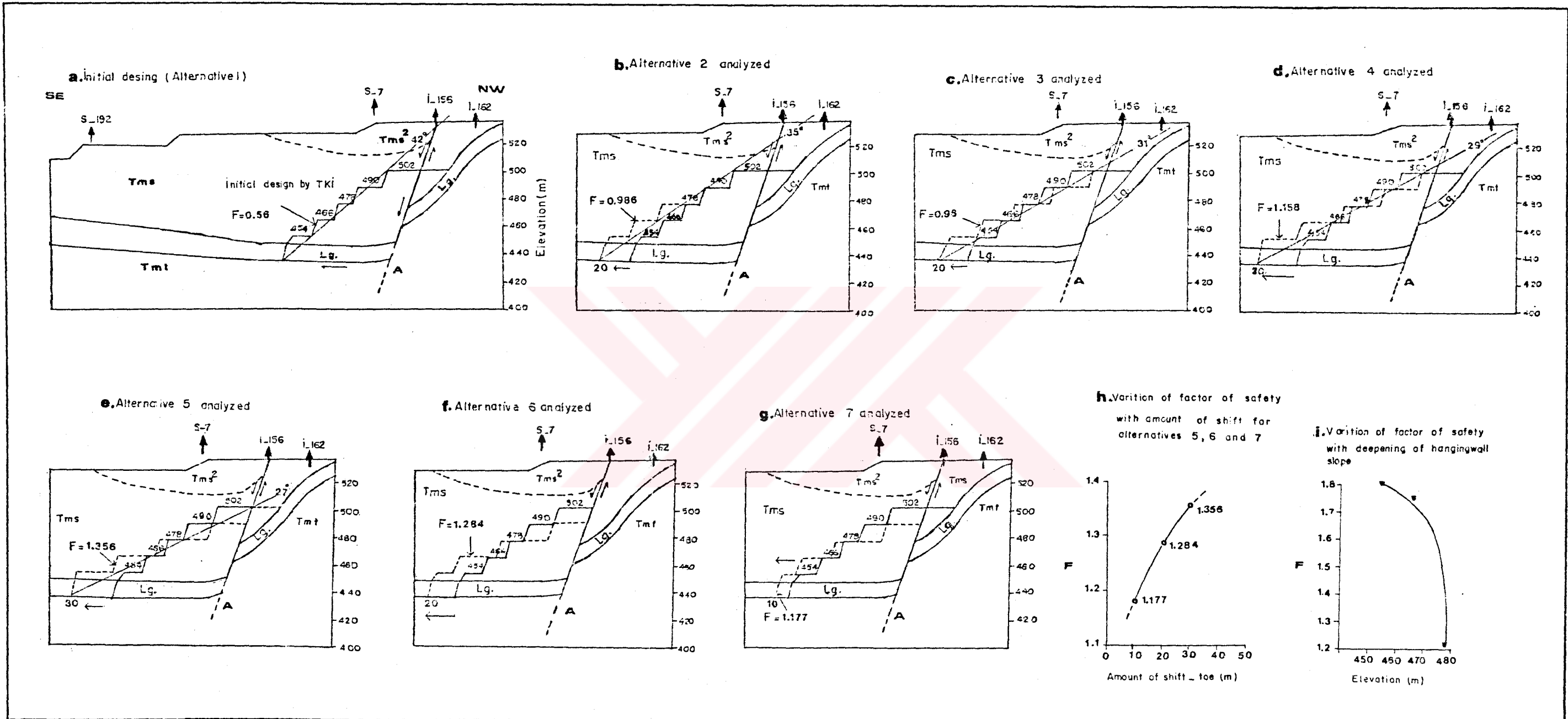
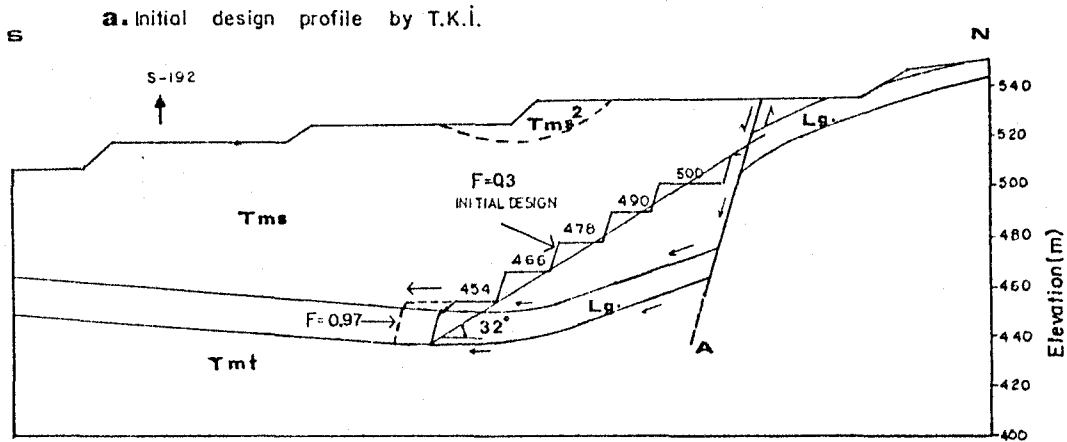


Figure 78: Multiplanar failure analyses for design section 3-3' at sector I.

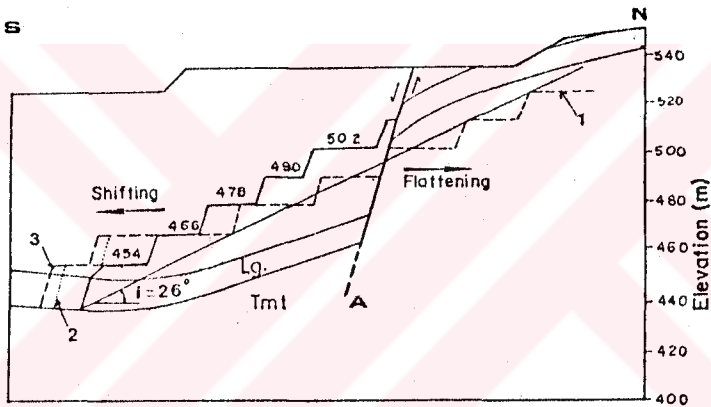
Section 5-5' : Initial design profile yielded a factor of safety of 0.3 which indicates stability of the profile is critical (Figure 80 a). Additional analyses on various slope configurations, shown in Figure 80 a and b, indicated that extending +466 bench and flattening the slope in conjunction with shifting the toe forward will be adequate (Figure 80 c). On the other hand, if overall slope is designed on the basis of a factor of safety of 1.3, the slope above the coal seam will be more stable having a higher factor of safety of 1.44.

Section 6-6' : The initial overall slope angle is 32.5° and it yields a factor of safety of 1.2 (Figure 81 a). In order to obtain higher factors of safety various geometrical configurations involving slope flattening and shifting the toe forward were examined (Figure 81 a and b). The results, as illustrated in the graphical form in Figure 81 c and d, showed that if the slope is reduced to 29° or +502 bench is extended in conjunction with shifting the toe 5 m forward with respect to its initial position, a factor of safety of 1.3 will be satisfied. Various stages of slope construction in hangingwall seems to be safe (Figure 81 e).

Section 7-7' : A factor of safety of 1.2 was obtained for the exposed footwall case with an overall slope angle of 30° (Figure 82 a). Flattening the entire slope to 27° , 25° and 23° (Figure 82 b and c) improves the overall stability. But this application requires more overburden removal. Thus, the initial position of the toe and the upper benches were shifted forward (Figure 82 d). As can be seen from Figure 82 e through g, improvement of the overall stability may be achieved by shifting the toe 5 m forward in conjunction with extended upper benches. On the other hand, the analyses showed that any instability is not expected in different stages of slope construction in hangingwall material (Figure 82h).



b. Profiles resulted from the combination of shifting and flattening



c. Factor of safety versus amount of shift forward

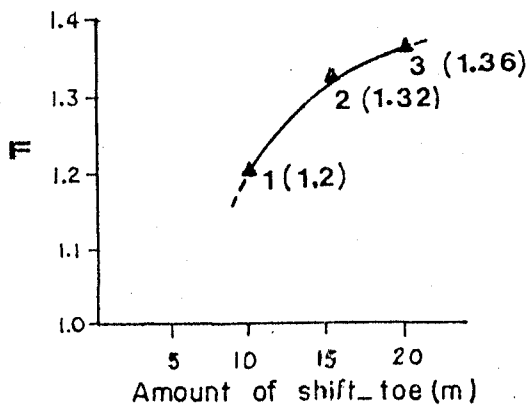
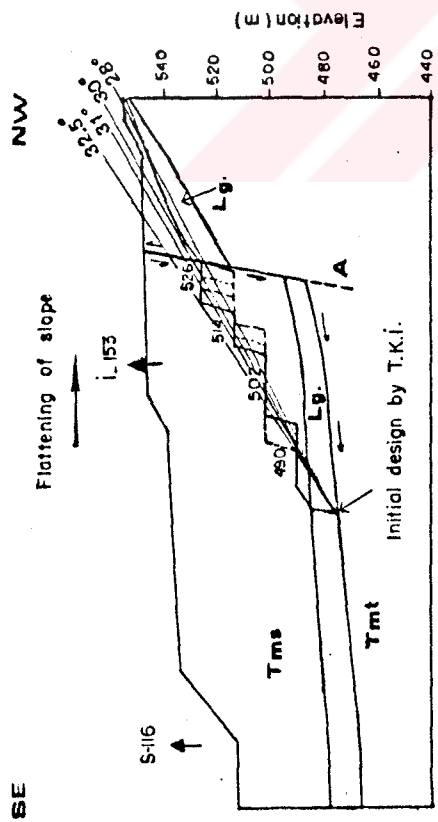
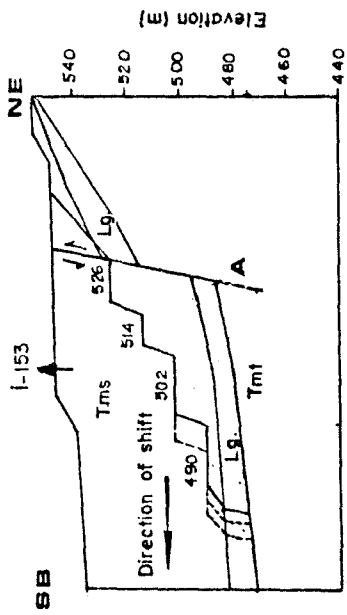


Figure 80: Multiplanar failure analyses for design section 5-5' at sector I.

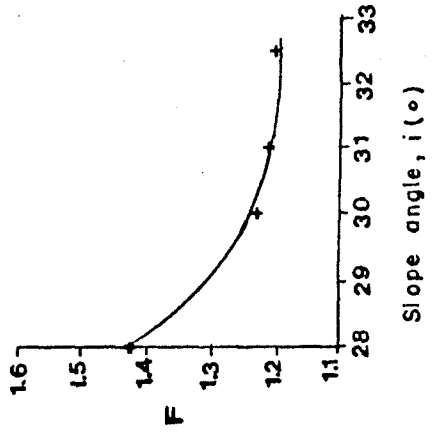
a. Initial design and flattening of slope (exposed footwall case)



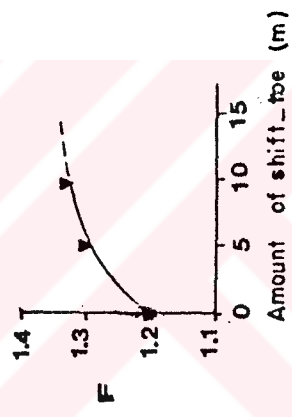
b. Shifting the toe forward (exposed footwall case)



c. Variation of factor of safety with flattening of slope (exposed footwall case)



d. Variation of factor of safety with amount of shift (exposed footwall case)



e. Variation of factor of safety with deepening of hangingwall slope

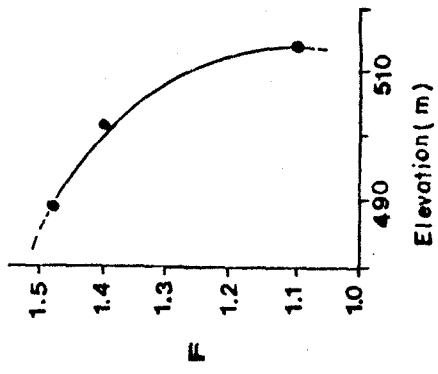


Figure 81: Multiplanar failure analyses for design section 6-6' at sector I.

BW

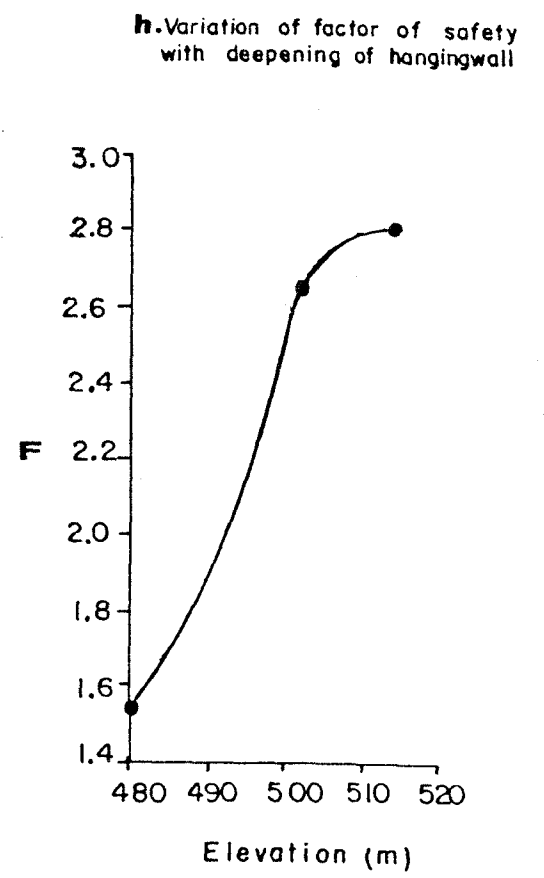
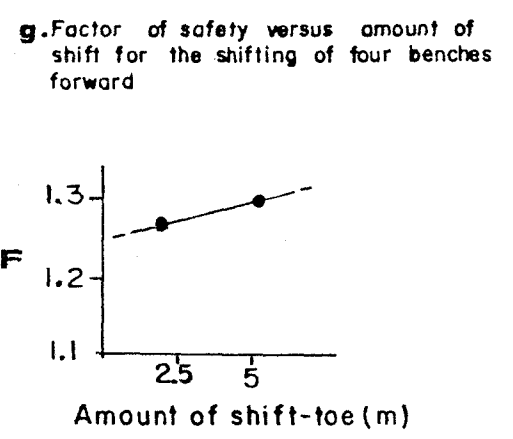
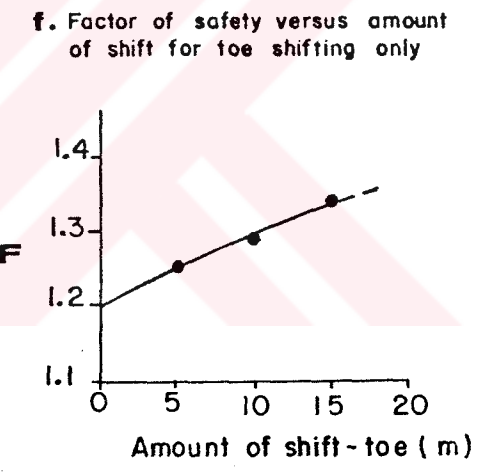
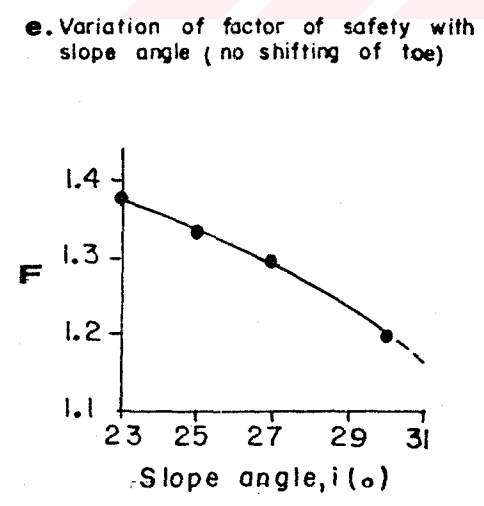
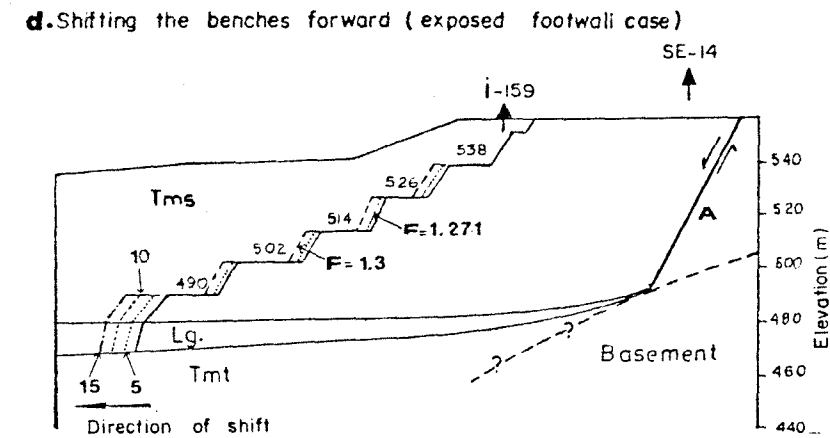
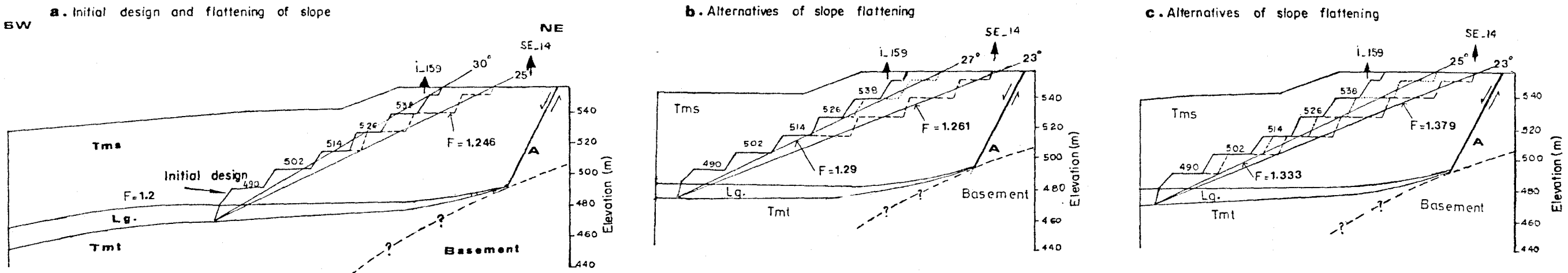


Figure 82: Multiplanar failure analyses for design section 7-7' at sector I.

Design Considerations : The results obtained from deterministic analyses on various sections showed that for the stability of the overall slope in design sector I exposed footwall case was the most critical. The stability highly depends on footwall dip which increases at the central part of the sector resulting in a drastic reduction in stability. In order to achieve a desirable factor of safety, flattening of the slope alone is not sufficient as a remedial measure. Because of the multiplanar nature of the failure surface, sliding forces can be minimized or balanced by increasing the length of flatter part of the sliding surface. This requirement may be best achieved by shifting the toe and upper benches forward rather than flattening slope case only.

The slope profile of each section satisfying a factor of safety of 1.3 was applied on the initial design project for comparison purposes (Figure 77). The most obvious difference between the initial and redesigned slope configurations appears in the central area bounded by the design sections 3-3' and 6-6' where bedding steepens.

Both at the eastern and western parts there is a close agreement between the slope configurations. Besides, an overall slope design based on the toe shifting alternative will also result in a higher safety for the portion of slope constructed in the hangingwall.

The lateral restraint is provided by the material on either side of a potential failure. It is clear that this restraint will be greater if the slope is concave than it would be if the potential failure is situated in a nose which has a freedom to expand laterally (Hoek and Bray, 1977). This suggests that convex slopes are less stable than concave slopes. The nose, in initial design project, at the west introduces a convex shape. But redesigned slope

profiles provide more gentle curvature and eliminate this possibility.

On the basis of equipment specifications, bench heights of 10 to 12 m have been selected and the analyses carried out indicate that there is no reason to amend this.

10.3. Southeast Wall (Design Sector II)

The permanent southeast wall at the south limit of dragline slices are planned parallel to the state highway (Figure 83). This wall generally cuts faulted blocks. The structural pattern, adversely oriented with respect to the wall orientation, may cause instabilities involving multiplanar mode of failure and subsidiary plane shear failure (Table 14).

Taking into consideration local variations in the orientation of main structural elements, stability conditions of the sector were evaluated on five design sections from the initial design project (Figure 83). As discussed previously, residual shear strength parameters of the faults and the bedding planes in overburden were employed in the analyses. On the other hand, in addition to the upper levels of Turgut formation black clay was also included in the analyses for some sections where this material appears.

The same groundwater model involving steady seepage condition, as in the sector I, was assumed. The stability conditions were examined with respect to the failures which occur along the faults and bedding planes both in overburden and footwall. The calculations were performed using the computer programs SWASE and MBPF. A series of analyses

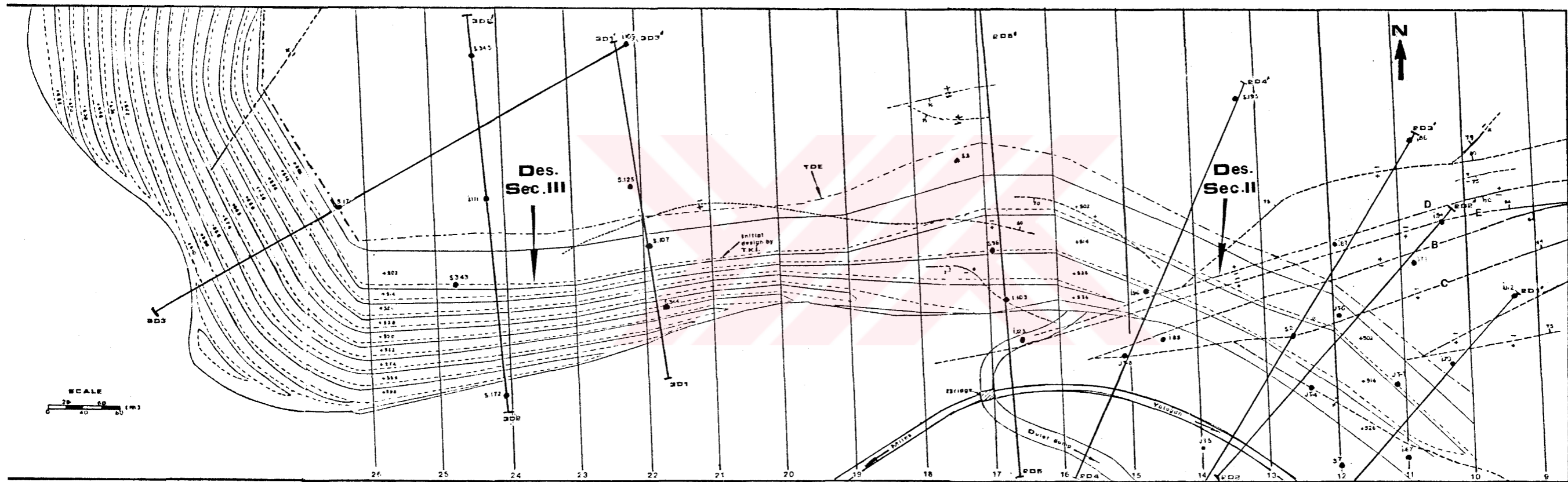


Figure 83: Design sections and mine layout based on the initial design by TKI at sectors II and III.

carried out on five design sections are summarized in the following sections.

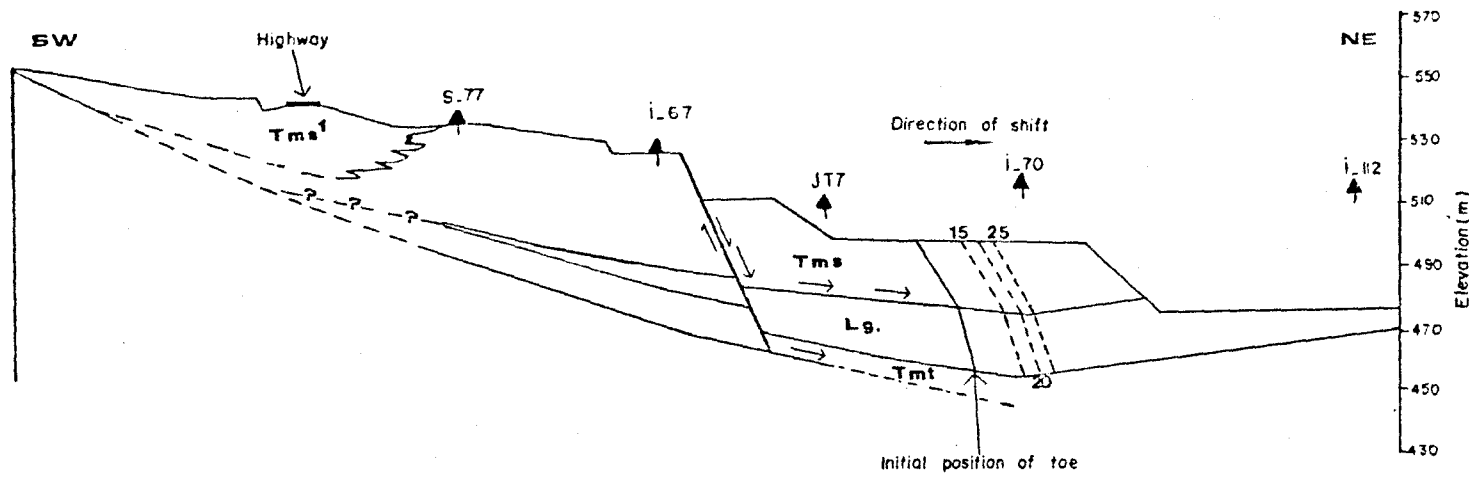
Section 2D1-1' : It is obvious from Figure 84a that the stability of slope profile is controlled by the fault and the two bedding planes with inclinations of 70° and 6° to 8° , respectively. Black clay is farther away from the block bounded by the fault and thus this material was not considered in this case. The overall slope profile (exposed footwall case), yielding a factor of safety of 1.03, is at the limit equilibrium. Thus, shifting the toe forward and slope flattening cases were examined for sliding along footwall and along the bottom of hangingwall (Figure 84 a, b).

The results (Figure 84 c and d) indicated the followings :

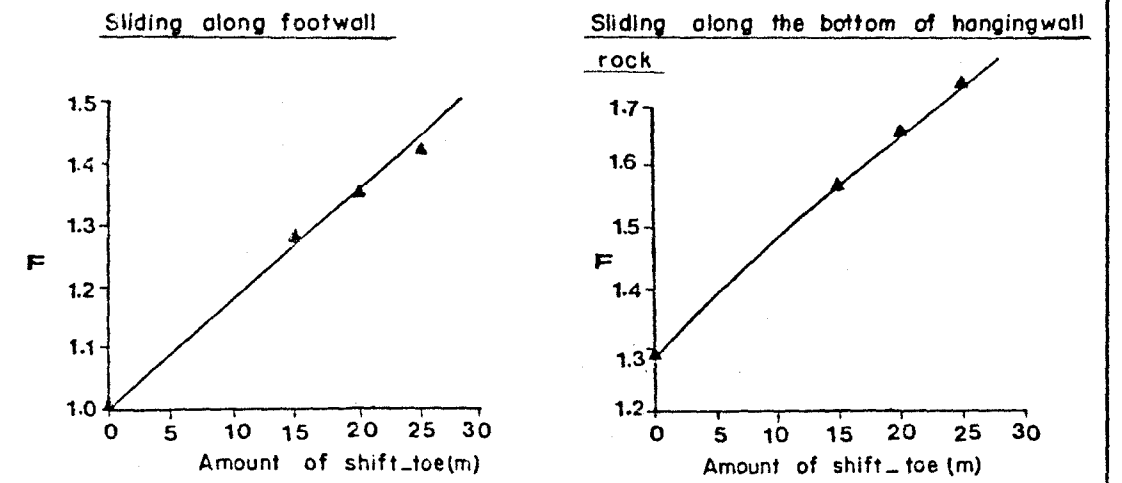
- 1) The stability of the overall slope is governed by the footwall strata and slope configuration in the hangingwall is more stable than the overall slope.
- 2) In order to achieve safer stability conditions such as satisfying a factor of safety of 1.4 or 1.5, it is necessary to flatten the slope to 20° - 21° . This alternative results in more overburden removal and very short distance (40 m) between the highway and slope crest which may be considered a critical distance. On the contrary, shifting the toe 25 m forward without slope flattening provides same safety conditions.

If a slope design based on the initial project is made and failure occurs, the possibility of plane failure in the mass behind the failed faulted block may increase. This case was examined for the bedding planes running to different depths and daylighting on the pre-failure surface (Figure

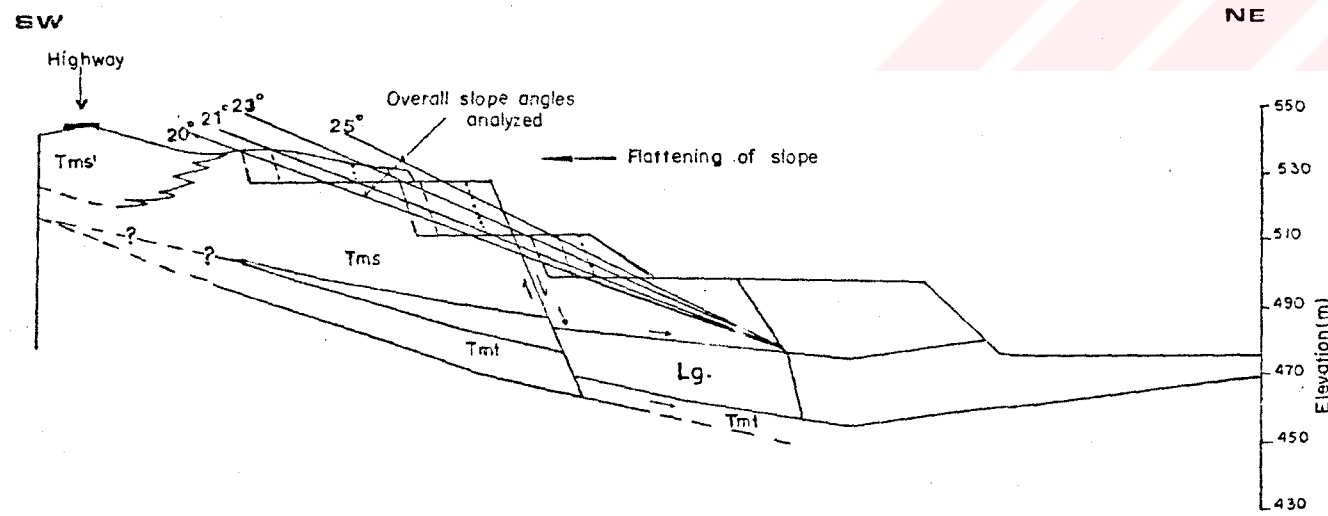
a) Initial design and shifting the toe forward



c) Variation of factor of safety with amount of shift (toe)



b) Flattening of slope



d) Variation of factor of safety with slope angle [flattening of slope case]

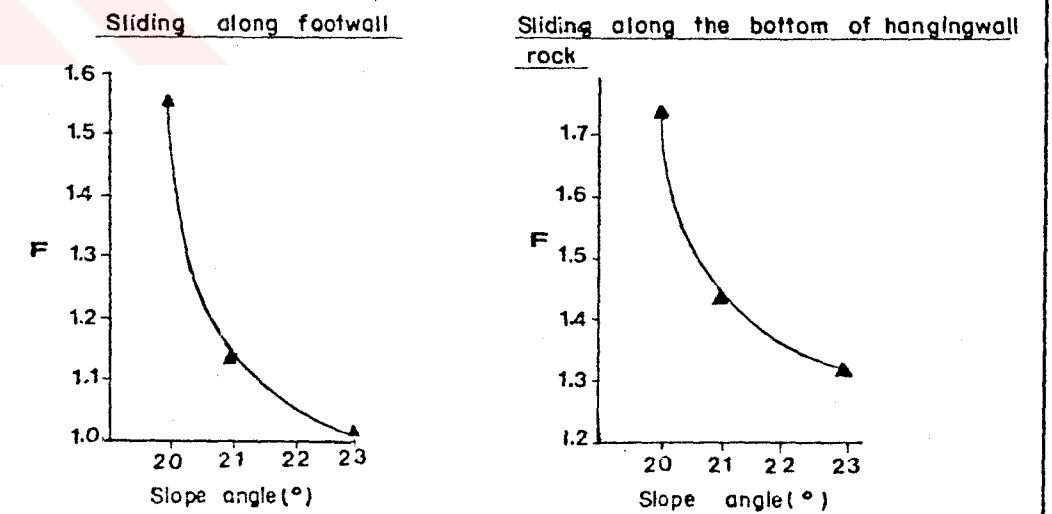


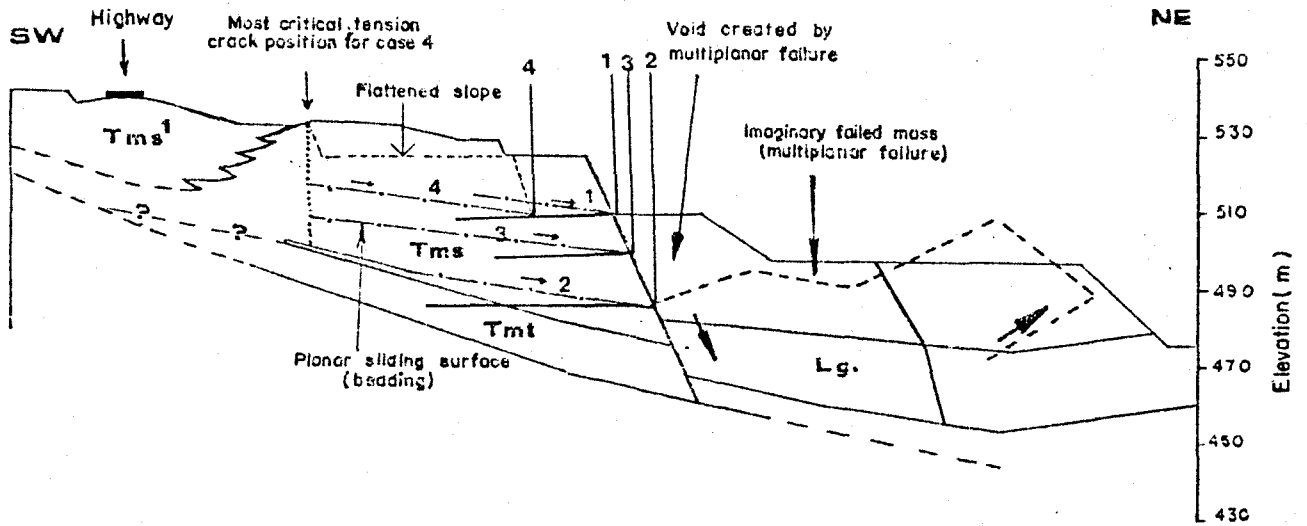
Figure 84: Stability analysis of various slope configurations for southeast wall-section 2D1-1', at sector II.

85). It was also assumed that the potential tension crack is located on a pre-existing geological feature such as a vertical joint. The tension crack position was stepped out from the crest to the highway and various water heights in tension crack were considered in performing sensitivity analysis.

The results of sensitivity analyses (Figure 85) suggest that the most critical tension crack position will develop 1 m from the slope crest and the plane failure will occur along deep seated bedding planes when the tension crack becomes water-filled as a consequence of rain storm. However, it is obvious that this type of instability involves a small amount of rock mass and its possibility seems to be minimal. Thus, it is concluded that the plane failure may occur if the conditions of heavy rainfall and steeper bedding are satisfied after a multiplanar failure is completed.

Section 2D2-2' : In this profile the fault behind borehole JT4 was considered as the upper bound of multiplanar failure surface (Figure 86 a). Black clay penetrated by borehole JT4 was also included in the analyses. The initial design profile for exposed footwall case yielding a factor of safety of 1.24 seems to be stable, while the profile above the coal seam is at the limiting equilibrium condition ($F = 1.09$).

If the benches are shifted 5 m back with the same toe configuration (slope flattening), the factor of safety decreases to 1.06 (Figure 86 a). This condition arises from the fact that due to increments in bedding dips towards south, removal of the overburden for slope flattening results in an increase in sliding forces. Thus, to achieve more stable conditions shifting the toe forward seems to be more effective measure (Figure 86b, c).



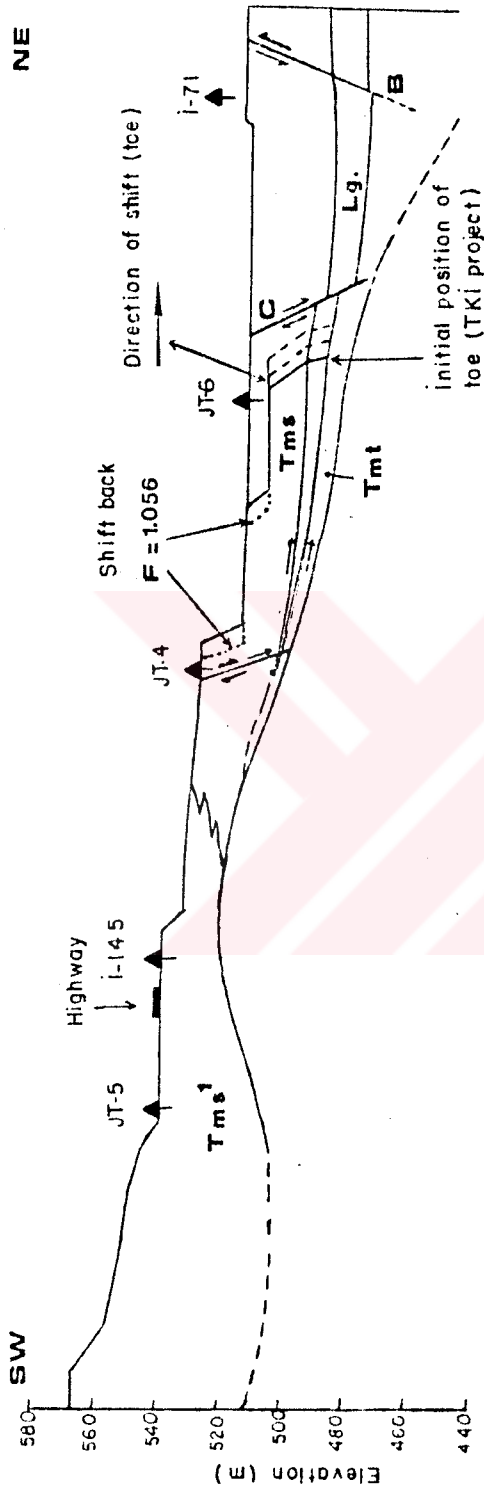
Results of plane failure analysis for section 2D1-1'

Number of sliding surface	Water condition in tension crack	Distance between slope crest and most critical tension crack (m)	Minimum factor of safety F
1	Filled with water	1	1.108
	Filled with water to 1st half	1	2.334
2	Filled with water	1	0.562
3	Filled with water	1	0.776
4*	Filled with water to 1st half	1	2.280

* Overall slope angle is 20° and benches are shifted back.

Figure 85: Analysis of planar failure developed after multiplanar failure in hangingwall at southeast wall-section 2D1-1', at sector II.

a) Design section and slope profiles analyzed



b) Variation of factor of safety with amount of shift
Multiplanar sliding along the bottom of hangingwall

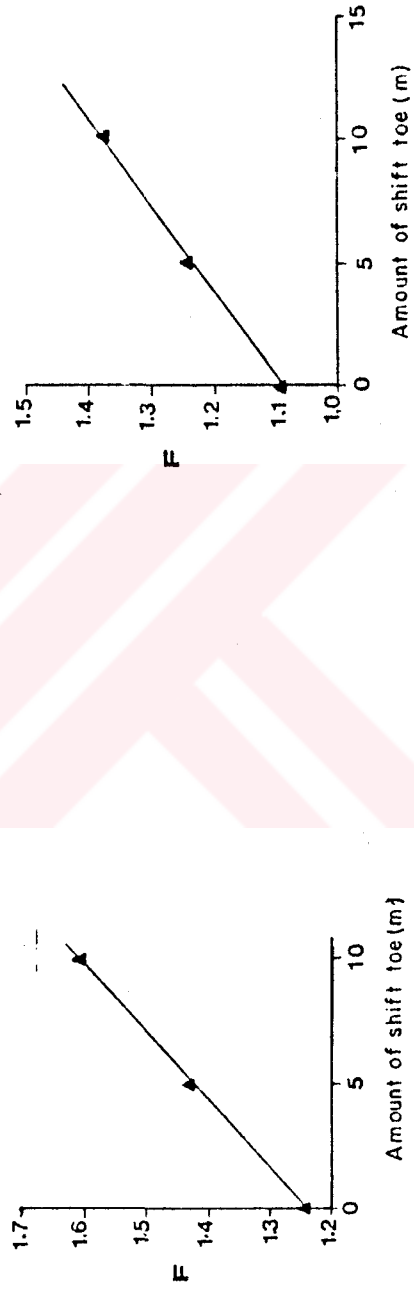


Figure 86: Stability analysis of various slope configurations for southeast wall-Section 2D2-2', at sector II.

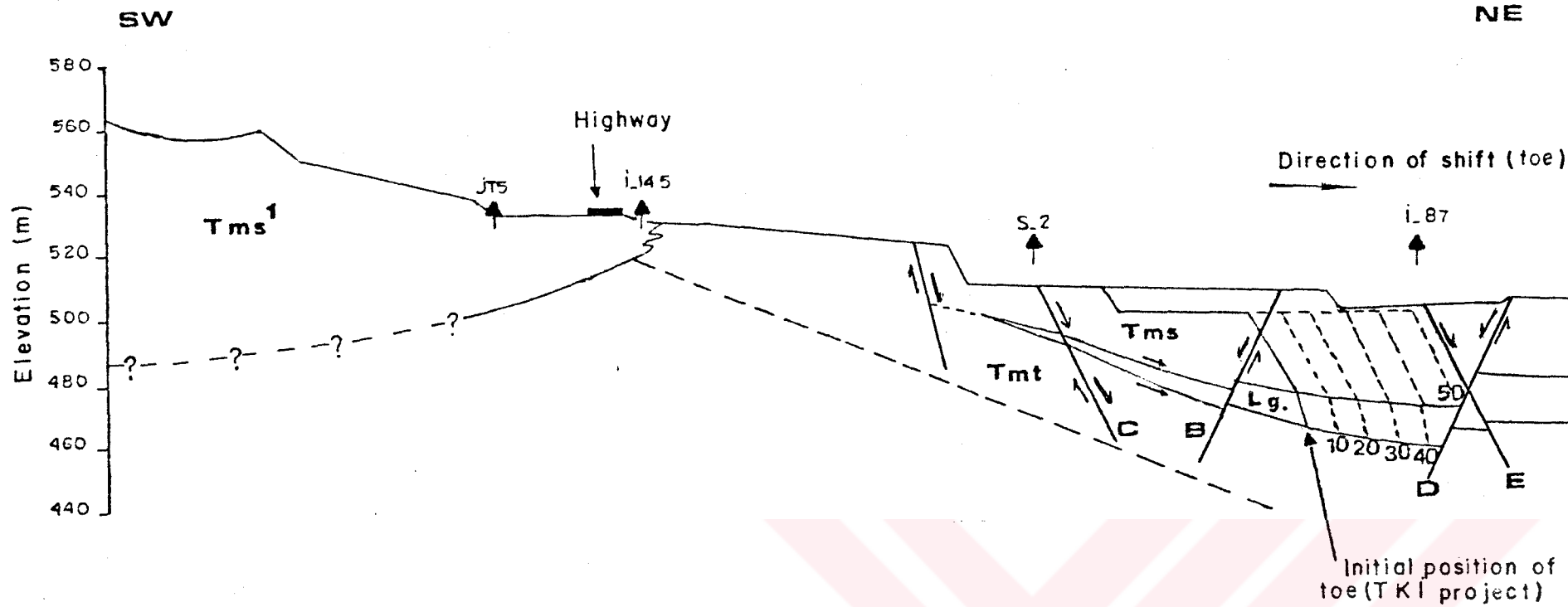
Section 2D3-3' : The entire profile in this case is cut by two faults. But the fault-C is more critical and contributes to multiplanar sliding surface (Figure 87a). Therefore, fault-C and the black clay at the central part was considered. The first series of analyses indicated that the slope profile with respect to initial design would be critical for footwall and hangingwall (Figure 87b). Slope flattening is also not an effective remedial measure, as in the previous section (Figure 87c). But it is obvious that shifting the toe by some amounts forward will provide adequate stability (Figure 87b).

Section 2D4-4' : The initially designed slope profile is bounded by fault-E from south and the bedding planes are nearly horizontal (Figure 88a). Besides, weak black clay does not contribute to sliding surface. These favorable conditions provide considerable higher factors of safety (Figure 88b). In order to produce more coal all benches were shifted back to south and the stability condition was examined in this case. The results (Figure 88b) showed that the overall slope is still stable, but the factor of safety decreases from 1.5 to 1.4.

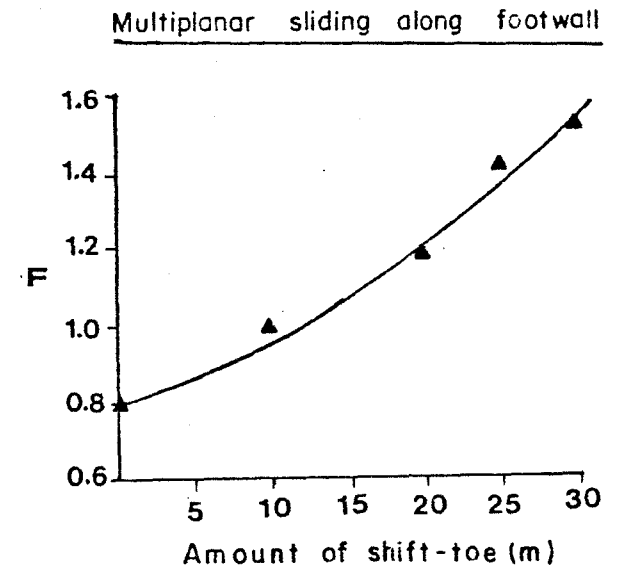
Section 2D5-5': This profile, involving gently dipping strata and thicker coal seam, runs very closely to highway bridge. The fault appearing between boreholes I98 and S3 is more likely to contribute to the failure than others (Figure 89a). Because of low factors of safety such as 0.6 and 1.17 obtained for exposed footwall and hangingwall cases, initial slope design is required to be revised.

Considering unimportant effect of slope flattening, only toe shifting case was examined. The results (Figure 89b) indicated that the overall stability was more critical than the stability of hangingwall and that shifting the toe 20 to 25 m forward would provide a factor of safety of 1.4.

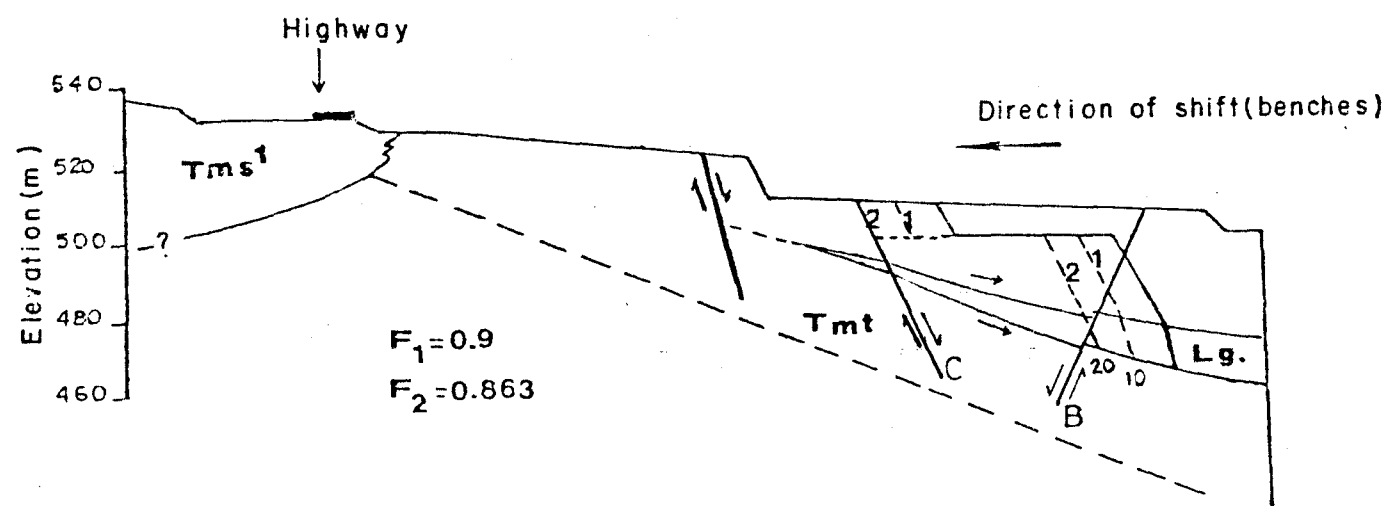
a) Slope profiles analyzed for shift forward case



b) Variation of factor of safety with amount of shift



c) Slope flattening and factors of safety



Multiplanar sliding along the bottom of hanginwall

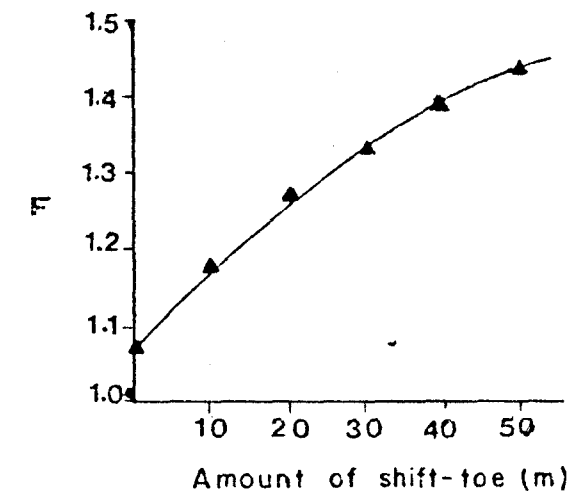
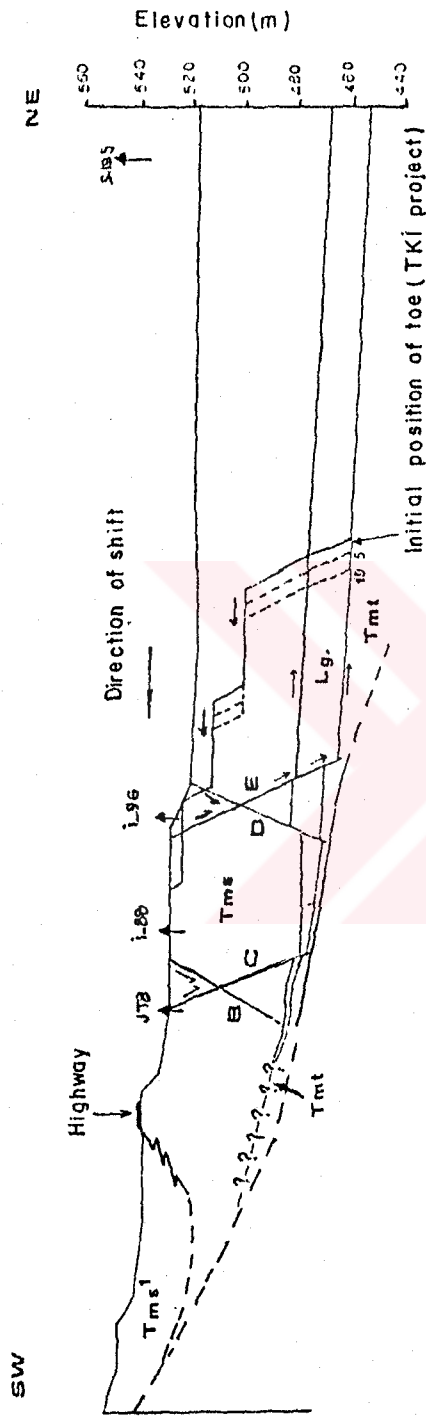


Figure 87: Stability analysis of various slope configurations for southeast wall-Section 2D3-3', at sector II.

a. Design section and slope profiles analyzed



b. Variation of factor of safety with amount of shift back

- A: Exposed footwall case
- B: Sliding along the bottom of hangingwall rock

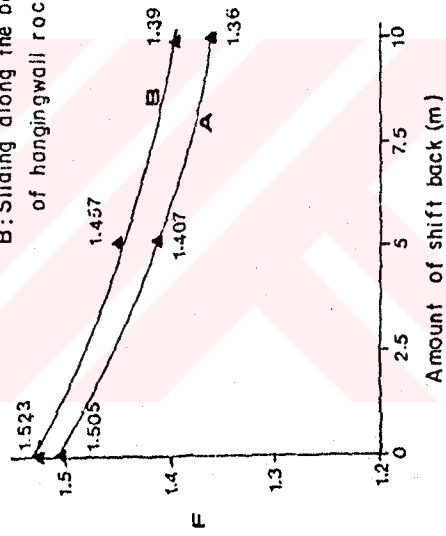
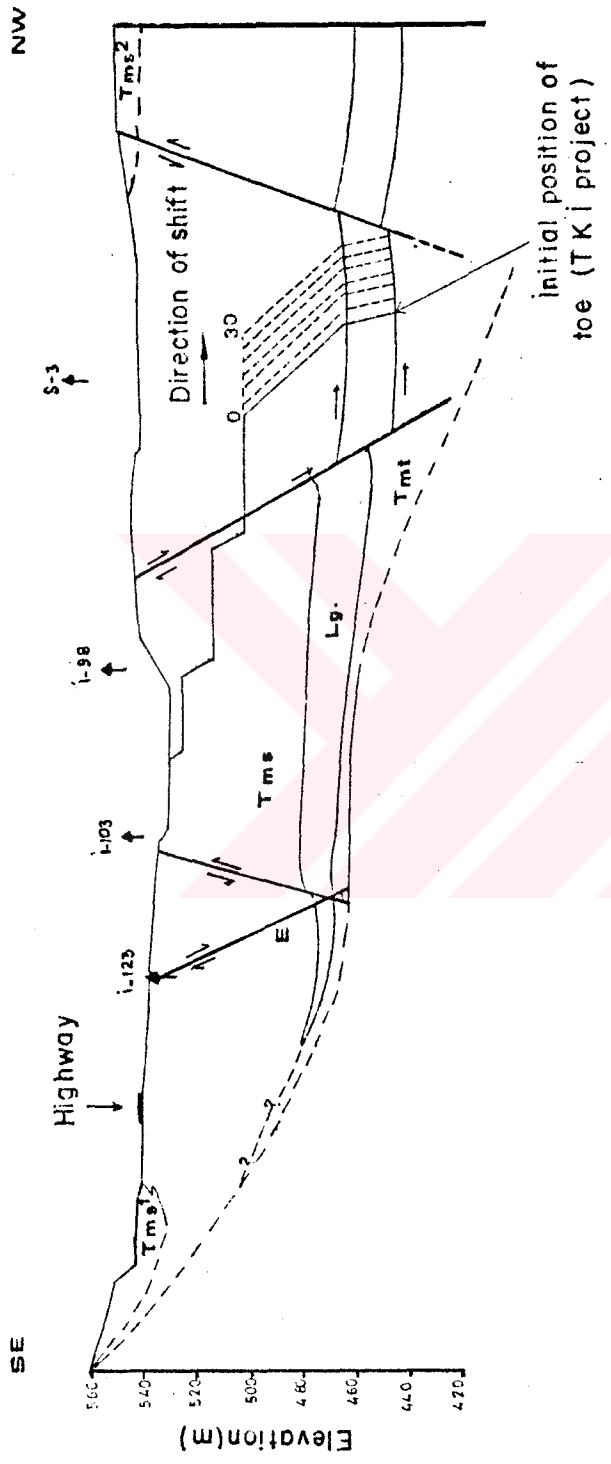


Figure 88: Stability analysis of various slope configurations for southeast wall-Section 2D4-4', at sector II.

a) Design section and slope profiles analyzed



b) Variation of factor of safety with the amount of shift

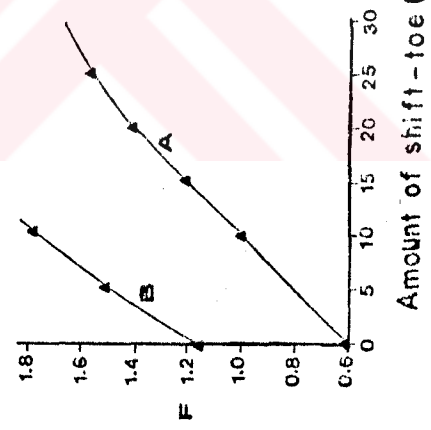


Figure 89: Stability analysis of various slope configurations for southeast wall-Section 2D5-5', at sector II.

Design Considerations : In this design sector multiplanar shear failure is the most critical mode of failure. The possibility of this type of failure to occur is higher, particularly, at the east and central parts of the sector where dips of strata increase and weak clay contributes to failure as a central sliding surface. On the basis of stability analyses initial design should be revised. As a remedial measure, shifting the toe forward to the north will provide better stability than slope flattening alternative.

The experience gained from these analyses also helped to understand the causes of movements observed by TKI personnel between the highway and permanent slopes at the southern edge of previous slices. Because of the increases in dips of bedding planes and removal of the coal seam extending back to the faulted blocks result in an exposed footwall case. Slope movement may be initiated along the footwall strata and then tension cracks may have been formed. However, immediate material filling into the void created by stripping has played a toe buttressing role and the movement was terminated. This approach was also confirmed by a similar movement at the end of ninth slice, in December 1990, which initiated when the stripping was exceeded in the faulted block to the toe limits as suggested by the results of analyses given herein.

For critical slopes adjacent to haul roads, important installations or important engineering constructions, such as highways, which should maintain their stability throughout their service life, a minimum factor of safety of 1.4, preferably 1.5, is suggested (Hoek and Bray, 1977; Huang, 1983). Due to the importance of design sector II and its position with respect to the highway, it is advisable that shifting the toe forward in each section should be based on a minimum factor of safety of 1.4. The amount of shift (toe) determined from the graphics given in Figures 84

through 89, on the basis of factors of safety 1.4 and 1.5 is tabulated in Table 15 for each design section. If a comparison is made between the profiles of initial design and the revised profiles, a small amount of coal will be left by the application of shifting the toe forward.

In order to avoid convex slope configuration after revision of the profiles, shifting should be based on the most critical section. On the other hand, the void resulted from the stripping should be filled in the shortest possible time after the removal of coal for better improvement of overall stability.

10.4. Southwest Wall (Design Sector III)

The permanent slopes planned in design sector III and in the southern part of sector IV (Figure 83) will be constructed in sandstone, transition zone and Sekköy formation. The strata are nearly horizontally bedded lacking shear or fault zones. The Sekköy formation cut by the slope is mainly represented by its upper weak sequence. Based on the kinematical evaluations, any structurally controlled failure is not anticipated along these walls. Hoek (1971), Jaworski and Zook (1979) reported approximately circular slip surfaces that cut across the bedding planes passing through the rock mass in the upper region of the slope, while in the lower regions they go nearly parallel to the bedding. Because of circular failure experienced in the transition zone soils and weak nature of the rock mass in Sekköy formation along basin margins the possibility of mass failure, as reported by above mentioned authors, is also investigated. In spite of the favorable orientation of structural elements with respect to slope orientation, this experience is required to understand the behaviour of the

Table 15: The amounts of shifting (toe) with respect to factors of safety of 1.4 and 1.5 for design sector II.

Design Section No	The amount of shift (m)		Critical sliding level (*)
	F = 1.4	F = 1.5	
2D1-1'	23	29	Footwall
2D2-2'	11	15	Bottom of hangingwall
2D3-3'	42	70	Bottom of hangingwall
2D4-4	(**)	Initial design	Footwall
2D5-5'	20	23	Footwall

* Indicates more critical sliding condition.

** F=1.5 with respect to initial design by TKI, for F=1.4 toe is shifted 5 m forward towards the highway.

cuts when high stresses develop in conjunction with the steepening and heightening of slopes

The stability of individual benches and slopes cut in each unit was analysed by first series analyses and the combined results were employed to investigate the stability of overall slopes which cut different units. In the analyses, the computer program MTASLP, based on Bishop's method (Bishop, 1955) for circular slip surfaces was used.

10.4.1. Stability of Slopes in Transition Zone Soils

The stability conditions of transition zone having a maximum thickness of 25 m was investigated on the basis of individual bench stability and overall stability. Based on the back analyses the residual shear strength of this zone (Table 12) and the mean unit weight (Table 6) were used in the analyses. Due to the lack of information on probable perched water levels in the zone, general water table (Plate 3) was considered and the dry slope case was analysed.

Individual benches of 12 m, 10 m, and 7 m high with respect to various inclinations such as 70°, 60° and 50° were examined for the slip surfaces passing through and behind the toe. The results (Figure 90 a) indicated that the toe failures yielded minimum factors of safety. In addition, to achieve factors of safety ranging between 1.1 and 1.2, which are acceptable values for an individual bench, 7 m high bench with a face inclination of 50° or 60° should not be exceeded.

By considering safer 7 m high benches, stability of overall slopes involving two or three benches (14 or 21 m) was analysed for various slope angles. The variations of factor of safety and slope height with overall slope angle

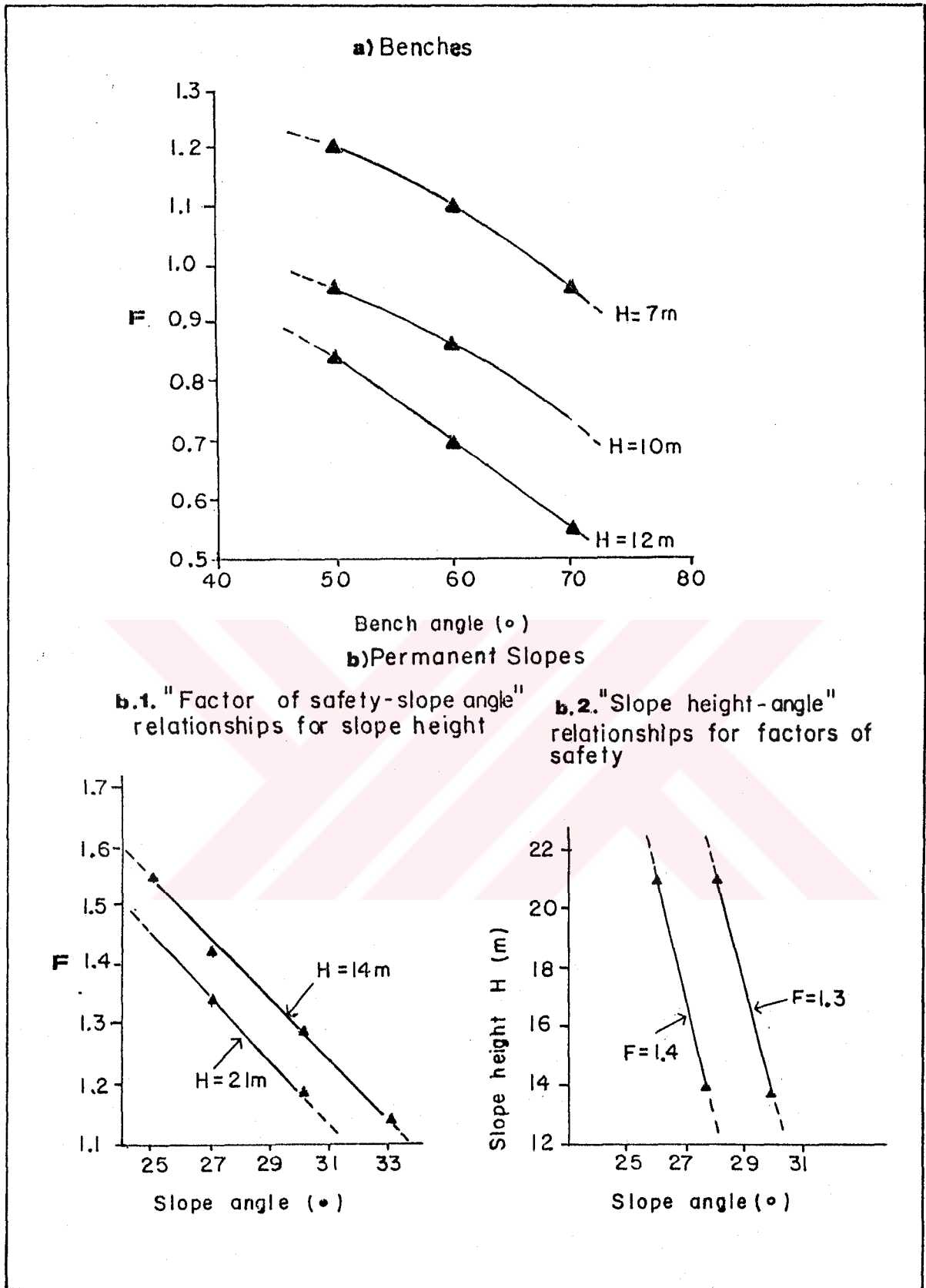


Figure 90: Slope stability curves for the soils of transition zone in southwest wall (Sector III)

are illustrated in Figure 90b1 and b2. It is obvious that in order to make a design on the basis of factor of safety of 1.3 or 1.4 the overall slope angle in this zone should be maintained at 28° or 30° and 26° and 27.5° for the 21 m and 14 m slopes, respectively.

10.4.2. Analysis of Mass Failure Possibility in Main Sekkōy Formation

In order to investigate any possibility of rock mass failure in main Sekkōy formation, which does not introduce structurally controlled failure in this sector, stability analyses were performed with respect to circular failure mode. On the basis of three design sections (Figure 91) vertically oriented to initially designed slopes (Figure 83), the maximum thickness of this rock mass ranges between 60 and 70 m. On the other hand, in the initial design a wide bench or toe just above the coal seam is left to provide a toe buttressing effect. This lowest bench was not considered in the analyses. In spite of the lack of valuable information on groundwater conditions in this sector, the same approach as in the previous case was made.

Classification of this rock mass under consideration gives an RMR rating of 43. Cohesion and internal friction angle of this rock mass are estimated from the relationships illustrated in Figure 60b2. The rock mass obeys the non-linear failure criterion. However, expected heights of slices in the circular failure arcs seem to be very similar to each other with the exception of a few slices located at the toe and crest areas. Thus, for the sake of simplicity in the analyses, it was concluded that employing the shear strength parameters corresponding to average normal stress

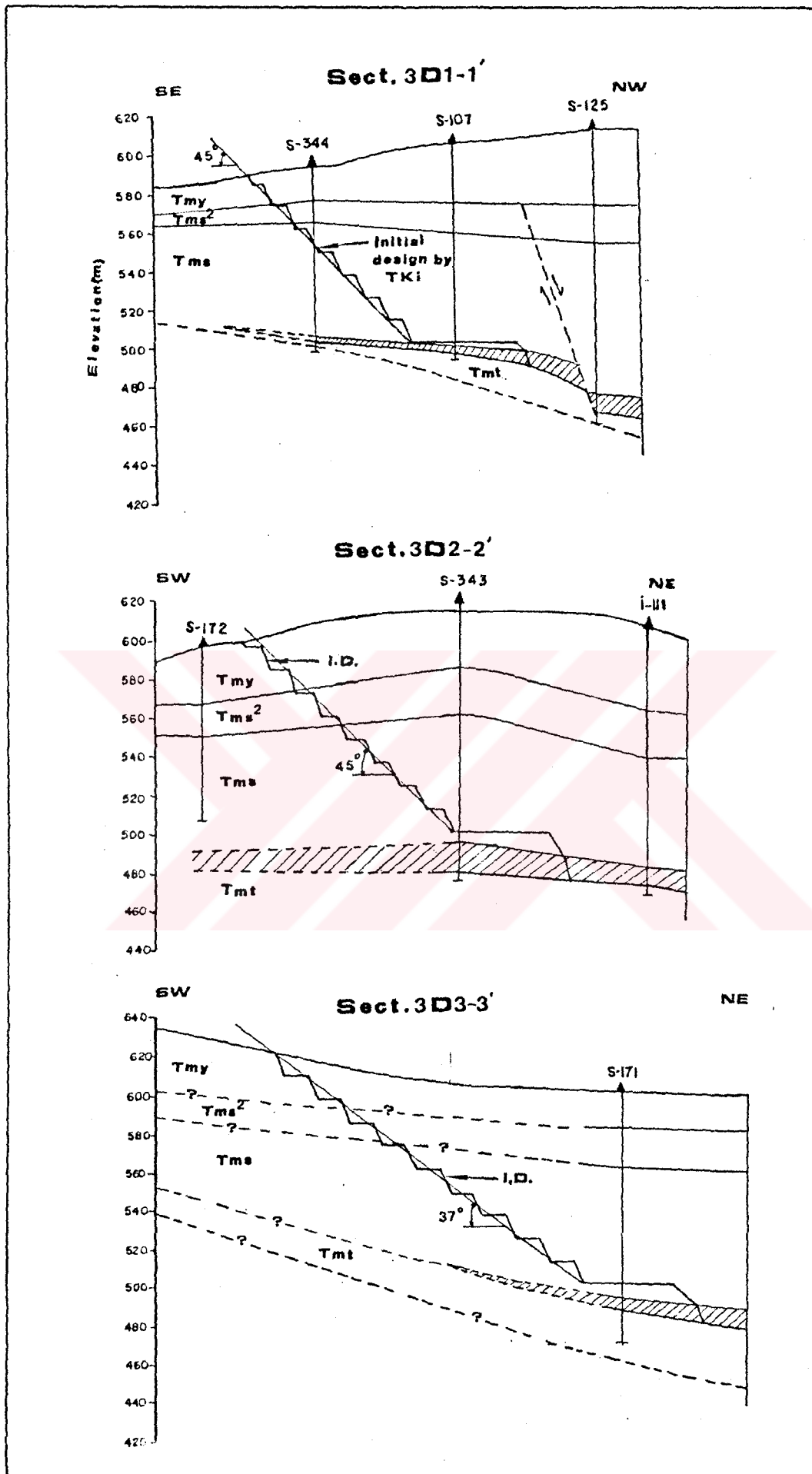


Figure 91: Design sections for design sector III.

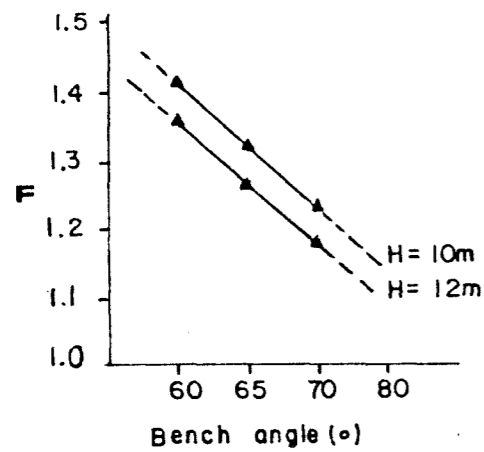
level acting along the slip surfaces would cause negligible effect on the results.

The first series of analyses indicated that a bench would be stable even if it was designed 12 m high with a face angle of 70° (Figure 92a). Considering the maximum thickness of the rock mass as 70 m, slopes of 70 m, 48 m and 36 m high were analysed with respect to various overall slope angles. The analyses show that slip surfaces passing through the toe yield the minimum factor of safety (Figure 92b). The results are introduced in the form of graphic illustrating the relationships between design parameters (Figure 92c).

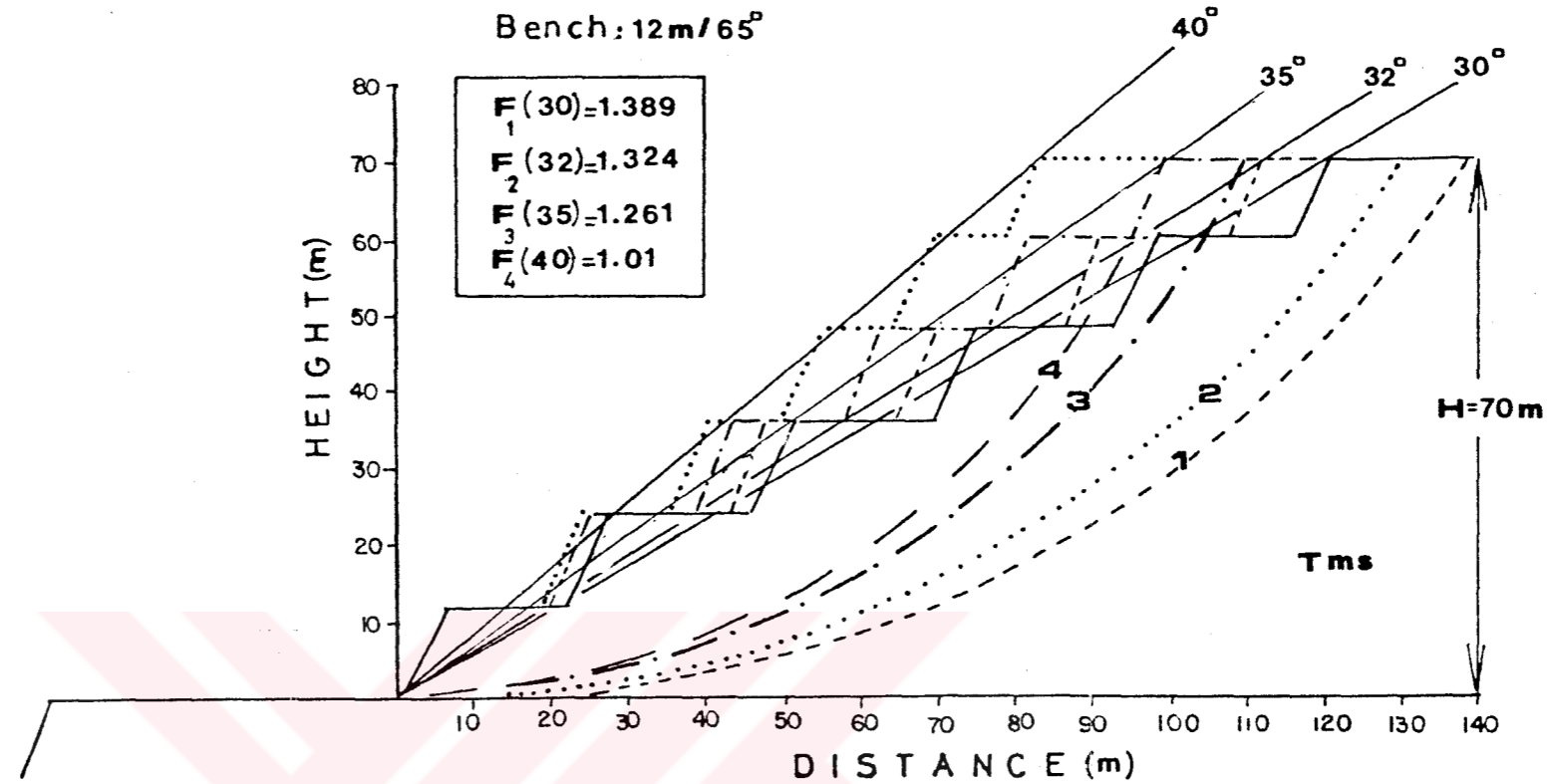
The southwest wall and the wall at the southern part of sector IV are considerably far from the highway indicating favorable condition for the stability of highway. However, it is advisable that an overall slope design based on a factor of safety of 1.3 may provide safer stability conditions against unexpected site conditions and earthquake acceleration risk. Thus, a slope in this rock mass of 70 m high should be designed with an overall angle of 34° instead of 45° proposed in the initial design.

In addition to above mentioned analyses, in order to investigate the effects of individual bench height and resulting bench configuration on overall slope stability, analyses were also performed. For this purpose, a 35° slope of 70 m high involving seven benches of 10 m each was examined. This configuration yielded a factor of safety of 1.278. This result indicates that 2 m of decrease in bench height results in an increase in the factor of safety by 1 % only when compared with slope involving 12 meters high benches ($F = 1.261$).

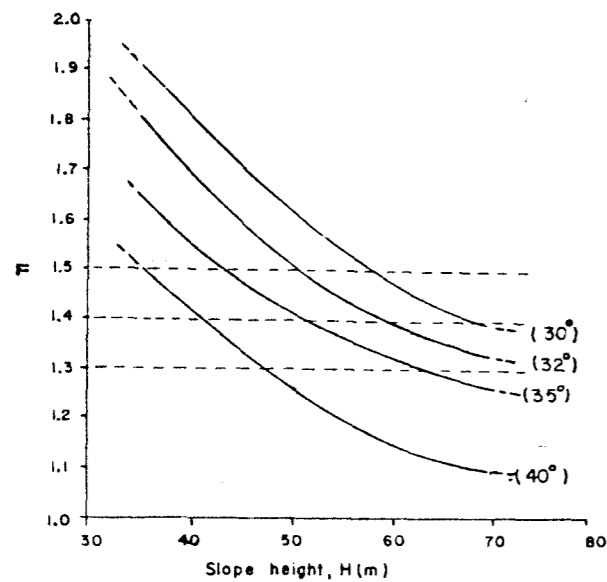
a. Factor of safety versus bench angle for benches 10 and 12m in height



b. Slope configurations analyzed and critical slip surface for a 70m height slope

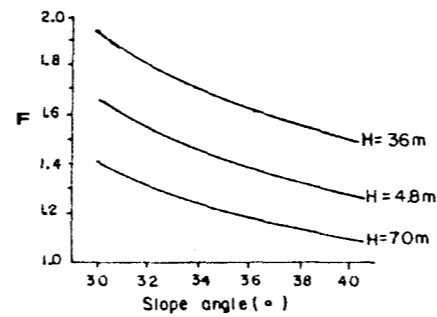


c.1. Slope height versus factor of safety for various slope angles



c. Slope stability curves

c.2. Slope angle versus factor of safety for various slope heights



c.3. Slope angle versus slope height for various factors of safety

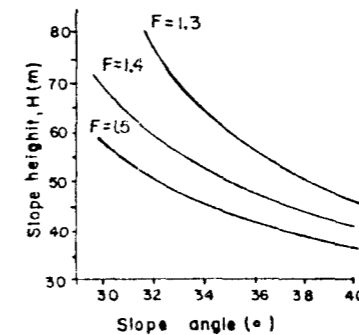


Figure 92: Stability analysis of weak portion of main Sekköy formation based on the mass failure.

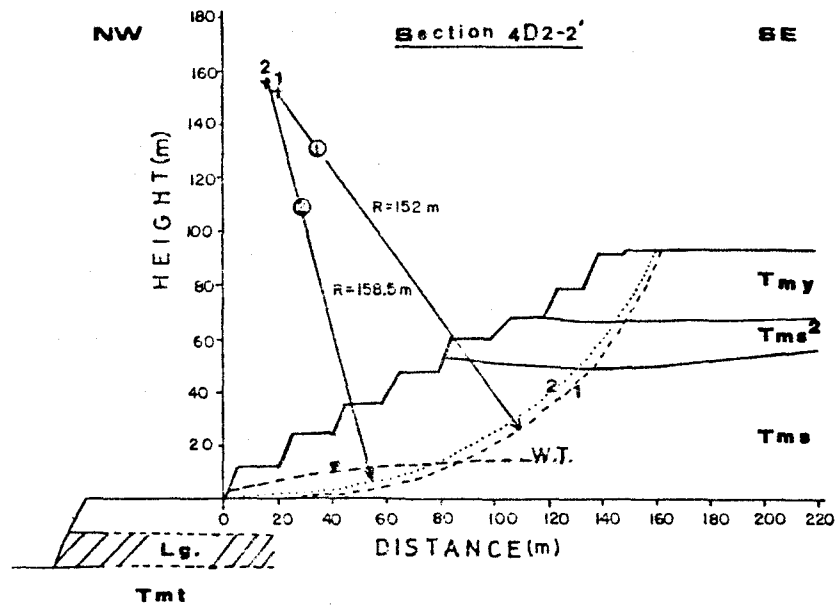
10.4.3. Overall Stability of Southwest Wall

The overall stability conditions at southwest wall were evaluated by considering different units in which the slope is cut. For this purpose the design section 4D2-2' was employed. In the first series of analyses the overall slope profile was constructed for a factor of safety of 1.3 with respect to the design parameters of each unit (Figure 91 and 92). Based on the observations performed on highly stable benches cut in the sandstone, slope angle was selected as 45° . The geometrical parameters employed in the analyses and the slope analysed are shown in Figure 93a. In spite of massive character of sandstone and the lack of distinct structural features, for the sake of simplicity, the failure is assumed to develop through the intact rock and shear strength parameters of moderately weathered portion of the unit (Table 11) was selected.

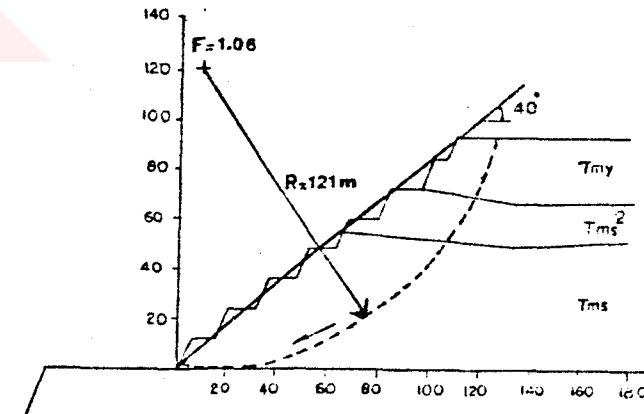
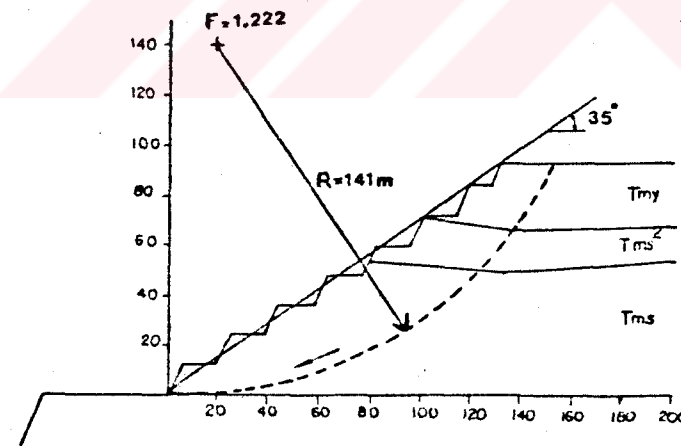
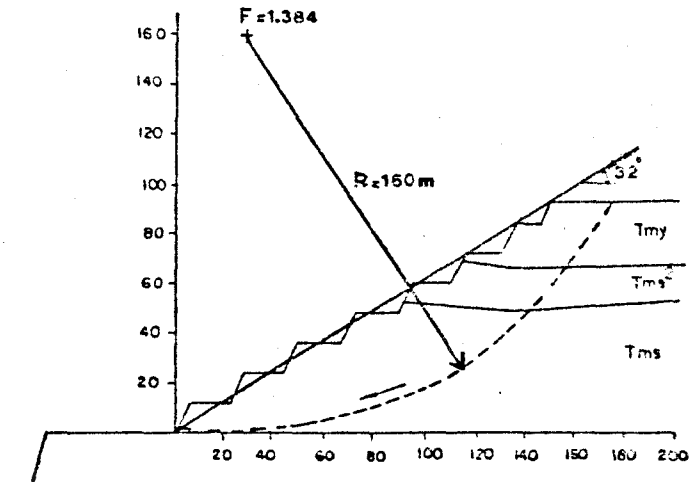
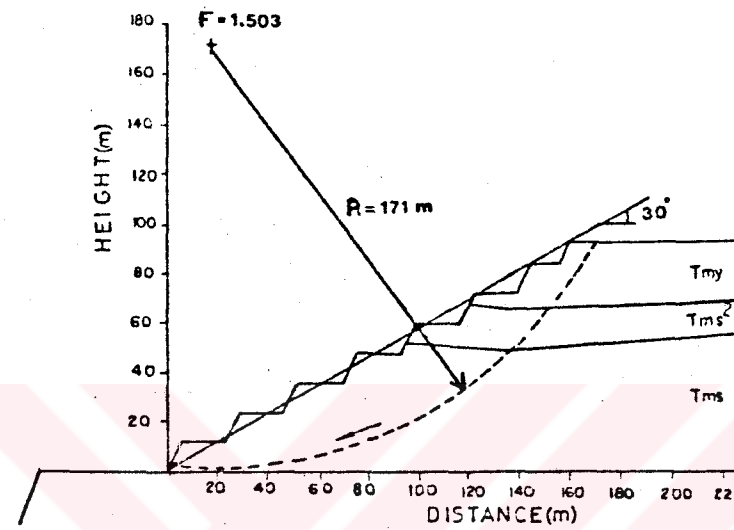
The resulting values of factor of safety are 1.312 and 1.29 for dry slope and the slope with steady state groundwater case, respectively (Figure 93a). This result indicates that overall slope design may confidently be made if the safe slope angle for each unit corresponding to a factor of safety of 1.3 is selected (Figure 90 and 92) and then they are applied to an overall slope configuration.

Planned slope heights are different for each unit in different parts of the design sector and this is reflected in the design angle. But, in practice, application of different slope angles may be restricted or introduces some difficulties because of variations in thickness of each unit. Therefore, designing of the slope with respect to the stability conditions for the dominant rock type seems to be more practical.

a. Overall slope profile analyzed and results of analyses for southwest wall 70m height



b. Overall stability analyses of different slope geometries and critical slip surfaces



Slope angles employed for each formation :

Tmy: 45°, Tms²: 29° (for F=1.3); Tms: 35° (for F=1.3)

Bench parameters:

Tmy: 12m/70°; Tms²: 7m/50°; Tms: 12m/70°

Slip circles:

No.1: Slope with water table (F=1.29)

No.2: Dry slope (F=1.312)

(*) Slope angles corresponding to F=1.3 from Figures 90b. and 92.c

Figure 93: Mass failure analyses for slopes involving different rock and soil units at sector III and south of sector IV.

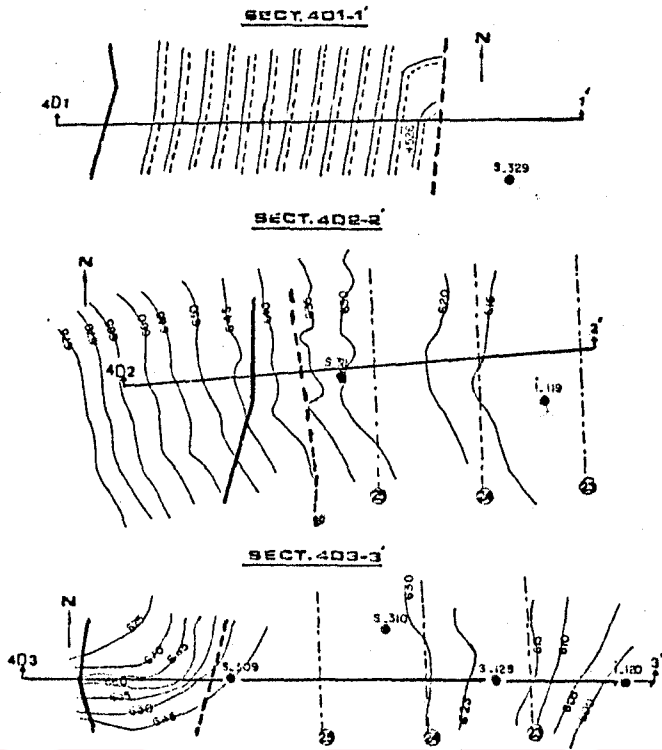
The alternative was investigated by taking into consideration the fact that rock mass in main Sekköy formation is dominant rock type. The analyses were performed for 30°, 32°, 35° and 40° slopes (Figure 93b). This revealed that the difference between the factor of safety of 32° slope designed with respect to dominant type of rock (Figure 93b) and 32° slope designed with different angles in different portions (Figure 93a) is only 5 % .

10.5. Stability of West and East Sidewalls (Design Sectors IV and V)

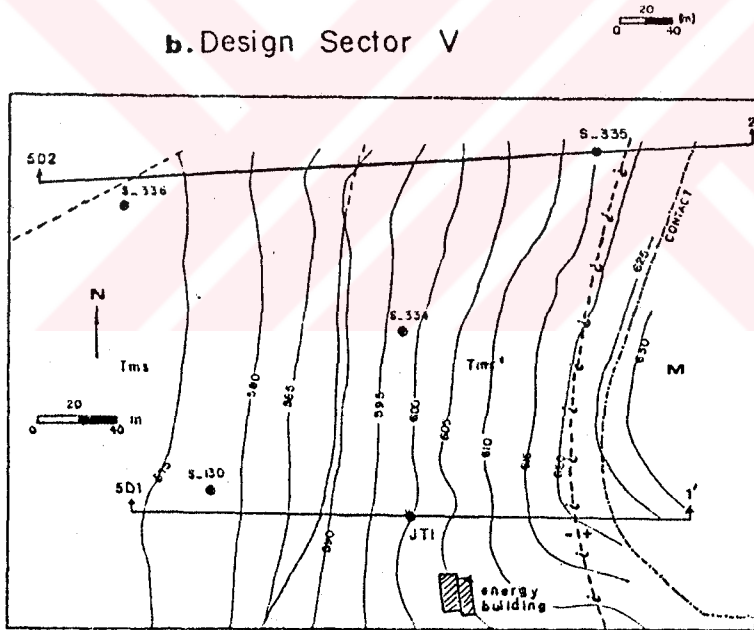
The permanent slopes or sidewalls along the basin margins will be constructed in the N-S direction, both at west and east. An initial design was made by TKİ for the west sidewall at a certain location (Ömeroglu Stream). Besides, dense vegetation cover and the lack of sufficient number of investigation boreholes along the basin margins introduced some uncertainties such as groundwater conditions, continuity of black clay, and localities where the coal seam is ended. However, the locations where more information were available, are determined and limited number of sections running through these locations are employed in the analyses (Figure 94).

On the basis of kinematic analyses plane shear failure mode was analysed using the computer program MBPF (Appendix E3). The slopes will cut all the units encountered in the study area with exception of transition zone deposits. A few analyses with respect to the sliding surfaces along the undulating planar bedding planes in limestones yielded considerably high factors of safety. It is then concluded that the overall stability of sidewalls is mainly controlled by the shear strength of bedding planes of the main Sekköy

a. Design Sector IV



b. Design Sector V



EXPLANATIONS



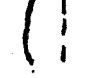
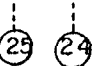
-  Section line
-  Initial design by T.K.I.
-  Toe and crest of slope
-  Slices

Figure 94: Design sections selected at sectors IV and V.

formation and the footwall material. Thus, further analyses were based on this argument.

In-situ observations performed on slide 1 adjacent to basin margin at Ertrans section (Figure 61) suggest that tension cracks occur in the slope face resulting in an unstable block and an unsupported rock mass behind it. After the initiation of the first slide the remainder unsupported mass further up of the face may tend to move retrogressively towards the void. Therefore, tension crack in the slope face was considered more critical for this case.

Because of some uncertainties involved at the basin margins, stability of sidewalls is required to be analysed by sensitivity approach. The conditions investigated are as follows:

- 1) Dry slope with tension crack,
- 2) Water in tension crack and along the sliding surface only (crack is filled with water to various depths, $z_w = 0.2, 0.3, 0.5$ (Appendix D1),
- 3) Non-linear water table daylighting at the marl/coal seam boundary and dry tension crack.

Water losses encountered in borehole JT1 drilled in limestone at the east margin (Figure 94b) and dips of strata probably suggest that limestone and conglomerate appearing in the upper benches may involve insignificant amount of water. Thus, on the basis of in-situ observations the groundwater table was assumed to lie just above the marl/coal seam boundary.

On the other hand, the approach employing one of shear strength parameter for the black clay or finest material of Turgut formation will lead to a conservative or an

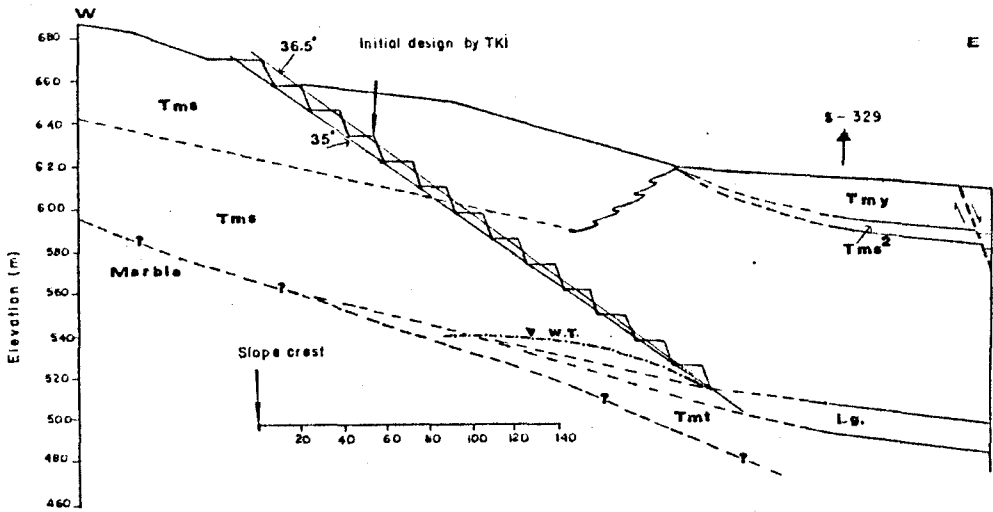
optimistic design. In order to avoid extreme assumptions, all experimental data derived from the peak and residual shear test results (Table B.10/C1, C2) were evaluated together. The regression analysis based on the linear fit yielded shear strength parameters as $c = 13.6$ kPa and $\phi = 27^\circ$. It is assumed that these parameters may balance the uncertainties resulting from the questionable conditions of footwall materials in these sectors. The shear strength parameters of bedding planes in the main Sekköy formation were taken as $c = 12.5$ kPa and $\phi = 26.5^\circ$ (Table 12).

The design sections, examined slope profiles and the results of sensitivity analyses are depicted in the graphical form in Figures 95 through 99. The graphs help to locate the position of tension crack which yields minimum factor of safety.

As it can be seen from the results, most critical conditions arise or minimum factor of safety is obtained in the case of tension crack filled with water coinciding with mid point of tension crack, and the sliding surface follows the bedding planes in footwall. These conditions become more critical if tension crack position is located close to the crest of slope. It also indicates the possibility of a large volume of unstable mass. However, in the same conditions factors of safety greater than unity are yielded for the portion of slope resting on the coal seam.

In the case of drawdown with no water pressure at the face of the benches in hangingwall, stability conditions are better than the case of tension crack filled with water. Because the water pressure is lower in this case. The tension cracks are located at the toe region, however, cause a sharp decrease in factor of safety, particularly in design sections 4D3-3', 5D1-1' and 5D2-2' where coal is thicker and consequently phreatic surface daylights at higher elevations. In this condition, however, most critical position of

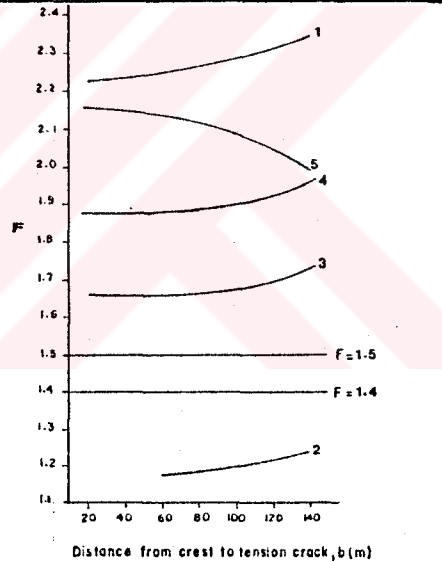
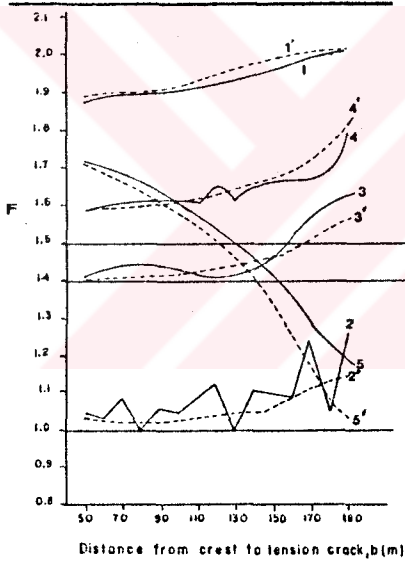
a. Design section and overall slope angles analyzed



b. Sensitivity plots

Planar sliding along footwall

Planar sliding along the bottom of hangingwall



— Multibenched slope profile
 --- Unbenched slope profile (36.5°)

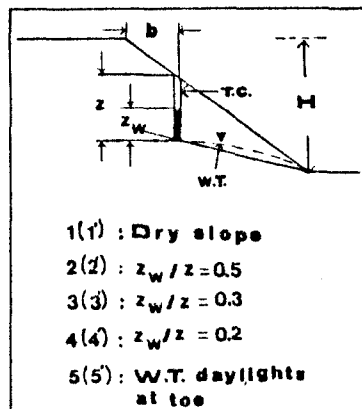
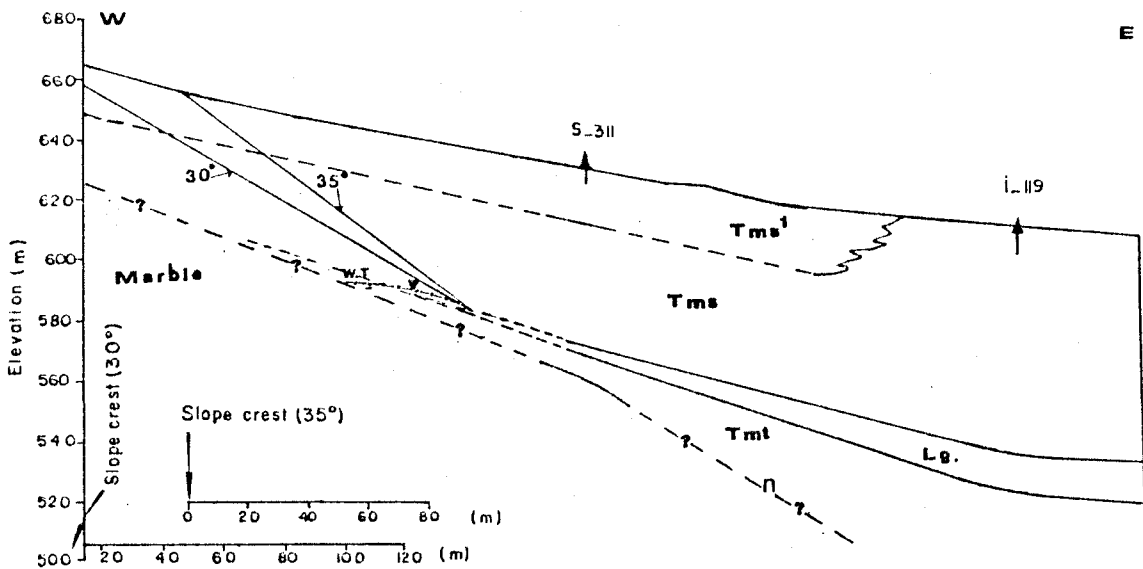
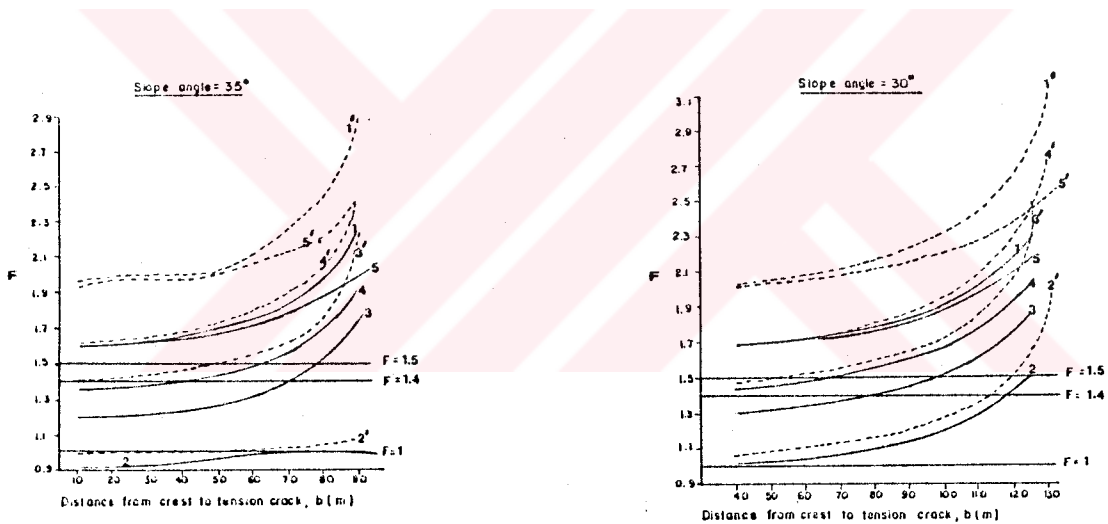


Figure 95: Design section 4D1-1' and computer solutions for the tension crack positions under different groundwater conditions (Sector IV).

a. Design section and overall slope angles analyzed



b. Sensitivity plots



— Planar sliding along footwall
 - - - Planar sliding along the bottom of hangingwall

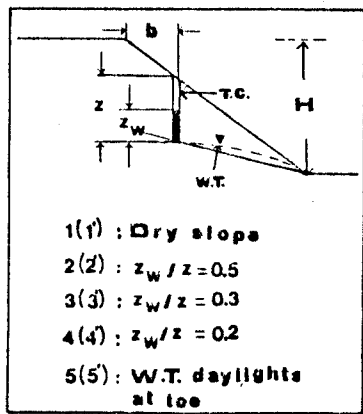
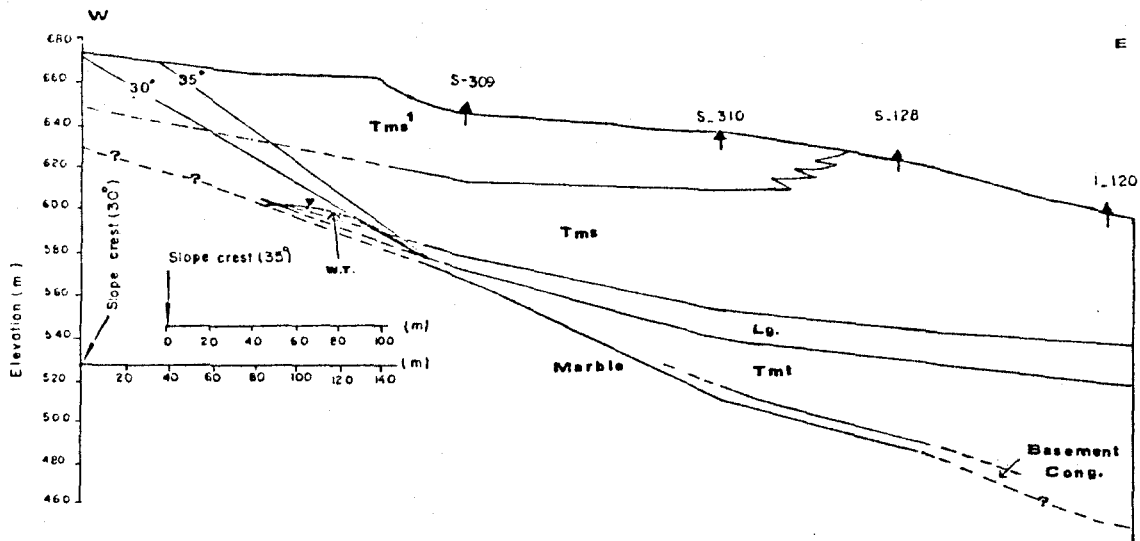
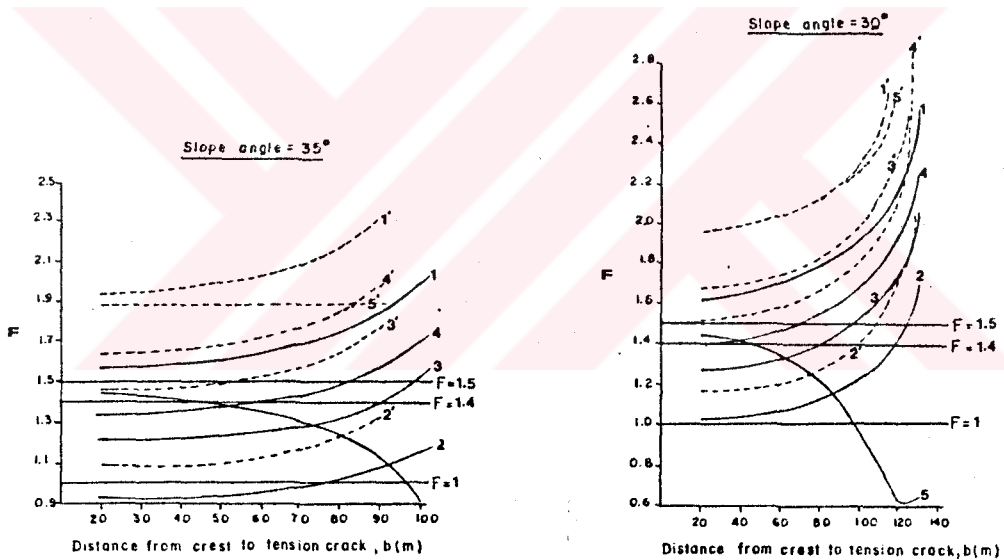


Figure 96: Design section 4D2-2' and computer solutions for the tension crack positions under different groundwater conditions (Sector IV).

a. Design section and overall slope angles analyzed



b. Sensitivity plots



— Planar sliding along footwall
 - - - Planar sliding along the bottom of hangingwall

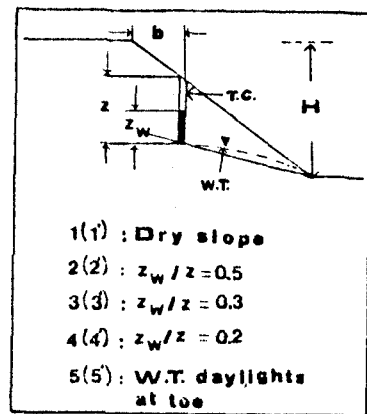
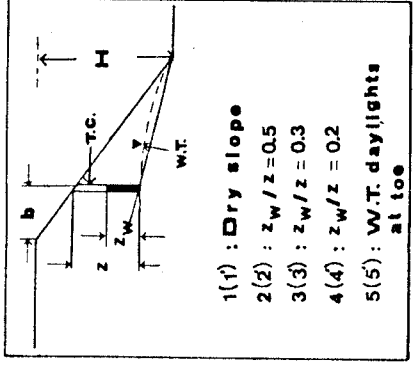
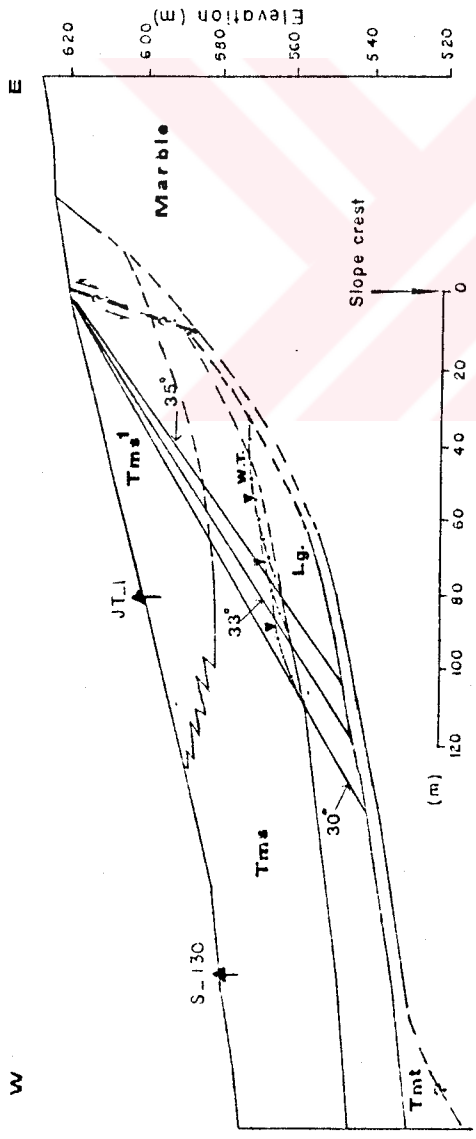


Figure 97: Design section 4D3-3' and computer solutions for the tension crack positions under different groundwater conditions (Sector IV).

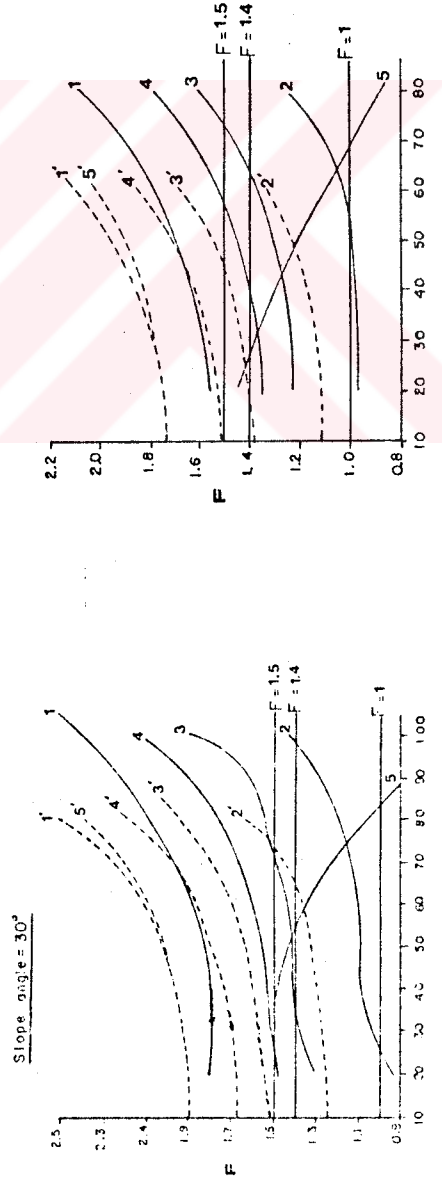
a. Design section and overall slope angles analyzed



— Planar sliding along footwall
 - - - - Planar sliding along the bottom of hanging wall

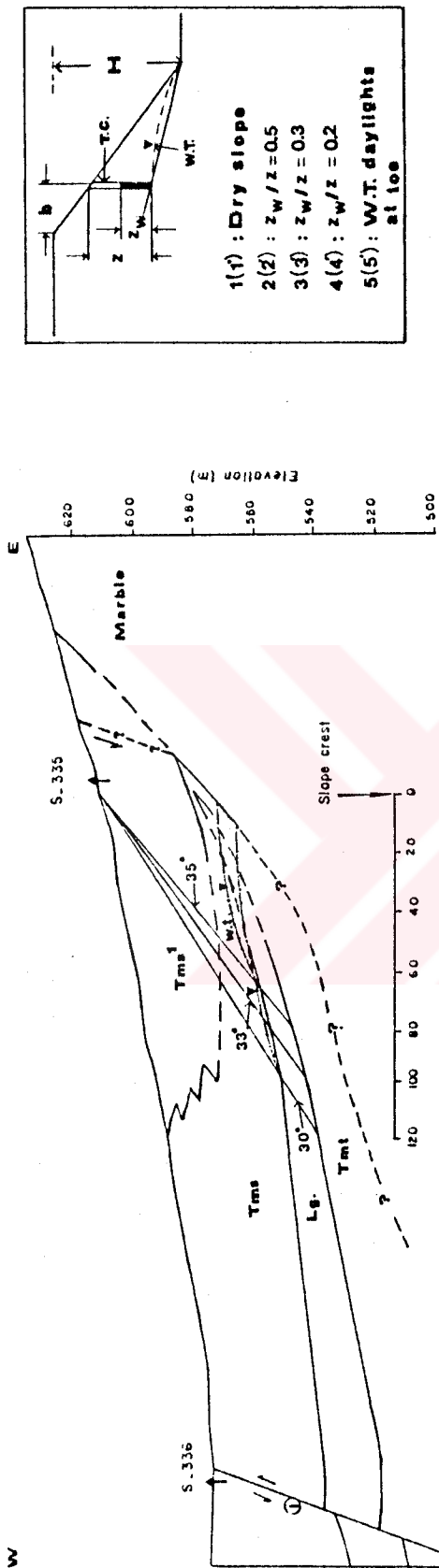
b. Sensitivity plots

Slope angle = 33°



DISTANCE FROM CREST TO TENSION CRACK, b (m)

Figure 98: Design section SD1-1' and computer solutions for the tension crack positions under different groundwater conditions (Sector V).



b. Sensitivity plots

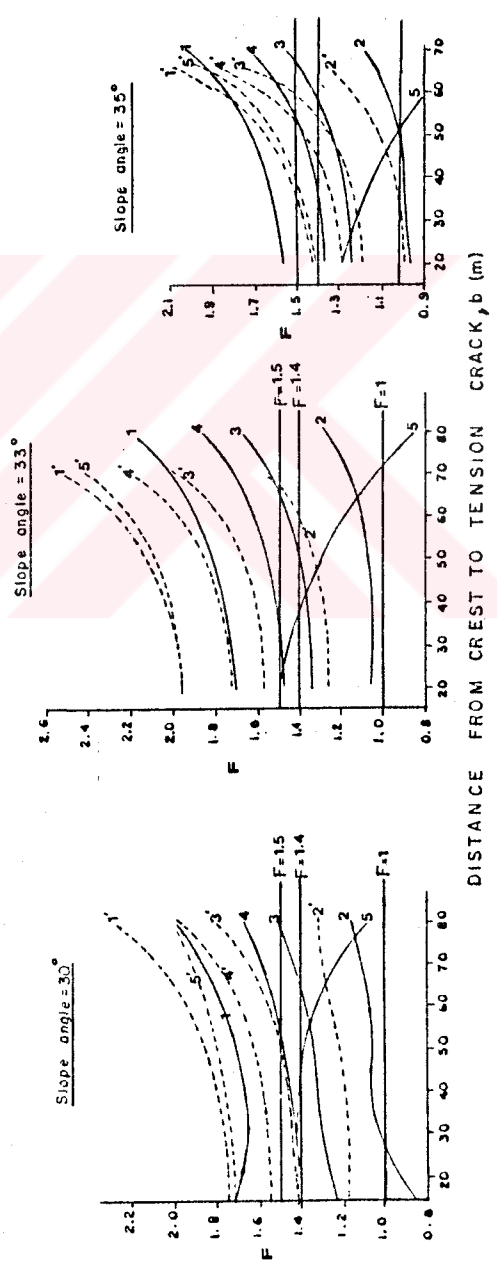


Figure 99: Design section 5D2-2, and computer solutions for the tension crack positions under different groundwater conditions (Sector V).

tension crack appears around the toe region resulting in small rock slides. It is considered that this slide may not threaten the stability of entire slope and may be controlled.

A tension crack filled with water to its mid point demonstrates the worst case amongst other cases investigated. This case may occur after a week or more of heavy rain and that this may be followed by an exceptionally heavy downpour filling an existing tension crack in the slope face. But, this is a very extreme case to occur. On the other hand, blasting for easy digging in limestones and conglomerates appearing in upper benches is necessary. This will produce an acceleration of an unknown magnitude. Thus, as a remedial measure against these adverse conditions an overall slope angle ranging between 30° to 33° seems to be safe.

10.6. Stability of Highwall Slopes

Stability of slopes surrounding the highwall, where dragline operates, are considered with respect to the following modes of failure:

- 1) Mass failure following a circular slip surface which may develop through the blasted highwall material, and
- 2) Failures controlled by major discontinuity sets.

On the basis of kinematical assessments, no structurally controlled failures are anticipated in design sector VII where dragline operates along N-S oriented highwalls. However, the possibility of mass failure, which may endanger the stability of the dragline, was

alternatively examined. In addition, stability of highwalls was investigated with respect to multiplanar mode of failure which is more critical in design sectors VIII and IX if the highwalls are oriented in the E-W direction.

10.6.1. Possibility of Mass Failure in Highwalls

The slopes of dragline panel or highwall (Figure 75) include:

- a) The slope in front of the dragline (cut face)
- b) The highwall of the slice where dragline operates (old highwall)
- c) The highwall of the slice to be excavated next (new highwall)

In the analysis of highwall slopes following assumptions were considered:

- 1) The bedding is horizontal or nearly horizontal.
- 2) The failure occurs along a circular slip surface through the rock mass.
- 3) On the basis of current mining practice the overburden thickness stripped by dragline ranges between 20 to 25 m.
- 4) Groundwater table may daylight on the wall face at different depths around the marl/coal seam boundary. Before the dragline moves on a new highwall, 1200 m long slice will be stripped by the dragline, thus there will be sufficient time for drainage to occur

along the highwall. Thus, the overburden material cut by old highwall is considered as a dry slope.

- 5) The shear strength parameters of blasted compact marl are determined from Figure 60 b.1 as $c = 60$ kPa and $\phi = 29^\circ$ for the 25 m high highwall.
- 6) On the basis of current mining practice and equipment specifications, highwalls of $55^\circ/70^\circ$ and $60^\circ/70^\circ$ (hangingwall/coal), and cut faces of 30° were analysed. In addition, cut faces of 45° were also examined.
- 7) When evaluating the impact of the dragline loading, the static load as well as the dynamic loading from the dragline operation should be considered. Since there is no available data on the nature and magnitude of the dynamic loading; the dynamic loading was not considered in the analyses. The dragline is assumed to produce strip loading and this load is entered into the computer program MTASLP. The dragline loading is not considered in the analysis of new highwall slope where the dragline does not operate.
- 8) Current operation suggests that minimum distance between the slope crest and the dragline pad is 12m.
- 9) Various slip circles passing through different points of the hangingwall were examined by means of iterations to obtain minimum factors of safety. The coal seam was not included in the analyses due to difficulty in obtaining suitable coal samples.

Due to the possible range of drawdown of the groundwater table and different slope angles, and overburden heights, sensitivity approach was used to see what effect these factors have on the predicted factor of safety.

Besides, three different positions of the dragline with respect to slope crest were also taken into consideration.

Slope geometries, possible positions of the dragline and the slip surfaces corresponding to minimum factors of safety for each highwall slope and cutface are introduced in Figure 100 a through c. The results are summarized in Table 16 and the sensitivity plots developed are also given in Figure 100 d.

Based on the results of the analyses followings are obtained:

- 1) New highwall slopes : The failure surfaces corresponding to minimum factors of safety are shallow seated slip surfaces passing through the toe (Figure 100 a). New highwall slopes seem to be stable under given conditions, even if the water tables lies above marl/coal seam boundary, as shown by the surface 3 in Figure 100 a. The current stable highwalls in the pit also confirm these results. However, because of the complex and shallow seated highwall failure which occurred in front of the temporary piles adjacent to new highwalls their effect on the stability should be taken into consideration. Thus, to account this effect indirectly by stipulating that a factor of safety of 1.3 may be used for purposes of establishing the design of new highwall (Jaworski and Zook, 1979).
- 2) Old highwall slopes : The position of predicted slip surface yielding a minimum factor of safety approaching unity for the dragline is of importance. As it can be seen from Figure 100 b, for 25 m thick overburden at 55° face angle, yields high factors of safety with respect to different dragline positions. However, predicted slip surfaces yielding

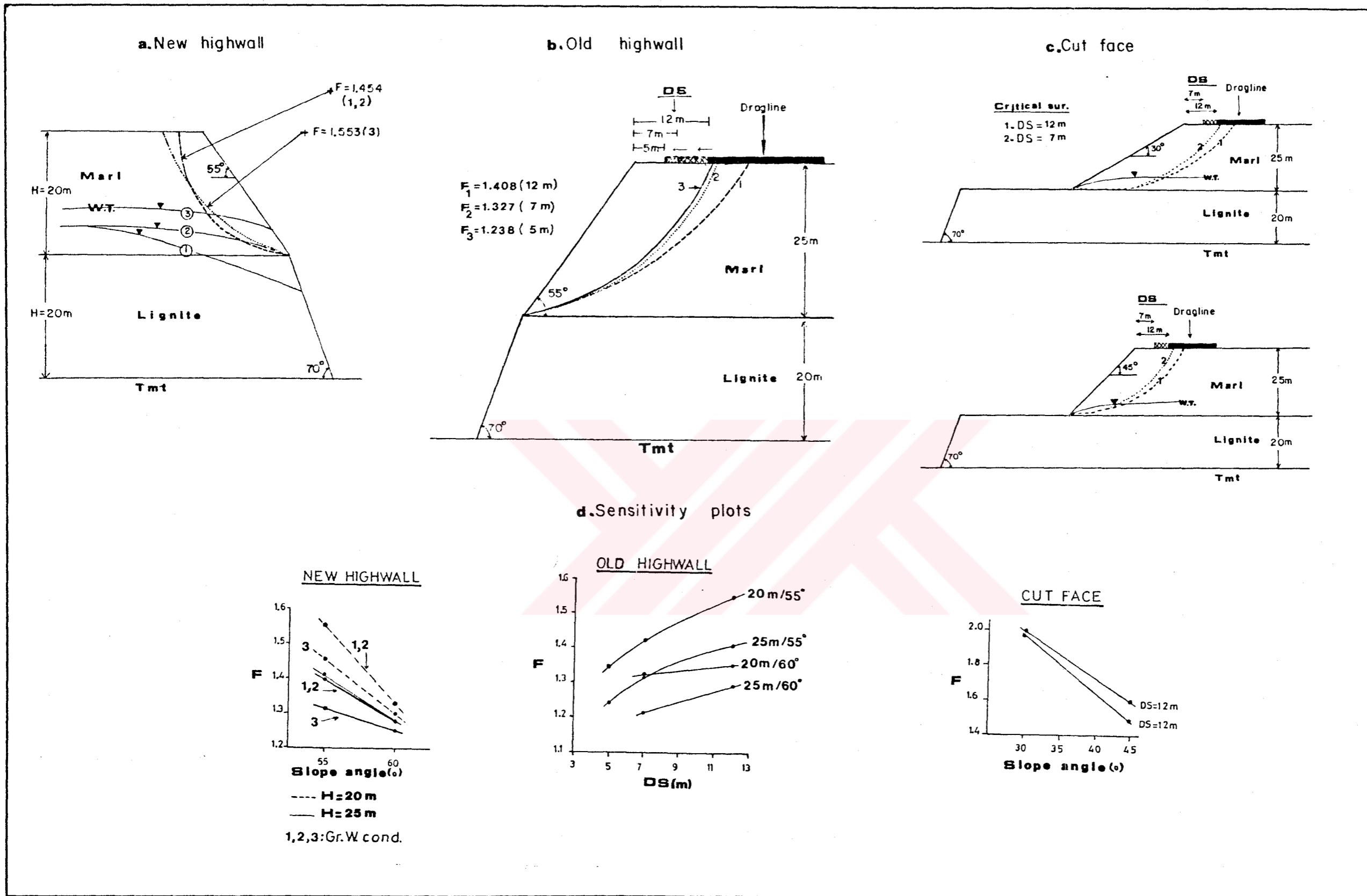


Figure 100: Stability analysis of highwall slopes constructed in blasted material with dragline load.

Table 16 : Results of the stability analyses for highwall slopes against mass failure

Thickness of marl (m)	Slope ⁺ Angle (°)	Factor of Safety, F												
		Old Highwall					New Highwall*					Cutface		
		Distance of dragline's tub from the crest		Position of groundwater table			Distance of dragline's tub from the crest		Position of groundwater table			12 m	7 m	
20	55°	12 m	7 m	5 m	1	2	3	12 m	7 m					
		1.553	1.425	1.349	1.553	1.553	1.454							
	60°	1.358	1.330	--	1.328	1.328	1.297							
25	55°	1.408	1.327	1.238	1.409	1.394	1.313							
	60°	1.290	1.215	--	1.280	1.279	1.251							
25	30°							2.06						1.98
	45°							1.605						1.492

* Reference should be made to Figure 100 a for the position of groundwater table

** Reference should be made to Figure 100 c for the position of groundwater table. Position 2 employed for new highwall is assumed for cutface.

+ Slope angles are given for overburden only (hangingwall material)

minimum factors of safety, undermine about half of the dragline pad and the stability conditions tend to decrease as dragline moves towards the crest (Table 16). Similar results on slip surface in the case of dragline with a capacity of 60 m³ were obtained by Jaworski and Zook (1979). Because of the uncertainties resulting from the dynamic loading of the dragline and the seismic coefficient as well as the importance of the dragline itself, it is important to select the factor of safety as 1.3, preferably 1.4 for the design of old highwalls. On the basis of current practice and the results of stability analyses a minimum distance between the dragline pad and the crest should be maintained at 12 m and there is no reason to amend this.

- 3) Cutface slopes : Based on a factor of safety of 1.4 a cutface slope seems to be highly safe against mass failure for both cases, that is slopes at 30° as in the current practice and slopes at 45° as an alternative, even if the overburden thickness is 25 m (Table 16). Thus, a cutface involving an overburden of 20 m thick is not required to be analysed.

10.6.2. Structurally Controlled Failure Analysis For Highwalls (Design Sector VIII and IX)

It is obvious from the kinematic assessments and the back analysis of slide 2 (Figure 65) that if slices and working benches are designed in the E-W direction the mode of multiplanar failure appears in certain parts of design sectors VIII and IX. This failure involves the faults and bedding planes striking NE-SW and adversely dipping into excavation.

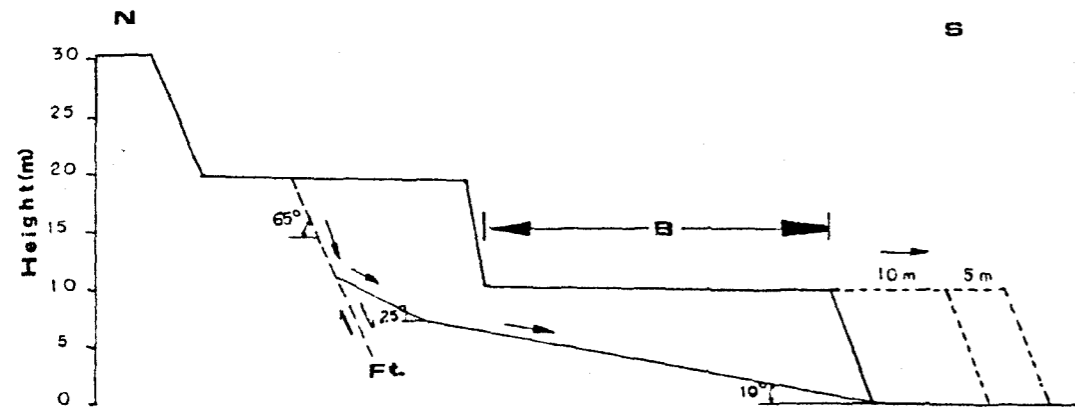
In order to investigate minimum safe bench width and the possibility of highwall failure in dragline panels at these sectors, deterministic stability analyses were carried out using the computer program SWASE (Huang, 1983) and residual shear strength parameters of discontinuities given in Table 12. The loading of the dragline was also taken into account.

The first series of analyses performed for safe bench width were based on the pre-failure slope configuration in section C-C' employed in back analysing of slide 2 (Figure 101a). A mean dip value of 65° was selected in the analyses for the fault planes in the sectors. As it can be seen from the graph given in Figure 101b, in order to obtain a factor of safety of 1.3, as recommended for temporary mine slopes (Hoek and Bray, 1977), the minimum distance between the working or advancing benches should be kept as 35 m.

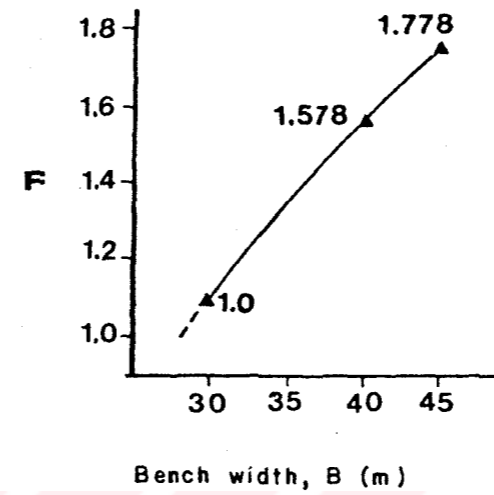
In the case of highwalls oriented in E-W direction, faults striking NE-SW and dipping SE run obliquely to the slope faces (Figure 101c). The highwall slopes are steeper than the cutface slopes. Therefore, it is considered that the mode of failure would be more critical for old highwalls. On the other hand, depending on the advance of the dragline on the highwall there will be many possible positions of the fault that may run behind or ahead of the dragline, as illustrated in Figure 101c. Assuming the most critical position of the dragline whose pad seats 12 m away from the crest, stability conditions resulting from the relationships between various positions of the dragline and the fault were investigated. For the purpose, a cross section parallel to dip direction of the discontinuities contributing to failure was employed (Figure 101d).

The variations in factor of safety with the distance between the fault and the crest are illustrated in Figure 101e. As it can be seen from the curve, factor of safety

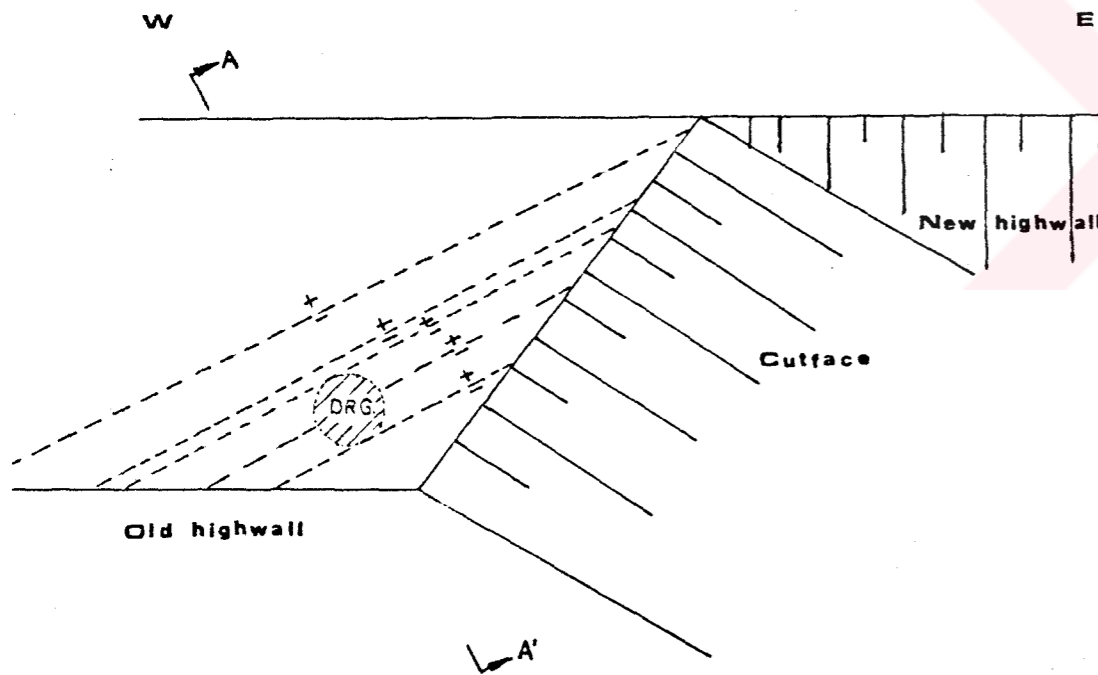
a. Determination of safe bench width against multiplanar failure



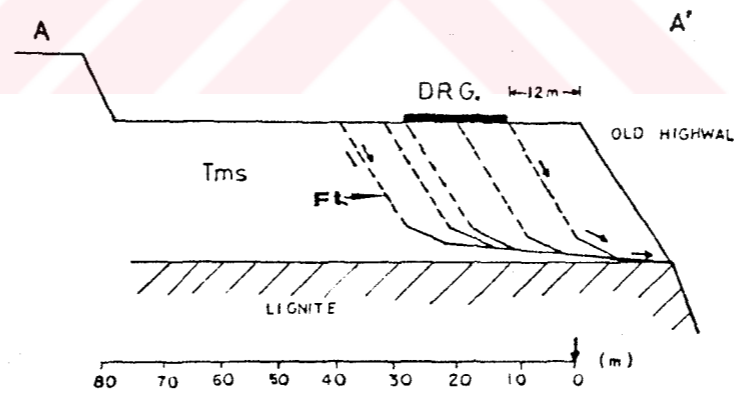
b. Factor of safety versus bench width



c. Block diagram of highwall oriented in E-W direction and different positions of fault with respect to dragline



d. A A' section and multiplanar failure surfaces



e. Variation of factor of safety with the distance between fault and slope crest

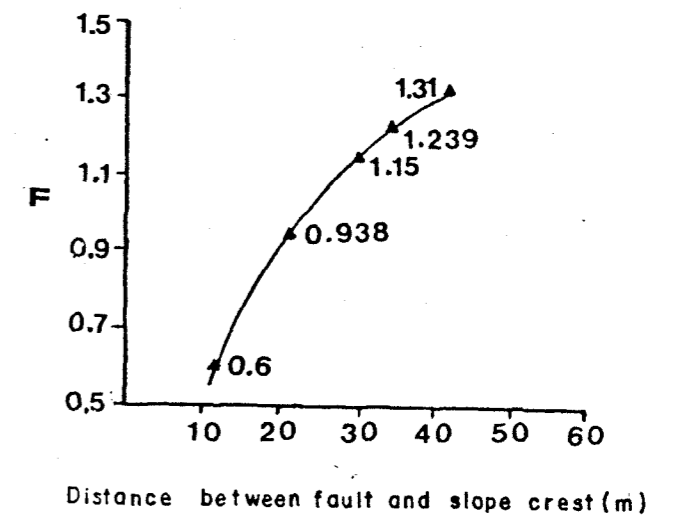


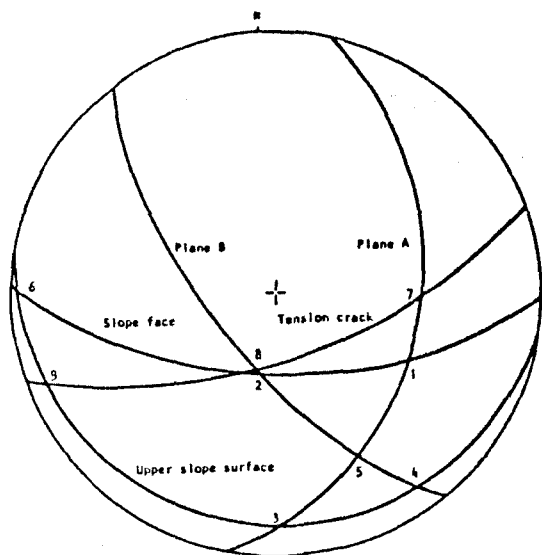
Figure 101: Analyses of safe bench width and combined effects of dragline and fault systems on the stability of slopes oriented E-W (Sector VIII and IX).

tends to decrease to unity, indicating a multiplanar shear failure risk, when the dragline seats very closely to the crest and the fault runs behind or in front of the dragline within a distance of 50 m from the crest. In these conditions when the distance between the old highwall crest and the fault is 50 m the factor of safety approaches to 1.31. Thus, if the highwalls are oriented in the E-W direction, as it is the case between the boundaries of 13th and 18th slices and in the vicinity of Ömeroglu Stream, where the major faults such as G and F cut the slopes obliquely (Plate 1), highwall instability problems can be encountered.

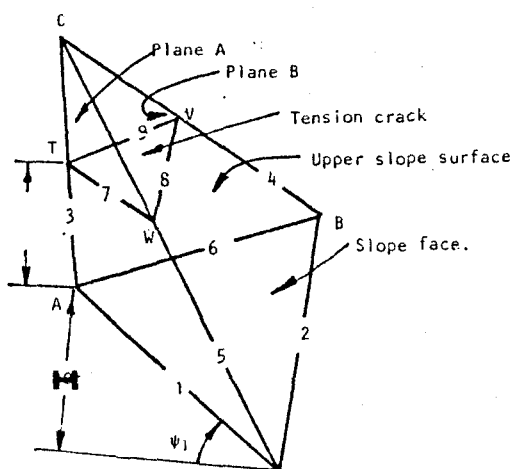
10.7. Analysis of Possible Wedge Failures

Kinematic assessments indicated that wedges are likely to develop in design sectors VI, VIII and IX. Wedge possibilities are confined to a working bench of 12 m high and overburden material of 25 m thick. Analytical method of analysis was employed to investigate the stability of these wedges considering various parameters. The calculations were carried out using the computer program WEDFA (Appendix E.4) modified to incorporate loading of the dragline.

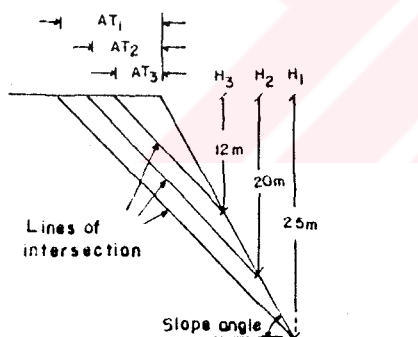
Input for directional data for each wedge was obtained from the kinematical analyses on the basis of the stereographic construction given in Figure 102a. The kinematic studies are based on the assumption of underground continuity of the surface plane of joints. This may not be the case, as indicated by the statistical analyses performed on joint persistence measurements. On the other hand, water percolating through joints or tension cracks may build up hydrostatic pressure during periods of rain. Above conditions are treated through sensitivity analyses. In the sensitivity analyses the following cases were considered :



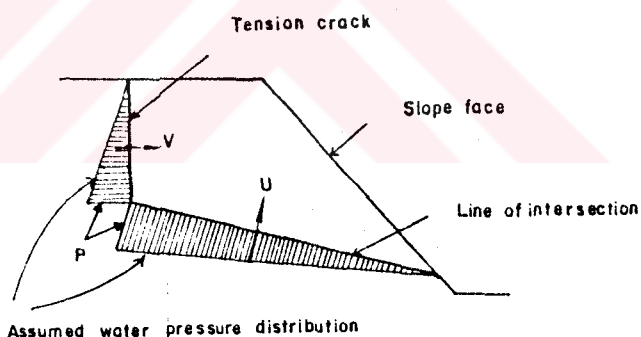
a. Great circle traces representing planes defined in wedge problem



b. Pictorial view of wedge problem to be analyzed showing numbering of intersections



c. Different positions of lines of intersection



d. Wedge geometry and water pressure distribution

Figure 102: Stereoprojections and sections showing the basic elements of wedge problem.

- 1) Dry slope with no tension crack,
- 2) Dry slope with tension crack behind the crest,
- 3) Slope with tension crack and hydrostatic pressure.

In the analyses various wedge heights (H) depending on daylighting location of the lines of intersection on the slope face (Figure 102 c) and tension crack positions behind the crest (Figure 102 b; distance AT) were also included. In the analyses it was assumed that water is free to enter the tension crack (trace TV in Figure 102 b) and that water pressure distribution is as shown in Figure 102 d.

As indicated by back analyses, the residual shear strength parameters of the faults and joints were employed as input parameters (Table 12). Overburden slopes 20 to 25 m high at 55° to 60° and working benches 12 m high at 70° were analysed.

10.7.1. Design Sector VI

The results of sensitivity analyses performed for the wedges involving faults and major joint sets ($I_{f1,j2}$ and $I_{f2,j2}$; Figure 76f) are tabulated in Table 17. It is obvious that the wedge involving fault 1 and joint set 1 is stable under various conditions. The plunge of the line of intersection $I_{f1,j1}$ is flatter than the internal friction angle of the joints. This situation results in high factor of safety.

The results indicate that the wedge involving fault 2 and joint set 2 is generally safe. It may tend to be critical, however, when the height and slope angle of the highwall increase to 25 m and 60°, respectively and the

Table 17 : Limiting equilibrium analysis of wedge failures-Design Sector VI

Type of slope	Slope angle (°)	Height of slope	Height of wedge H* (m)	Tension crack position AT** (m)	Water condition	External loading	Factor of Safety F
a) $I_{f1,j1} = 30/068$ (Figure 76f), slices oriented in the N-S direction							
Highwall	55°	25	25	None	Dry	None	5.589
Highwall	55°	25	25	None	Dry	Dragline	3.315
Highwall	55°	25	20	None	Dry	None	4.519
Highwall	55°	25	20	None	Dry	Dragline	3.218
b) $I_{f2,j2} = 48/108$ (Figure 76f), slices oriented in the N-S direction							
Highwall	55°	25	25	None	Dry	None	1.613
Highwall	55°	25	20	None	Dry	None	1.803
Highwall	55°	25	12	None	Dry	None	2.438
Highwall	55°	25	25	4	Dry	None	1.596
Highwall	55°	25	20	4	Dry	None	1.794
Highwall	55°	25	12	4	Dry	None	2.414
Highwall	55°	25	25	4	W. pressure	None	1.218
Highwall	55°	25	20	4	W. pressure	None	1.562
Highwall	55°	25	12	4	W. pressure	None	2.660
Highwall	60°	25	25	None	Dry	None	1.414
Highwall	60°	25	20	None	Dry	None	1.554
Highwall	60°	25	12	None	Dry	None	2.023
Highwall	60°	25	25	None	Dry	None	1.381
Highwall	60°	25	20	None	Dry	None	1.522
Highwall	60°	25	12	None	Dry	None	2.016
Highwall	60°	25	25	None	W. pressure	None	0.768
Highwall	60°	25	20	None	W. pressure	None	1.021
Highwall	60°	25	12	None	W. pressure	None	1.864
Working bench	70°	12	12	None	Dry	None	1.591
"	70°	12	12	4	Dry	None	1.539
"	70°	12	12	2	W. pressure	None	1.505

* Reference should be made to Figure 102 c

** Reference should be made to Figure 102 b

$I_{f1,j1} = 30/068$, "plunge/trend" of line of intersection

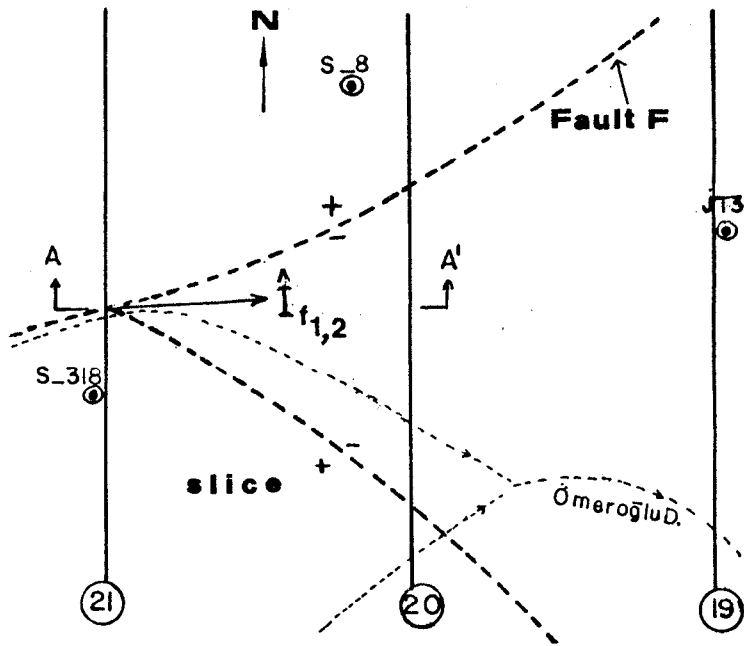
joint set is continuous throughout the entire wall. This case also involves a tension crack filled with water appearing 4 m behind the crest. The persistence data, however, showed that a continuous joint running throughout a 25 m thick overburden is rather unlikely.

10.7.2. Design Sector VIII

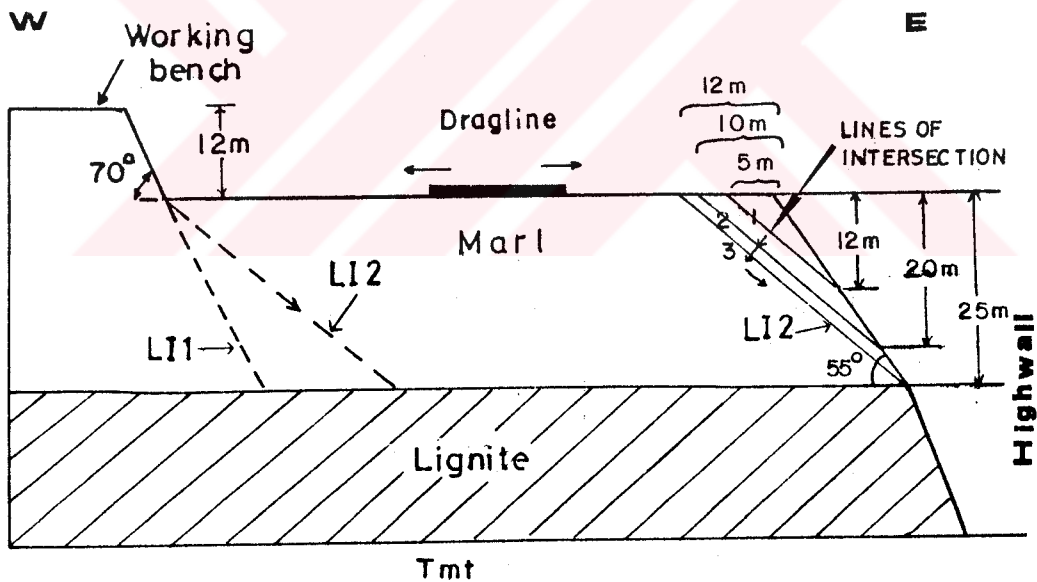
The results of the analytical solutions for the wedges outlined in Table 14 are tabulated in Table 18. Major faults striking NW-SE and NE-SW intersect each other at the eastern boundary of the 21th slice and the line of intersection plunges 62° east (Figure 103a) The line of intersection, however, does not daylight on the wall face (Figure 103b; line LI1) and the wedge is stable in this case. However, if the dips of faults under consideration reduce to 50° due to local variations in their orientations, plunge of the line of intersection tends to be flatter approaching to 40° as shown by the line LI2 in Figure 103b. Even in this case the line of intersection will not be daylighted by the highwall slope. The width of the panel is 80 m and this geometrical configuration makes daylighting impossible. As a conclusion, this wedge cannot be activated unless the current position of the slices are changed. On the contrary, if the slice boundaries are shifted 5 to 10 m toward east, the line of intersection may appear on the next highwall face, as demonstrated in Figure 103 b, and then the factor of safety falls below unity (Table 18a).

Wedges involving faults and joints ($I_{f1,j2}$, $I_{f2,j3}$) may develop critical conditions if the joint sets are continuous throughout the overburden even if no water pressure develops. Turning to persistence of joints in the overburden, the possibility of occurrence of these wedges seems to be minimum. However, surcharge effect of temporary

a) Sketch showing the intersection point of faults and position of slices



b) Section A A' and position of lines of intersection



LI1: Lines of intersection of faults determined from stereo-projection
 ($\hat{I}_{r12} = 62^\circ / 084$)

LI2: Line of intersection of faults if their clips are 50°

1,2,3: Lines of intersections if they appear near highwall crest

Figure 103: Plan and section views of wedge problem and most critical wedge occurrences along highwalls at design sector VIII.

Table 18 : Limiting equilibrium analysis of wedge failures-Design Sector VIII

Type of slope	Slope angle (°)	Height of slope	Height of wedge H (m)	Tension crack position AT (m)	Water condition	External loading	Factor of Safety F
a) $I_{f1,2} = 40/084^*$ (Figure 76 h.1) slices oriented in the N-S direction							
Highwall	55°	25	25	None	Dry	None	0.876
Highwall	55°	25	20	None	Dry	None	0.985
Highwall	55°	25	12	None	Dry	None	1.348
Working bench	70°	12	12	None	Dry	None	0.967
	70°	12	12	10	Dry	None	0.954
b) $I_{f1,j2} = 40/110$ (Figure 76h.1), slices oriented in the N-S direction							
Highwall	55°	25	25	None	Dry	None	0.609
Highwall	55°	25	20	None	Dry	None	0.93
Highwall	55°	25	12	None	Dry	None	1.998
Working bench	70°	12	12	None	Dry	None	0.863
c) $I_{f2,j3} = 43/200$ (Figure 76h.2), slices oriented in the E-W direction							
Highwall	55°	25	25	None	Dry	None	0.798
Highwall	55°	25	20	None	Dry	None	1.166
Highwall	55°	25	12	None	Dry	None	2.393
Highwall	60°	25	25	None	Dry	None	0.5
Highwall	60°	25	20	None	Dry	None	0.794
Highwall	60°	25	12	None	Dry	None	1.771
Working bench	70°	12	12	None	Dry	None	1.08
	70°	12	8	None	Dry	None	1.956
"	70°	12	4	None	Dry	None	4.586

* Orientation of faults is not taken as in Figure 76.h1. Their dip is assumed as 50°, then resulting line of intersection is employed in the analyses.

piles dumped near the crest of the slope should be considered.

10.7.3. Design Sector IX

Possible wedges involving faults and joints (Figure 76i) were treated analytically for two possible highwall orientations. Because of the close agreement between the plunges of lines of intersection and wall inclination, majority of the cases yielded considerably high factor of safety (Table 19). Sensitivity analyses indicate that where joints are continuous, tension cracks are filled with water, slope angles reach to 60° , and the overburden thickness approaches 25 m shallow seated wedge failures may occur.

Due to the shallow seated wedges involving tension cracks located 3 to 4 m behind the crest and also considering the possible position of the dragline, loading of the dragline was not taken into account in the analyses. On the other hand, on the basis of factor of safety calculated, wedge failure seems to be more critical along the walls oriented in the E-W direction than the walls running in the N-S direction.

Table 19 : Limiting equilibrium analysis of wedge failures-Design Sector IX

Type of slope	Slope angle	Height of slope	Height of wedge	Tension crack position AT	Water condition	External loading	Factor of Safety F
	(°)	(m)	H (m)	(m)			
a) $I_{f1,j2} = 52/110$ (Figure 76i.1), slices oriented in the N-S direction							
Highwall	55°	25	25	None	Dry	None	1.709
Highwall	55°	25	20	None	Dry	None	1.928
Highwall	55°	25	12	None	Dry	None	2.657
Highwall	55°	25	25	2	Dry	None	1.677
Highwall	55°	25	20	2	Dry	None	1.896
Highwall	55°	25	12	2	Dry	None	2.646
Highwall	55°	25	25	2	W. pressure	None	1.076
Highwall	55°	25	20	2	W. pressure	None	1.390
Highwall	55°	25	12	2	W. pressure	None	2.445
Highwall	60°	25	25	None	Dry	None	1.613
Highwall	60°	25	20	None	Dry	None	1.808
Highwall	60°	25	12	None	Dry	None	2.457
Highwall	60°	25	25	3	Dry	None	1.574
Highwall	60°	25	20	3	Dry	None	1.765
Highwall	60°	25	12	3	Dry	None	2.443
Highwall	60°	25	25	3	W. pressure	None	0.797
Highwall	60°	25	20	3	W. pressure	None	1.102
Highwall	60°	25	12	3	W. pressure	None	2.131
Working bench	70°	12	12	None	Dry	None	1.632
"	70°	12	12	3	Dry	None	1.563
"	70°	12	12	None	Dry	None	1.982
"	70°	12	12	None	Dry	None	3.110
"	70°	12	12	None	W. pressure	None	1.320
b) $I_{f1,j3} = 52/198$ (Figure 76i.2), slices oriented in the E-W direction							
Highwall	55°	25	25	None	Dry	None	2.039
Highwall	55°	25	20	None	Dry	None	2.554
Highwall	55°	25	12	None	Dry	None	4.272
Highwall	55°	25	25	1	Dry	None	2.034
Highwall	55°	25	20	1	Dry	None	2.550
Highwall	55°	25	12	1	Dry	None	4.271
Highwall	55°	25	25	1	W. pressure	None	1.948
Highwall	55°	25	20	1	W. pressure	None	2.477
Highwall	55°	25	12	1	W. pressure	None	4.237
Highwall	60°	25	25	None	Dry	None	0.901
Highwall	60°	25	20	None	Dry	None	1.13
Highwall	60°	25	12	None	Dry	None	1.902
Highwall	60°	25	25	3	Dry	None	0.89
Highwall	60°	25	20	3	Dry	None	1.122
Highwall	60°	25	12	3	Dry	None	1.894
Highwall	60°	25	25	3	W. pressure	None	0.737
Highwall	60°	25	20	3	W. pressure	None	0.975
Highwall	60°	25	12	3	W. pressure	None	1.773
Working bench	70°	12	12	None	Dry	None	0.812
"	70°	12	8	None	Dry	None	1.229
"	70°	12	4	None	Dry	None	2.48
"	70°	12	12	2	Dry	None	0.785
"	70°	12	8	1	Dry	None	1.185
"	70°	12	4	2	W. pressure	None	0.627

CHAPTER 11

CONCLUSIONS AND RECOMMENDATIONS

Based on the results of geological, geotechnical and hydrogeological investigations, back analyses and design considerations following conclusions can be derived for the Eskihisar strip coal mine :

1. An integrated approach was developed for stability analysis and design of slopes.
2. The relationship between the orientation of structural pattern and configuration of slopes in different parts of the open pit plays a major role on the stability of slopes.
3. The coal seam acts as the principal aquifer. The drawdown pattern directed towards compact marl/coal seam boundary indicate a steady seepage condition, which is considered in the stability analyses.
4. Direct recharge through moderately spaced joints in the carbonate and clay rich overburden rocks has considerable adverse effects on the discontinuity shear strength parameters. This effect may locally be important even when the slope is dry.
5. On the basis of normal stress levels anticipated in the pit, use of shear strength parameters derived from linear Coulomb relationship for the design of slopes will not cause any noticeable departure from in-situ conditions.
6. The shear strength of the basal failure plane, that is the weak black clay bed appearing along the basin margins, is significantly important in determining overall stability of sidewalls than the strength of bedding planes in the hangingwall.

7. The Hoek - Brown empirical strength criterion in conjunction with rock mass classification offers an alternative means of estimating rock mass strength from the examination of borehole cores and surface exposures, coupled with simple field or laboratory tests. If the assessments are based on the correct measurements a close agreement between the analysis and existing stability conditions can be achieved.
8. Majority of ratings derived from Bieniawski's (1989) RMR system and modified RMR system for stratified and clay bearing rock masses proposed by Ünal and Özkan (1990) show close agreement. However, below the rating value of 40 modified values show noticeable variation and wider band of RMR values. Modified RMR system seems as a better tool for describing the specifications of weak and very weak classes of stratified and clay-bearing rock masses. But, in modified RMR system joint orientation index is lower and this parameter is not clearly defined in Bieniawski's system for slopes. Thus, joint orientation index proposed by Singh and Gahrooe (1989) provides better and more clear definition for slope stability evaluations.
9. As experienced in many strip coal mines in the different parts of the world, majority of the failures occurred in hangingwall and footwall materials at Eskihisar open pit can be explained by the modes of multiplanar and plane shear failures. However, retrogressive mass failures developing along circular slip surfaces are valid for the soil materials encountered in the pit.
10. In multiplanar failure mode, which controls the stability around the faulted blocks, faults cut by parallel or oblique slopes act as rear release

surfaces and failure occurs along the fault and adversely dipping bedding planes resulting in discrete block. The zone of failure may extend for a considerable horizontal distance back from the toe, depending on the inclination of basal bedding plane and the distance between the fault and the toe.

11. In the case of multiplanar failure the stability is sensitive to changes in the length of the lower part of the basal sliding surface, toe configuration, and shear strength.
12. In order to improve the overall stability against multiplanar failure, leaving more buttress of unblasted rock resulting in an increase in the length of gently or horizontally dipping portion of the sliding surface is the better remedial measure than slope flattening.
13. Residual shear strength in terms of conventional linear relationship is more representative for various types of smooth-planar and clay coated discontinuities and soil materials than their peak strength for designing of slopes at Eskihisar open pit. This result supports the argument that residual shear strengths may be used when high clay material is involved in a slope stability study. It may also be concluded that laboratory derived shear strength parameters of similar materials can be considered as a first approximation for the preliminary or prefeasibility stage of open pit coal mine design.
14. Temporary spoil piling near the crest of highwalls may contribute to development of a complex, shallow seated but controllable failures which occur with

the combination of failure along discontinuities and through the rock mass.

15. From the stability point of view, there is no reason to change the bench height, which were fixed as 10 m or 14 m in the overburden. But, due to retrogressive nature of the failure experienced in the transition zone, bench heights should not exceed 7 m.
16. Designing the slopes within weak rocks and soils lacking adverse structural features with an overall slope angle of 45° , as conventionally preferred for most mine slopes in Turkish mines, may drastically result in mass failures. The stability assessments suggest that in such materials sidewall slopes are marginally stable against circular failures for factor of safety of 1.3 if the designing of the slopes is based on the stability conditions of dominant rock type.
17. In order to minimize excavation and to provide steep slopes, it was hoped to cut the rock at sidewalls in both west and east at about 35° . However, as a result of sensitivity analyses a maximum overall slope angle ranging between 30 to 32° seems more suitable.
18. The results of stability analysis indicate that there is no reason to change the highwall geometry currently practiced in the pit. It should also be emphasized that existing N-S oriented slices provide adequate stability conditions. On the contrary, if their directions are changed to E-W, considerable decrease in the stability resulting in multiplanar shear failure will be possible.

19. Possible wedges are limited to benches and highwalls only. These are small-scale shallow seated wedges developing by the combination of faults and joints. However, on the basis of persistence data of joints and in-situ observations, the possibility of wedge failures is low, but a few controllable wedges can be expected if the walls are designed parallel to E-W direction after heavy precipitation resulting in hydrostatic pressure built-up.

20. In this study, similar failure modes and material behaviours, as reported for open pit coal mines abroad, were examined. On the other hand, the study emphasizingly indicated that the initial design by TKI should be revised to improve the stability for further development of the pit.

For future researches and safe mining operations in the Eskihisar strip coal mine the following recommendations can be made :

1. Higher normal loads than anticipated in-situ, which cause greater damage on discontinuity surfaces particularly in weak and clay bearing rocks, result in lower determined internal friction angle and conservative design. For this reason to achieve the requirements of ISRM's test procedure using the shear box developed for soil testing having strain control facility and residual measurements even under lowest normal loads are recommended.
2. Modified RMR system, with some modifications required for slopes, seems to be reliable and descriptive for weak stratified rocks. Similar studies may also be conducted in open pit mine slopes constructed in clay-bearing, and stratified

weak rocks. These studies may lead to more generalized results about the applicability of this classification to slope stability problems experienced in weak or very weak rock masses.

3. Paying close attention to probable departures from anticipated conditions during the advancement of the pit and uncertainties from seismic risk, on the basis of worldwide experiences, it is recommended that for designing marginally stable slopes at Eskihisar open pit, factors of safety ranging between 1.3 and 1.5 should be selected depending on the importance of the slope under consideration. For the purpose, the graphs given for the variations in factor of safety with various design parameters should be employed.
4. Considering the long-term service life of the state highway, initial toe configuration of the southeast sidewalls should be shifted a few ten meters forward, to north. In addition, the void resulted from the previous strip should be filled as soon as possible.
5. In order to improve highwall stability, orientation of slices in the N-S direction should not be changed. However, the last stage of stripping, which involves removal of twentysixth slice in the west, will result in a very long and unsupported excavation along the west sidewall where weak basal plane will expose. For this reason, it is recommended as a remedial measure that stripping may be carried out by operating dragline to the end of twentyfourth slice in the N-S direction and then the overburden between the west sidewall and the unexcavated last two slices may be removed by excavators operating in the E-W direction with the

construction of small benches. This application will result in a narrow unsupported excavation, which can be filled as soon as possible, and provides the control of sidewall stability. This procedure is also suggested for east sidewalls in the northeast.

6. Operating distance of the dragline to highwall crest should not exceed 12 m.
7. Preventing infiltration by installing sealed interception ditches behind the slope crest and back filling of the tension cracks are recommended where possible.
8. For seismic design decisions peak horizontal ground accelerations caused by blasting should be determined through suitably located seismographs.
9. Construction of convex slopes should be avoided.
10. Some of the future observations needed to improve knowledge and increase in mining efficiency should include the followings:
 - a. Geological and geotechnical development work should be continued, particularly for the west and east sidewalls along the basin margins by drilling closely spaced and fully cored boreholes planned along the lines vertical to sidewalls.
 - b. Additional studies for groundwater level monitoring in virgin areas and around major faults should be planned.
 - c. Instabilities should be monitored employing available equipment to provide valuable

information for further design requirement or revisions and remedial measures.

- d. A database compiling past and future instabilities, which is an important deficiency in most mines, should be prepared.



REFERENCES

- Abdallah, T. and Helal, H., 1990, Risk evaluation of rock mass sliding in El-Deir El-Bahary Valley, Luxor, Egypt, Bull. Engineering Geology, No. 42, pp. 3-9.
- Abdüsselamoğlu. Ş., 1965, Muğla-Yatağan Çevresinde Görülen Jeolojik Formasyonların Korelasyonları Hakkında Rapor, Unpublished report, MTA archive no. 3497, 33 p.
- A.S.T.M (American Society For Testing and Materials), 1985, Annual Book of ASTM Standarts-Soil and Rock, Building Stones, Section-4, Construction, V. 04.08, ASTM Publication, 972 p.
- Atalay, Z., 1980, Muğla-Yatağan ve yakın dolay karasal Neojenin stratigrafi araştırması, TJK Bülteni, C. 23, No. 1, pp. 93-99.
- Attewell. P.B. and Farmer, I.W., 1982, Principles of Engineering Geology, Chapman and Hall, London, 1045 p.
- Ayday, C., 1989, Statistical analysis of discontinuity parameters of Gölbaşı (Ankara) andesites, Süpren (Eskişehir) marble, and Porsuk Dam (Eskişehir) peridotite, Unpublished Ph.D. Thesis, Middle East Tech. Univ., Geological Engng. Dept., 186 p.
- Barton, N., 1973, Review of a new shear strength criterion for rock joints, Engineering Geology, 7, pp. 287-332.
- Barton, N., 1976, The shear strength of rock and joints, Int. J. Rock Mech. and Geomech. Abstr., V. 13, pp. 255-279.

Barton, N., Lien, R. and Lunde, J., 1974, Engineering classification of rock masses for the design of tunnel support, *Rock Mechanics*, Vol. 6, No. 4, pp. 183-236.

Barton, N. and Choubey, V., 1977, The shear strength of rock joints in theory and practice, *Rock Mechanics*, Vol. 10, pp. 1-54.

Becker - Platen, J.D., 1970, Lithostratigraphische untersuchungen'in Känozoikum Sudwest-Anatoliens (Turkei), *Beih. Geol. Jb.*, 97, 244 p.

Bell, F.G., 1981, *Foundation Engineering in Difficult Ground*, Butterworths Comp., pp. 498-510.

Benda, L., 1967, Yatağan-Eskihisar (Muğla) bölgesinin linyit etüdü, Unpublished report, MTA archive no. 6042, 5 p.

Bieniawski, Z.T., 1973, Engineering classification of jointed rock masses, *Trans. S. Afr. Int. Civ. Eng.*, Vol. 15, pp. 335-344.

Bieniawski, Z.T., 1984, *Rock Mechanics Design in Mining and Tunneling*, A. A. Balkema, Rotterdam, 272 p.

Bieniawski, Z.T., 1989, *Engineering Rock Mass Classification*, Mc Graw Hill, New York, 237 p.

Bishop, A.W., 1955, The use of the slip circle in the stability analysis of slopes, *Geotechnique*, 5, pp.7-17.

Broch, E. and Franklin, J.A., 1972, The point-load strength test, *Int. J. Rock Mech. Min. Sci.*, 9, pp. 669-697.

B.S.I. (British Standards Institution), 1975, *Methods of Test for Soils for Civil Engineering Purposes- BS 1377*, British Standards Institution, 147 p.

- B.S.I. (British Standards Institution), 1981, Code of Practice for Site Investigations-BS 5930, British Standards Institution, 147 p.
- Call, R.D., 1982, Monitoring pit slope behaviour, Third Int. Conf. on Stability in Surface Mining , Vancouver, Canada, V.3, pp. 229-248.
- Canik, B., 1975, Yatağan (Muğla) linyit sahasının hidrojeoloji etüdü, Unpublished report, MTA archive no. 5449, 11 p.
- Carter, M. and Bentley, S.P., 1985, The geometry of slip surfaces beneath landslides: predictions from surface measurements, Can. Geotech. J., 22, pp. 234-238.
- Cassagrande, A., 1948, Classification and identification of soils, Trans. ASCE, 113, pp. 901-992.
- Cavounidis, S. and Sotiropoulos, E., 1979, Strain softening marly rock, Fourth Int. Congress on Rock Mechanics, Montreux, Switzerland-1979, A. A. Balkema, Rotterdam, V. 2, pp. 63-66.
- Chandler, R.J., 1977, Back analysis techniques for slope stabilization works: a case record, Geotechnique, 27, No. 4, pp. 479-495.
- Chowdhury, R.N., 1978, Slope Analysis, Elsevier Sci. Pub. Comp., Amsterdam, 423 p.
- Chugh, Y.P., 1980, Surface mining of minerals by draglines in the U.S.A., Inst. Min. Metall. , Sec. A, Min. Industry, pp. 198-204.

Coates, D.F., 1964, Classification of rocks for rock mechanics, Int. J. Rock Mech. Min. Sci., V. 1, No. 3, pp. 421-429.

Darton Software, 1987, SPLIT for the analysis of structural data-User's Manual, Darton Software, Rapid City, U.S.A., 34 p.

Davis, J.C., 1973, Statistics and Data Analysis in Geology, John Wiley and Sons, New York, pp. 237-242.

Deen, R.C., Hopkins, C.T. and Allen, D.L., 1977, Some uncertainties of slope stability analyses, Transportation Res. Record, No. 640, pp. 7-13.

Deere, D.U. and Miller, R.P., 1966, Engineering classification and index properties for intact rock, Tech. Rept. No. AFWL-TR-65-116, Air Force Weapons Lab., Kirtland Air Force Base, New Mexico, 308 p.

Demirok, Y., 1978, Muğla-Yatağan Linyit Sahaları Jeoloji ve Rezerv Ön Raporu, Unpublished report, MTA archive no. 6234, 17 p.

Engin, O., 1965, Muğla-Yatağan-Eskihisar Kömür Zuhurlarının Prospeksiyonu, Unpublished MTA report, 5 p.

Englund, E. and Sparks, A., 1988, GEO-EAS (Geostatistical Environmental Assessment Software) User's Guide, Environmental Monitoring Systems Laboratory, Office of Research and Development, U.S. Environmental Protection Agency, Nevada, 194 p.

Ercan, T., Günay, E. and Türkecan, A., 1984, Bodrum Yarımadasındaki mağmatik kayaların petrolojisi ve kökensel yorumu, TJK Bülteni, C. 27, No. 2, pp. 85-98.

Erdik, M., Doyuran, V., Gülkan, P. and Akkaş, N., 1985, Türkiye'de deprem tehlikesinin istatistiki açıdan değerlendirilmesi, ODTÜ Deprem Mühendisliği Araştırma Merkezi, Ankara, 116 p.

Ersoy, R., 1957, Yatağan Ovası Hidrojeoloji Raporu, Unpublished report, MTA archive no. 2738, 11p.

Fazio, A.L. and Tommasi, P., 1990, Sheared bedding joints in rock engineering: Two case histories in Italy, Proc. of the Int. Symp. on Rock Joints, Leon, Norway, 4-6 June 1990, Balkema, Rotterdam, pp. 83-90.

Franklin, J.A., 1977, The monitoring of structures in rock, Int. J. Rock Mech. Min. Sci. and Geomech. Abstr., V. 14, p. 163-192.

Franklin, J.A. and Chandra, R., 1972, The slake durability test, Int. J. Rock Mech. Min. Sci. and Geomech. Abstr., V. 9, pp. 325-341.

Franklin, J.A., Broch, E. and Walton, G., 1971, Logging the mechanical character of rock, Inst. Min. Metall., 80, pp. A1-A9.

Geological Society of America, 1963, Rock-color chart.

Geological Society of London: Engineering Group Working Party, 1970, The logging of rock cores for engineering purposes. Q.J. Eng. Geol., V. 3, No. 1, pp. 1-24.

Geological Society of London: Engineering Group Working Party, 1972, The preparation of maps and plans in terms of engineering geology, Q.J. Eng. Geol., V. 5, No. 4, pp. 295-381.

- Geological Society of London: Engineering Group Working Party, 1977, The description of rock masses for engineering purposes, Q.J. Eng. Geol., V.10, pp.355-388.
- Gillette, D.R., Strue, S., Ko, H.Y., Gould, M.C. and Scott, G.A., 1983, Dynamic behaviour of rock joints, 24th U.S. Symposium on Rock Mechanics, Texas, pp. 163-179.
- Golden Software, Inc., 1986, GRAPHER CSM User's Guide, Golden Software, Inc., U.S.A., 24 p.
- Goodman, R.E., 1976, Methods of Geological Engineering, West Publishing Comp., New York, 472 p.
- Goodman, R.E., 1980, Introduction to Rock Mechanics, John Wiley and Sons, New York, pp. 254-285.
- Gökçen, N., 1982, Denizli ve Muğla çevresi Neojen istifinin Ostrakod biyostratigrafisi, Yerbilimleri, 9, pp. 111-131.
- Gökmen, V., 1975, Muğla-Yatağan-Eskihisar Kömür Yatağı Fizibilite Raporu, Cilt 1: Jeoloji, Unpublished MTA report, 37 p.
- Göktaş, F., 1989, (MTA Aegean Regional Directority-Personnal communication).
- Grim, R.E., 1962, Applied Clay Mineralogy, Mc Graw Hill Book Comp., Inc., New York, 422 p.
- Hanna, T.H., 1985, Field Instrumentation in Geotechnical Engineering, Trans Tech Publication, 842 p.
- Has, F., Gürsoytrak, E., Tokan, A., and Bakkaloğlu, A., 1975, Muğla-Yatağan-Eskihisar Kömür Yatağı Fizibilite Araştırması-Cilt 2:Rezerv, Unpublished MTA Report, 87p.

- Hassani, F.P. and Scoibe, M.J., 1982, Properties of weak rocks, with special reference to the shear strength of their discontinuities encountered in British surface coal mining, The Aus. I.M.M. Central Queensland Branch Symp. On Strip Mining-45 m and beyond.
- Hawkins, A.B. and Privett, K.D., 1985, Measurements and use of shear strength of cohesive soils, Ground Engineering, V. 18, pp. 22-29.
- Hawley, P.M., Martin, D.C. and Acott, C.P., 1986, Failure mechanism and design considerations for footwall slopes, CIM Bulletin, 79, pp. 47-53.
- Hencher, S.R., 1981, Friction parameters of design of rock slopes to withstand earthquake loading, Proc. Conf. on Dams and Earthquakes, London, Inst. Civil Engineers, pp. 79-88.
- Hencher, S.R. and Richards, L.R., 1989, Laboratory direct shear testing of rock discontinuities, Ground Engineering, V. 22, pp. 24-31.
- Herget, G., 1981, Pit Slope Manual, Chapter 2, Structural Geology, CANMET, CANMET Report No. 17-41, 123 p.
- Hocking, G., 1976, A method for distinguishing between single and double plane sliding of tetrahedral wedges, Int. J. Rock Mech. Min. Sci. and Geomech. Abstr., V. 13, pp. 225-226.
- Hoek, E., 1971, Influence of rock structure on the stability of rock slopes, Proc., 1st Int. Conf. on Stability of Open Pit Mining, The American Inst. Min. Metall. and Petr. Engrs., Inc., New York, pp. 49-63.

Hoek, E., 1982, Analysis of slope stability in very heavily jointed or weathered rock masses, Third Int. Conf. on Stability in Surface Mining, Vancouver, Canada, V. 3, pp. 375-406.

Hoek, E., 1983, Strength of jointed rock masses, Geotechnique, 33, pp. 187-223.

Hoek, E., 1990, Estimating Mohr - Coulomb friction and cohesion values from Hoek-Brown failure criterion, Int. J. Rock Mech. Min. Sci. and Geomech. Abstr., V. 27, No. 3, pp. 227-229.

Hoek, E. and Bray, J.W., 1977, Rock Slope Engineering, Institution of Mining and Metallurgy, Stephen Austin and Sons Ltd., London, 402 p.

Hoek, E. and Brown, E.T., 1980 (a), Underground Excavations in Rock, Institution of Mining and Metallurgy, Stephen Austin and Sons Ltd., London 527 p.

Hoek, E. and Brown, E.T., 1980 (b), Empirical strength criterion for rock masses, J. Geotech. Engg. Div. ASCE, 106, pp. 1013-1035.

Hoek, E. and Brown, E.T., 1988, The Hoek-Brown failure criterion- a 1988 update, Proc. 15th Canadian Rock Mech. Symp., Univ. of Toronto, pp. 31-38.

Huang, Y.H., 1983, Stability Analysis of Earth Slopes, Van Nostrand Reinhold Comp., New York, 305 p.

Hutchinson, J.N., 1983, Methods of locating slip surfaces in landslides, Bull. Assoc. Engng. Geol., V. 20, No. 3, pp. 235-252.

Hutchinson, J.N., Somerville, S.H. and Petley, D.J., 1973, A landslide in periglacially disturbed Etruria Marl at Burry Hill, Staffordshire, Quart. J. Engng. Geol., V. 6, pp. 377-404.

I.S.R.M. (International Society for Rock Mechanics), 1981, Rock Characterization, Testing and Monitoring-ISRM Suggested Methods, Pergamon Press, Oxford, Brown, E.T. (ed.), 211p.

Jaworski, W.E. and Zook, R.L., 1979, Considerations in the stability analyses of highwalls in Tertiary rocks, Proc. 1st Int. Symp. on Stability in Coal Mining, Vancouver, 1978, pp. 46-64.

Jaeger, J.C., 1970, The behaviour of closely jointed rock, Proc. 11th Symp. on Rock Mech., Berkeley, pp. 57-68.

Jaeger, J.C., 1971, Friction of rocks and stability of rock slopes, Geotechnique, V. 21, No. 2, pp. 97-134.

Jennings, J.E., Brink, A.B.A. and Williams A.A.B., 1973, Revised guide to soil profiling, Trans. S. African Instn. Civil Engrs., V. 15, No. 1, pp. 3-12.

Jeran, P.W. and Mashey, J.R., 1970, A computer program for the stereographic analysis of coal fractures and cleats, U.S.B.M. Inf. Circular 8454, 34 p.

Jumikis, A. R., 1967, Introduction to Soil Mechanics, Van Nostrand Comp. Inc., 436p.

Kasap, A. and Ünal, D., 1987(a), Muğla-Yatağan-Eskihisar Linyit Sektörü 1986 Yılı çalışma Raporu, Unpublished report, MTA archive no. 8327, 5 p.

Kasap, A. and Ünal, D., 1987^(b), Muğla-Yatağan-Eskihisar Linyit Sektörü 1987 Yılı çalışma Raporu, Unpublished report, MTA archive no. 8329, 6 p.

Kezdi, A., 1974, Handbook of Soil mechanics-Soil Physics, Elsevier Scientific Publishing Company, Amsterdam, 294 p.

Khan, F. Z. and Nikols, D., 1989, Toe buttressing procedure to stabilize dragline stripping operations, CIM Bulletin, V. 82, No. 925, pp. 37-47.

Koçak, Ç., Ergüder, I. and Kızıldağ, I., 1991, G.E.L.İ. Yatağan-Eskihisar Ocağı Yeraltısuyu Jeofizik-Rezistivite Etüdü, Unpublished T.K.İ. Report, 5 p.

Lambe, T.W. and Whitman, R.V., 1969, Soil Mechanics, John Wiley and Sons, New York, 533 p.

Leonards, G.A., 1962, Foundation Engineering, Mc Graw Hill Book Comp., Tokyo, 1136 p.

Lupini, J.F., Skinner, A.E. and Vaughan, P.R., 1981, The drained residual shear strength of cohesive soils, Geotechnique, 31, pp. 181-213.

Major, G., Kim, H.S. and Ross-Brown, D., 1977, Pit Slope Manual, Supplement 5.1-Plane Shear Analysis, CANMET, CANMET Report 77-16, Canada, 307 p.

Means, R.E. and Parcher, J.W., 1963, Physical Properties of Soils, Charles E. Merrill Publishing Comp., Columbia, Ohio, 467 p.

Miller V.J., 1982, The northeast tripp slide-a 11.7 million cubic meter wedge failure at Kennecott's Nevada Mine Division, Canada, V. 3, pp.725-743.

Mitchell, J.K., 1975, Fundamentals of Soil Behaviour, John Wiley and Sons, New York, 422 p.

Munn, F.J., 1985, Coping with fall failures, CIM Bulletin, 78, pp. 59-62.

Newcomen, H.W. and Martin, C. D., 1988, Geotechnical assessment of the southeast wall slope failure at Highmont Mine, British Columbia, CIM Bulletin, V. 81, No. 917, pp. 71-76.

Özgenoğlu, A., 1990, In-situ shear testing of blasted rock mass associated with a slope stability analysis, Proc. Int. Conf. on Mech. of Jointed and Faulted Rock, Tech. Univ. of Vien, 18-20 April, 1990, pp. 365-370.

Papaliangas, T., Lumsden, A.C., Hencher, S.R. and Manolopoulou, S., 1990, Shear strength of modelled filled rock joints, Proc. of the Int. Symp. o Rock Joints, Loen, Norway, 4-6 June 1990, Balkema, Rotterdam, pp. 275-282.

Paşamehmetoğlu, A.G., Karpuz, C., Müftüoğlu, Y., Özgenoğlu, A., Bilgin, A., Ceylanoğlu, A., Bozdağ, T., Toper, Z. and Dinçer, T., 1988, TKİ Dekapaj İhale Panoları İçin Makina Parkı Seçimi, Maliyet Analizi ve Birim Maliyetin Saptanması, Cilt:2, Müesseselere Ait Jeoteknik ve Performans Bilgileri, O.D.T.ü. Maden Müh. Böl., Ankara, Unpublished report, pp. 89-97.

Piteau, D.R., 1973, Characterizing and extrapolating rock joint properties in engineering practice, Rock Mechanics, Suppl. 2, pp. 5-31.

Piteau, D.R. and Martin, D.C., 1982, Mechanics of rock slope failure, Third Int. Conf. on Stability in Surface Mining, Vancouver, Canada, V. 3, pp. 113-169.

- Platen, B. and Bering, A., 1966, Yatağan (Muğla) Sahasının Linyit Etüdü, Unpublished report, MTA archive no. 5995, 13 p.
- Priest, S.D. and Hudson, J. A., 1976, Discontinuity spacing in rock, *Int. J. Rock Mech. Min. Sci. and Geomech. Abstr.*, V.13 , pp. 135-148.
- Priest, S.D. and Brown, E.T., 1983, Probabilistic stability analysis of variable rock slopes, *Trans. Inst. Min. Metall.*, 92, pp. A1-A12.
- Rosenbaum, M.S. and Jarvis, J., 1985, Probabilistic slope stability analysis using a microcomputer, *Q.J. Eng. Geol.*, V. 18, No. 4, pp. 353-356.
- Richards, B.G., Coulthard, M.A and Toh, C.T., 1981, Analysis of slope stability at Goonyella Mine, *Can. Geotech. J.*, 18, pp. 179-194.
- Sancio, R.T. , 1981, The use of back-calculations to obtain the shear and tensile strength of weathered rocks, *Proc. Int. Symp. on Weak Rocks, Tokyo, 21-24 Sept. 1981*, V. 2, pp. 647-652.
- Schneider, H.J., 1978, The laboratory direct shear test-an analysis and geotechnical evaluation, *Bull. Int. Assoc. Engng. Geology* , 18, pp. 121-126.
- Sharp, J.C., Ley, G.M.M. and Sage, R., 1977, Pit slope Manual, Chapter 4: Groundwater, CANMET, CANMET Report 77-13, Canada, 240 p.
- Singh, R.N. and Gahrooee, D.R., 1989, Application of rock mass weakening coefficient for stability assessment of slopes in heavily jointed rock masses, *Int. J. Surface Mining*, 3, pp. 207-219.

- Skempton, A.W., 1953, The colloidal activity of clays, Proc. 3rd Int. Conf. Soil Mech. Found. Eng., Switzerland, V. 1, p. 57.
- Skempton, A.W., 1964, Long term stability of clay slopes: Fourth Rankie Lecture, Geotechnique, V. 14, No. 2, pp. 75-102.
- Skempton, A.W., 1985, Residual strength of clays in landslides, folded strata and the laboratory, Geotechnique, V. 35, No. 1, pp. 3-18.
- Smith, G.N., 1974, Elements of Soil Mechanics for Civil and Mining Engineers, Crosby Lockwood Staples, London, pp. 141-144.
- Stead, D., 1990, The back analysis of rock slope failures in U.K. surface coal mining practice, Int. Symp. on Mine Planning and Equipment Selection, Balkema, Rotterdam, pp. 343-352.
- Stapledon, D.H., 1968, Discussion of paper "classification of rock substances" by D.F. Coates, Int. J. Rock Mech. Min. Sci., V. 5, No. 4, pp. 371-373.
- Stimpson, B., 1979, Simple equations for determining the factor of safety of a planar wedge under various groundwater conditions. Q.J. Engng. Geol., V. 12, pp. 3-7.
- Şen, Z. and Kazı, A., 1984, Discontinuity spacing and RQD estimates from finite length scanlines, Int. J. Rock Mech. Min. Sci. and Geomech. Abstr., V.21, pp. 203-212.
- Townsend, F.C. and Gilbert, P.A., 1973, Test on measure residual shear strength of some clay shales, Geotechnique, 23, No. 2, pp. 267-271.

Udd, J.E. and Pakalnis, R., 1979, Determination of a friction angle for an alkaline igneous rock, CIM Bulletin, V. 76, No. 809, pp. 86-90.

Udd, J.E. and Betournay, M.C., 1983, Slope stability in the Trenton limestone of a Montreal area quarry, CIM Bulletin, V. 76, NO, 856, pp. 72-78.

U.S.B.R. (United States Dept. of Interior Bureau of Reclamation), 1974, Earth Manual, A Water Resources Technical Publication, Denver, 810 p.

Ünal, E. and Özkan, I., 1990, Determination of clasifiction parameters for clay-bearing and stratified rock mass, 9th Int. Conf. on Ground Control in Mining, West Virginia Univ., 4-6 June 1990, Peng S.S. (ed.), pp.250-259.

Van Der Merwe, D.H., 1964, The prediction of heave from plasticity index and percentage clay fraction of soils, S. African Civil Engr., 6, pp. 103-107.

Walton, G. and Atkinson, T., 1978, Some geotechnical considerations in the planning of surface coal mines, Trans. Int. Min. Metall., Section A, 87, pp. A147-A171.

Wyllie, D.C. and Munn, F.J., 1979, The use of movement monitoring to minimize production losses due to pit slope failures, Proc. First Int. Symp, on Stabily in Coal Mining, Vancouver, 1978, pp. 75-94.

Yücelay, A, 1970, Muğla İli Yatağan-Eskihisar Civarındaki Kömürlü Sahanın Jeoloji Etüdü, Unpublished report, MTA archive no. 4436, 23 p.

APPENDIX A

Results of Petrographical-Mineralogical

And

X-Ray Diffraction Analyses

Table A.1: Results of petrographical-mineralogical analysis of rock samples taken from Eskihisar area

Field Sample No.	Petrographical description	Field Sample No.	Petrographical description	Petrographical description
PT1	Intra micrite (limestone)	PT48	Clayey micritic limestone	Calcarenite
PT2	Intra sparite (limestone)	PT49	Micrite (limestone)	Sandy limestone
PT3	Micro-zero crystalline limestone	PT50	Diatomite with calcite	"
PT4	Intra micrite (limestone)	PT51	Clayey micrite (limestone)	Intra biosparite (limestone)
PT5	Micritic limestone	PT52	"	Bio micrite (limestone)
PT6	Intra micrite (limestone)	PT53	Carbonated and clayey tuffite	Sandstone
PT7	Tuff	PT54	Micritic limestone	Sandstone (carbonate cemented)
PT9	Micritic limestone	PT55	Crystal tuff	Marl
PT10	"	PT56	Tuffite	"
PT11	"	PT57*	Sparitic limestone	Cryptocrystalline limestone
PT12	"	PT58*	Claystone	with microfossils
PT13	"	PT59*	Marl	Marly cryptocrystalline limestone "
PT14	"	PT60*	Sandy limestone	"
PT15	Marl	PT61*	Bio micrite	Macrocrystalline limestone
PT16	Micritic limestone		Schist	Serisite-graphite-biotite-quartz schist
PT17	Intra micrite (limestone)	PT62	Recrystallized limestone	Carbonated sandstone
PT18	Micritic limestone	PT63	Quartz-serisite marble	"
PT19	"	PT64	Muscovite-biotite-quartz schist	"
PT20	Biointrasparite (limestone)	PT65	Quartz-calc schist	"
PT21	Marble	JTS/LB21†	Limestone breccia	Clayey sandy limestone
PT22	Intra micritic sparite	JTS/LB28†	Cryptocrystalline limestone	Claystone
PT23	Biotite-muscovite-plagioclase schist		Calcarenite (sandstone)	
	Limestone conglomerate		Limestone with diatomite	
			Sandy limestone	

* Core samples from borehole JT1

x Core sample from borehole JT6

+ Core samples from borehole JT9

Table A.2: Results of X-ray diffraction analyses of soil samples taken from Eskihisar area

Specimen No.	Formation or lithological name	Minerals in the order of abundance
Z1 (LB1)	Fault gouge	Illite, a few amount of montmorillonite, kaolinite, calcite, quartz, aragonite, dolomite, cristobalite and very few alunite(?).
Z2 (LB6)	Fault gouge	Montmorillonite, illite, kaolinite, dolomite, aragonite, calcite, very few quartz and feldspar.
Z3 (LB20)	Fault gouge	Aragonite, a few illite, fewer calcite.
Z4	Fault gouge	Montmorillonite, kaolinite, illite, calcite and a few amount of quartz and aragonite and very few feldspar.
Z5 (LB12)	Fault gouge	Montmorillonite, kaolinite, illite, aragonite, calcite, quartz and very few feldspar.
Z6 (LB8)	Fault gouge	Illite, montmorillonite, fewer amount of kaolinite, dolomite, calcite, aragonite, quartz and very few feldspar.
Z7	Fault gouge	Montmorillonite, a few amount of illite, kaolinite, calcite and very few quartz.
Z10 (LB23)	Fault gouge	Illite, kaolinite, montmorillonite, quartz, fewer feldspar.
Z12 (LB35)	Fault gouge	Montmorillonite, a few amount of illite, kaolinite, quartz, and very few feldspar.
Z8 (LB21)	Tns ²	Illite, Ca-montmorillonite, kaolinite, fewer quartz and muscovite, very few feldspar.
LB26	Tns ²	Montmorillonite, illite, kaolinite, quartz, a few feldspar.
LB40	Tns ²	Montmorillonite, illite, kaolinite, a few amount of quartz and calcite, very few feldspar.
LB30	Tst	Kaolinite, illite, a few montmorillonite and quartz, very few feldspar.
LB44	Tst	Chlorite, illite, very few amount of montmorillonite, sepiolite, quartz, feldspar, calcite and dolomite.
LB48	Tst	Kaolinite, illite, very few montmorillonite and quartz.
LB50	Tst	Ca-montmorillonite, kaolinite, quartz, muscovite and very few feldspar.

Tns² : Fine grained soils of transition zone.

Tst : Fine grained soils of Turgut formation.

(Montmorillonites identified are mostly in the type of Na-Ca montmorillonite)



APPENDIX B

Rock And Soil Mechanics Laboratory

Test Results

Table B.1: Results of the Schmidt hammer tests on non-planar bedding surfaces developed in the limestone of detritic facies.

Test No.	Mean from 10 sets of readings	Unit weight (kN/m ³)	Joint roughness coefficient JRC
1	47.6	25.6	6-8
2	44.2	25.4	6-8
3	46.0	24.9	6-8
4	44.2	24.1	6-8
5	43.2	24.7	6-8
6	46.4	24.8	6-8
7	42.8	22.7	4-6
8	36.8	24.7	6-8
9	35.6	24.0	6-8
10	35.4	24.8	6-8
11	41.0	25.3	4-6
12	32.0	26.0	6-8
13	47.0	26.5	6-8

Table B.2.1: Summary of Atterberg Limit tests and grain size distribution analyses

Sample No.	Lithology or Formation	Grain size distribution				Moisture Content (w) (%)	Atterberg Limits			Unified Soil Classification Group Symbol
		Gravel (%)	Sand (%)	Silt (%)	Clay (%)		LL (%)	PL (%)	PI (%)	
LB1	Fault gouge	--	12	71	17	67	76	49	27	MH-OH
LB2	" "					44	62	38	24	MH-OH
LB6	" "	7	73	(20)*		--	Non-plastic			SM
LB7	" "					--	42	20	22	CL
LB8	" "	--	10	76	14	--	82	45	37	MH-OH
LB12	" "					51	87	28	59	CH
LB20	" "	9	72	(19)*		--	Non-plastic			SM
LB23	" "					8	70	31	39	CH
LB35	" "	--	15	74	11	76	106	51	55	MH-OH
LB36	" "					--	88	35	53	CH
Z7	" "					--	34	19	15	CL
Z4	" "					--	65	36	29	MH-OH
JT/Z1	Claystone					--	42	21	21	CL
JT2/2	"					--	58	32	26	MH-OH
JT8/2	"					--	60	34	26	MH-OH
LB30	Turgut formation	--	2	65	33	19	63	30	33	CH
LB31	" "					--	76	46	30	MH-OH
LB32	" "	--	73	24	3	--	Non-plastic			SM
LB44	" "	--	2	68	30	12	36	22	14	CL
LB46	" "					22	87	46	41	MH-OH
LB50	" "	--	7	53	40	--	82	30	52	CL
LB51	" "	23	69	(8)*		--	Non-plastic			SN-SM
LB21	Transition zone	--	15	75	10	21	59	37	22	MH-OH
LB22	" "	2	46	44	8	--	41	26	15	ML-CL
LB24	" "	--	65	35	5	--				SM
LB26	" "	--	19	75	6	6	54	31	23	MH-OH
LB27	" "	--	10	81	9	13	77	34	43	CH
LB39	" "	--	13	70	17	--	59	29	30	CH
LB40	" "	--	13	72	15	25	52	37	25	MH-OH
LB41	" "	1	59	35	5	--	Non-plastic			SM
LB42	" "	--	60	36	4	--	51	30	21	SC
LB43	" "	--	57	34	9	--				SM

* Percentage of fine grained material (silt and clay) are given together

* Claystone in the upper alternation of main Bekköy formation

Table B.2.2: Coefficient of uniformity and curvature for sand sized samples

Sample No.	D ₁₀ (mm)	D ₃₀ (mm)	D ₆₀ (mm)	C _u (mm)	C _c (mm)	Grading	Soil Material
LB6	0.004	0.16	0.61	152.5	10.5	Poorly graded	Fault material
LB20	0.01	0.175	0.61	61.0	5.0	" "	" "
LB32	0.012	0.067	0.15	12.5	2.5	Well graded	Turgut formation
LB51	0.075	0.22	0.5	6.7	1.3	" "	" "
LB24	0.0038	0.03	0.1	26.3	2.4	" "	Transition zone
LB41	0.0062	0.047	0.09	14.5	3.95	Poorly graded	" "
LB42	0.007	0.03	0.12	17.1	1.1	Well graded	" "
LB43	0.0025	0.025	0.11	44.0	2.3	" "	" "

W. B.
 Geological Engineering
 Department

Table B.3: Summary of slake durability test results of marl

Borehole No.	Sample No.	Interval (m)	Slake durability index (I_{d2}) (%)
JT2	20	22.65-23.35	96.69
JT3	3	5.3 - 5.7	93.30
JT3	22	33.65-33.90	93.80
JT7	3	22.30-22.80	89.75
JT9	39+40	92.85-93.65	94.24

Table B.4: Intact rock shear strength data obtained from triaxial tests

Borehole or block No.	Specimen No.	Stress at failure		Shear strength parameters		Rock unit
		Lateral σ_3 (Mpa)	Axial σ_1 (Mpa)	c (Mpa)	ϕ (degree)	
JT9	11	1	7.25	0.6	42	SANDSTONE, moderately weathered.
	12/1	2	10.09			
	12/2	3	12.03			
JT9	10/1	1	9.30	1.0	42	" "
	10/2	1.5	11.36			
	9	2	14.05			
JT9	13/1	1	8.97	0.9	42.5	" "
	13/2	1.5	11.48			
	13/3	2	14.04			
JT9	8/1	1	20.57	2.5	64	SANDSTONE, well cemented, unweathered.
	8/2	1.5	33.43			
	8/3	2	35.19			
LB34 (Block)	C7	1	29.79	4.5	48	" "
	C8	3	41.59			
	C1	4	49.80			
LB34 (Block)	C2	1	21.82	3.75	44	" "
	C11	2	28.35			
	C9	5	43.85			
LB34 (Block)	B1	1	19.19	4.1	35	" "
	B2	2	21.31			
	B5	4	26.42			
JT9	14	1	11.89	0.3	54	SANDSTONE, slightly weathered, medium hard.
	16	1.5	15.43			
	17	2	20.00			
JT9	15/1	1	12.85	0.5	55	" "
	15/2	1.5	19.02			
	15/3	2	23.88			
JT9 LB34 LB34	6	1	9.53	0.35	51	" "
	C3	1.5	14.55			
	C10	2	17.31			
LB34 (Block)	C5	1	15.67	1.75	49	" "
	B4	2	23.50			
	B6	3	30.03			
JTS	1/4	1	48.80	4.5	60	CONGLOMERATE, occasionally limonitized including and small cavities (Tms ¹)
	1/5	2	70.00			
	1/3	3	80.45			

Table B.4 (Continued)

Borehole or block No.	Specimen No.	Stress at failure		Shear strength parameters		Rock unit
		Lateral σ_3 (Mpa)	Axial σ_1 (Mpa)	c (Mpa)	ϕ (degree)	
JT5	4/1	1	32.00	3.0	58	CONGLOMERATE, occasionally limonitized including and small cavities (Tms ¹)
	4/2	1.5	34.00			
	4/3	2	46.70			
	4/4	3	62.60			
JT5	1/3	1	42.60	3.3	61	" "
	1/2	2	62.30			
	1/1	3	73.80			
JT5	6/1	1	41.71	6.3	49	CONGLOMERATE, moderately weathered, including a few small cavities
	6/2	2	49.54			
	6/3	3	53.50			
JT5	7B/1	1	51.30	9.0	48	CONGLOMERATE, slightly weathe- red, including small cavities and coarse rock fragments.
	7B/3	2	57.00			
	7B/2	3	66.20			
JT1	1/2	1	22.00	2.0	54	LIMESTONE, moderately weathered, fractured, including small cavities (Tms ¹)
	1/3	2	31.00			
	1/1	3	41.00			
LBS4 (Black)	A1	1	56.00	7.3	55	" "
	A2	2	64.00			
	A3	3	72.50			
JT2	14	1	7.77	1.6	29	MARL (Tms)
	19	2	10.64			
	20A/1	3	13.74			
JT2	20A/2	1	10.90	2.6	26.5	" "
	20B/1	2	13.65			
	20B/2	3	16.00			
JT3	17/1	1	8.60	2.4	19	" "
	22/1	2	10.80			
	22/2	3	12.50			
JT3	26/1	1	9.22	2.6	19	" "
	26/2	1.5	10.22			
	26/3	2	11.30			
JT3	29	1	8.90	1.3	37	" "
	30	2	13.70			
	31/2	3	17.00			

Table B.4 (Continued)

Borehole or block No.	Specimen No.	Stress at failure		Shear strength parameters		Rock unit
		Lateral σ_3 (Mpa)	Axial σ_1 (Mpa)	c (Mpa)	ϕ (degree)	
JT7	3/1	1	8.00			MARL (Tnt)
	3/2	1.5	9.77			
JT9	40	2	13.20			1.3 33.4
	42	3	15.14			
JT9	38	1	8.76			" "
	39/1	2	11.31			
	39/2	3	14.80	2	26	
JT7	4B1/1	1	11.66			" "
	4B1/2	2	13.14			
	4B1/3	3	14.95	3.8	16	
LB58 (Block)	C/7	1	12.93			" "
	C/8	2	13.96			
	C/9	3	15.74	3.75	18	

Table B.5: Direct shear test data of natural smooth-planar joints developed in the main Sekkōy formation

Sample No.	Normal stress σ (kPa)	Shear Strength	
		Peak τ_p (kPa)	Residual τ_r (kPa)
LB18A	5.4	9.8	4.0
LB11B	10.9	15.2	8.4
LB18B	20.2	24.4	20.4
LB18C	25.7	27.0	20.4
LB18D	31.1	30.2	25.3
LB11E	58.3	45.5	37.3

Table B.6: Direct shear test data of smooth-planar bedding surfaces developed in the main Sekköy formation

Test Set No.	Sample No.	Normal Stress σ (kPa)	Shear Strength		Shear Strength Parameters *						Description of the rock unit and bedding surface
			Peak	Residual	Peak			Residual			
			τ_p (kPa)	τ_r (kPa)	c_p (kPa)	θ_p (°)	r	c_r (kPa)	θ_r (°)	r	
1	LB3/A2	41.9	48.8	20.9	17.9	42.1	1	5.2	25.4	1	Grayish olive (10Y 4/2), thinly bedded MARL; smooth-planar and very thinly clay coated surface
	A3	82.8	100.8	50.1							
	A4	164.7	167.2	82.8							
	B4	246.4	238.1	121.6							
2	LB4/A2	41.9	44.0	30.0	23.3	30.6	1	19.3	28.7	0.97	Grayish yellow (5Y 8/4), thinly bedded MARL; smooth-planar and thinly clay coated surface
	A1	82.8	77.5	72.2							
	D3	164.7	120.2	114.4							
	A3	246.4	168.0	146.0							
3	LB5/A2	41.9	35.1	20.0	6.2	39.5	0.99	2.0	27.5	0.96	Pale olive (10Y 6/2) thinly to moderately bedded MARL; smooth-planar and very thinly clay coated surface
	A3	82.8	73.1	39.9							
	J1	164.7	159.3	107.9							
	J2	246.4	199.6	119.4							
4	LB9/A1	41.9	73.1	17.2	18.6	41.8	0.99	5.6	29.9	0.98	Grayish olive (10Y 4/2), thinly bedded MARL; smooth-planar and clay coated surface
	A2	82.8	85.0	54.1							
	B1	164.7	152.2	113.4							
	B4	246.4	230.6	162.4							
	B5	328.1	325.6	177.9							
5	LB13/A1	41.9	37.3	20.9	16.7	32.9	0.99	5.3	24.9	0.98	Grayish olive (10Y 4/2), thinly bedded MARL; smooth-planar and thinly clay coated surface
	A2	82.8	70.9	44.8							
	A3	164.7	136.9	77.5							
	A5	246.4	168.6	137.5							
	A6	328.1	227.9	146.1							
6	LB19/B4	41.9	55.5	23.5	31.9	35.4	0.99	25.7	19.9	0.95	Moderate olive brown (5Y 4/4), thinly bedded MARL; smooth-planar and thinly clay coated surface
	B5	82.8	97.3	63.8							
	B2	164.7	145.7	101.7							
	B3	246.4	214.6	119.4							
	B1	328.1	259.4	133.5							
7	LB38/A1	41.9	42.6	25.4	25.9	33.5	0.99	23.5	20.4	0.97	Moderately olive brown (5Y 4/4), thinly bedded MARL; smooth-planar, a few clay coated surface
	A2	82.8	87.2	65.2							
	A4	164.7	148.2	95.7							
	A5	246.4	181.4	107.9							
	A6	328.1	241.7	144.3							
8	LB14/A1	41.9	79.7	26.0	32.9	34.1	0.99	4.9	33.9	0.99	Moderate olive brown (5Y 4/4), hard, compact MARL; smooth-planar and very thinly clay coated surface
	B3	110.0	105.7	72.2							
	B1	164.7	164.1	125.3							
	D1	219.2	189.4	152.6							
	B2	246.4	194.7	172.6							
	D2	328.1	246.1	219.1							

* Shear strength parameters, cohesion (c) and internal friction angle (θ) are based on linear regression analysis

r Coefficient of correlation

Table B.7: Direct shear test data of artificial discontinuities prepared from limestones (T_{ms}^1)

Sample No.	Normal	Shear	Description
	stress	strength	
	σ (kPa)	τ (kPa)	
LB54/C1	58.3	44.4	Very pale orange
C2	85.6	42.0	coarse crystallized
C3	112.8	77.0	(10YR 8/2) LIMESTONE
C4	167.2	117.6	with occasional very
C5	221.9	149.6	small cavities.
C6	276.4	178.3	

Table B.8: Direct shear test data of bedding surfaces with small asperities developed in the limestone of detritic facies

Sample No.	Normal stress σ (kPa)	Shear Strength		Description
		Peak	Residual	
		τ_p	τ_r	
		(kPa)	(kPa)	
LB47/D	5.0	11.1	1.4	Grayish yellow
C	20.3	24.0	8.2	(5Y 8/4), slightly
D1	31.1	30.4	24.0	fractured, occasio-
A1	41.9	39.4	27.2	nally including very
D2	50.3	44.8	32.2	small cavities
B	80.0	106.1	61.2	LIMESTONE; slightly
E	151.1	170.3	92.9	rough and clay-limonite
A	200.0	180.5	112.2	coated bedding surface.

Table B.9: Direct shear test data-fault gouge

Test Set No.	Sample No.	Normal Stress σ (kPa)	Shear Strength		Shear Strength Parameters *						Soil Description
			Peak τ_p (kPa)	Residual τ_r (kPa)	Peak			Residual			
					c_p' (kPa)	ϕ_p' (°)	r	c_r' (kPa)	ϕ_r' (°)	r	
1	LB12C/1	58.3	38.2	20.0	25.3	15.2	0.98	11.3	12.4	0.96	Pale olive (5Y 6/3), homogenous, highly plastic Clay (CH)
	C/2	112.8	60.3	42.6							
	B	221.7	84.1	58.0							
2	LB36/D	58.3	49.3	28.4	14.5	31.4	0.99	1.6	25.5	0.99	Pale yellow (5Y 7/3), sticky, plastic, soft CLAY (CH)
	A1	112.8	85.0	57.2							
	A2	167.2	115.8	80.3							
3	LB35/A1	58.3	21.9	23.1	4.9	24.2	0.99	3.7	17.3	0.99	Olive (5Y 5/4), soft, highly plastic, including organic matter, clayey SILT (MH-OH)
	A3	167.2	77.9	51.9							
	A4	221.7	106.1	67.2							
4	LB23/D2	58.3	40.2	30.0	20.2	30.5	0.93	15.6	17.6	0.98	Olive gray (5Y 5/2), homogenous, medium to high plasticity clayey SILT (MH-OH)
	C2	112.8	108.3	57.6							
	D1	221.7	143.7	84.0							
5	LB8/A	58.3	56.8	27.8	14.4	34.6	1	0.0	22.4	0.98	Olive (5Y 5/4), homogenous, highly plastic, clayey SILT (MH-OH)
	E1	58.3	52.4	27.9							
	G	112.8	92.0	38.5							
	D2	221.7	167.2	92.9							
6	LB20/B1	58.3	75.3	40.8	9.0	51.4	1	4.2	32.6	1	Olive (5Y 5/3), silty and clayey fine SAND (SM) with a few fine rock fragments
	B2	112.8	160.6	77.2							
	A	221.7	283.6	145.5							
7	LB6/A2	58.3	69.3	39.9	8.6	42.1	0.98	2.2	35.5	0.98	Pale olive (5Y 6/3), silty and clayey fine SAND (SM) with a few fine rock fragments
	A1	112.8	125.6	97.2							
	B	221.7	203.6	155.6							

* Effective shear strength parameters are determined from linear regression analyses
 r Coefficient of correlation

Table B.10: Direct shear test data-soil materials

Sample No.	Normal Stress σ (kPa)	Shear Strength		Shear Strength Parameters *						Soil Description
		Peak τ_p (kPa)	Residual τ_r (kPa)	Peak			Residual			
				c_p' (kPa)	ϕ_p' (°)	r	c_r' (kPa)	ϕ_r' (°)	r	
<u>(a) Clay in main Sekköy formation:</u>										
JT8/2A	58.3	39.5	26.3	15.53	22.86	0.99	8.43	14.14	0.95	Pale olive (5Y 6/3), plastic CLAY
2B	112.8	60.8	35.8							
2C	167.2	92.4	43.1							
2D	221.7	105.5	69.6							
JT2/2A	58.3	40.0	28.1	15.86	22.77	0.99	8.08	14.41	0.94	Pale olive (5Y 6/3), plastic CLAY
2B	112.8	62.0	34.3							
2C	167.2	90.3	42.3							
2D	221.7	106.4	73.0							
<u>(b) Soils of transition zone:</u>										
LB39/A	20.3	55.0	10.4	60.23	22.06	0.99	4.56	16.60	0.99	Dark gray (5Y 4/1), micaceous, plastic clayey elastic SILT
C1	33.9	66.0	15.0							
C2	44.7	69.1	21.0							
LB21/A1	41.9	58.5	18.6	57.07	25.37	0.91	0.0	23.81	0.93	Olive gray (5Y 5/2), plastic, sandy, clayey SILT
A2	82.9	109.8	42.6							
D	164.7	154.4	56.8							
F	246.4	159.7	115.9							
LB22/A	20.3	62.1	17.7	57.32	23.60	0.99	11.88	19.80	0.97	Olive gray (5Y 5/2), low plasticity, clayey sandy SILT
B1	33.9	68.7	24.9							
B2	55.6	78.7	33.9							
B3	82.8	89.4	40.4							
<u>(c.1) Soils of Turgut formation (finest portion) :</u>										
LB50/A1	41.9	71.3	15.9	56.86	19.65	0.99	2.56	14.50	0.99	Dark gray (5Y 4/1), highly plastic silty CLAY
A2	82.8	87.2	24.0							
A3	164.7	115.4	50.6							
A4	273.6	180.3	80.6							
LB44/C1	41.9	46.1	24.8	22.22	31.64	0.99	4.18	24.28	0.99	Very dark gray (5Y 3/1), low plasticity clayey SILT
C2	82.8	74.7	36.8							
A1	164.7	126.9	83.2							
A2	273.6	189.4	126.0							
<u>(c.2) Black clay (Turgut formation-sliding surface) :</u>										
LB48/A	20.3	17.7	6.3	7.59	24.71	0.98	0.0	17.21	1	Very dark gray (5Y 3/1), highly plastic CLAY
B	39.4	23.1	11.4							
D	58.3	37.3	17.8							
E	77.5	42.2	24.0							

* Effective shear strength parameters are determined from linear regression analyses

r Coefficient of correlation



APPENDIX C

Rock Mass Classification Systems

Table C.1: The Rock Mass Rating System (Geomechanics Classification of Rock Masses)^a

A. Classification parameters and their ratings

PARAMETER		RANGES OF VALUES						
1	Strength of intact rock material	Point-load strength index > 10 MPa	4 - 10 MPa	2 - 4 MPa	1 - 2 MPa	For this low range - uniaxial compressive test is preferred		
		Uniaxial compressive strength > 250 MPa	100 - 250 MPa	50 - 100 MPa	25 - 50 MPa	5-25 MPa	1-5 MPa	< 1 MPa
	Rating	15	12	7	4	2	1	0
2	Drill core quality RQD	50% - 100%	75% - 90%	50% - 75%	25% - 50%	< 25%		
	Rating	20	17	13	8	3		
3	Spacing of discontinuities	> 2 m	0.6 - 2 m	200 - 600 mm	60 - 200 mm	< 60 mm		
	Rating	20	15	10	8	5		
4	Condition of discontinuities	Very rough surfaces. Not continuous. No separation. Unweathered wall rock.	Slightly rough surfaces. Separation < 1 mm. Slightly weathered walls.	Slightly rough surfaces. Separation < 1 mm. Highly weathered walls.	Slackenaided surfaces OR Gouge < 5 mm thick OR Separation 1-5 mm. Continuous.	Soft gouge > 5 mm thick OR Separation > 5 mm. Continuous.		
	Rating	30	25	20	10	0		
5	Ground water	Inflow per 10 m tunnel length	None	< 10 litres/min	10-25 litres/min	25 - 125 litres/min	> 125	
		Ratio joint water pressure major principal stress	OR 0	OR 0.0-0.1	OR 0.1-0.2	OR 0.2-0.5	OR > 0.5	
		General conditions	Completely dry	Damp	Wet	Dripping	Flowing	
	Rating	15	10	7	4	0		

B. Rating adjustment for discontinuity orientations

Strike and dip orientations of joints		Very favourable	Favourable	Fair	Unfavourable	Very unfavourable
Ratings	Tunnels	0	-2	-5	-10	-12
	Foundations	0	-2	-7	-15	-25
	Slopes	0	-5	-25	-50	-60

C. Rock mass classes determined from total ratings

Rating	100-81	80-61	60-41	40-21	< 20
Class No	I	II	III	IV	V
Description	Very good rock	Good rock	Fair rock	Poor rock	Very poor rock

D. Meaning of rock mass classes

Class No	I	II	III	IV	V
Average stand-up time	10 years for 15 m span	6 months for 8 m span	1 week for 5 m span	10 hours for 2.5 m span	30 minutes for 1 m span
Cohesion of the rock mass	> 400 kPa	300 - 400 kPa	200 - 300 kPa	100 - 200 kPa	< 100 kPa
Friction angle of the rock mass	< 45°	35° - 45°	25° - 35°	15° - 25°	< 15°

E. Rating adjustment for joint orientation.^b

Joint Orientation	No mode of failure	One possible mode of failure	One mode of failure	Two mode of failures	Several mode of failures
Rating	0	-5	-25	-50	-60

F. Assessment of discontinuity conditions in coal mines for the Geomechanics Classification (RMR)^c

Separation of bedding	None	Hairline	< 1 mm	1-5 mm	> 5 mm
Roughness of surfaces	Very rough	Rough	Smooth	Slackenaided	Slackenaided
Weathering of surfaces	Fresh, hard	Slightly weathered	Highly weathered	Highly weathered	Completely weathered
Infilling (gouge)	None	None	Minor clay	Stiff clay, gouge	Soft clay, gouge
Continuity	All bedding planes continuous across entry				
Rating	30	25	20	10	0

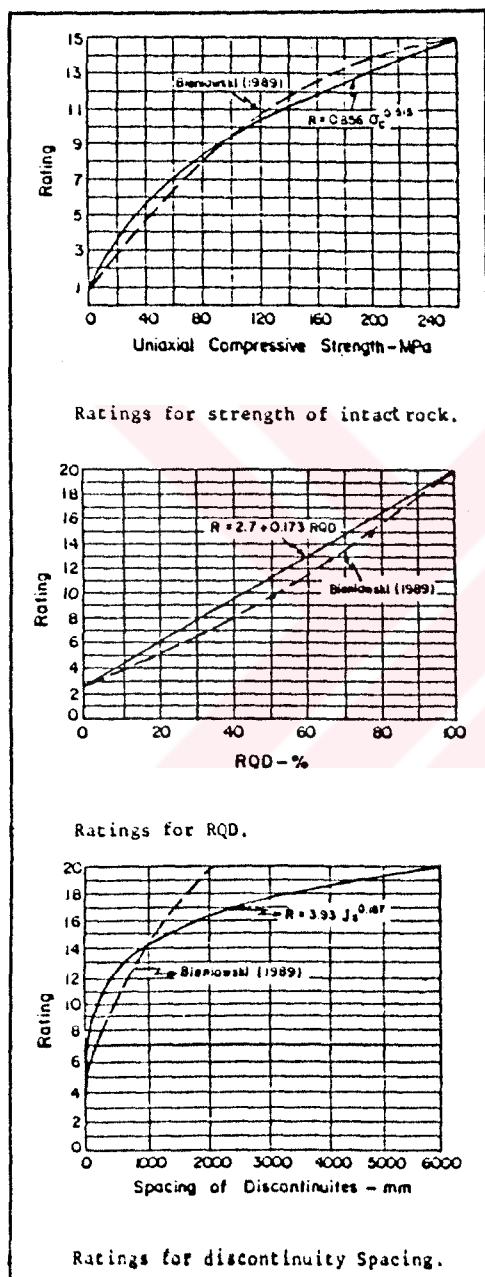
^a After Bieniawski (1989)

^b After Singh and Gahrooe (1989)

^c After Bieniawski (1984)

Table C.2.: Modified RMR System for clay-bearing and stratified rock masses (after Ünal and Özkan, 1990)

Table C.2.1: Intervals and ratings for "spacing", "groundwater" and "joint orientation" index



SPACING INDEX (SI)	
CONDITION	RATING
Sand	1
Clay + Gravel	2
$SP \leq 20$ ■■	3
$20 \leq SP < 60$ ■■	5
$60 \leq SP < 200$ ■■	8
$200 \leq SP < 600$ ■■	10
$600 \leq SP < 2000$ ■■	15
$2000 \leq SP < 6000$ ■■	18
$SP \geq 6000$ ■■	20

GROUNDWATER INDEX (WI)	
CONDITION	RATING
Completely dry	15
Damp	10
Wet	7
Dripping	4
Flowing	0

JOINT ORIENTATION INDEX (OI)	
CONDITION	RATING
Intact Core Recovery (ICR) < 5 %	-12
5 % \leq ICR < 15 %	-10
15 % \leq ICR < 25 %	-8
ICR \geq 25 %	-5

Rating for "uniaxial compressive strength", "RQD" and "discontinuity spacing" employed in RMR and modified RMR systems.

Table C.2.2: Intervals and ratings for "joint condition" index

JOINT CONDITION INDEX (CI)			
PARAMETER	CONDITION	RATING	
I. WEATHERING "A"	Unweathered	8	
	Slightly weathered	7	
	Moderately weathered	6	
	Highly weathered	4	
	Very highly weathered	2	
	Decomposed	0	
II. ROUGHNESS "P"	Undulating	Very rough	8
		Rough	6
		Slightly rough	4
		Smooth	2
		Slickensided	1
	Planar	Very rough	4
		Rough	3
		Slightly rough	2
		Smooth	1
		Slickensided	0
III. CONTINUITY "Y"	Very low	3.5	
	Low	3	
	Medium	2	
	High	1.5	
	Very high	1	
IV. APERTURE "Z"	0.0 - 0.01 mm	4	
	0.01 - 1.0 mm	3	
	1.0 - 5.0 mm	2	
	> 5 mm	0	
V. FILLING "D"	None	1	
	0 - 1 mm	4	
	1 - 5 mm (Soft)	3.5	
	1 - 5 mm (Hard)	3.0	
	< 5 mm (Soft)	2.0	
	< 5 mm (Hard)	0	

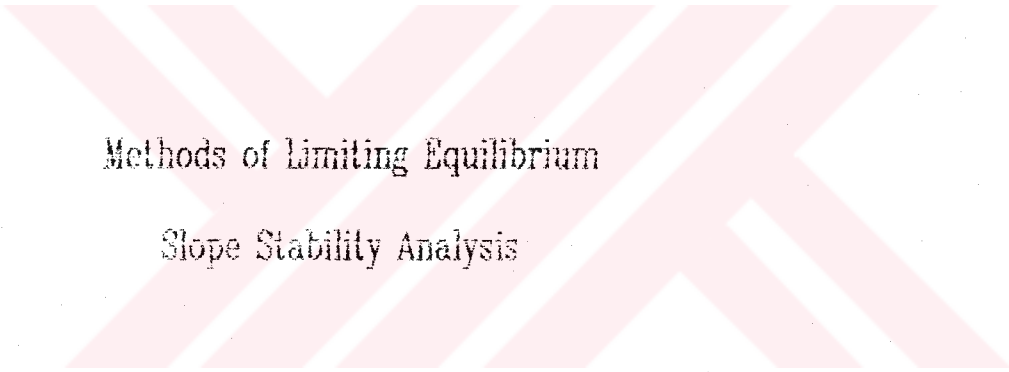
The modified RMR values are obtained from the following equation:

$$RMR_m = [(\sigma_C + RQD + JC) F_C] + SI + WI - OI$$

where,

- σ_C : Rating for uniaxial compressive strength
- F_C : Coefficient for slake durability index
- JC : A + P + (Y * Z * D)
- A, P, Y, Z and D is obtained from Table C.2.2.

APPENDIX D



Methods of Limiting Equilibrium

Slope Stability Analysis

APPENDIX D. 1

PLANE FAILURE ANALYSIS

Slope failures in which sliding occurs down a single planar surface are the most simple type to analyse using limiting equilibrium technique and have been treated in a number of publication and text, e.g., Hoek and Bray, 1977; Major, et. al., 1977; Stimpson, 1979. In order that sliding should occur on a single plane, the following geometrical conditions must be satisfied (Hoek and Bray, 1977; Stimpson, 1979):

- a. The plane on which sliding occurs must strike parallel or nearly parallel (within approximately $\pm 20^\circ$) to the slope face. If a tension crack is present, it is assumed to be parallel to the slope crest and vertical (Figure D.1).
- b. The failure plane must "daylight" in the slope face. This means that its dip must be smaller than the dip of the slope face.
- c. The dip of the failure plane must be greater than the angle of friction of this plane.
- d. Release surface which provides negligible resistance to sliding must be present in the rock mass to define the lateral boundaries of the slide.

In analysing two dimensional slope problems, it is usual to consider a slice of unit thickness taken at right angles to the slope face. This means that the area of the sliding surface can be represented by the length of surface visible on a vertical section through the slope and the volume of the sliding block is represented by the length A in Figure D.1.a.

The geometry of the slope considered in this analysis is defined in Figure D.1. Note that three cases is considered:

- a. A slope having a tension crack in its upper surface (Figure D.1.a).
- b. A slope with a tension crack in its face (Figure D.1.b).
- c. A slope with non-linear phreatic surface and tension crack or no tension crack (Figure D.1.c).

The groundwater pressure distributions for the cases considered are as shown in Figure D.1. The factor of safety, given by the total force resisting sliding to the total force tending to induce sliding, is

$$F = \frac{cA + (W \cos\psi_p - u - V \sin\psi_p) \tan\phi}{W \sin\psi_p + V \cos\psi_p} \quad (1)$$

If the seismic acceleration, α , due to the earthquake or blasting is taken into consideration equation 1 can be written as

$$F = \frac{cA + [W (\cos\psi_p - \alpha \sin\psi_p) - u - V \sin\psi_p] \tan\phi}{W(\sin\psi_p + \alpha \cos\psi_p) + V \cos\psi_p} \quad (2)$$

where, from Figure D.1 :

$$A = (H - z) \operatorname{Cosec}\psi_p \quad (3)$$

$$u = \frac{1}{2} \gamma_w \cdot z_w (H - z) \operatorname{Cosec}\psi_p \quad (4)$$

$$V = \frac{1}{2} \gamma_w \cdot z_w^2 \quad (5)$$

for tension crack in the upper slope surface (Figure D.1.a)

$$W = \frac{1}{2} \gamma H^2 \{ [1 - (z/H)^2] \cot\psi_p - \cot\psi_f \} \quad (6)$$

and, for the tension crack in the slope face (Figure D.1.b)

$$W = \frac{1}{2} \gamma H^2 \{ (1 - z/H)^2 \cot\psi_p (\cot\psi_p \tan\psi_f - 1) \} \quad (7)$$

For a slope with a phreatic surface and no tension crack (Figure D.1.c), equation 2 reduces to,

$$F = \frac{cA + [W (\cos\psi_p - \alpha \sin\psi_p) - u] \tan\phi}{W(\sin\psi_p + \alpha \cos\psi_p)} \quad (8)$$

where,

$$u = \frac{1}{2} \gamma_w \cdot H^2_w \operatorname{Cosec}\psi_p \quad (9)$$

The simpler pore pressure equation (9) given above were modified for various cases involving combination of non-linear phreatic surface and different tension crack positions by incorporating the slice definition in the computer program MBPF developed by the author (Appendix E.3).

APPENDIX D.2

MULTIPLANAR SHEAR FAILURE ANALYSIS

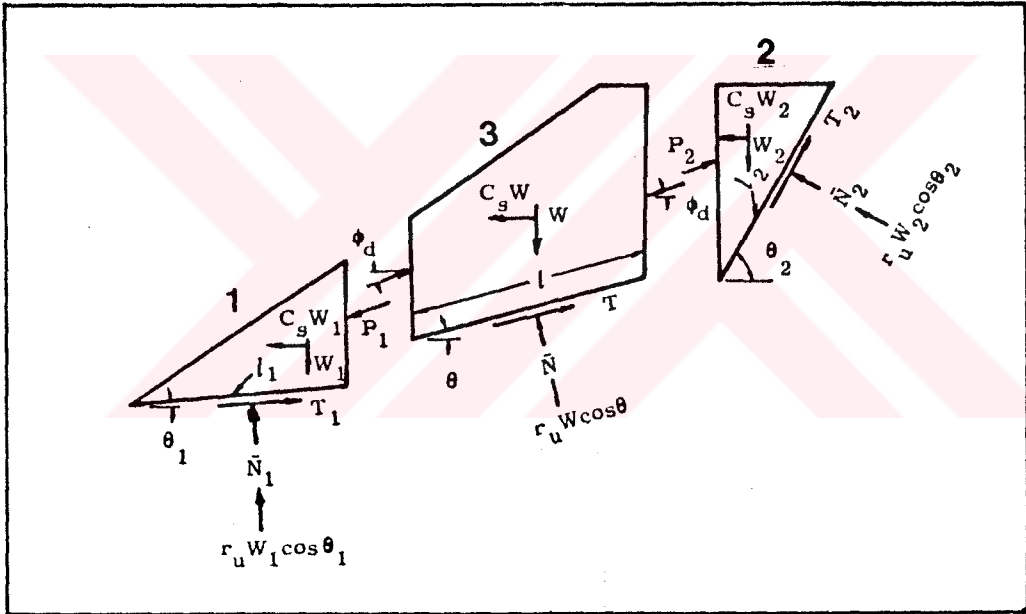


Figure D.2: Free-body diagram for three blocks
(After Huang, 1983).

Figure D.2 is the free-body diagram showing the forces on each block. There are total six unknowns (P_1 , P_2 , N_1 , N_2 , and the factor of safety, F), which can be solved by six equilibrium equations, two for each block.

For the bottom block (block 1) summing all forces in the vertical directions

$$W_1 + P_1 \sin \theta_D - \bar{N}_1 \cos \theta_1 - r_u W_1 \cos^2 \theta_1 - T_1 \sin \theta_1 = 0 \quad (1)$$

in which $\theta_D = \tan^{-1} [(\tan \theta)/F]$ is the angle of internal friction of two blocks and T_1 is the shear force on failure plane at bottom, which can be expressed as

$$T_1 = (c_1 l_1 + \bar{N}_1 \tan \theta_1) / F \quad (2)$$

Summing all forces in the horizontal direction

$$P_1 \cos \theta_D + \bar{N}_1 \sin \theta_1 + r_u W_1 \sin \theta_1 \cos \theta_1 + C_S W_1 - T_1 \cos \theta_1 = 0 \quad (3)$$

From equations 1, 2 and 3

$$N_1 = \{W_1 [\cos \theta_D - r_u \cos \theta_1 \cos (\theta_D - \theta_1)] - C_S \sin \theta_D + [c_1 l_1 \sin (\theta_D - \theta_1)] / F\} / \{ \cos (\theta_D - \theta_1) - [\tan \theta_1 \sin (\theta_D - \theta_1)] / F \} \quad (4)$$

From equation 3

$$P_1 = (T_1 \cos \theta_1 - N_1 \sin \theta_1 - r_u W_1 \sin \theta_1 \cos \theta_1 - C_S W_1) / \cos \theta_D \quad (5)$$

For the top block (block 2)

$$W_2 - P_2 \sin \theta_D - N_2 \cos \theta_2 - r_u W_2 \cos^2 \theta_2 - T_2 \sin \theta_2 = 0 \quad (6)$$

$$T_2 = (c_2 l_2 + N_2 \tan \theta_2) / F \quad (7)$$

$$P_2 \cos \theta_D - \bar{N}_2 \sin \theta_2 - r_u W_2 \cos \theta_2 \sin \theta_2 - C_S W_2 + T_2 \cos \theta_2 = 0 \quad (8)$$

From the equations 6, 7 and 8

$$N_2 = \{w_2 [\cos \theta_D - r_u \cos \theta_2 \cos (\theta_D - \theta_2)] - C_S \sin \theta_D + [c_2 l_2 \sin (\theta_D - \theta_2)] / F\} / \{ \cos (\theta_D - \theta_2) - [\tan \theta_2 \sin (\theta_D - \theta_2)] / F \} \quad (9)$$

From equation 8

$$P_2 = (\bar{N}_2 \sin \theta_2 - T_2 \cos \theta_2 + r_u W_2 \cos \theta_2 \sin \theta_2 + C_s W_2) / \cos \theta_d \quad (10)$$

for the middle block (block 3)

$$W + P_2 \sin \theta_d - P_1 \sin \theta_d - \bar{N} \cos \theta - r_u W \cos^2 \theta - T \sin \theta = 0 \quad (11)$$

$$T = (c_1 + \bar{N} \tan \theta) / F \quad (12)$$

$$-P_2 \cos \theta_d + P_1 \cos \theta_d - \bar{N} \sin \theta - r_u W \cos \theta \sin \theta + T \cos \theta - C_s W = 0 \quad (13)$$

From Equations 11, 12 and 13

$$N = \{W(1 - r_u \cos^2 \theta) + (P_2 - P_1) \sin \theta_d - (c_1 \sin \theta) / F\} / [\cos \theta + (\tan \theta \sin \theta) / F] \quad (14)$$

Equation 13 can be written as

$$\text{Function } (F) = (P_1 - P_2) \cos \theta_d - \bar{N} \sin \theta - r_u W \cos \theta \sin \theta + T \cos \theta - C_s W = 0 \quad (15)$$

in which P_1 , P_2 , T and \bar{N} are a function of F and can be determined from Equations 5, 10, 12 and 14, respectively. A subroutine from the IBM 360 Scientific Subroutine Package was used to solve for F (International Business Machines Corporation, 1970; in Huang, 1983).

Note: For more information reference should be made to Huang (1983) and Chowdhury (1978).

APPENDIX D.3

WEDGE FAILURE ANALYSIS

A mode of failure involving the sliding of a wedge on two intersecting discontinuity planes is frequently encountered in rock slopes. The method briefly summarized hereunder includes an inclined upper slope surface, a tension crack running behind the slope crest and the influence of water pressure in tension crack and along the sliding surface. The stabilization of the slope by means of cable anchors or rockbolts is also included in this analytical method of analysis, which is proposed by Hoek and Bray (1977).

The following assumptions are made:

- a. The wedge remains in contact with both discontinuity surfaces during sliding.
- b. The influence of moments is neglected.
- c. The shear strength of the sliding surfaces is defined by a linear relationship.
- d. Sliding of the wedge is kinematically possible.

The factor of safety can be determined for the following conditions:

- a. A dry slope with no tension crack.

- b. A dry slope with the tension crack.
- c. With the slope surface flooded with water which can enter the top of the tension crack.
- d. With an external force due to cable anchors or rock bolts.

As an initial step of analysis the various planes which bound the wedge (Figure D.3.1) are plotted as great circles on the stereonet (Figure D.3.2) for the determination of dip directions of lines of intersection. In other steps, rigorous solutions by using various equations are required. These steps and related equations are summarized as in the form of a calculation table in Figure D.3.3. For derivation of equations and further information, reference should be made to Hoek and Bray (1977; App.1).

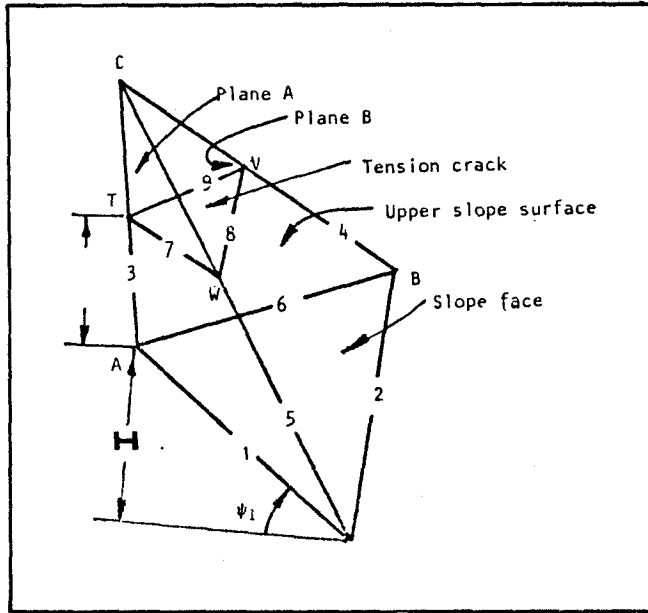


Figure D.3.1: Pictorial view of wedge problem to be analysed showing numbering of intersection lines (After Hoek and Bray, 1977).

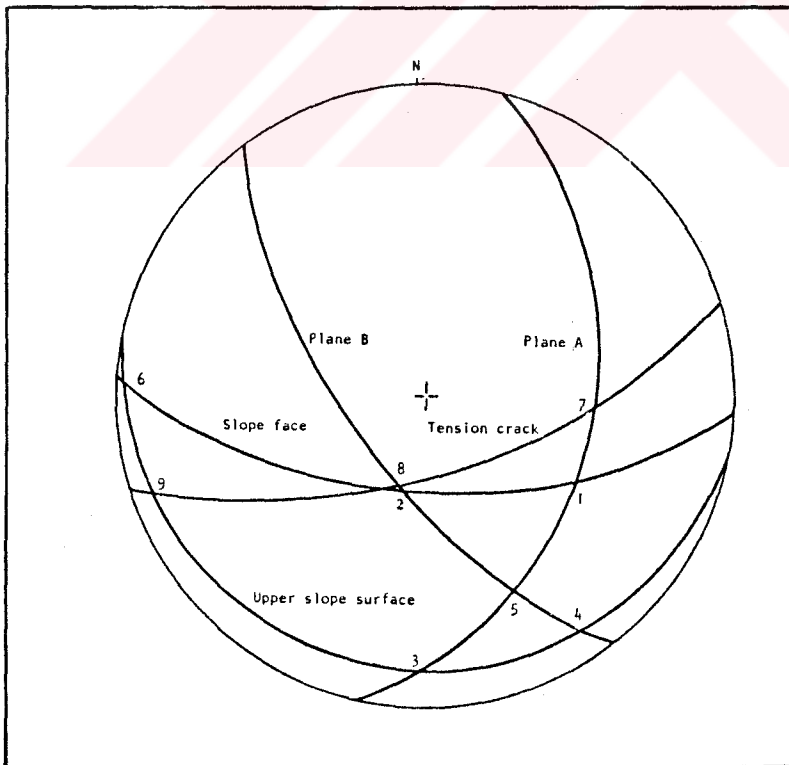


Figure D.3.2: Great circle traces representing planes defined in Figure D.3.1. Intersection points of great circles represent lines of intersection of planes (After Hoek and Bray, 1977).

Step 1: Calculation of dip directions of lines of intersection

Fig. D.3.2

Input data:

- ψ_a - dip of plane A
- α_a - dip direction of plane A
- ψ_b - dip of plane B
- α_b - dip direction of plane B
- ψ_f - dip of slope face
- α_f - dip direction of slope face
- ψ_s - dip of upper slope surface
- α_s - dip direction of upper slope surface

Calculation:

$$\alpha_1 = \arctan \left\{ \frac{\tan \psi_a \cdot \cos \alpha_a - \tan \psi_f \cdot \cos \alpha_f}{\tan \psi_f \cdot \sin \alpha_f - \tan \psi_a \cdot \sin \alpha_a} \right\}$$

$$\alpha_2 = \arctan \left\{ \frac{\tan \psi_b \cdot \cos \alpha_b - \tan \psi_f \cdot \cos \alpha_f}{\tan \psi_f \cdot \sin \alpha_f - \tan \psi_b \cdot \sin \alpha_b} \right\}$$

$$\alpha_3 = \arctan \left\{ \frac{\tan \psi_a \cdot \cos \alpha_a - \tan \psi_s \cdot \cos \alpha_s}{\tan \psi_s \cdot \sin \alpha_s - \tan \psi_a \cdot \sin \alpha_a} \right\}$$

$$\alpha_4 = \arctan \left\{ \frac{\tan \psi_b \cdot \cos \alpha_b - \tan \psi_s \cdot \cos \alpha_s}{\tan \psi_s \cdot \sin \alpha_s - \tan \psi_b \cdot \sin \alpha_b} \right\}$$

$$\alpha_5 = \arctan \left\{ \frac{\tan \psi_a \cdot \cos \alpha_a - \tan \psi_b \cdot \cos \alpha_b}{\tan \psi_b \cdot \sin \alpha_b - \tan \psi_a \cdot \sin \alpha_a} \right\}$$

$$\alpha_6 = \arctan \left\{ \frac{\tan \psi_f \cdot \cos \alpha_f - \tan \psi_s \cdot \cos \alpha_s}{\tan \psi_s \cdot \sin \alpha_s - \tan \psi_f \cdot \sin \alpha_f} \right\}$$

$$\alpha_7 = \arctan \left\{ \frac{\tan \psi_a \cdot \cos \alpha_a - \tan \psi_t \cdot \cos \alpha_t}{\tan \psi_t \cdot \sin \alpha_t - \tan \psi_a \cdot \sin \alpha_a} \right\}$$

$$\alpha_8 = \arctan \left\{ \frac{\tan \psi_b \cdot \cos \alpha_b - \tan \psi_t \cdot \cos \alpha_t}{\tan \psi_t \cdot \sin \alpha_t - \tan \psi_b \cdot \sin \alpha_b} \right\}$$

$$\alpha_9 = \arctan \left\{ \frac{\tan \psi_s \cdot \cos \alpha_s - \tan \psi_t \cdot \cos \alpha_t}{\tan \psi_t \cdot \sin \alpha_t - \tan \psi_s \cdot \sin \alpha_s} \right\}$$

Step 2 continued:

$$\psi_6 = \arctan (\tan \psi_f \cdot \cos (\alpha_f - \alpha_6))$$

$$\psi_7 = \arctan (\tan \psi_a \cdot \cos (\alpha_a - \alpha_7))$$

$$\psi_8 = \arctan (\tan \psi_b \cdot \cos (\alpha_b - \alpha_8))$$

$$\psi_9 = \arctan (\tan \psi_s \cdot \cos (\alpha_s - \alpha_9))$$

Step 3: Calculation of angles between lines of intersection.

Input data: from steps 1 and 2.

Calculation:

$$\theta_{13} = \arccos (\cos \psi_1 \cdot \cos \psi_3 \cdot \cos (\alpha_1 - \alpha_3) + \sin \psi_1 \cdot \sin \psi_3)$$

$$\theta_{15} = \arccos (\cos \psi_1 \cdot \cos \psi_5 \cdot \cos (\alpha_1 - \alpha_5) + \sin \psi_1 \cdot \sin \psi_5)$$

$$\theta_{24} = \arccos (\cos \psi_2 \cdot \cos \psi_4 \cdot \cos (\alpha_2 - \alpha_4) + \sin \psi_2 \cdot \sin \psi_4)$$

$$\theta_{25} = \arccos (\cos \psi_2 \cdot \cos \psi_5 \cdot \cos (\alpha_2 - \alpha_5) + \sin \psi_2 \cdot \sin \psi_5)$$

$$\theta_{34} = \arccos (\cos \psi_3 \cdot \cos \psi_4 \cdot \cos (\alpha_3 - \alpha_4) + \sin \psi_3 \cdot \sin \psi_4)$$

$$\theta_{35} = \arccos (\cos \psi_3 \cdot \cos \psi_5 \cdot \cos (\alpha_3 - \alpha_5) + \sin \psi_3 \cdot \sin \psi_5)$$

$$\theta_{37} = \arccos (\cos \psi_3 \cdot \cos \psi_7 \cdot \cos (\alpha_3 - \alpha_7) + \sin \psi_3 \cdot \sin \psi_7)$$

$$\theta_{45} = \arccos (\cos \psi_4 \cdot \cos \psi_5 \cdot \cos (\alpha_4 - \alpha_5) + \sin \psi_4 \cdot \sin \psi_5)$$

$$\theta_{48} = \arccos (\cos \psi_4 \cdot \cos \psi_8 \cdot \cos (\alpha_4 - \alpha_8) + \sin \psi_4 \cdot \sin \psi_8)$$

$$\theta_{49} = \arccos (\cos \psi_4 \cdot \cos \psi_9 \cdot \cos (\alpha_4 - \alpha_9) + \sin \psi_4 \cdot \sin \psi_9)$$

$$\theta_{57} = \arccos (\cos \psi_5 \cdot \cos \psi_7 \cdot \cos (\alpha_5 - \alpha_7) + \sin \psi_5 \cdot \sin \psi_7)$$

$$\theta_{58} = \arccos (\cos \psi_5 \cdot \cos \psi_8 \cdot \cos (\alpha_5 - \alpha_8) + \sin \psi_5 \cdot \sin \psi_8)$$

$$\theta_{79} = \arccos (\cos \psi_7 \cdot \cos \psi_9 \cdot \cos (\alpha_7 - \alpha_9) + \sin \psi_7 \cdot \sin \psi_9)$$

$$\theta_{89} = \arccos (\cos \psi_8 \cdot \cos \psi_9 \cdot \cos (\alpha_8 - \alpha_9) + \sin \psi_8 \cdot \sin \psi_9)$$

Step 2: Calculation of dips of lines of intersection

Input data from step 1.

Calculation:

$$\psi_1 = \arctan (\tan \psi_a \cdot \cos (\alpha_a - \alpha_1))$$

$$\psi_2 = \arctan (\tan \psi_b \cdot \cos (\alpha_b - \alpha_2))$$

$$\psi_3 = \arctan (\tan \psi_a \cdot \cos (\alpha_a - \alpha_3))$$

$$\psi_4 = \arctan (\tan \psi_b \cdot \cos (\alpha_b - \alpha_4))$$

$$\psi_5 = \arctan (\tan \psi_a \cdot \cos (\alpha_a - \alpha_5))$$

Step 4: Calculation of areas of planes

Input data: from step 3 and from measured lengths AC and TC.

Supplementary calculation of lengths AC and TC

$$AO = H / \psi_1$$

$$AC = AO \cdot \frac{\sin \theta_{15}}{\sin \theta_{35}}$$

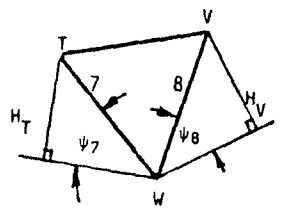
$$TC = AC - AT$$


Figure D.3.3: Calculation table for wedge analysis (After Hoek and Bray, 1977)

Calculation:

$$A_A = \frac{1}{2} \left\{ AC^2 \cdot \frac{\sin^2 \theta_{13}}{\sin^2 \theta_{15}} - TC^2 \cdot \frac{\sin^2 \theta_{37}}{\sin^2 \theta_{57}} \right\} \sin \theta_{35}$$

$$A_B = \frac{1}{2} \left\{ AC^2 \cdot \frac{\sin^2 \theta_{13} \cdot \sin^2 \theta_{25} - TC^2 \cdot \sin^2 \theta_{37} \cdot \sin^2 \theta_{58}}{\sin^2 \theta_{15} \cdot \sin^2 \theta_{24}} - \frac{\sin^2 \theta_{37} \cdot \sin^2 \theta_{58}}{\sin^2 \theta_{57} \cdot \sin^2 \theta_{48}} \right\} \sin \theta_{45}$$

$$A_T = \frac{1}{2} TC^2 \cdot \frac{\sin \theta_{35} \cdot \sin^2 \theta_{35} \cdot \sin \theta_{79}}{\sin^2 \theta_{45} \cdot \sin^2 \theta_{57}}$$

Step 5: Calculation of weight of wedge

Input data: Angles from step 3 plus lengths AC and TC.

Calculation:

$$K = (1 - \cos^2 \theta_{34} - \cos^2 \theta_{35} - \cos^2 \theta_{45} + 2 \cos \theta_{34} \cos \theta_{35} \cos \theta_{45})^{\frac{1}{2}}$$

$$W = \frac{1}{6} \gamma K \left\{ AC^3 \cdot \frac{\sin^2 \theta_{13} \cdot \sin^2 \theta_{25}}{\sin^2 \theta_{15} \cdot \sin^2 \theta_{24}} - TC^3 \cdot \frac{\sin^2 \theta_{37} \cdot \sin^2 \theta_{58}}{\sin^2 \theta_{57} \cdot \sin^2 \theta_{48}} \right\}$$

Step 6: Calculation of forces due to water pressure.

Input data: From steps 2, 3 and 4.

Calculation:

$$p = \gamma_w \cdot \frac{TC \cdot \sin^2 \theta_{35}}{2 \cdot \sin^2 \theta_{57}} \left\{ \sin \theta_{79} + \frac{\sin^2 \theta_{79}}{\sin^2 \theta_{69}} \cdot \sin \psi_5 \right\}$$

$$V = \frac{1}{3} \cdot p \cdot A_T$$

$$U_A = \frac{1}{3} \cdot p \cdot A_A$$

$$U_B = \frac{1}{3} \cdot p \cdot A_B$$

Step 7: Calculation of coefficients for resolution of forces

Input data: original data on planes and step 2.

Calculation:

$$m_{na.nb} = \sin^2 \psi_a \cdot \sin^2 \psi_b \cdot \cos(\alpha_a - \alpha_b) + \cos^2 \psi_a \cdot \cos^2 \psi_b$$

$$m_{w.na} = -\cos \psi_a$$

$$m_{w.nb} = -\cos \psi_b$$

$$m_{v.na} = \sin^2 \psi_a \cdot \sin^2 \psi_t \cdot \cos(\alpha_a - \alpha_t) + \cos^2 \psi_a \cdot \cos^2 \psi_t$$

$$m_{v.nb} = \sin^2 \psi_b \cdot \sin^2 \psi_t \cdot \cos(\alpha_b - \alpha_t) + \cos^2 \psi_b \cdot \cos^2 \psi_t$$

$$m_{t.na} = \cos^2 \psi_t \cdot \sin^2 \psi_a \cdot \cos(\alpha_t - \alpha_a) - \sin^2 \psi_t \cdot \cos^2 \psi_a$$

$$m_{t.nb} = \cos^2 \psi_t \cdot \sin^2 \psi_b \cdot \cos(\alpha_t - \alpha_b) - \sin^2 \psi_t \cdot \cos^2 \psi_b$$

$$m_{w.5} = \sin^2 \psi_5$$

$$m_{v.5} = \cos^2 \psi_5 \cdot \sin^2 \psi_t \cdot \cos(\alpha_5 - \alpha_t) - \sin^2 \psi_5 \cdot \cos^2 \psi_t$$

$$m_{t.5} = \cos^2 \psi_5 \cdot \cos^2 \psi_t \cdot \cos(\alpha_5 - \alpha_t) + \sin^2 \psi_5 \cdot \sin^2 \psi_t$$

Step 8: Calculation of coefficients for determination of effective normal reactions N_{ae} and N_{be} .

Input data: from step 7

Calculation:

$$q = (m_{na.nb} \cdot m_{w.nb} - m_{w.na}) / (1 - m_{na.nb}^2)$$

$$r = (m_{na.nb} \cdot m_{v.nb} - m_{v.na}) / (1 - m_{na.nb}^2)$$

$$s = (m_{na.nb} \cdot m_{t.nb} - m_{t.na}) / (1 - m_{na.nb}^2)$$

$$x = (m_{na.nb} \cdot m_{w.na} - m_{w.nb}) / (1 - m_{na.nb}^2)$$

$$y = (m_{na.nb} \cdot m_{v.na} - m_{v.nb}) / (1 - m_{na.nb}^2)$$

$$z = (m_{na.nb} \cdot m_{t.na} - m_{t.nb}) / (1 - m_{na.nb}^2)$$

Step 9: Calculation of Factor of Safety

$$F = \frac{c_A A_A + c_B A_B + (qW + rV + sT - U_A) \tan \phi_A + (xW + yV + zT - U_B) \tan \phi_B}{m_{w.5} W + m_{v.5} V + m_{t.5} T}$$

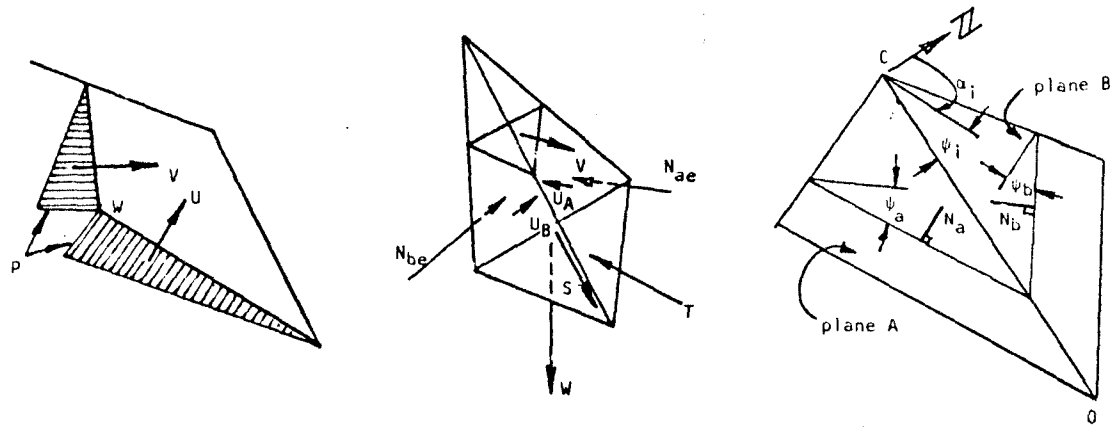


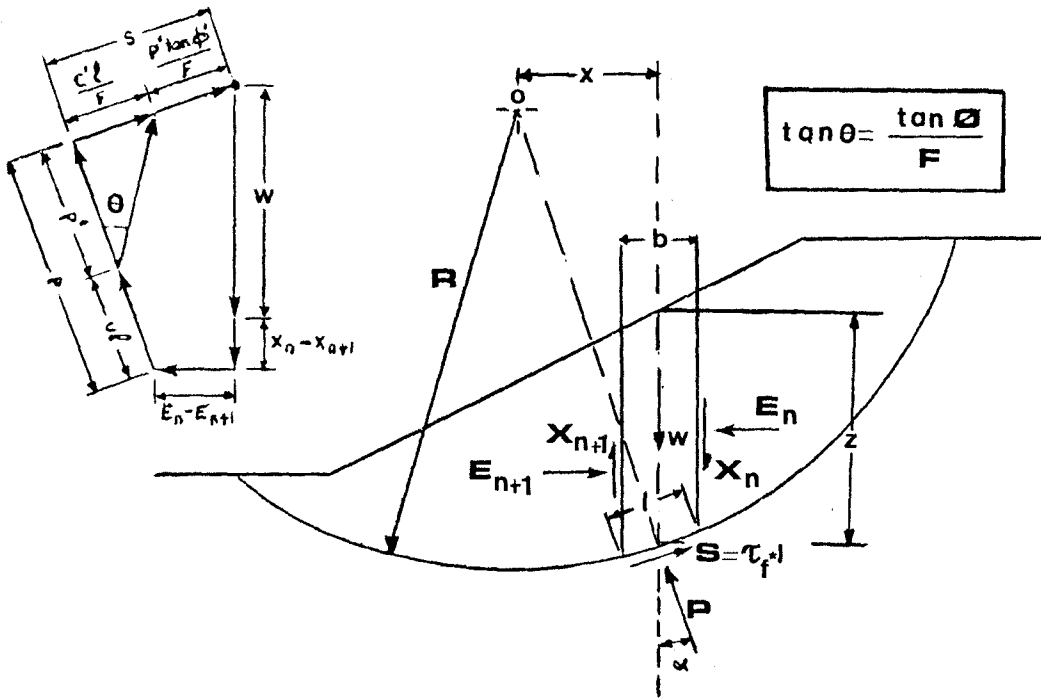
Figure D.3.3 (Continued)

APPENDIX D.4

CIRCULAR FAILURE (Bishop's Method)

In this method the potential failure surface, in section, is assumed to be a circular arc with centre O and radius R . The soil mass (ABCD) above a trial failure surface $O(AD)$ is divided by vertical planes into a series of slices of width, b , as shown in Figure D.4. The base of each slice is assumed to be a straight line. For any slice the inclination of the centre-line, is z . The factor of safety is defined as the ratio of available shear strength to the shear strength which must be mobilized to maintain a condition of limiting equilibrium.

Force equilibrium conditions introduce E or X forces (Figure D.4) and an assumption must be made to render the problem statically determinate. In what is usually termed the simplified Bishop method (Bishop, 1955), force equilibrium of a slice in the vertical direction is taken and the variation in X forces across a slide is ignored. This is tantamount to assuming zero shear between slices and ignoring the requirement for equilibrium in the horizontal direction. Resolving the forces combined with the Mohr-Coulomb criterion results in the expression of factor of safety given in Figure D.4.



- W = weight of slice
- P = total normal force acting on base of slice
- T = shear force acting on base of slice
- z = height of slice
- b = breadth of slice
- l = length of BC (taken as a straight line)
- α = angle between P and the vertical
- x = horizontal distance from centre of slice to centre of rotation, O.
- u = pore pressure
- R = diameter of slip circle
- X = Vertical shear force
- E = Resultants of the total horizontal forces

Factor of Safety:

$$F = \frac{1}{\sum W \sin \alpha} \sum \left[(c'b + W(1 - r_u) \tan \phi') \frac{\sec \alpha}{\frac{\tan \phi' \tan \alpha}{F} + 1} \right]$$

Figure D.4: Effective stress analysis by Bishop's method: forces acting on a vertical slice and factor of safety equation (arranged from Bishop (1955) and Smith (1974)).

APPENDIX E

Flow Charts of The Computer Programs

Developed For The Study

APPENDIX E. 1

COMPUTER PROGRAMS "SHEAR" AND "REVERSE" FOR DIRECT SHEAR TEST

The computer program SHEAR is written in Fortran language and developed for the calculation of shear stresses corresponding to incremental deformations recorded in forward shear tests, peak shear stresses and shear strength parameters cohesion, c , and internal friction angle, ϕ . The test readings taken from tested many specimens, which represent a soil or a discontinuity sample, can be evaluated as an individual test set. The shear strength parameters of the sample examined are computed from the determined peak shear and normal stresses of each specimen by linear regression technique.

The program REVERSE is used for evaluating the reverse shear test results. Its flow chart is the same as the program SHEAR, but the test gauge constants as an input parameter are different than those of program SHEAR. This program calculates residual shear strength parameters.

Because of the similarities between these two programs, their flow charts are introduced in a combined form in Figure E.1 with input data required to run the programs.

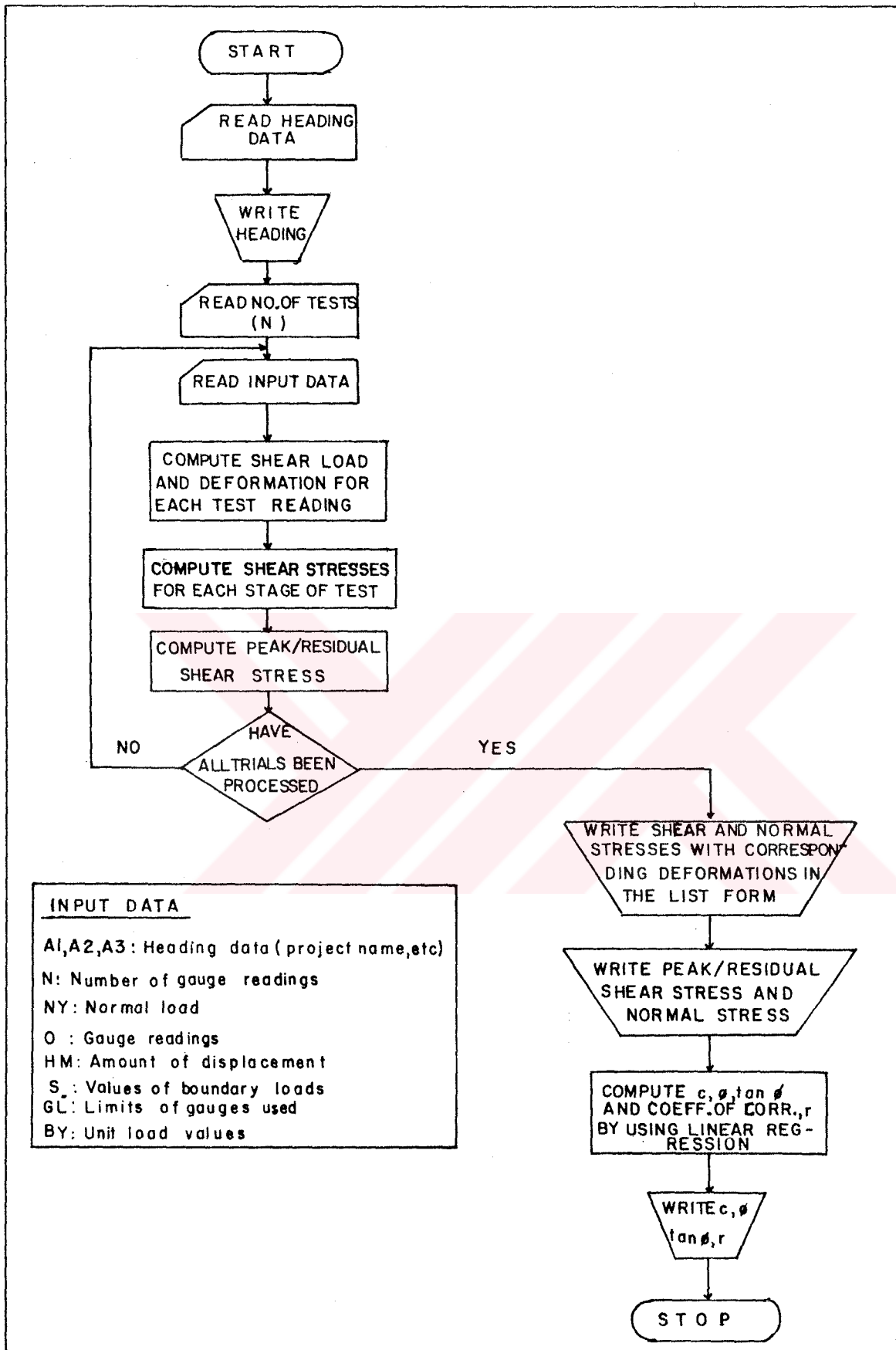


Figure E.1: Combined flow chart for computer programs "SHEAR" and "REVERSE" with the list of input data.

APPENDIX E.2

COMPUTER PROGRAM "HOBR"

Program HOBR, written in Fortran language, has been developed to calculate the shear strength parameters of rock masses. The logic of the program is based on the non-linear failure criterion proposed by Hoek and Brown (1980 a,b) in conjunction with the rock mass classification.

In the first part of the program uniaxial compressive strength and material constant m_i with coefficient of correlation, r , are calculated using the triaxial test data pairs obtained from intact rock specimens. m_i is the value of m for the intact rock. Calculations are based on the linear regression analysis as pointed out in Hoek and Brown (1980 a).

The program calculates the constants m and s for the given rock mass category using the following equations (Hoek and Brown, 1988):

a) Disturbed rock masses:

$$m/m_i = \exp\left(\frac{\text{RMR} - 100}{14}\right) ; \quad s = \exp\left(\frac{\text{RMR} - 100}{6}\right) \quad (1 \text{ a,b})$$

b) Undisturbed or interlocking rock masses:

$$m/m_i = \exp\left(\frac{\text{RMR} - 100}{28}\right) ; \quad s = \exp\left(\frac{\text{RMR} - 100}{9}\right) \quad (2 \text{ a,b})$$

Finally, using the above values and following the calculation sequence mentioned in Hoek and Brown (1988) internal friction angle, cohesion and shear stress values are computed for different normal stress values which can be pre-determined by the user.

A flow chart of this program is given in Figure E.2.

INPUT DATA

N : Number of triaxial test data pairs
SG1, SG3 : σ_1, σ_3
RMR : Rock mass rating
IC : Rock mass category control
SIGC : Uniaxial compressive strength of intact rock
K : Number of normal stress values
SIGMAN : Normal stress value which is selected by the user

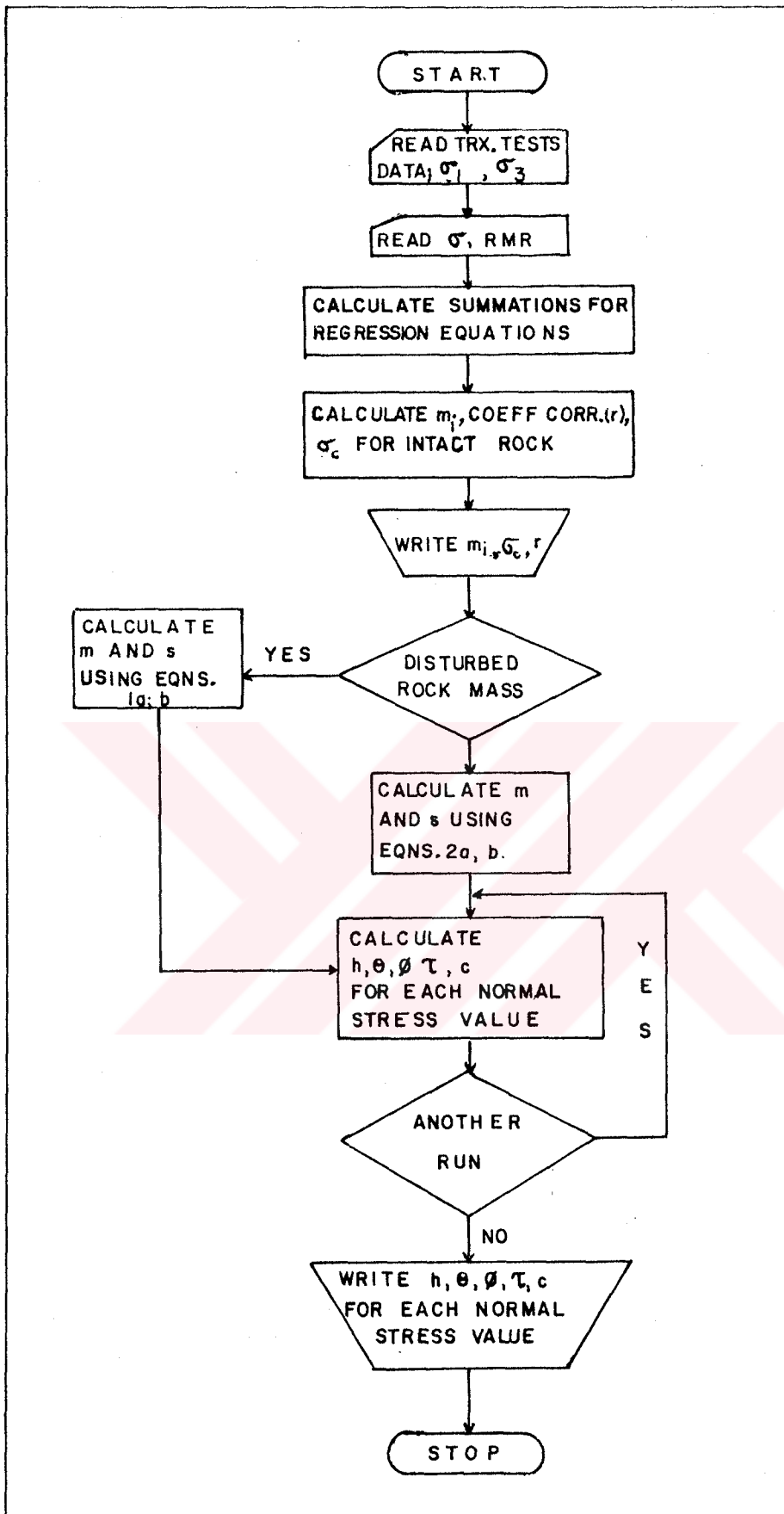


Figure E.2: Flow chart for computer program "HOBR".

APPENDIX E.3

COMPUTER PROGRAM "MBPF" FOR PLANE SHEAR FAILURE ANALYSIS

Program MBPF performs a limiting equilibrium analysis for the case of a slope which may slide along a single discontinuity plane. If it is desired, the program also allows for the inclusion of a vertical tension crack which may be located behind the slope crest (Figure E.3.1) or in the slope face, the effect of externally applied static loads as may result from a dragline.

The advantageous of the program are that the analysis of slopes consisting of many benches in different geometries and involving various units can be easily performed. In addition, the top surface may be inclined. In the case of a slope with nonlinear groundwater table, the linear segmented phreatic surface line enables any water distribution to be easily modeled. Up to 30 segments can be used. The shear strength of the sliding surface is assumed to be composed of frictional and cohesive component according to the linear relationship. The external loads are taken into consideration according to their locations on the sliding mass (Figure E.3.1). The mass above a trial sliding surface is divided by vertical planes into a series of slices. The weight of the sliding mass and water pressure are calculated in terms of slices.

Input data for the program includes slope geometry, conditions of water table or water pressure in tension crack, external loading conditions and the material

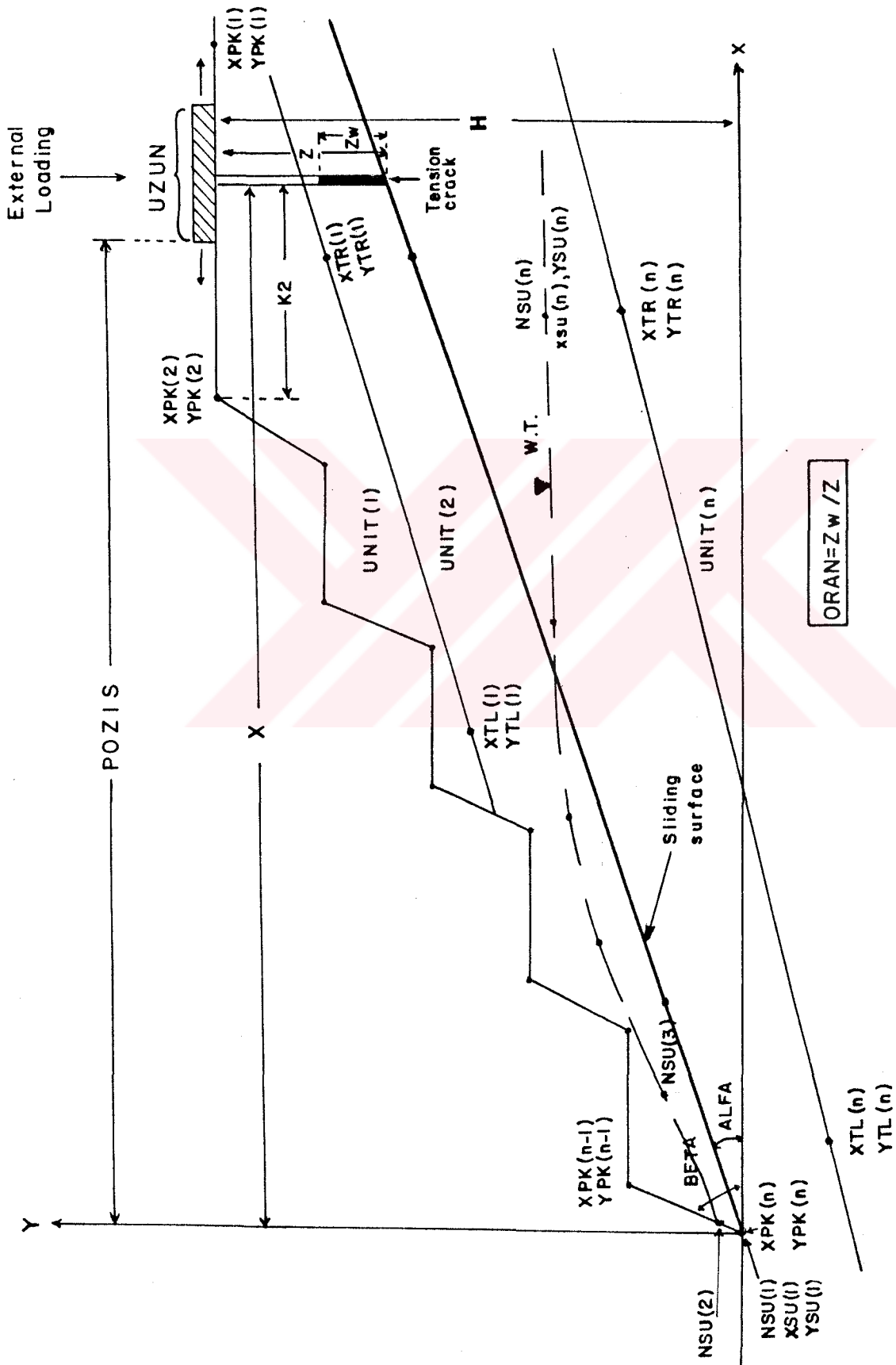


Figure E.3.1: Slope geometry and input parameters of plane sliding employed in program "MBPF".

properties. It will also prompt to user to enter the interval required to be evaluated and the increment of tension crack position. Output consists of a table of input data, a list of factors of safety, weight of sliding mass, water pressures at each position of evaluation. Figure E.3.2 shows a flow chart for this program.

The following cases are included in the program:

- a. Dry slope with or without tension crack.
- b. A slope with non-linear phreatic surface without tension crack.
- c. A slope with non-linear phreatic surface and vertical tension crack.
- d. A slope with tension crack and water pressure acting along tension crack and sliding surface only.
- e. A slope with external loading and with or without tension crack and various groundwater conditions.

INPUT DATA

A1, A2, A3 : Heading input (Project name, location, etc.)

NBAS : Number of benches

XPK, YPK : Coordinates of points defining slope profile

COH, GAMS, SEISM : Cohesion mobilizing along sliding surface, unit weight of water, seismic coefficient

NSTRAT : Number of strata (geological units)

GAMK : Unit weight of each strata

XTL, YTL, XTR, YTR : Coordinates of left and right points of strata bases

H : Slope height

BETA, ALFA, FI : Overall slope angle, inclination of sliding surface, internal friction angle mobilizing along sliding surface.

IEXT : External loading control:
 If IEXT = 1, no loading
 If IEXT = 2, external loading
 POZIS : See Figure E.3.1 (If IEXT =2)
 WBIRIM : Unit weight of material caused
 external loading (If IEXT = 2)
 UZUN : See Figure E.3.1 (If IEXT =2)
 GECAT : Tension crack control:
 GECAT = 1, tension crack is on the
 slope face
 GECAT = 2, tension crack is behind
 the crest
 GECAT = 3, no tension crack
 NAKFER : Groundwater condition control:
 NAKFER = 1, dry slope
 NAKFER = 2, phreatic surface (free
 aquifer case)
 NAKFER = 3, water pressure along
 tension crack and
 sliding surface only
 ORAN : Pre-determined ratio between the
 depth of tension crack and height of
 water in tension crack (If NAKFER=3)

 NSU : Number of points defining phreatic
 surface
 XSU, YSU : Coordinates of points defining
 phreatic surface
 K2, L2, M2 : Initial position of tension crack
 with respect to slope crest,
 intervals of increments for tension
 crack position, maximum distance of
 tension crack from crest (last
 tension crack position)

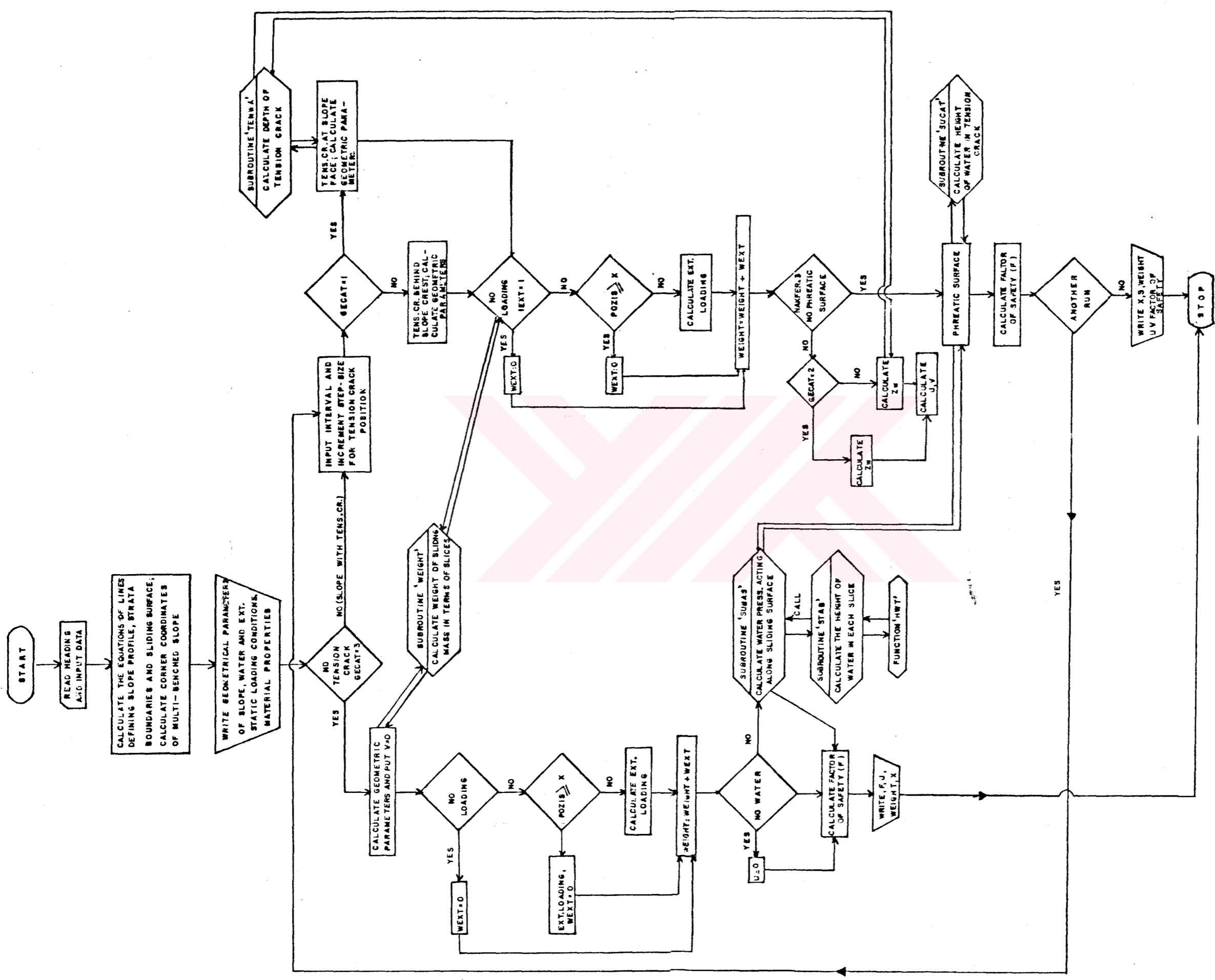


Figure E.3.2: Flow chart for program "MBPF".

APPENDIX E.4

COMPUTER PROGRAM "WEDFA" FOR WEDGE FAILURE ANALYSIS

The computer program WEDFA is written in Fortran language. Basically, this program calculates the factor of safety for the wedge which may involve a tension crack behind the crest and water pressure or may not. The program is based on the limiting equilibrium method of analysis proposed by Hoek and Bray (1977) which is summarized in Appendix D.3. It also provides analysis of many wedges in different heights in the same run. The flow chart of the program is given in Figure E.4.

The input data required to run the program are as follows:

A1, A2, A3 : Heading data (project name, etc.)
N : Number of wedges to be analysed
H : Height of wedge
WEXT : Weight of external load
IW : Water pressure control:
ISU = 1, no pressure
ISU = 2, water pressure does exit
ITECR : Tension crack control:
ITECR = 1, no tension
ITECR = 2, tension crack is behind the
slope crest

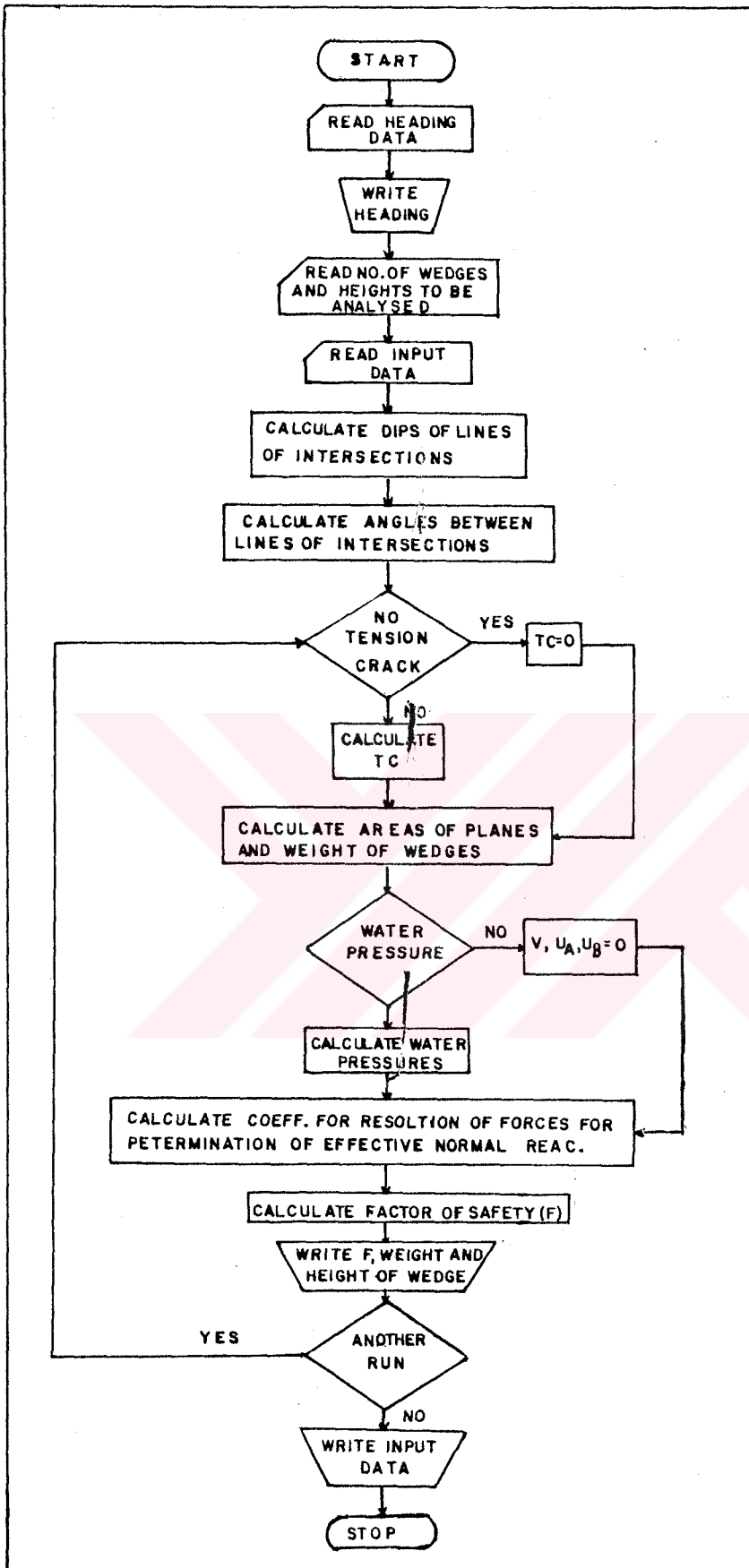


Figure E.4: Flow chart for computer program "WEDFA".

VITA

Reşat ULUSAY was born in Izmir, on September 1, 1952. After graduation from Eskişehir Atatürk High School in 1969, he attended the department of Geological Engineering of the Hacettepe University, where he received his M.S. degree in June 1975. He was elected as the most successful student and received İhsan Doğramacı award for outstanding success.

In 1975 he joined the General Directorate of the Mineral Research and Exploration. In 1978 he attended the training course held in England on "Geotechnical Investigation and Design for Mining Feasibility Studies". In 1982 he attended the UNESCO sponsored seminar on "Theory and Application of Rock Mechanics" and the course "Rock Fracture Mechanics" held at Udine, Italy.

Mr. Ulusay took part in eighteen research projects as principal investigator and/or the team leader. He is the author of two books and eight papers.

Reşat Ulusay is married and has one child.